QUEEN SQUARE INSTITUTE OF NEUROLOGY

UCL

NOVEL TOOLS TO INVESTIGATE CORTICAL ACTIVITY IN PAROXYSMAL DISORDERS

Damandeep Singh Rathore

UCL Institute of Neurology

March 2022

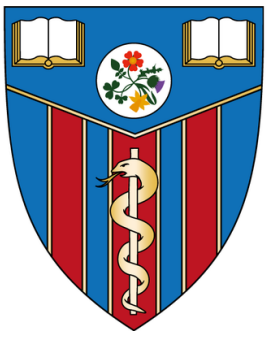

A thesis submitted for the degree of

Doctor of Philosophy (PhD)

Abstract

This PhD project is at the interface between academic research and industry, and is jointly sponsored by the BBSRC and the industrial partner– Scientifica UK. The goal of this research is the development of new instruments and approaches to monitor and manipulate neuronal network activity in disease states. Firstly, (I) I collaborated with Scientifica to develop and utilise the newly developed Laser Applied Stimulation and Uncaging (LASU) system. The combined usage of the LASU system, alongside novel spatially-targeted channelrhodopsin variants, has allowed me to test the limits of single-photon optogenetic stimulation in achieving specific activation of targeted neurons. The presented findings demonstrate that, although high-resolution stimulation is achievable in the rodent cortex, single-photon stimulation is insufficient to achieve single-cell resolution stimulation. Secondly, (II) I have combined the high temporal resolution of novel, transparent 16-channel epicortical graphene solution-gated field effect transistor (gSGFET) arrays with the large spatial coverage of bilateral widefield Ca^{2+} fluorescence imaging; to perform investigations of the relationship between spreading depolarisation (SD) and cortical seizures in awake head-fixed mouse models of epilepsy. To analyse these complex datasets, I developed a bespoke, semi-automated analysis pipeline to process the data and probe the seizure-SD relationship. I present the advantages of this dual-modality approach by demonstrating the strengths and weaknesses of each recording method, and how a synergistic approach overcomes the limitations of each technique alone. I utilise widefield imaging to perform systematic classification of SD and seizures both temporally and spatially. Detailed electrophysiological analysis of gSGFET data is then performed on extracted time periods of interest. This work demonstrates the complex interaction between seizures and SD, and proposes several mechanisms describing these interactions. The technological and analytical tools presented here lay the groundwork for insightful and flexible experimental paradigms; altogether, able to probe paroxysmal activity in profound detail.

Impact Statement

The research presented in this thesis is focused around the development, characterisation and implementation of novel technology to provide insight into neurological disorders.

Communication in the nervous system is an incredibly fascinating, yet complex phenomenon. Coordinated electrical signalling within millions of neurons leads to a diverse range of essential functions. However, the delicate balance of this coordinated signalling leads to an increased susceptibility to adverse events. An example of this is in epilepsy, wherein a network imbalance leads to massive breakdown of coordinated communication. The result is the occurrence of transient, unpredictable events with often profound impacts on quality of life. This thesis presents new means to study these events and the pathological mechanisms by which they arise.

The research presented here can be separated into two primary sections. The first, involves the investigation of an affordable, commercially-available laser system to stimulate specific groups of neurons in intact brain tissue using channelrhodopsins. The development and characterisation of this system provides more researchers with the ability to investigate complex neural dynamics and pathological network alterations with a high-level of detail.

The second core body of research in this thesis is focused on the generation and application of new methodologies to study seizures and spreading depolarisation in detail. These phenomena surround alterations of widespread brain networks, and the presented novel methods are able to dissect activity across these widespread regions with high spatial and temporal resolution. To achieve this, novel imaging methods are combined with powerful graphene transistor-based technology. The research presented here demonstrates the first combined application of graphene-transistors with fluorescence imaging. Considerable work has recently demonstrated the power for graphene-based neural interfaces in unravelling complex disease mechanisms (Masvidal-Codina et al., 2019, 2021; Bonaccini Calia et al., 2021; Garcia-Cortadella et al., 2021). The research presented here contributes to the body of knowledge promoting the commercialisation and clinical translation of this tech-

nology. Moreover, a powerful, novel analysis pipeline is generated to use these elaborate datasets to produce meaningful insight into disease mechanisms, and to probe epileptiform activity.

The research presented here demonstrates the use of these novel methodologies to gain insight into cortical network activity. Future work will build considerably upon these findings to provide powerful insight into disease mechanisms. Moreover, outputs will be used to guide computational models of complex disease processes.

Acknowledgements

Firstly, I would like to thank the relevant funding bodies, without whom, this work could not have been possible. I would like to thank the Biotechnology and Biological Sciences Research Council (BBSRC) and the London Interdisciplinary Doctoral Programme (LIDo) for funding this studentship and allowing me to carry out this work. I thank Epilepsy Research UK (ERUK) for funding the *in vivo* work carried out in this thesis. I thank Scientifica UK for their contribution to funding the LASU investigations in this thesis. Lastly, I would like to thank the European Commission-funded Graphene Flagship for subsidising the cost of the graphene transistor arrays used in this work.

Next, I would like to acknowledge the animal models that were essential for the work presented throughout this thesis, and to thank the UCL Biological Services (Denny Brown Lab) staff who have done an amazing job ensuring the highest standards of care for the mice used to generate this data.

Now, onto the individuals without whom this work would not have been possible. I would like to start by thanking my primary supervisor, Prof. Kirill Volynski (UCL Institute of Neurology, UK), for all the guidance and support throughout this PhD project. Thanks to Kirill's support, I have been able to effectively carry out the work in this project. Moreover, I am very grateful for the opportunities to explore my own ideas and develop as an independent researcher. I have very much appreciated Kirill's open and honest feedback throughout my time at UCL, and his interest in my scientific development. Throughout this PhD, I have grown considerably as a scientist and developed many research skills. Without the guidance of Kirill, this would not have been possible; and, therefore, I will always appreciate his guidance throughout my future scientific endeavours.

I also thank my secondary supervisor, Dr. Rob Wykes (UCL Institute of Neurology, UK), for his continual support during the *in vivo* epilepsy investigations presented in this thesis. Rob provided very helpful guidance throughout this PhD relating to epilepsy and spreading depolarisation. I would also like to thank Rob for the many opportunities to collaborate on other projects and assist in the devel-

opment of graphene neural interfaces. These other projects were very insightful and have allowed me to gain extensive experience in the design and implementation of novel *in vivo* recording interfaces. Additionally, at the start of these *in vivo* studies, Rob took the time to train me in all required surgical and experimental procedures. I am very grateful for all of this knowledge Rob has shared with me.

Next, I would like to thank Scientifica UK for allowing me the opportunity to learn about neurotechnology development in the industry sphere. I would like to thank Dr. Christian Wilms and Dr. Alex Murray for supervising the Scientifica-related aspects of this PhD project. With regards to LASU development, I would like to thank Swathi Kamble for frequent support in debugging LASU software issues and developing this software for research purposes. I would also like to thank many individuals in the sales, marketing and research & development teams of Scientifica. These individuals allowed me to contribute to each department and develop knowledge of the multiple departments of a biotechnology company.

I would now like to express much gratitude towards the many collaborators, without whom, this work could not have been possible. Firstly, I would like to thank Prof. Yulia Timofeeva and Adam Smith (University of Warwick, UK) for their assistance in constructing the *in vivo* imaging analysis pipeline. It was a pleasure to work closely with Adam in developing these novel analysis tools. Together, we outlined the steps required to efficiently process the experimental data. Adam then used his computational expertise to construct the code for all analysis stages until and including event detection. These tasks were very challenging and I am very thankful to have assistance in solving the complex problems that arose along the way. During this collaborative work, I was fortunate to develop my Python analysis skills by learning from Adam. As a result, I was able to construct Python code for the later stages of analysis myself (all stages occurring after event detection), and therefore, I am very grateful for all I have learnt through this collaboration.

Another essential collaboration that allowed this work to be performed was with Dr. Anton Guimerá-Brunet and Dr. Eduard Masvidal-Codina (IMB-CNM, Spain). Anton and Eduard were both essential in the design and fabrication of the graphene transistor arrays used throughout this thesis. I am very grateful to Eduard for his work optimising and fabricating low-autofluorescence parylene C graphene transistor arrays. I thank Anton and Eduard for their continual assistance with electrophysiology analysis tasks, for many interesting discussions, and for helping me to further develop my Python analysis skills. I would also like to thank Enrique Fernandez-Serra for his help in designing the 64-channel graphene transistor arrays, and his future work in fabricating these devices. I also thank Prof. Jose Garrido and

Dr. Andrea Bonaccini Calia (ICN2, Spain) for their work designing and fabricating the intracortical graphene transistor probes presented in the appendix.

I am very grateful to Prof. Ed Boyden and Dr. Or Shemesh (MIT, USA) for providing the unpublished spatially-targeted optogenetic tools used in this thesis. These tools were essential to fully investigate the LASU system resolution, and I am thankful for the opportunity to be involved in their large, collaborative research project.

Now, I would like to thank many individuals in the Department of Clinical and Experimental Epilepsy (DCEE) at the UCL Institute of Neurology. Firstly, starting with those who have worked in the Volynski lab, I thank Dr. Elizabeth Nicholson for teaching me the initial surgeries required for LASU experiments and for guidance in slicing and patch-clamp techniques. Next, I thank all other members of the Volynski lab for the regular feedback and assistance over the years. I would also like to thank many individuals in the Wykes lab. A very large thank you to Dr. T. Martin Smith for many interesting scientific discussions. Martin always took the time to give me advice and help me develop as a scientist, which I am very grateful for. Moreover, Martin's work developing the Simulink model to allow recordings from two 16-channel arrays simultaneously was essential for the dual intracortical-epicortical gSGFET recordings presented in the appendix. Lastly, I thank the many individuals in DCEE, UCL. I have learned a lot through our weekly seminars and discussions. Moreover, I have really enjoyed the environment created by the many passionate and kind researchers throughout the department, and I'm very grateful for the many laughs and good times.

From other institutions, I would like to thank Dr. L. Federico Rossi (UCL, Institute of Ophthalmology) for interesting analytical discussions regarding the *in vivo* data presented in this thesis. I would also like to thank the many individuals in the Wykes lab at the University of Manchester (Nanomedicine Lab) for many interesting weekly discussions regarding the use of gSGFET technology to study neurological diseases.

Lastly, I would like to thank many individuals in my person life who have continually supported me throughout this project. I express my deepest gratitude to my family, Mohinder, Rani and Taran Rathore. Throughout my life they have provided me with the love and support to allow me to pursue my ambitions. I thank Dio for sharing part of this journey with me. I would also like to thank the many friends who have accompanied me on this journey. These many individuals have been there to help and support me over the years, and I will always be grateful for all the kindness they have shown.

Contents

List of Figures

Acronyms

4-AP 4-aminopyridine

AC alternating-current

aCSF artificial cerebrospinal fluid

AgCl silver chloride

ASIC1a acid-sensing ion channel 1a

ATP adenosine triphosphate

CBS cortex-buffered saline

CCD charge-coupled device

ChR channelrhodopsin

CMOS complementary metal-oxide semiconductor

CSD cortical spreading depression

DC direct-current

DP double-peak

DPh double-peak with hyperpolarisation

ECoG electrocorticography

EEG electroencephalography

EMCCD electron-multiplying charge-coupled device

FETs field-effect transistors

FHM familial hemiplegic migraine

FPGA field-programmable gate array

GABA gamma-Aminobutyric acid

GPCR G-protein coupled receptor

gSGFET graphene solution-gated field effect transistor

HET Heterozygous

HFOs high-frequency oscillations

HOM Homozygous

I_{ds} drain-source current

IOS Intrinsic optical signalling

ISA infraslow activity

KCl potassium chloride

LASU Laser Applied Stimulation and Uncaging

LED light-emitting diode

LFP local field potential

MUA multi-unit activity

NMDA N-methyl-D-aspartate

PBS phosphate-buffered saline

PCB printed circuit board

PDs paroxysmal disorders

PFA paraformaldehyde

PGES postictal generalised EEG suppression

PIDs peri-infarct depolarisations

PSRR post-spike recovery ratio

PunctCoChR Punctate CoChR

SD spreading depolarisation

SNR signal-to-noise ratio

SoCoChR Somatic CoChR

SP single-peak

SPh single-peak with hyperpolarisation

SUDEP sudden unexpected death in epilepsy

TBI traumatic brain injury

TTL transistor-transistor logic

$\mathbf{V}_{ds}$ drain-source voltage

$\mathbf{V}_{gs}$ gate-source voltage

WT wild-type

Chapter 1

Introduction

1.1 Recording Electrical Activity in the Brain

Since the discovery of electrically active biological tissue (Galvani, 1792), technological development of new recording methods have allowed researchers to dissect and understand the encoding of fast communication within, and between, excitable cells. The electrical nature of nervous communication, and the reliance on charge displacement for this communication to occur, led to the development of novel tools that are able to provide the sensitivity to record biological signals with high fidelity. Conventionally, these recording techniques have been focused around capturing changes in potential difference in response to the displacement of ions during certain periods or phases of activity (Rubaiy, 2017). More recently, the repertoire of tools has grown to include optical reporters of activity that have revolutionised our understanding of the spatial dynamics in neuronal networks (C. K. Kim et al., 2017).

1.1.1 Current Electrophysiological Tools

Electrophysiological tools are able to provide insight into electrical communication in excitable tissue on multiple scales. This, depending on the chosen recording configuration, can allow dissection of activity ranging from the scale of charge flowing through single ion channels in the plasma membrane (Maki et al., 2014); to the scale of activity of entire ensembles of neurons (Juavinett et al., 2019). Here I will discuss currently employed electrophysiological tools used to probe communication in the nervous system.

Historically, basic insight into bioelectrical communication was achieved using simple metal electrode configurations. In this paradigm, a metal electrode is in-

serted into, or close to, a tissue region of interest. Another electrode is then either; internally inserted into a different area, or attached externally in contact with the specimen to act as a reference. The reference subtracted signal can then be amplified and digitised to investigate activity across a large distance. A similar configuration is still commonly used in clinical environments to achieve non-invasive recording of brain activity in multiple regions of the cortex. This method, known as electroencephalography (EEG), utilises metal electrodes coated in silver chloride (AgCl) that are placed across the surface of the skull, close to brain regions of interest (Buzsaki et al., 2012a).

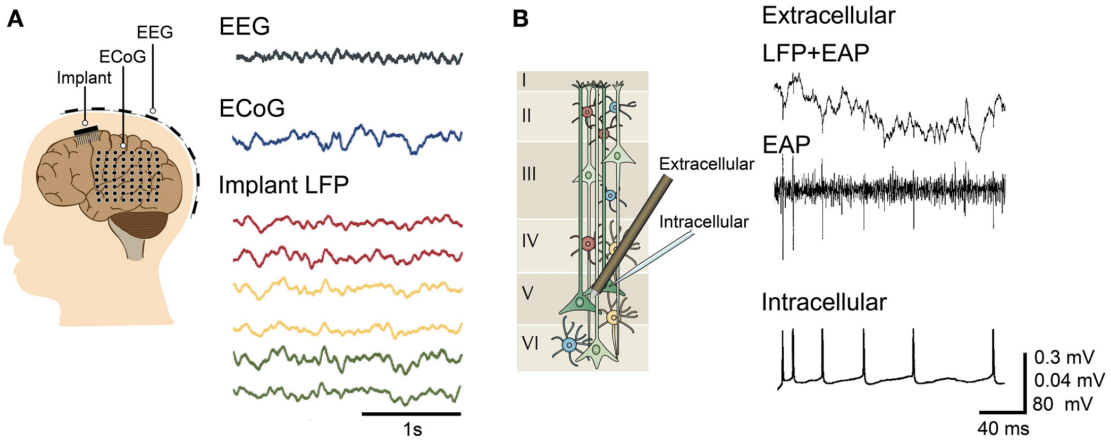

Figure 1: Diagram comparing extracellular and intracellular recording techniques. **A)** EEG recording through skull shown with lower signal-to-noise ratio (SNR) compared to ECoG and Implant local field potential (LFP). **B)** Comparison of LFP, extracellular action potential and intracellular recordings. Adapted from Buzsaki et al. (2012a)

Although EEG is a leading technique in the area of cortical electrophysiology, it suffers from several limitations. A major limitation arises from the shape and thickness of the skull: recording through bone results in dispersion of the signal leading to poorer signal localisation and distortion of signal properties (Chauveau et al., 2004a). As a result, to gain a more detailed glimpse into electrical communication in the cortex, similar metal electrodes are often placed directly in contact with neural tissue in a technique known as electrocorticography (ECoG) (Buzsaki et al., 2012a). These studies are especially relevant in the case of epilepsy, whereby the use of ECoG was pioneered to map out epileptogenic zones for surgical resection (Reif et al., 2016a).

ECoG can be performed epidurally or subdurally, wherein the sterile recording device is placed either above or below the dura mater respectively. Furthermore, the silver chloride coating of electrodes used for EEG recordings is not used in ECoG,

or with any other techniques requiring invasive insertion. Silver chloride coated electrodes allow increased baseline stability during recordings due to a reduction in electrode polarisation. However, chronic AgCl exposure to biological tissue delivers a toxic effect, limiting these electrodes to external use only (Masvidal-Codina et al., 2019).

To provide a further level of detail regarding neuronal population activity, metal electrodes can be inserted into the tissue at the region of interest. This allows selective extracellular recording from a region of interest, and combining this technology with stereotaxic methods can allow recording from specific sites within laminar structures. For example, progression of an electrode through the cortex will allow recording from first, mainly dendritic arbours (Layer 1/2); secondly, neuronal soma (Layer 2/3); third, axon terminals (Layer 4); and fourth, deeper soma (Layer 5/6) (see Figure 2). This would not be achievable if the recording site is located at the cortical surface, wherein the recorded signal would be a composite signal dominated by activity in superficial layers (Buzsaki et al., 2012a).

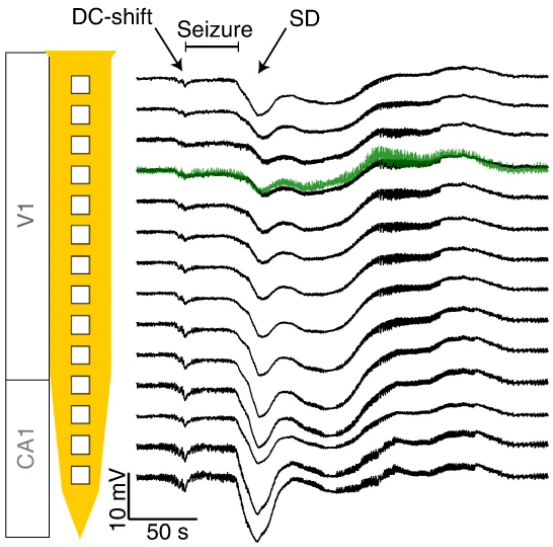

Figure 2: Full bandwidth recording of 4-aminopyridine (4-AP)-induced epileptiform activity and spreading depolarisation (SD) using a graphene solution-gated field effect transistor depth probe (black). Recording shown for multiple layers of the visual cortex and hippocampus with a micropipette simultaneously recording from the visual cortex (green) (Bonaccini Calia et al., 2021)

.

To further increase recording resolution, intracellular recordings can be performed. These are often performed in excised tissue due to the difficult and time-consuming nature. In the case of intracellular recordings, the impedance of metal electrodes requires a size insufficient for recording from excitable cells. In recent

years, intracellular electrodes are typically comprised of an electrolyte-filled glass micropipette in contact with a AgCl wire. Since, their initial use in plant tissue in the early 1900s, glass micropipette-mediated recordings have become widely used to record from small structures in the nervous system (Bretag, 2017). Multiple classical studies have used methods such a two electrode voltage-clamp, whereby two glass electrodes are inserted into a cell of interest; with one used to record potential, and the other used to deliver current to the cell. This configuration, although highly useful in studying isolated currents in large environments (e.g. in oocyte ion channel expression studies), requires insertion of multiple electrodes, creating a configuration too complex for routine intracellular neuronal recording (Wang et al., 2017). Consequentially, in the 1970s, considerable research was invested to develop a recording technique able to record intracellularly from single neurons with high stability.

The revolutionary solution, known as the patch-clamp, was presented by Sakmann and Neher. This technique utilises a single, pressurised, finely-pulled, polished glass micropipette. The use of a polished glass micropipette allows formation of a gigaohm seal onto the membrane of the cell of interest. The micropipette is filled with an artificial solution created to mimic the environment of the cell being studied. In contact with this solution is a conductive wire connected to intricate operational amplifier circuitry. These initial developments allowed local activity to be recorded using a single micropipette (Neher & Sakmann, 1976). Following this seminal paper, considerable developments occurred. Altogether, these developments resulted in the generation of many flexible experimental paradigms. The recording circuitry allowed the potential of a neuron to be clamped relative to a reference point and for any charge deviation from this clamp point to be measured through the application of an opposing current (voltage-clamp). Additionally, under other circumstances, constant current can be delivered to the electrode tip to allow the measurement of any deviations in potential (current-clamp). These two circuitry configurations are powerful in revealing complex mechanisms of signal transduction in the nervous system at both a micro- and mesoscopic level (Kornreich, 2007).

These developments resulted in the ability to construct a variety of insightful experimental paradigms. Firstly, the use of a singular fine-tipped glass pipette allows recording from small cells of interest, such as neurons and astroglia (Henneberger & Rusakov, 2012). Secondly, the high-resistance seal onto the surface of the membrane allows recordings to be acquired in multiple configurations, including intracellularly using a 'whole-cell' configuration and extracellularly through the membrane using a 'cell-attached' configuration. Thirdly, the sealed membrane can be

excised to allow recording from individual currents in the small area of membrane in either inside-out or inside-in configuration (Leech & Holz, 1994; Rubaiy, 2017). Additionally, the patch pipette can be used infuse various chemicals into the cell-of-interest, and therefore, generate complex, information-rich experimental paradigms. Lastly, the fine tip of the micropipette can allow recording from minuscule sub-compartments of neurons; such as synaptic terminals (Novak et al., 2013), and dendrites (Beaulieu-Laroche et al., 2018), with a minimal leak current. Altogether, patch-clamp electrophysiology is an incredibly powerful method, showing powerful versatility, and existing as an essential component of the modern electrophysiologist's toolbox (Verkhratsky & Parpura, 2014).

Alongside the development of patch-clamp electrophysiology, glass micropipettes are also utilised as a powerful tool in studying the activity of large populations of neurons simultaneously. Filling the micropipette with a solution to mimic the extracellular environment of neurons allows external recording from multiple cells, while overcoming some of the limitations presented by metal electrode configurations. Moreover, extending beyond the precision of metal electrodes, these configurations are able to utilise the high resistance tip to record locally from specific areas and even extracellularly from few soma (Buzsaki et al., 2012a).

1.1.2 Limitations of Conventional Extracellular Recording Techniques

Standard metal electrode recording techniques demonstrate several limitations. A large limitation of these techniques comes from the limited bandwidth of these recording configurations. Due to polarisation at the electrode surface, raw signals recorded using these interfaces typically suffer from considerable direct-current (DC) drift. Since the amplifier used to augment this signal has a limited dynamic range, this slow drift, if uncorrected, will inevitably lead to saturation and clipping of any subsequent activity. To circumvent this issue, these signals are high-pass filtered in real-time to remove any slow DC drift. As a result, no slow DC fluctuations are recorded by the amplifier and saturation is avoided. However, of considerable importance in nervous tissue are slow oscillations, and of course, when trying to study DC events, removing low frequency components from a recording limits the ability to dissect these phenomena (Masvidal-Codina et al., 2019).

Glass micropipettes, as mentioned previously, are able to overcome these limitations in recording bandwidth due to the layer of Cl^- ions on the AgCl wire resulting in minimal polarisation and minimal DC drift (Bonaccini Calia et al.,

2021). However, micropipette-mediated recordings suffer from a variety of other limitations. Similar to metal electrodes, these devices are rigid and cause damage to tissue upon insertion, as well as when implanted chronically: the rigidity prevents electrode movement with the tissue during natural pulsation, resulting in greater damage over time (Masvidal-Codina et al., 2019). Moreover, due to the complexity of the recording site, glass micropipette techniques are fragile and difficult to organise into multi-channel arrays, thus limiting their use in spatial mapping of activity in the nervous system.

Consequentially, significant work is underway to develop recording configurations that allow the recording of low frequency activity at multiple sites in the nervous system, without suffering from the limitations seen by the systems presented thus far.

1.1.3 Full-bandwidth recording in the Nervous System

Generally, the recording of full-bandwidth activity in the nervous system is limited by three factors. The first, is the availability of stable recording interfaces that minimise slow DC drift. The second, is a recording interface with high tissue contact and low impedance; to minimise noise and reduce inherent high-pass filtering of signals by the recording configuration. The third is the availability of an amplifier with a dynamic range large enough to avoid signal saturation (Masvidal-Codina et al., 2019). Additional to these factors, other desired properties exist. These include low noise, biocompatibility, flexibility and the ability to be organised into multi-site arrays (Hess et al., 2013).

Multiple passive electrode-based recording techniques have attempted to overcome the previous limitations in stability. Several techniques used clinically to study infraslow activity (ISA) involve Pt, Pt iridium, or Pt black electrode-based recording. Although, these electrodes are inert and allow recording of low-frequency activity, they still suffer from considerable baseline drift (Hartings et al., 2017). Moreover, miniaturisation of these metal electrode-based techniques, which is often required for multi-site recording, can result in signal attenuation, particularly at lower frequencies, due to increases in electrode impedance that can not be overcome by amplifier gain (Masvidal-Codina et al., 2019).

In recent years, interest into diamond electrodes has grown considerably. Moreover, the doping of diamond electrodes with boron has resulted in electrode properties that are highly suitable for recording from the nervous system. Historically, boron-doped diamond electrodes have suffered from rigidity limitations. However, recently, they have been embedded in flexible substrates to allow multi-site record-

ing. Consequentially, boron-doped diamond electrodes are able to satisfy several of the required criteria for a neural interface. These include multi-site recording, chemical inertness, biocompatibility and a wide potential window. Nonetheless, little evidence has been presented that these devices are fully able to capture ISA without suffering from noise limitations. Moreover, the cost of materials required for fabrication make them somewhat inaccessible (Torres-Martinez et al., 2019).

Attempts have been made to overcome the impedance issues created when using passive electrode-mediated recording devices. Generally, these issues are created through the limited surface contact between tissue and electrode resulting in inherent high pass filtering of the signal of interest. To circumvent this issue, focus shifted to the fabrication of stable electrodes with a high surface area. This can be seen in the case of Pt black, where the surface area is increased, and impedance reduced, by coating of the electrode surface with rough layers (Desai et al., 2010). Another example of this can be seen with carbon nanotube-based recording devices. These facilitate large contact with neural tissue while allowing high conductivity. Nonetheless, these devices are seen to suffer from the common issues associated with other passive electrode techniques, essentially making them suboptimal for recording ISA. Furthermore, due to a requirement for nanoscale catalyst patterning, these devices are difficult and often costly to fabricate (Voge & Stegemann, 2011).

1.1.4 Active Recording Devices

Emerging from this demand for a system able to capture ISA with high fidelity is the development of active recording devices for neuroscience applications. Passive electrode-based systems record potential differences between the tissue and a reference. The electrode impedance, if approaching amplifier impedance (which is often the case for low frequency signals), results in large reductions in SNR. Active recording systems, such as those using transistors, are able to circumvent these limitations (Masvidal-Codina et al., 2019; Bonaccini Calia et al., 2021).

The use of transistors and their associated circuitry results in the recording of a signal undergoing intrinsic amplification. Consequentially, recording signal-to-noise ratio (SNR) is no longer dependent on the interplay between electrode and amplifier impedance. Instead, signal fidelity is determined by intrinsic transistor noise and transconductance. Transistors are semiconductor devices found widely throughout electronic devices, with each generally consisting of three terminals. Transistor function typically relies on the modulation of current flow between two terminals through the application of a potential to a third terminal (Hess et al., 2013).

Specifically used in neural recording devices are field-effect transistors (FETs).

FETs utilise a semi-conductive material bridging two terminals, the source and drain; with a nearby third terminal, the gate, applying an electrical field to the source and drain. This electrical field can be controlled by applying a voltage to the gate and alters the current flow between the source and drain (Khodagholy et al., 2013). The result is a significant reduction in noise susceptibility due to active voltage-to-current amplification. Conventional FETs, although powerful at recording activity with minimal noise, suffer from limitations: firstly, the materials required to achieve high charge carrier mobility and a high SNR are rigid and damaging to tissue; and secondly, the materials used often struggle to withstand the harsh, aqueous biological environment. The incorporation of graphene monolayers into this structure resulted in a large increase in suitability for electrophysiological recording (Hess et al., 2013; Masvidal-Codina et al., 2019).

1.1.5 Graphene Solution-Gated Field Effect Transistors (gSGFETs)

In recent years, there has been considerable growing interest in the utilisation of graphene. Graphene is a single atomic layer thick allotrope of carbon. Each atom in a graphene sheet interacts with three neighbouring atoms via sigma bonding. A fourth electron from each atom is contributed to a conduction band surround the graphene layer. As a result, graphene is surrounded by free charged particles, allowing efficient electrical conduction (see Figure 3). Additional to the conductive properties of graphene, the material also has other desirable properties, including high mechanical stability, biocompatibility and optical transparency when present in a monolayer (Hébert et al., 2018). Altogether, these properties led to the investigation of graphene as a material highly suited to interface with nervous tissue.

Due to recent fabrication advancements, the body of literature characterising graphene-based electrodes has grown considerably (Kwon et al., 2018). Several studies have demonstrated the successful use of graphene electrodes to record bioelectrical activity with high SNR in the cortex (D. W. Park et al., 2018; Lee et al., 2021). However, a further recent advancement is the incorporation of graphene monolayers into FET devices, wherein the graphene acts as the semi-conductor bridging the source and drain. The result is a graphene solution-gated field effect transistor (gSGFET) device, overcoming several of the limitations associated with conventional FETs, while maintaining the benefits. These benefits include high stability, active signal amplification, inert composition, flexibility and transparency (Hébert et al., 2018).

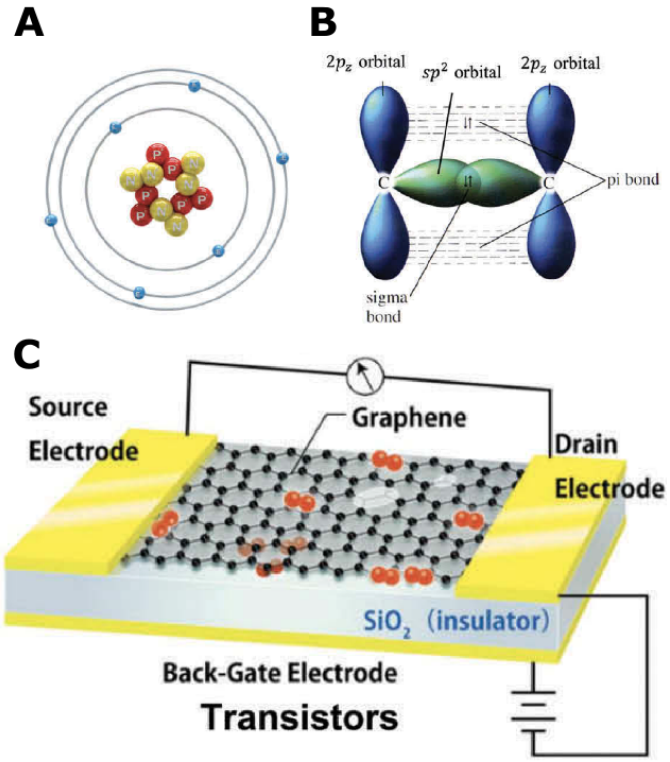

Figure 3: Chemical properties of graphene and integration into transistor circuity. **A)** Image of carbon atom showing positions of protons, neutrons and electrons. **B)** Interaction of two carbon atoms in graphene showing strong sigma bonding between atoms and weaker pi bonding from overlapping p-orbitals. **C)** Integration of graphene structure into transistor technology. Graphene used to bridge source and drain electrodes with pi bonds allowing electrical conduction. Adapted from G. Yang et al. (2018)

Several studies have been performed characterising the performance of gSGFETs, in particular their ability to record wide-band electrographic signals. In the major first study characterising gSGFET arrays, collaborators from IMB-CNM and ICN2 (Spain) performed in depth characterisation of gSGFET technology, along with the efficacy in recording low frequency electrophysiological signals (Masvidal-Codina et al., 2019).

Firstly, the study discusses fabrication procedures and device characterisation. gSGFETs have been organised into array-like structures to allow multi-site recording from different cortical regions simultaneously (Figure 4B). One design, the epicortical or epidural array, involves 16 gSGFET channels arranged in a thin sheet-like structure. The other major design in use, the intracortical probe, has either 14 or 15 gSGFET channels arranged down the length of a thin shank. This flexible intracortical probe, can be inserted into nervous tissue to record at multiple depths

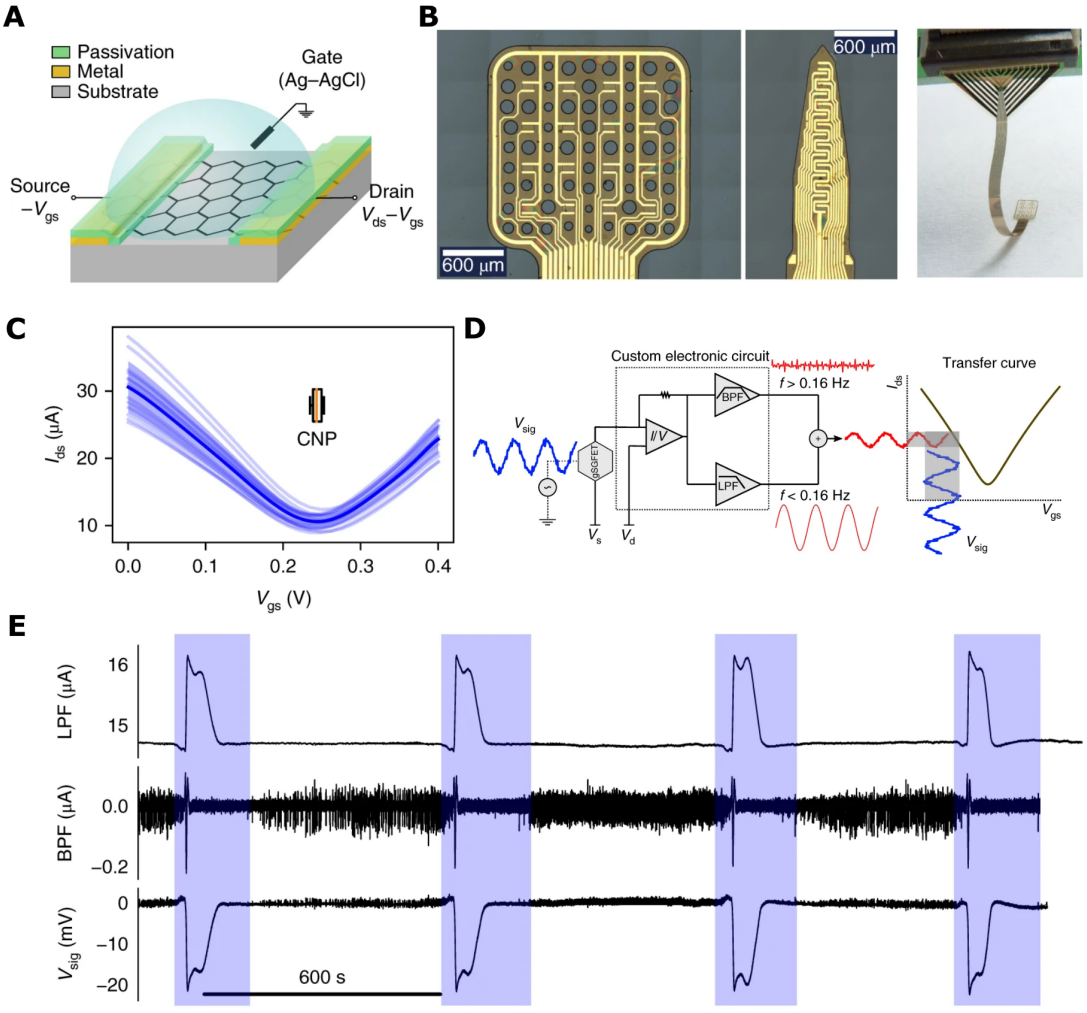

Figure 4: gSGFET structure, calibration and recording. **A)** gSGFET structure showing graphene monolayer bridging source and drain with nearby gate modulating current flow. **B)** gSGFET epicortical (left) and intracortical array (middle) shown with epicortical array inserted into zero-force connector (right). **C)** gSGFET transfer curve generated during calibration procedure. Relationship between gate potential and current flow between source and drain shown, with charge neutrality point (CNP) marked. **D)** Custom electronic circuit used for gSGFET calibration and recording shown. Low frequency (f<0.16Hz) and high frequency (f>0.16Hz) currents, amplified separately, with field potential signal reconstructed using the previously generated transfer curve. **E)** KCl-induced SD showing low-frequency current (LPF), high frequency current (BPF) and the reconstructed extracellular field potential signal (V_{sig}). Adapted from Masvidal-Codina et al. (2019)

from different areas of interest simultaneously.

Each batch of gSGFET devices are fabricated using a silicon wafer. Using photolithographic techniques and reactive-ion etching, graphene channels, metal terminals and associated wiring (Ni, Ti and Au composition) are embedded into an inert substrate. For investigations prior to this thesis, the inert substrate used was polyimide (Masvidal-Codina et al., 2019; Garcia-Cortadella et al., 2021; Bonaccini Calia et al., 2021). The end result is a wafer containing multiple gSGFET epicortical arrays which can be detached from the wafer and inserted into a zero-force connector to allow bioelectrical interfacing.

Each device once detached from the wafer undergoes a series of testing to characterise the performance of each transistor. In a common-gate mode, the drain-source voltage (V_{ds}) is fixed and the gate-source voltage gate-source voltage (V_{gs}) is varied while the transistor and AgCl reference are in contact with a conductive solution (Figure 4A demonstrates gSGFET terminal arrangement). Since graphene behaves as a near-ideally polarisable molecule, following generation of a potential between source and gate, charge accumulates at the graphene surface and results in minimal charge transfer across the interface. As the gate-source potential is altered, the drain-source current (I_{ds}) is modulated. This allows generation of a V_{gs}-I_{ds} curve demonstrating the modulation of charge flow across each graphene transistor, along with the charge neutrality point. Using this characterisation curve, an optimal V_{gs} is selected as the gate-source potential with the maximum mean transconductance value across all working transistors. This optimal V_{gs} is selected as the value below the charge neutrality point to allow hole transport, wherein charge transfer occurs through a positively-biased graphene monolayer (Figure 4C).

gSGFET-mediated full-bandwidth recordings are acquired using a custom-built amplifier. Both low frequency and high frequency signals are processed and amplified separately (Figure 4D). The raw signal is both lowpass filtered at 0.16Hz and bandpass filtered between 0.16-10kHz. Each current-frequency group across the graphene monolayer is amplified differently to avoid amplifier saturation from large amplitude infraslow events. The original signal is then reconstructed by combining the low and high frequency components. Then, using the generated V_{gs}-I_{ds} curve, the raw current signal is calibrated and converted into a field potential (Figure 4E).

Following potassium chloride (KCl)-meditated induction of spreading depolarisation (SD), gSGFET recording capabilities were compared with that of Au and Pt black electrodes. Au electrodes display high conductivity, stability and biocompatibility (Vafaiee et al., 2019), while Pt black electrodes are known to facilitate low impedance recording through a high surface area (Desai et al., 2010): both

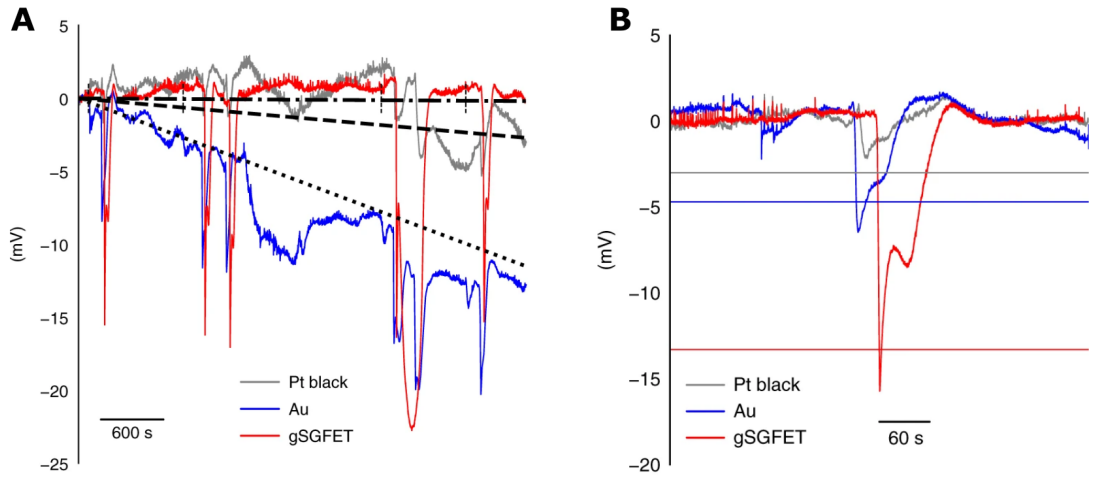

Figure 5: Comparison of gSGFET with platinum black (Pt black) and gold (Au) microelectrodes demonstrating superior stability and ability to resolve DC events. **A)** Graph comparing stability of gSGFET in comparison to Pt black and Au microelectrodes over long recording periods. **B)** Graph showing recorded amplitude for different recording techniques after KCl-induced SD. Adapted from Masvidal-Codina et al. (2019)

electrode types are considered the 'gold standard' in stable wide-band electrophysiological recording. This initial comparison revealed remarkable baseline stability in gSGFET recordings compared to the aforementioned recording methods. Additionally, gSGFETs were able to record low frequency activity with high fidelity and accurately capture the full amplitude of DC events across multiple sites of the cortex (Figure 5). Moreover, findings in this study demonstrate successful gSGFET-mediated multi-site recording. Data is presented showing SD mapping across the surface of the cortex (using epicortical grids) and through the depth of the cortex using intracortical probes (Masvidal-Codina et al., 2019). The characterisation of gSGFET technology in these configurations was an essential foundation for the investigations performed in this thesis. The findings of these investigations clearly demonstrate the ability for gSGFET devices to capture infraslow activity in high detail; and therefore, advance the current understanding of DC events in the context of disease pathology. Further discussion of preliminary gSGFET-related investigations will be performed in the coming section titled 'Spreading Depolarisation'.

1.2 Optogenetics

Although electrophysiology is a powerful tool in dissecting communication in the nervous system, it suffers from limitations due to invasiveness, lack of specificity

and uncertain spatial sampling. Optogenetic techniques are able to overcome many of these limitations; by allowing fast, non-invasive, targeted activity modulation. Optogenetics involves the gene-mediated expression of proteins that respond to light, in order to generate a desired cellular response. In general, photoreceptive molecules are expressed in cells of interest and light is delivered to these targeted regions. The delivery of the genes encoding these light-activated modulators is achieved through genomic expression in transgenic lines, or through viral transduction, often in targeted cell types or regions. The result of stimulation is generally the induction of a quasi-physiological response through either ion channel opening, ionic pump activation or G-protein coupled receptor (GPCR) activation (C. K. Kim et al., 2017).

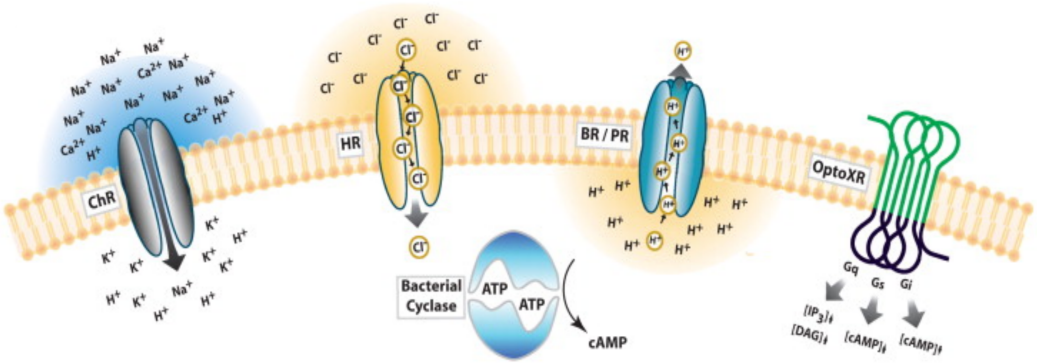

Figure 6: Different optogenetic actuators with their associated molecules. **L-to-R:** Channelrhodopsin (ChR) showing non-selective cation permeability; Halorhodopsin (HR) showing Cl^- permeability; Archaerhodopsin (BP/PR) active pump showing proton displacement; G-protein coupled OptoXR activation leading to intracellular cascades depending on G_q, G_s or G_i. Adapted from Yizhar et al. (2011)

1.2.1 Optogenetics for Modulating Neural Activity

Genetically encoding and expressing a protein to allow the pairing of a photonic input to a desired cellular output is unparalleled in the ability to non-invasively achieve high spatial and temporal control over neuronal dynamics. Optogenetic modulation of neuronal activity at both the single-cell level and on a population-wide scale is powerful in dissecting information transmission and integration in mammalian cortical networks. Moreover, following the continuous development of the field, currently available optogenetic tools allow powerful flexibility in output selection (see Figure 6): tools are now able to achieve precise modulation of activity in the forms of excitation, inhibition or GPCR activation (C. K. Kim et al., 2017).

These pioneering developments are a result of the collaborative efforts of different research institutions working together over the last 20 years.

In 2003, studies of the unicellular algae Chlamydomonas reinhardtii pointed to a strong starting point for developing opsins— the rhodopsin-based microbial ChR2. Rhodopsin-based photoreceptors share a similar core structure containing a 7-transmembrane domain helix covalently linked to an all-trans retinal molecule. Chlamydomonas reinhardtii utilises rhodopsin for phototaxis to enable the efficient collection of light for photosynthesis (Nagel et al., 2003). Although the role of rhodopsin in algae phototaxis was discovered in 1991 (Takahashi et al., 1991), detailed investigations of photoreceptor currents and kinetics only took place in the early 2000s.

In 2003, the sequences of Chop1 and Chop2 in algae were acquired through identification due to sequence homology with microbial rhodopsin. The complexity of algae phototransduction still remained a mystery and following conjugation to all-trans retinal, extensive electrophysiological investigations were performed to understand the functional roles of Chop1 and Chop 2 in allowing efficient phototaxis. Following these investigations, Chop2 (coined ChR2 from Chop2 + retinal) became the centre of focus due to recordings from Xenopus oocytes suggesting that the gene encodes an ion channel conducting a mixture of cations. Moreover, stimulation in different extracellular solutions revealed extensive information about pore size and selectivity for cations, both mono- and divalent. Evidence revealed high selectivity for Na^+ and Ca^{2+}, suggesting the channel would be effective in modifying signalling systems in mammalian cells. Patch-clamp experiments in HEK293 cells revealed rapid channel activation with fast kinetics (Nagel et al., 2003), suggesting a direct link from photon to channel without the requirement for diffusible molecule supplementation; as seen in the case of the first generation optogenetic tool, chARGE (Zemelman et al., 2002). Moreover, calculation of the ChR2 reversal potential as 0mV revealed the occurrence of purely passive conductance through the channel. Lastly, the peak excitation wavelength of the channel was calculated to 460nm increasing the specificity of stimulation beyond the photon, to the level of photon energy delivered (Nagel et al., 2003).

ChR2 was then investigated as a tool to modulate neuronal activity. Research focused on characterising hippocampal neurons following expression of ChR2. Lentiviral transduction of ChR2 fused to YFP was performed and neuronal properties extensively characterised by patch-clamp electrophysiology. Results showed that spiking could be driven reliably and repeatedly following photostimulation. Furthermore, ChR2 activation in different cell populations revealed considerable diversity

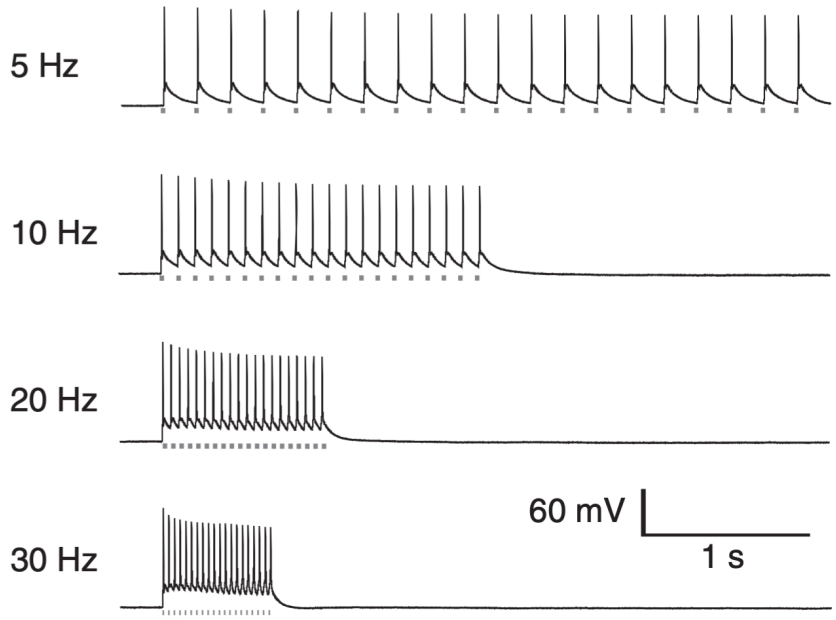

Figure 7: Response of first generation ChR2-expressing neurons to pulsed light stimulation at 5, 10, 20 and 30Hz. Evoked action potentials seen to be tightly synchronised to light delivery. Adapted from Boyden et al. (2005)

as a tool to probe neuronal networks; while investigations into neuronal function revealed no changes to the permeability, excitability and passive membrane properties.

Importantly, the data showed that ChR2 could overcome the limitations associated with the then-existing tools: firstly, light delivery and neuronal activity could be tightly synchronised to result in complex patterns of stimulation with fine control; secondly, the level of all-trans retinal available in neuronal populations was shown to be sufficient to allow repetitive ChR2 stimulation without the requirement for supplementation; lastly, due to ChR2 having fast kinetics with no intermediate messenger in the pathway, activity returns to baseline levels immediately after removal of the light stimulus. This pioneering study (Boyden et al., 2005) revolutionised neuroscientific investigations and has led to multiple subsequent developments and discoveries.

1.2.2 Recent Advancements in Optogenetic Modulation

Since ChR2 set the benchmark for optogenetics in 2005, several expansions and optimisations have been performed to equip neuroscientists with a growing repertoire of tools. Numerous different channelrhodopsin (ChR) variants are dispersed through nature and have been purposefully engineered through targeted mutation

to have desirable characteristics. One of the desired characteristics is the ability to produce fast, reliable inhibition of neuronal populations following photostimulation. Optical inhibition of neurons can be achieved through multiple diverse mechanisms, with some utilising anion-permeable channels (GtACR2 (Messier et al., 2018)), others utilising anion-permeable pumps (eNpHR3.0 (Gradinaru et al., 2010)), and some manipulating the outward movement of protons to elicit hyperpolarisation (ArchT (Han et al., 2011)). Lastly, optogenetics can now allow controlled modulation on a longer time scale using chimeric OptoXRs. OptoXRs are photo-activatable GPCR-derived constructs that allow slow modulation of specific pathways, e.g. Gαs activation in β2 adrenoceptors (J. M. Kim et al., 2005).

A large evolution regarding optogenetic tools has come from the generation of ion channels that activate upon long wavelength illumination. This provides considerable flexibility, particularly regarding in vivo experiments, wherein deeper brain structures can be selectively targeted with reduced photon scattering compared to low wavelength illumination (J. Y. Lin et al., 2013). Additionally, a useful feature of optogenetic experiments is their complementary nature when combined with imaging. Mutliple methods are able to optically quantify both population and subcellular activity (Hochbaum et al., 2014). These fluorescent reporters include Ca^{2+} indicators (Akerboom et al., 2013), voltage sensitive dyes (Hochbaum et al., 2014) and neurotransmitter reporters (Marvin et al., 2013)). A plethora of both red and blue light-excited optogenetic tools and optical reporters are available that permit imaging and optogenetics to occur in parallel due to the ability to select constructs with distinct spectral properties. Therefore, powerful complex optical experimental paradigms can be constructed.

Optogenetic tools exhibit diversity in additional properties besides excitation wavelength. These include spatial distribution, kinetics and photocurrent. Therefore, this allows control of neuronal dynamics with greater precision. For example, in the case of ChR-mediated excitation, if the opsin has slow off-kinetics (e.g. CnChR2 (Klapoetke et al., 2014)), delivery of a single light pulse will result in ionic influx for a considerable period of time, resulting in the induction of multiple action potentials with limited control over firing frequency (Berndt et al., 2011). To produce high frequency stimulation, an opsin with fast kinetics (e.g. Chronos (Klapoetke et al., 2014)) is essential to allow strong coupling between light pulse delivery and neuronal activity. The availability of constructs with varying on- and off-kinetics allows the construction of complex stimulation paradigms, tailored to specific cell populations and research questions.

1.2.3 Spatially Targeted Optogenetic Modulators

Optogenetic modulators are powerful tools to investigate cellular contributors to various forms of electrical communication in the nervous system. Opsin expression can be selectively restricted to particular cell types of interest. This can be achieved through multiple methods, all generally relying on selective promoter-driven expression. A common method to achieve this is to use transgenic animal lines with the sequence for an opsin following the sequence of a particular promoter (Arenkiel et al., 2007). Another method of targeted expression is to use viral transduction, often using adeno-associated viruses or lentiviral constructs, to insert a sequence of nucleotides containing the promoter of interest attached to the selected opsin (as performed in Masvidal-Codina et al. (2021)). Only the transduced cells with the endogenous transcriptional machinery to interface with the promoter will have the functional opsin present. Other studies utilise a combination of both transgenic animal lines and viral transduction. These paradigms take advantage of Cre-Lox recombination systems to target expression to particular cell types. Transgenic lines expressing Cre-recombinase under a particular promoter are transduced with a virus containing an opsin of interest flanked with LoxP sites. Within the viral construct, the opsin gene is inserted in reverse. Upon insertion of the nucleotide sequence into a Cre-recombinase-expressing cell, the Cre-recombinase will recognise the LoxP sites, and reverse the orientation of the opsin gene back to a readable orientation. The result is selective opsin expression targeted to infected cells of interest (C. K. Kim et al., 2017). Generally, the spatial targeting of these opsin constructs is limited by the availability of defined promoters with characterised expression in different cell types. Nonetheless, many promoters have been characterised, with this allowing selective expression in different neuronal subtypes, such as pyramidal (Masvidal-Codina et al., 2021), parvalbumin-expressing, somatostatin expressing (Magloire, Cornford, et al., 2019a) and cholecystokinin expressing (Nguyen et al., 2020); as well as glial populations, such as astrocytes (Pelluru et al., 2016) and microglia (Yi et al., 2021). The result is the ability to generate targeted expression restriction, leading to focused activation of specific cell types; a near-impossible feat with classical electrical stimulation paradigms.

Concurrent technological advancements in photostimulation devices have enabled stimulation with high spatial resolution. As a result, focus has shifted to advancing optogenetic tools to increase the utility of different devices. Frequently, photostimulation is achieved through widefield light-emitting diode (LED) illumination of large cell populations (Zemelman et al., 2002; Boyden et al., 2005). Recently, developments in complex photo-modulation devices have allowed the selective illu-

mination of individual cells (Andrasfalvy et al., 2010), and targeted cellular compartments (Packer et al., 2012). To match this advancement, interest in the spatial restriction of opsin tools on a subcellular-scale has grown considerably.

In recent years, opsin constructs have been conjugated to fusion proteins acting to guide the spatial distribution of the channel (Figure 8). In 2017, the fast, high-photocurrent channel CoChR was shown to achieve soma-targeted expression following conjugation to amino acids 1-150 of the receptor subunit KA2 of the kainate receptor (Somatic CoChR (SoCoChR) (Shemesh et al., 2017)). Since then, fusion protein optimisation has been performed to increase the density of channel expression in the soma. As a result, the similarly-targeted Punctate CoChR (PunctCoChR) (unpublished) was generated by the Synthetic Neurobiology Group at MIT (Boyden group). Punctate CoChR utilises various myosin-binding domains to restrict the distribution of CoChR to distinct puncta. These investigations utilise these novel, targeted ChR constructs combined with the recently developed Scientifica Laser Applied Stimulation and Uncaging (LASU) system to test the spatial limits of single-photon stimulation.

1.2.4 Technology for Optogenetic Stimulation

Different device configurations, depending on the number and size of the structures to be stimulated, demonstrate varying efficacy in providing experimental insight. Generally, these configurations can be separated by the method of opsin stimulation; the first classification being either single-photon or multi-photon mediated (Figure 9). Single-photon stimulation uses the energy of a single photon to excite each opsin molecule and generate a response. The desired illumination wavelength is frequently focused to the tissue of interest using an imaging objective. However, in *in vivo* applications, a mounted optic fibre may be used (Laxpati et al., 2014). Since each delivered photon contains energy sufficient to excite the expressed modulator, molecules are excited entirely along the plane of delivery. This can be commonly seen in the case of widefield LED stimulation whereby an entire tissue volume is illuminated with the excitation wavelength (Klapoetke et al., 2014). The result is activation of all exposed cells and a lack of targeting in all three spatial dimensions. The spatial resolution may be improved through targeted stimulation in X and Y dimensions using lasers, a restrictive pinhole, or both. Nonetheless, single-photon-mediated, high spatial resolution stimulation is difficult to achieve in the Z-dimension, due to out-of-focus activation along the illumination axis.

Multi-photon opsin stimulation is able to circumvent these limitations considerably. This method of stimulation utilises the energy of multiple photons (typically

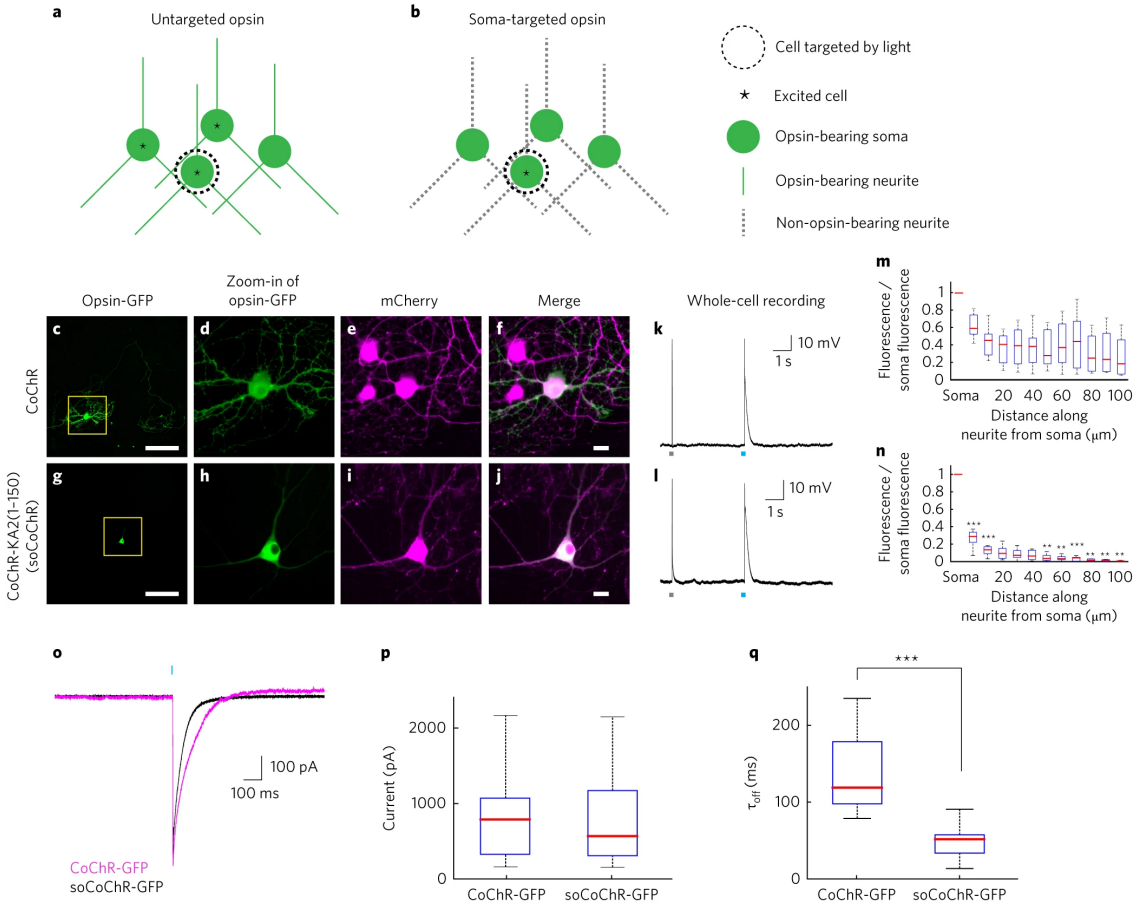

Figure 8: Characterisation of soma-targeted channelrhodopsin. **A)** Schematic of cells expressing an untargeted opsin: stimulation of the light-targeted cell will lead to activation of neighbouring neurons due to stimulation of adjacent neurites. **B)** Schematic of soma-targeted opsin expressing cells: stimulation of targeted cell will result in minimal activation in neighboring cells. **C-J)** Fluorescence images of opsin-expressing hippocampal cultured neurons. Strong mCherry overlap seen only for soma of SoCoChR-expressing cells. **K-L)** Whole-cell recordings of hippocampal cultured neurons after electrical and optical stimulation of untargeted and targeted CoChR. **M-N)** Plots showing GFP fluorescence restricted to the soma in SoCoChR-expressing cells but not for untargeted CoChR. **O)** Representative current traces for both opsins tested in hippocampal cultured neurons using voltage-clamp. **P)** Comparison of evoked photocurrent following opsin stimulation. Soma targeting has a neglible influence on generated photocurrent. **Q)** Off-kinetics for different opsin molecules. Somatic targeting reduces time required for recovery. Adapted from Shemesh et al. (2017)

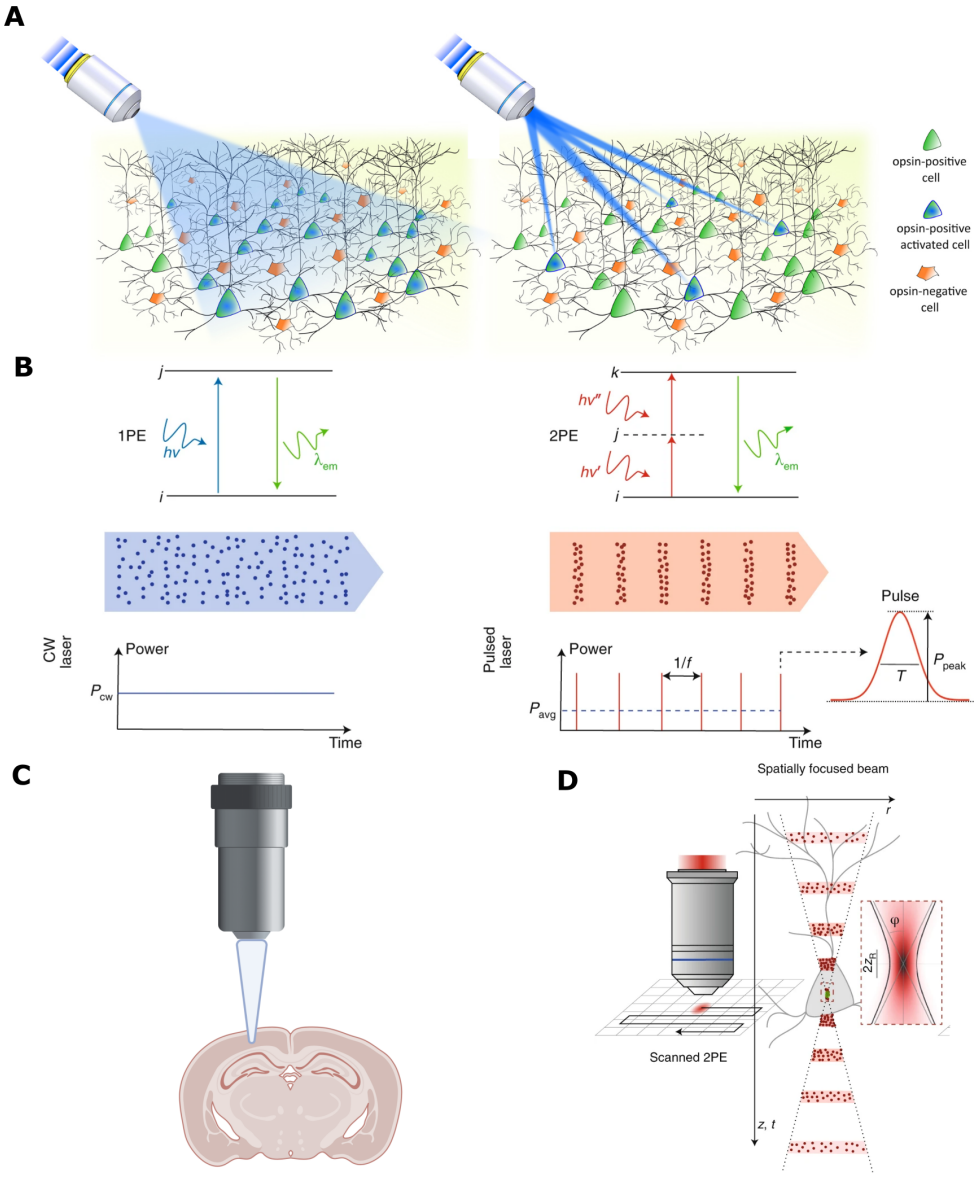

Figure 9: Schematics showing difference between single-photon and multiphoton excitation. **A)** Simultaneous widefield illumination of multiple neurons (Left) and targeted illumination using multiphoton excitation allowing stimulation of specific cells (Right). Adapted from Ronzitti et al. (2017). **B)** Left: Single-photon excitation using continuous illumination. A single photon (hv) contains sufficient energy to excite opsin from 'i' to 'j' state. Right: Two-photon excitation using pulsed illumination. The combined energy of two photons (hv) allows transition to state 'k'. Adapted from Papagiakoumou et al. (2020). **C)** Widefield stimulation resulting in activation of large areas of the cortex simultaneously. Created using Biorender. **D)** Scanning two-photon excitation showing pulsed stimulation leading to high spatial resolution and subcellular specificity. Adapted from Papagiakoumou et al. (2020).

two) to activate a single opsin molecule. Multiple low energy photons are focused at the tissue plane of interest using an imaging objective. Since the energy of multiple photons is required to activate a single opsin molecule, excitation is targeted to the plane of focus and is minimal in the Z-axis above and below the level of interest, whereby singular photon energy is insufficient for activation. Due to the utilisation of lasers to achieve this stimulation, high X and Y spatial resolution is also achieved (Oron et al., 2012).

Nonetheless, two-photon devices suffer from several limitations. Several of these limitations arise due to the small volume of tissue illuminated at any one given time. Since the area of photon energy combination is minute, few opsin molecules are stimulated at any one given time. Thus, two-photon stimulation often struggles to cause sufficient activation to generate the desired response. To address this, mirror galvanometers are used to move the laser position in X and Y to recruit multiple opsin molecules. Mirror galvanometers are mirrors along the illumination path which, when a voltage is applied, adjust their position with fine precision. This facilitates the adjustment of stimulation position, however, results in the frequency of stimulation being limited by the speed of mirror adjustment. Moreover, the lengthy focused illumination on the tissue has been observed to result in increases in tissue temperature, and consequentially, may disrupt physiological processes (Picot et al., 2018). Additionally, since the experimental paradigm requires powerful infrared lasers with the associated guiding components, these configurations are often costly.

Several strategies have been presented to overcome these limitations. One of recent interest is the use of patterned holograph generators. These devices are compatible with either single-photon or multi-photon systems and allow simultaneous light delivery to a specified three-dimensional volume of interest (Shemesh et al., 2017). These devices, although effective, are often custom-built, requiring expert knowledge for operation, and are costly in time and money to construct.

1.2.5 Scientifica LASU System

The LASU system is a single-photon optogenetics and uncaging system, aiming to provide a simple, commercially available method of high-resolution optogenetic stimulation and uncaging (Figure 10). The LASU system is a low-noise, air table-mountable laser, guided into two mirror galvanometers before being beamed into the light path of the microscope. The laser point is focused on the sample by the microscope objective with the mirror galvanometers allowing fine movement of the laser point in X and Y. The result is a user-friendly single-photon system aiming to provide efficient high-resolution, high-frequency controlled stimulation. The soft-

ware, constructed in National Instruments LABVIEW, allows communication with both the mirror galvanometers and laser system. Due to the novelty of the system and the software, considerable steps were performed during this project to optimise functionality and characterise LASU stimulation resolution.

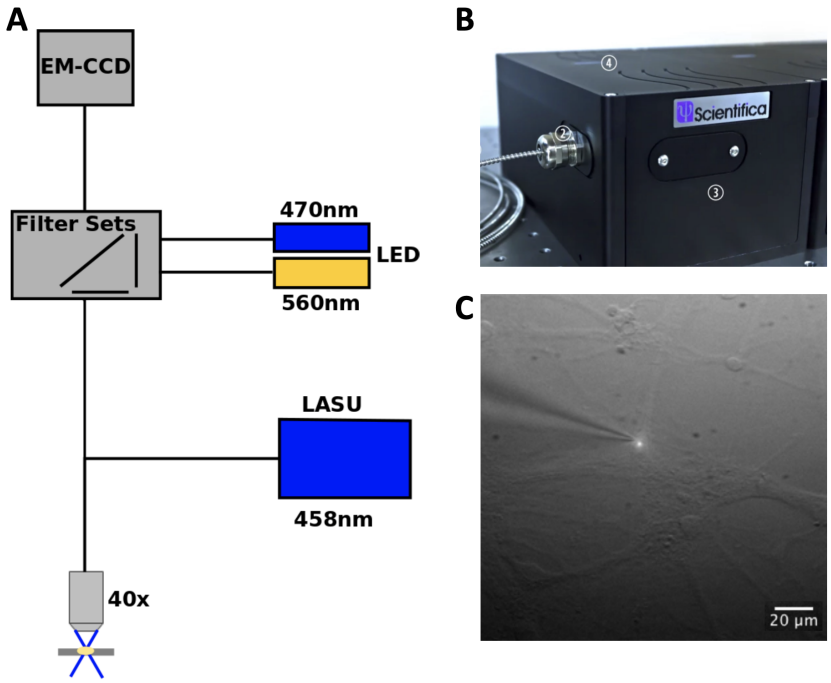

Figure 10: Diagram showing Scientifica Slicescope with LASU system. **A)** Schematic of LASU rig with 458nm LASU laser focused by a 40x objective. A 470nm LED used for GFP visualisation and a 560nm LED to allow concurrent imaging. **B)** Diagram showing table-mounted LASU housing unit. **C)** Image of primary neuronal culture showing size of patch pipette and LASU stimulation point under a 40x objective.

The research presented in this thesis probes the spatial resolution of the LASU system in stimulating cortical neurons expressing somatic (SoCoChR), punctate (PunctCoChR) and non-targeted (CoChR) ChR variants.

1.3 Imaging Tools to Record Neural Activity

The ability to measure neuronal activity in multiple cells with high spatial resolution was revolutionised by the development of imaging for neuroscience (reviewed in Rossi et al. (2018)). Similarly to optogenetic modulators, a photoreceptive peptide is expressed in targeted cells, and upon illumination, photons of a specific wavelength are emitted, with a quantity proportional to a particular ionic or molecular concentration.

1.3.1 Genetically-Encoded Fluorescent Reporters

Genetically-encoded fluorescent indicators of activity typically consist of a circularly permuted fluorophore that contains a binding site for a physiologically-relevant molecule. When the concentration of a molecule of interest increases, a larger proportion of indicator binding sites are occupied, resulting in a conformational change to fluorophore structure and an increase in fluorescence (M. Z. Lin & Schnitzer, 2016).

As for optogenetic modulators, genetically encoding a fluorescent reporter allows targeted expression in specific cell types of interest. Conjugation of the fluorescent reporter nucleotide sequence to an endogenous promoter allows selective recording from defined cell types. This method has been demonstrated effective in probing activity in multiple different neuronal subtypes, such as pyramidal (Asrican & Song, 2021), somatostatin (Adler et al., 2019), cholecystokinin (Asrican & Song, 2021), parvalbumin (Deng et al., 2019); and glial subtypes, such as astrocytes (Asrican & Song, 2021) and microglia (Umpierre et al., 2020). A large proportion of these studies utilise viral transduction to achieve selective expression through combination with transgenic Cre-expressing animals.

Gene-mediated expression of fluorescent reporters can probe activity in either single or multiple cells at a population level. These indicators include voltage-sensitive dyes (Abdelfattah et al., 2019a), K^+ reporters (J. Liu et al., 2020) and, the most established of these, Ca^{2+} indicators (Dana et al., 2014). During the rising phase of the action potential, membrane depolarisation results in the opening of voltage-gated Ca^{2+} channels. As a result, membrane depolarisation, and therefore neuronal activation, are tightly coupled with intracellular Ca^{2+} concentration. Ca^{2+} indicators (such as GCaMP and RCaMP) bind to Ca^{2+} with a given affinity and the attached circularly permuted fluorophore adjusts conformation upon Ca^{2+} binding. Consequentially, as a neuron becomes depolarised and intracellular Ca^{2+} concentration increases, a localised increase in fluorescence can observed (Akerboom et al., 2013).

Several studies have demonstrated the efficacy of genetically-encoded Ca^{2+} reporters in revealing communication in the nervous system. These studies allow insight to be gained from the scale of individual dendritic spines, using two-photon imaging (Jia et al., 2011); to entire cortical regions, using widefield imaging (Rossi et al., 2017).

Each of these methods have their own limitations, usually determined by both the nature of the biological process generating the signal, and the inherent properties of light itself. In the case of recording from small structures, such as individual den-

dritic spines, acquisition of an accurate signal is limited by the quantity of photons generated by a single event. Therefore, in these circumstances, a Ca^{2+} indicator with high sensitivity is required to readout these events. On the contrary, in the case of widefield imaging, due to light scattering and diffraction, a single imaging pixel will acquire composite information on a large population of neurons. In this case, the generated signal is large, however, the recording modality accompanies different limitations to those seen for two-photon dendritic imaging. One of these issues is that the signal may be excessively large and may lead to saturation of the recording device detector. Therefore, it is important to have an indicator with adequate sensitivity and fast kinetics. Additionally, the limitations of a particular indicator will be determined by the nature of the signal being recorded. For example, in the case of high frequency, large amplitude epileptiform activity, the signal is prone to saturation; and if indicator kinetics are slow, important information regarding activity dynamics will not be acquired. As a result, for each experimental paradigm, it is essential to select a fluorescent indicator that maximises the information obtained from each recording session.

1.3.2 Advancements in Genetically-Encoded Imaging Tools

Since the first generation of the genetically-encoded GCaMP family of Ca^{2+} indicators, several modifications have been made to the peptide sequence; each undergoing optimisation for different purposes. The latest generation of these optimisations have resulted in multiple variations of the construct jGCaMP7 (jGCaMP7s, jGCaMP7b, jGCaMP7c and jGCaMP7f; Figure 11). Each of these constructs were designed with a specific purpose in mind. jGCaMP7s exhibiting high sensitivity and slow kinetics, is suitable for imaging low amplitude signals. jGCaMP7b has a brighter baseline and a high response to single action potentials, making it useful for localising dendritic spines for two-photon imaging and for recording low amplitude events. jGCaMP7c was optimised for low baseline fluorescence and high contrast imaging. Lastly, jGCaMP7f was optimised for fast imaging with a large dynamic range (Dana et al., 2019). Due to investigations here focusing on high frequency, large amplitude epileptiform activity, jGCaMP7f was selected.

Similar in structure to genetically-encoded Ca^{2+} indicators, fluorescent neurotransmitter reporters have become increasingly available in recent years. Powerful insight into neuronal communication has been provided through the growing use of fluorescent glutamate reporters. These molecules, such as iGluSNfR, similarly consist of circularly-permuted GFP. However, activation of iGluSNfR-mediated fluorescence is triggered through binding to the major excitatory neurotransmitter

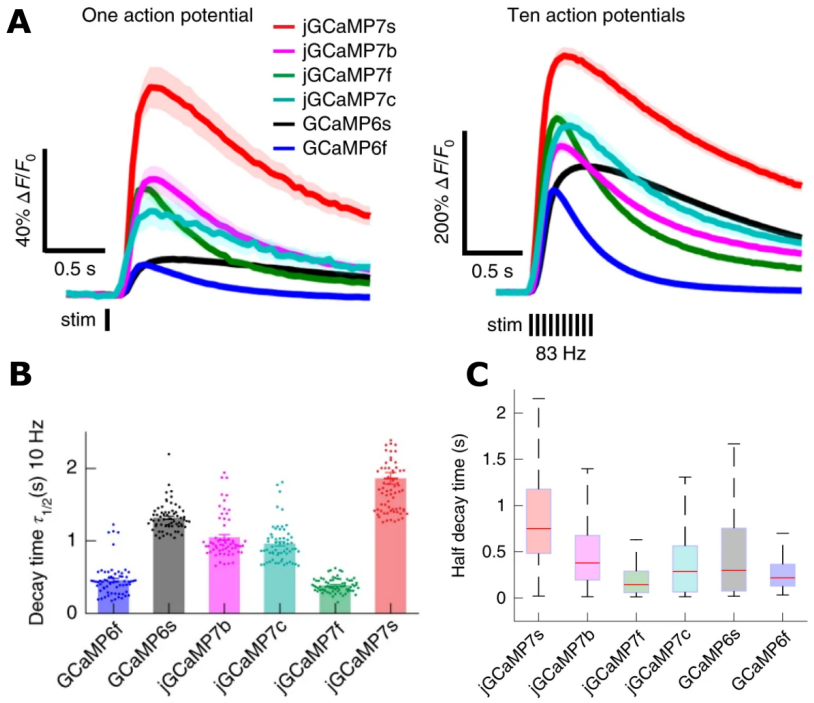

Figure 11: Comparison of recently developed genetically-encoded Ca^{2+} indicators showing fast kinetics of newly developed GCaMP7f. **A)** Comparison of the fluorescence response of dissociated neurons expressing different jGCaMP7 constructs. Data shown after single action potential induction (Left) and stimulation with a train of 10 action potentials at 83Hz (Right). jGCaMP7 displays greater responses to stimulation compared with GCaMP6 constructs. **B)** Fluorescence half decay time of responses from Drosophila neuromuscular junction boutons, showing low decay time of jGCaMP7f. **C)** Fluorescence half decay time of responses from the mouse primary visual cortex following grated light stimulation. Adapted from Dana et al. (2019).

glutamate. Consequentially, fluorescence imaging of expressing cells is able to provide insight into synaptic communication, as well as how this communication is altered in disease states (Marvin et al., 2013). Previous studies demonstrating the efficacy of both fluorescent Ca^{2+} and glutamate reporters in probing pathological events will be discussed in the section titled 'Spreading Depolarisation'.

1.3.3 Technology for Fluorescent Imaging Recordings

Depending on the number and size of the structures to be recorded from, different configurations are able to probe communication to varying degrees. Similarly to optogenetic stimulation, these configurations can be separated by the method of fluorophore activation; either single-photon, or multi-photon mediated (Figure 12). As for optogenetic stimulation, single-photon and multi-photon stimulation can

be distinguished by the number of photon energies required to activate a single photoreceptive molecule.

Single-photon imaging of genetically-encoded fluorescent indicators suffers from similar limitations to that seen for optogenetics. Predominantly, these limitations surround the detection of out-of-focus fluorescence above and below the focal plane of interest. Consequentially, localisation of detected fluorescence is difficult to attribute to a particular source of interest, especially in three-dimensional tissues such as *ex vivo* acute slices and *in vivo* brain tissue. Nonetheless, the ability to simultaneously image large regions of interest is not achievable with multi-photon imaging. Throughout these investigations, I use single-photon illumination to investigate population dynamics in large regions of the cortex; with a focus on paroxysmal events.

1.3.4 Limitations of Widefield Calcium Imaging and Associated Non-linearity

The use of Ca^{2+} fluorescence dynamics as a proxy for neuronal activity suffers from several limitations. These arise due to multiple factors; such as the physical arrangement of neurons, the inherent properties of light, and the properties of the genetically-encoded Ca^{2+} indicator.

The cortical arrangement of neurons typically results in a high density of dendrites in superficial layers. These dendrites are contacted by synapses from both local and distal neuronal populations. The cell soma are typically present in deeper layers below this arrangement of dendrites. Therefore, when imaging a given volume from a dorsal perspective, recorded fluorescence will likely be dominated by activity in the large cloud of dendrites present in superficial cortical layers. Somatic signals will still be present in these recordings, however, the recorded fluorescence will be dominated by activity in neural processes which may be dispersed over large distances. Consequentially, when recording Ca^{2+} fluorescence using widefield imaging, it may be difficult to attribute fluorescence signals to a particular brain region/population.

Another limitation of widefield imaging of Ca^{2+} fluorescence signals surrounds the properties of light. Since photons travel a considerable distance before reaching the camera pixel, localisation of fluorescence is difficult to achieve. Firstly, as a photon travels a distance to reach the camera photo-detector, the photon will undergo diffraction. Secondly, each recorded photon will undergo scattering, whereby the photon will interact with neighbouring tissue resulting in a change in direction.

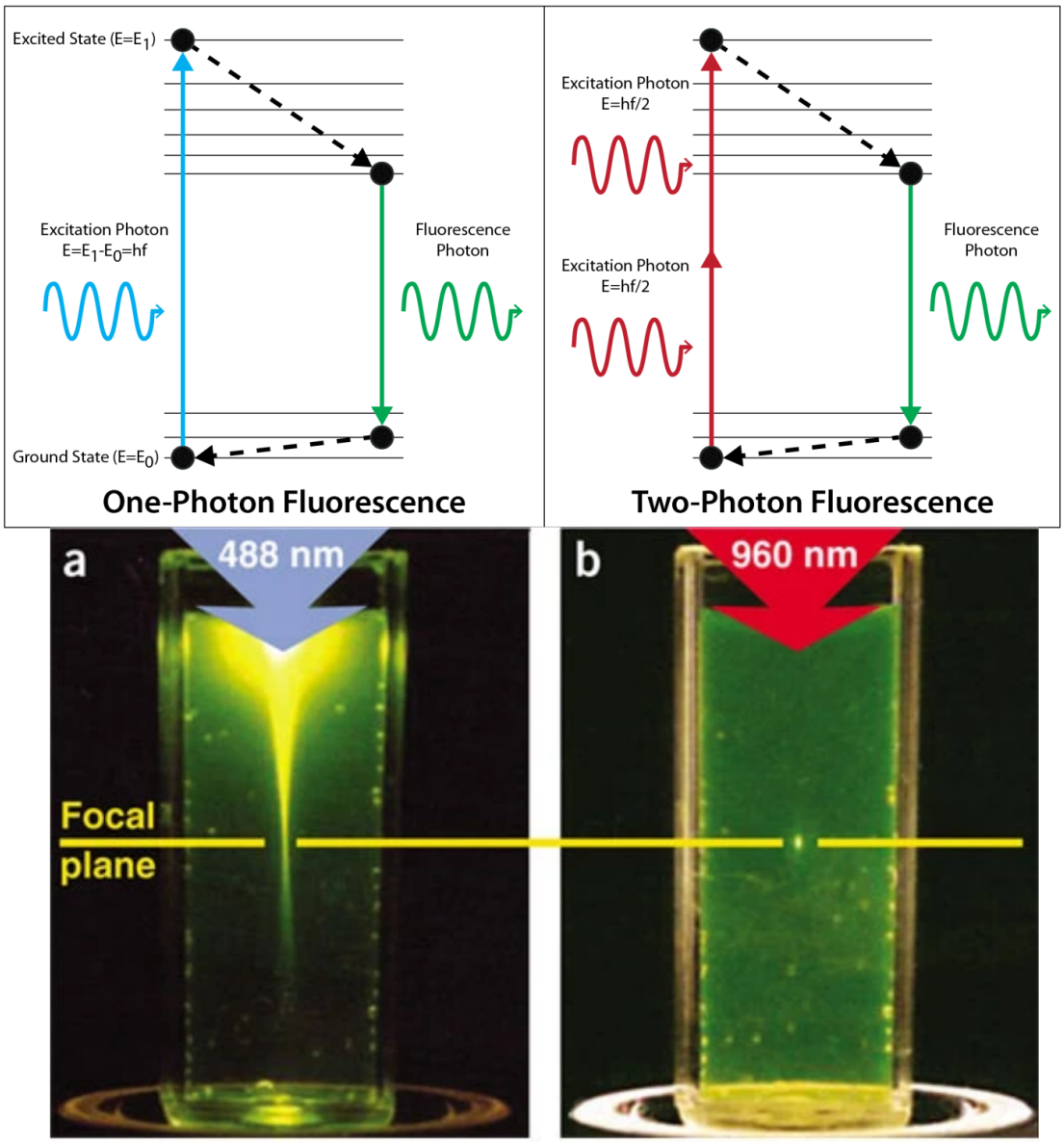

Figure 12: Comparison of single-photon and two-photon illumination for functional imaging. Two photon illumination results in selective excitation at the focal plane due to combination of pulsed photon energies. Adapted from https://i.stack.imgur.com/uLMeH.png and Zipfel et al. (2003).

Therefore, this can result in each camera pixel acquiring photons from a mixture of brain regions in different proportions; thus, reducing the spatial specificity of the acquired fluorescence signal.

A major limitation of Ca^{2+} fluorescence imaging surrounds the properties of genetically-encoded indicators. Each GCaMP molecule will bind and unbind Ca^{2+} with a given affinity and kinetics. This process has several limitations. Firstly, since GCaMP is constructed to be analogous to endogenous Ca^{2+} buffers, the indicator may alter Ca^{2+} dynamics through altered Ca^{2+} buffering. Secondly, GCaMP molecules are present in a finite quantity in a given cellular compartment, and are able to bind and unbind at a defined rate. Therefore, if there is a large, sudden increase in Ca^{2+} concentration, the response within a single cellular compartment may become saturated; thus preventing any further increase in Ca^{2+} fluorescence following further activity. This limitation is especially relevant in the cases of seizures and SD demonstrated in this thesis. These non-linearities between neuronal activity and Ca^{2+} fluorescence may lead to difficulties in attributing observed fluorescence to a given populations of neurons when performing mesoscale imaging, wherein single-cell dynamics can not be directly observed.

Nonetheless, irrespective of these limitations, widefield calcium imaging remains a powerful method to spatially dissect the complex interactions between paroxysmal events in the rodent cortex.

1.4 Paroxysmal Disorders

The defining feature of all paroxysmal disorders (PDs) is the sudden unexpected development of usually recurrent symptoms. Neurological manifestations of these disorders have been characterised in human patients and include epilepsy, migraine (Cianchetti et al., 2017), dyskinesias (Meneret et al., 2013) and episodic ataxia (Choi & Choi, 2016). Due to the unpredictable nature of PDs, system-level investigations of activity preceding, during and following pathological events are essential. Moreover, understanding the underlying network alterations resulting in the increased propensity for these events to occur is of importance in understanding the transition to and from paroxysmal states. Insight into these states can allow characterisation of shared alterations between multiple PDs, leading to an increased understanding of disease mechanisms and multiple potential therapeutic avenues.

1.4.1 Epilepsy

Epilepsy is a highly debilitating disorder, present in approximately 4% of the population and characterised by the recurrence of paroxysmal seizures (England et al., 2012). These seizures can vary according to classification (focal, generalised, tonic-clonic, absence etc.), however, all share the electrophysiological hallmark of abnormally synchronous neuronal discharges. Moreover, seizure presentation varies largely from patient-to-patient: many cases are genetically-linked and become apparent during early childhood years; in other cases, traumatic events are able to chronically alter the physiological environment to permanently increase seizure susceptibility. These traumatic events include stroke, infection, prolonged oxygen deprivation and others (Stafstrom & Carmant, 2015).

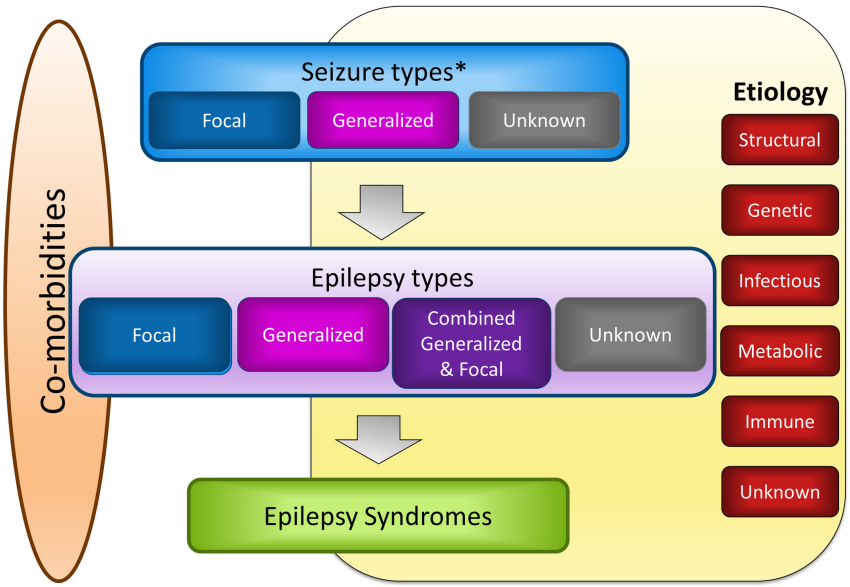

Figure 13: Structure of classification procedure for epilepsies, showing types and causes. Upon development of seizures, seizure type is classified into focal (unilateral and spatially restricted), generalised (bilateral and affecting subcortical networks) or those unknown due to recording difficulties. Information about the type of seizure allows classification of epilepsy type based on similar criteria. Many of these types of epilepsy have shared co-morbidities (e.g. migraine) and arise as a result of one of six etiologies (Scheffer et al., 2017).

Several patient cases and studies have provided insight into the aetiology of epileptic disorders. Some arise sporadically, whilst others have a clear genetic or environmental origin. Cases of head trauma patients have revealed a link between structural damage and epileptic seizures (Ding et al., 2016). The proposed mechanisms leading to the transition from a healthy to epileptic network involve inflammatory pathways and alterations in tissue excitability (Bugay et al., 2020).

Furthermore, genetic cases also provide insight. These often lead to imbalances in the fine control of network excitation and inhibition, eventually leading to periods of unregulated electrical discharges (Ketzef & Gitler, 2014). Sporadic cases are rare and are often attributed to category of unknown origin (Scheffer et al., 2017).

Seizures can manifest behaviourally in patients in multiple ways. The phenotypic signs of a seizure are heavily dependent on the type of seizure and therefore, different seizures demonstrate considerable variability in their presentation. Several types of seizure-associated behaviour have been observed and this has led to the classification of epileptiform activity into several groups. Depending on the presentation of the different types of seizures, the time of presentation, and the hypothesised cause, patients are diagnosed with one or more of different types of epileptic disorders, where these seizures persist over time (Scheffer et al., 2017). Here I will discuss the physical manifestations of different types of seizures that lead to this classification.

Myoclonic seizures are associated with large, involuntary, sudden jerking movements. These are frequently seen following periods of sleep and, although each myoclonic jerk lasts a short time period (approximately 1 second), they are often seen to repeatedly occur in bouts. These events can occur in healthy individuals during periods surrounding sleep, however, the frequency in which they present in epileptic patients is far greater. These seizures often predominate in the upper limbs and can vary in amplitude (Genton & Gelisse, 2013; Kiziltan et al., 2020). Myoclonic seizures vary in their presentation and depending on the specific case, will either affect patients unilaterally or bilaterally. Similarly to other seizure types, these events can be precipitated by tiredness, stress, fevers, alcohol and photic stimulation (Stafstrom & Carmant, 2015).

Tonic-clonic seizures, or as previously known, Grand Mal seizures are another major presentation of epileptic symptoms. These seizures are associated with both a tonic phase, where muscle rigidity is observed, and a clonic phase, characterised by involuntary muscle twitching. These seizures last approximately one to three minutes and can lead to loss of consciousness depending on the scale of brain networks affected. Additionally, tonic-clonic seizures are often associated with other manifestations including involuntary vocal outbursts, loss of involuntary muscle control, headaches and tiredness following regaining of consciousness. Tonic-clonic seizures will manifest differently depending on the affected brain regions (Stafstrom & Carmant, 2015), which will be further discussed in the next section with regards to electrophysiological signatures of epileptiform activity.

Absence seizures, or petit mal seizures, are a type of seizure strongly associated with loss of awareness or consciousness. During these events, a patient will become

unresponsive and lose awareness for a period lasting seconds to minutes. Due to the loss of consciousness, these seizures are often unnoticed by the patients themselves. Absence seizures are commonly seen in children during adolescent periods, with over 57% of these individuals no longer having seizures at later ages. Additionally, these patients appear to suffer no lasting consequences of these events (Albuja & Khan, 2021).

Atonic, or akinetic, seizures are associated with a sudden loss in muscle strength or tone. This loss of muscle tone can be seen across a widespread area, often affecting both the face and body. These seizures last approximately 15 seconds and are likely to cause secondary injuries due the muscle atonia leading to falls (Baraldi et al., 2015).

Additionally, seizures may be classified as either focal, generalised or unknown (Scheffer et al., 2017). Focal seizures usually manifest in neural circuits unilaterally, commonly affecting the limbic system or neocortex, while generalised seizures are seen to affect the brain bilaterally, having profound effects on whole-brain activity and thalamocortical networks. Focal and generalised seizures can be further subdivided into those with motor and non-motor manifestations. Focal onset seizures either present with retained or impaired awareness, whereas generalised seizures typically accompany an impairment to consciousness (Thijs et al., 2019). Myoclonic (Genton & Gelisse, 2013), atonic (Aihara et al., 1997) and absence seizures (Avoli, 2012a) are often seen to manifest bilaterally in epileptic patients, whereas tonic-clonic seizures often have a focal onset preceding a secondary generalisation (Xu et al., 2021; Stafstrom & Carmant, 2015). Classification of epilepsies into the categories of either focal or generalised onset is frequently guided by the electrophysiological techniques described in the previous sections.

1.4.2 Electrophysiological Signatures of Epileptic Activity

Characterisation of epileptic activity is frequently assisted by electrophysiology. EEG is frequently performed due to the non-invasive nature of scalp electrodes. Precise placement of multiple EEG electrodes enables acquisition from multiple areas of the brain; creating a powerful tool for non-invasively mapping pathological brain regions (Reif et al., 2016b). Moreover, generation of EEG montages through subtraction of neighbouring electrode signals creates a powerful tool for signal source localisation; an important task in the characterisation of seizure focus and epileptic phenotypes (Acharya & Acharya, 2019). Nonetheless, a large limitation of EEG recordings comes from the location of the recording sites: since the electrodes are located on the scalp, signals are dispersed through bone leading to difficulties in

precise signal localisation (Chauveau et al., 2004b). Additionally, the recorded signal is dominated by radial dipoles formed in superficial cortical neurons (Buzsaki et al., 2012b). Consequentially, insight into subcortical activity is often difficult to achieve. As a result, ECoG techniques are often employed to generate further insight.

ECoG recordings, although invasive, provide powerful insight into pathological activity. Greater contact with tissue, without a recording medium of bone, results in an improved signal-to-noise ratio. Studies use ECoG techniques to gain greater insight into cortical activity, while others use these techniques to record from deeper structures and gain insight into afflicted subcortical regions. Since the recording sites can be placed in direct contact with brain tissue, ECoG enables recordings of high frequency (>500Hz), local neuronal firing; thus increasing the insight gained into epileptic phenotypes even further. Additionally, ECoG techniques are essential for effective surgical resectioning of epileptic tissue: ECoG is often utilised to determine precise regions of epileptic zones to be targeted for removal, while also mapping regions of 'eloquent cortex' to minimise the risk of undesired post-surgical complications (Reif et al., 2016a). The combination of both EEG and ECoG techniques in human patients has revealed insight into the pathological electrical changes associated with the different types of epileptic activity.

Myoclonic seizures can typically be easily identified by physical manifestations, however, several electrophysiological investigations have probed the electrical correlate of these events. Alongside direct electrical recordings from activated muscle groups, jerk-time-locked averaging of EEG activity has shown large, mostly bilateral, synchronous discharges (Genton & Gelisse, 2013; Kiziltan et al., 2020).

Electrophysiological investigation of tonic-clonic seizures has revealed common elements in multiple diverse electrical events. Typically, tonic-clonic seizures originate at a focus and propagate through brain tissue at varying speeds, often <1mm/sec (Liou et al., 2018; Proix et al., 2018), preferentially spreading to functionally connected regions (Rossi et al., 2017). In some cases, these seizures can spread to subcortical regions and become generalised. In these cases of generalisation, the seizure is interacting with multiple brain regions bilaterally, and this is often associated with changes in patient awareness (Falco-Walter et al., 2018). The physical manifestation of a tonic-clonic seizure will vary depending on affected brain regions. Focal tonic-clonic seizures will often produce symptoms associated with the region currently displaying pathological activity, e.g. visual disturbances from visual cortices, motor disturbance from precentral gyri and sensory disturbances from post-central gyri (Stafstrom & Carmant, 2015). These disturbances

may present together and may precede the presentation of other phenotypes that occur following spreading of the seizure to widespread bilateral networks during secondary generalisation. Tonic-clonic seizures may also have a generalised onset, where the seizure affects bilateral circuits from the onset (Falco-Walter et al., 2018). Generally, tonic-clonic seizures can be divided into four phases; prodromal, aura, ictal and post-ictal (Kodankandath et al., 2021). These classifications may also be extended to the other types of seizure but are often considered more applicable to tonic-clonic seizures. For example, myoclonic seizures are brief and generally do not have a post-ictal phase; whereas, this phase can be profound following tonic-clonic seizures (Pottkamper et al., 2020). The prodromal phase can occur hours-to-days before the presentation of a seizure and is associated with mood disturbances and tremors. Following the prodromal phase, in some cases, is the aura, whereby patients experience sensory disturbances shortly before a seizure. The two previously mentioned stages can act as a predictive warning to patients that the ictal phase will soon follow. The ictal phase is associated with the seizure itself where abnormal synchronous discharges are seen to dominate the electrophysiological trace. As mentioned previously, the physical manifestation of this phase will vary depending on affected brain regions. Lastly, the ictal phase can be followed by a post-ictal phase, where for a period varying in length, patients may experience symptoms such as tiredness, confusion, nausea and headaches (Pakozdy et al., 2014). Since tonic-clonic seizures are of a major focus in this thesis, seizure initiation, propagation and termination will be discussed in detail in the following section.

Absence seizures have a characteristic electrical signature. Typically, these seizures are thought to be associated with 3Hz spike-and-wave discharges occurring in cortico-thalamocortical networks (S. J. Smith, 2005). The circuitry thought to be associated with these events includes deep cortical glutamatergic transmission (D'Antuono et al., 2006), thalamic relay neurons and neurons of the thalamic reticular nucleus (Avoli, 2012b). These circuits are associated with wakefulness and arousal, and pathological discharges in these circuits are central to the proposed mechanisms underlying impaired consciousness. Epidemiological evidence suggests a particular susceptibility of these networks during developmental periods. Absence seizures are more common preceding adulthood, and in around 75% of cases resolve with no known long-term consequences (Stafstrom & Carmant, 2015).

Atonic seizures, although often characterised by a clear phenotype, can also be probed using EEG techniques. EEG investigations have revealed a wide range of abnormal electrical events that vary considerably from patient-to-patient. Commonly seen are generalised spikes and paroxysmal fast activity associated with 10Hz bursts

of rhythmic discharges (Baraldi et al., 2015).

The previously mentioned types of seizure can vary in severity between and within patients. Some events can be relatively short and mild, while others long and greater in intensity. For each mentioned type of seizure, if the duration exceeds five minutes, or multiple seizures occur in a five minute period without resumption of normal consciousness, the time period is classified as status epilepticus. Status epilepticus is a problematic condition where processes leading to seizure termination fail, leaving patients susceptible to long-term nervous system damage or sudden unexpected death in epilepsy (SUDEP). Rapid pharmacological treatment of these events are essential for ensuring a positive long-term outcome for patients (Sharma et al., 2018).

The recorded electrical potentials in the brain during the aforementioned seizure types vary considerably from patient-to-patient. From EEG studies, several different pathological waveform signatures corresponding with different events have been identified. Based on their properties, these waveforms are generally classified into one of several groups.

Spikes are single large amplitude discharges caused by the synchronous firing of a large population of neurons. Spikes can occur as singular events in isolation or be associated with other events, such as other spikes. These short trains of spikes are known as polyspikes or complex spikes, characterised by multiple spikes occurring together (Silfverhuth et al., 2011). Additionally, other events are seen where each spike is followed by a slower wave, considered to be a result of gamma-Aminobutyric acid $(GABA)_B$-mediated currents. These events are known as spike-and-wave discharges and are strongly associated with absence seizures, as well as other seizure types (Destexhe, 1998). Another electrical event known as sharp waves, are also commonly observed in EEG recordings from epileptic patients, and these differ from spikes in their duration. While spikes have a duration of approximately 70ms, sharp waves range from 70 to 200ms in duration. Although several studies have pooled these two phenomena, others have hypothesised that understanding the distinct mechanisms leading to the two events may improve our understanding of therapeutic limitations (Jaseja & Jaseja, 2012). These discussed epileptiform waves are capable of permanently altering neuronal excitability and plasticity in neuronal circuits (C. Yang et al., 2020; Choy et al., 2021); further increasing the complexity of the pathophysiology of epilepsy.

Generally, the aforementioned waveforms are observed in varying combinations in epileptic patients, often during seizure-free periods. EEG studies are often able to diagnose patients through the presence of these pathological waveforms in routine

tests. The occurrence of these discharges during periods without seizures has led to their classification as interictal discharges. The role of these interictal discharges has been a topic of considerable investigation and speculation. Several recordings have revealed an increase in frequency prior to ictal events, while others have revealed a converse decrease in frequency (Karoly et al., 2016). This has resulted in ambiguity as to the role interictal spikes play in seizure initiation. Nonetheless, the prevailing presence of these events in epileptic tissue, and absence in healthy tissue, demonstrates a strong association with epileptic networks. Moreover, the long-term changes induced by the presence of interictal spikes is of importance (Staley et al., 2011), especially when predicting surgical outcomes following resectioning (Krendl et al., 2008). In rare cases, spontaneous seizures are coincidentally captured during routine EEG studies. In other cases, usually more severe, seizures can be induced through photic stimulation during EEG or ECoG recordings to allow mapping of the epileptic focus, often to aid mapping for surgical resectioning (Curatolo et al., 2000; S. J. Smith, 2005). Recordings of activity from epileptic patients have shown a mixture of these waveforms usually occurring with large amplitudes and at a high frequency (Emmady & Anilkumar, 2021).

Altogether, different seizure types exist, leading to multiple epilepsy classifications. Moreover, a single patient may present a complex mixture of pathological waveforms that occur both ictally and interictally (Figure 14). Further understanding the network alterations that lead to the increased propensity for these discharges to occur is essential in generated new therapeutic targets.

1.4.3 Seizure Initiation

Several structural and functional changes associated with neuronal and glial populations can lead to a seizure-prone state. As mentioned previously, these include genetic alterations and traumatic events; such as stroke, infection, physical damage and oxygen deprivation (Scheffer et al., 2017). Nonetheless, seizures are paroxysmal events with the aforementioned changes simply resulting in a state of increased seizure probability. The transition from controlled physiological brain function into a pathological state is an elusive topic of interest. Patient studies have revealed several triggers that lead to an increased probability of seizure initiation. These triggers include sleep deprivation, illness, photic stimulation, drug use, natural hormonal fluctuations, hypoglycaemia and caffeine (Schachter, 2009; Imad et al., 2015; Jailani et al., 2020). Although these triggers have assisted in generating patient guidelines to reduce the likelihood of seizures occurring, large knowledge gaps continue to surround the cellular processes leading to seizure initiation.

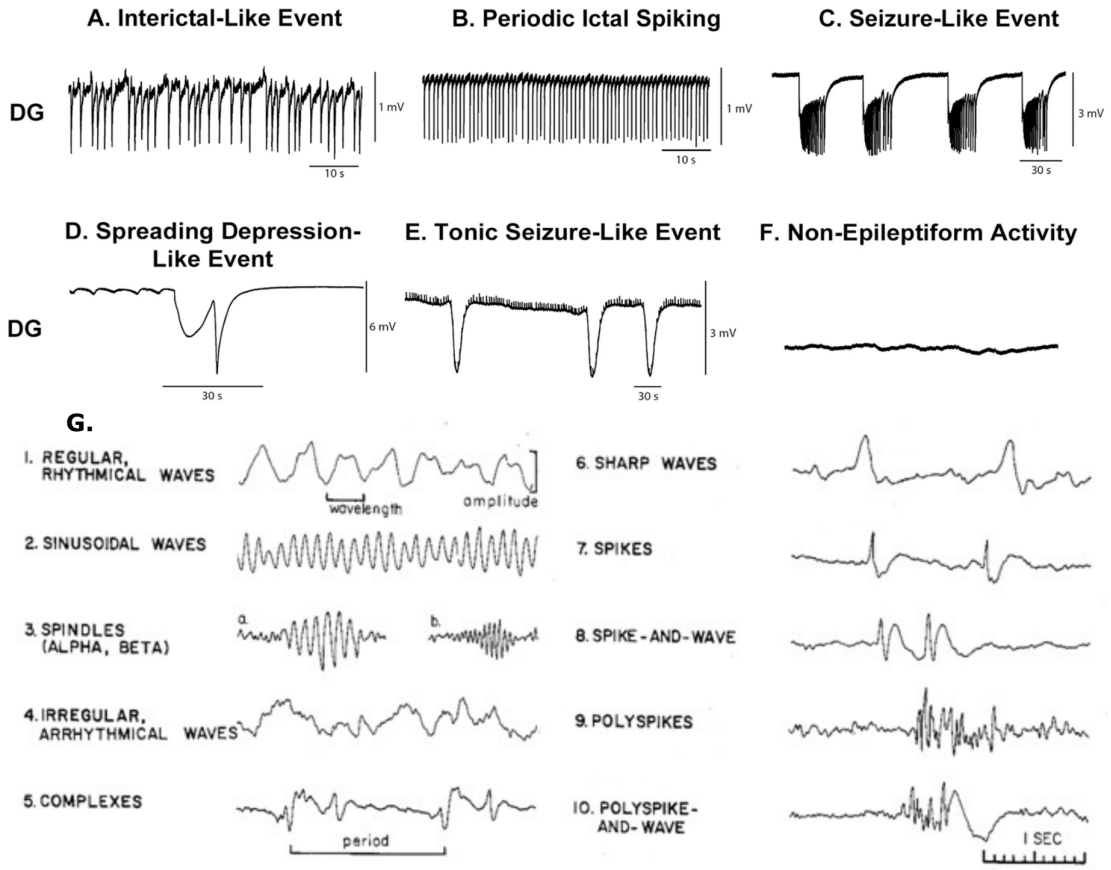

Figure 14: Diverse epileptic waveforms found in human tissue. **A-F)** Different signatures of healthy and epileptiform activity recorded with extracellular electrodes inserted into the dentate gyrus of resected human hippocampus. Adapted from Reyes-Garcia et al. (2018). **G)** Different signatures of healthy and epileptiform activity recorded using scalp EEG in human patients. Adapted from https://slideplayer.com/slide/4642577/.

Several studies have probed the mechanisms leading to seizure initiation. Here I will discuss these mechanisms with particular relevance to tonic-clonic seizures. Evidence from both patient studies (Shen et al., 2021) and animal models (Choy et al., 2021) suggest network changes beyond the location of the initial insult leading to a chronic state of susceptibility. A particularly clear example of this can be seen in animal models following acute status epilepticus induction. Following recovery from status epilepticus, chronic spontaneous seizures can be observed, commonly originating from networks associated with the temporal lobe (Nissinen et al., 2000; Bumanglag & Sloviter, 2008). These studies demonstrate the greater susceptibility of specific networks to drive epileptic activity. Moreover, these studies illustrate that these networks can be distinct from the location of the initial insult.

EEG recordings from human patients have revealed mild suppression of back-

ground neural activity immediately before the seizure onset (de Curtis & Avoli, 2015). Coinciding with this is the appearance of low-voltage fast activity in the 20-100Hz (β to γ) range (Gnatkovsky et al., 2011). Similarly observed at seizure onset, are hypersynchronous large amplitude spikes (Ogren et al., 2009). These two events are often focal to epileptic networks and serve as a powerful measure of afflicted brain regions (Figure 15). Often these periods of activity have been observed together and their presence during these seizure onset periods has been confirmed in animal models (de Curtis & Avoli, 2015).

Further investigation of both low-voltage fast activity and large hypersynchronous spikes in animal models have revealed information regarding their cellular contributors. Recordings of high-frequency oscillations from pilocarpine-treated epileptic rats have revealed ripples (80-200Hz) associated with the low-voltage fast activity, and fast ripples (250-500Hz) associated with hypersynchronous large amplitude activity. Previous investigations have probed the origin of these high-frequency oscillations, and evidence suggests that ripples are generated by activity in inhibitory neurons, while fast ripples are generated by synchronous pyramidal cell firing (de Curtis & Avoli, 2015). These relationships have been observed both *in vivo* (Levesque et al., 2012) and in slice models (Fujiwara-Tsukamoto et al., 2010).

The dominant presence of inhibitory activity and its electrographic signature, low-voltage fast activity, during seizure onset has been hypothesised as a mechanism to prevent seizure initiation through feedforward inhibition. When this inhibitory restraint fails, synchronous pyramidal cell activity increases considerably and gives rise to the hypersynchronous phase that is seen to follow (Trevelyan et al., 2006; Magloire, Mercier, et al., 2019). These phenomena have been observed in brain slice investigations whereby initial activity is dominantly GABAergic and shortly after, depolarisation block of interneurones is observed at the time of seizure onset (Cammarota et al., 2013). However, this depolarisation block has not been observed in *in vivo* models of epilepsy (de Curtis & Avoli, 2015); possibly due to differences in tissue perfusion through an intact vascular system.

Profound inhibitory neuron activation has been consistently observed at seizure onset in multiple models of epilepsy. However, it remains unclear as to whether these interneurons are active during these periods in an attempt to counteract seizure initiation or whether they play a fundamental role in seizure initiation itself (de Curtis & Avoli, 2015). Nonetheless, in silico modeling of interneuron dynamics has revealed bistability that make these neurons particular susceptible to transitioning into a synchronous firing state following perturbation, or even background excitatory synaptic activity (Rich et al., 2019). Altogether, the evidence from studies in

different models has revealed a key role for inhibitory interneurons and a disruption to the excitation-inhibition balance in the time-period immediately preceding a seizure.

Further evidence for the complex role of inhibitory interneurons has been demonstrated by several studies. Firstly, disruption of GABAergic activity through receptor antagonism is a commonly used method of seizure induction (Rossi et al., 2017; Soares-Silva et al., 2021); suggesting a strong role for inhibition in seizure suppression. Recent work has demonstrated that the role of inhibitory populations in seizure initiation is dependent on both the location of inhibitory input onto pyramidal cells, as well as the timing of input arrival. Support for this notion can be seen through seizure-time-locked *in vivo* optogenetic stimulation of different interneuron populations using real-time field-programmable gate array (FPGA)-mediated processing. Stimulation of perisomatic parvalbumin-positive interneurons at seizure onset demonstrated anti-ictal properties. However, stimulation with a delay from onset revealed pro-epileptic effects. Overexpression of the K^+/Cl^- cotransporter KCC2 prevented the aforementioned change to a pro-epileptic effect; demonstrating a dependence on loss of pyramidal cell Cl^- electrochemical drive in mediating this pro-epileptic effect. Moreover, these findings could not be replicated with dendrite-targeting somatostatin interneurons. Altogether, this evidence suggests a complex role for inhibitory populations, placing dysfunction in these cells at the precipice marking the transition between physiological function and pathological activity (Magloire, Cornford, et al., 2019b).

Further insight into seizure initiation mechanisms has been gained through the use of fluorescence imaging. Large-scale two-photon imaging of GCaMP fluorescence in the cortex during 4-aminopyridine (4-AP)-induced seizures has revealed complex mechanisms surrounding seizure initiation. Close to the injection site, representative of the seizure focus, investigations have revealed activation of small neuronal ensembles during seizure initiation. This event has been termed a microseizure and is absent from nearby electrophysiological measurements. As time progresses, this ensemble of neurons will grow until breaking into neighbouring cortical regions (Wenzel et al., 2019). In a different study, widefield imaging combined with electrographic field recordings in a picrotoxin seizure model revealed that seizure initation appears identical to the interictal spikes seen to occur between ictal events. Following this initiation, seizures propagate to areas both local and distal from the ictal focus (Rossi et al., 2017).

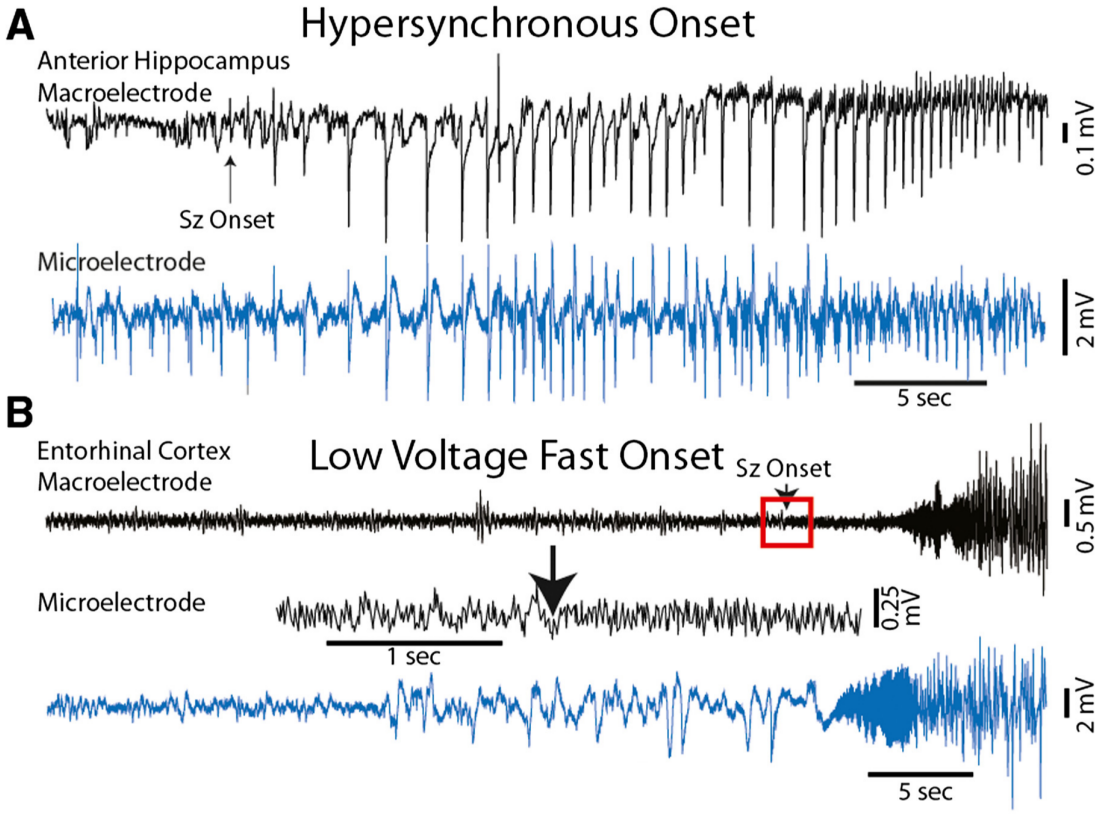

Figure 15: EEG and microelectrode recordings from epileptic patients. **A)** Hypersynchronous firing at onset of seizure shown for macroelectrode and microelectrode recording from hippocampus. **B)** Low-voltage fast onset activity at seizure onset shown for both macroelectrode and microelectrode recording from the entorhinal cortex. Adapted from Weiss et al. (2016).

1.4.4 Seizure Propagation

Once a seizure has been initiated, propagation to other areas has been hypothesised to result from multiple contributing factors. Evidence for this can be seen from the variability in seizure propagation velocity, with this spanning a large range between 0.1 and 100mm/s (Khateb et al., 2021). Several hypotheses regarding seizure propagation are focused on the failure of an inhibitory surround to the seizure focus: seizures are often thought have a focal onset in an epileptogenic zone, and the seizure remains focal to this region due to surrounding inhibition. If this inhibition fails, the seizure is able to spread and propagate to other brain regions (Liou et al., 2018).

An observed contributing factor to seizure propagation is an alteration in extracellular potassium concentration (Heinemann et al., 1977). Increased extracellular potassium levels have been hypothesised to result from excessive interneuron fir-

ing during the initiation phase (Avoli et al., 1996). This has been hypothesised to result from K^+ efflux during action potentials, as well as intracellular chloride accumulation leading to KCC2 co-transporter overactivity (Viitanen et al., 2010). An increase in extracellular potassium is known to increase the excitability of neuronal populations through multiple mechanisms. One of these mechanisms is the increase of neuronal resting membrane potential through alteration of the equilibrium potential of K^+ (Hodgkin & Huxley, 1952). Another, is the reduction of the Cl^- electrochemical drive, leading to loss of inhibition (de Curtis & Avoli, 2015). As a result, extracellular K^+ concentration plays an important role in seizure propagation and generalisation.

Further regarding Cl^- concentration, evidence suggests that excessive interneuron firing can result in eventual loss of inhibitory drive on pyramidal cells. Repeated activation of $GABA_A$ receptors results in the accumulation of intracellular Cl^- in pyramidal cells. Although KCC2 acts to remove this excess Cl^- (with deleterious effects on extracellular K^+ concentration), excess intracellular Cl^-, has been demonstrated to result in the reversal of Cl^- gradients. Therefore, upon $GABA_A$ activation, Cl^- will flow according to the electrochemical gradient, exiting pyramidal cells and leading to further depolarisation, thus exacerbating the epileptic state (Huberfeld et al., 2007).

Other mechanisms have been observed to contribute to seizure propagation. These include increased Ca^{2+} concentration in presynaptic terminals, leading to increased neurotransmitter release (Sztriha et al., 1985). Additionally, removal of N-methyl-D-aspartate (NMDA) receptor depolarisation block is able to lead to greater depolarisation and activation of post-synaptic Ca^{2+}-mediated secondary messengers that alter neuronal excitability (Ghasemi & Schachter, 2011). Together, these alterations further exacerbate the disruption of the E/I-balance in neuronal networks.

The previously mentioned mechanisms all describe how a seizure is able to progressively advance through tissue by altering the internal and external environment of neurons. However, recent evidence suggests that this propagation does not occur passively in a radial manner from the focus. Instead, seizures appear to preferentially propagate between functionally connected regions (Rossi et al., 2017). Evidence to support this notion was obtained through widefield Ca^{2+} imaging of neuronal activity. Since this study served as an important precursor for the work presented in this thesis, this work will be discussed in detail. The authors performed retinotopic mapping of the visual cortex in awake mice using widefield Ca^{2+} imaging. Additionally, pupil dilation and overall movement was concurrently mea-

sured. Following successful retinotopic mapping in response to light grates moving in different orientations, a glass micropipette was used to induce epileptiform activity through picrotoxin delivery, while simultaneously recording extracellular field potential.

These experiments resulted in several important findings. Firstly, the authors observed that the initial phase of each seizure had similar properties to interictal spikes. These interictal spikes were seen to manifest as standing waves where the response in all affected regions followed a similar time course. Seizures initially demonstrate this behaviour, however, quickly diverge and begin to spread to wider areas of the cortex. Comparison of areas invaded by the seizure with the previously characterised retinotopic map revealed a preference for propagation to occur to homotopic areas: seizures showed favourable propagation to co-activated visual areas during retinotopic mapping. Therefore, the authors present two mechanisms by which epileptiform activity is able to propagate through the cortex; contiguously and homotopically. Contiguous propagation will occur to areas neighbouring the focus, while homotopic propogation will occur to areas demonstrating functional connectivity, such as similar orientation tuning in the visual cortex. Moreover, in some cases, spiral wave propagation was seen to occur with activity pin-wheeling around a centre with lower-amplitude (Rossi et al., 2017).

Altogether, the findings from this study, along with others (Liou et al., 2020), demonstrate complex propagation dynamics that vary depending on event properties. The slower, variable timescale of seizure propagation suggests the contribution of multiple factors beyond conventional synaptic transmission. These factors appear to surround slower changes in cellular excitability caused by alterations in the extracellular environment and activation of intracellular cascades over longer timescales (de Curtis & Avoli, 2015). Nonetheless, once initiation and propagation has occurred, seizures generally tend to sporadically terminate. In some more rare cases, the seizure may be prolonged, leading to status epilepticus; wherein inhibition-potentiating drugs, such as benzodiazepenes (Sharma et al., 2018), are required to halt the seizure, minimise lasting adverse consequences and reduce the risk of SUDEP (Auzmendi et al., 2018). Nonetheless, the majority of seizures are seen to terminate without intervention and the following section will discuss the mechanisms by which this termination is precipitated.

1.4.5 Seizure Termination

In order to minimise long-term deterioration of memory and cognition, as well as to minimise risk of death, seizure termination in a timely manner is essential

(Mathern et al., 2002; Postnikova et al., 2017). Although several studies have proposed hypotheses surrounding the mechanisms bringing about this termination, the exact process remains elusive. Multiple events have been observed to coincide with seizure termination, however, the exact contribution of each remains unclear.

Adenosine, a product of adenosine triphosphate (ATP) metabolism, has been demonstrated to play a large role in seizure dynamics. Shown to be an endogenous inhibitor of excitatory transmission (Boison, 2007), adenosine demonstrates anti-epileptic properties in animal models. Intraventricular implantation of adenosine-secreting cells has been shown to suppress seizures in a rat model of epilepsy (Huber et al., 2001). Moreover, exogenous adenosine application has been shown to halt seizures in multiple animal models (Akula et al., 2008; Van Dycke et al., 2010). Other studies using electrographic and electrochemical recordings from the brains of both animal models (Van Gompel et al., 2014) and human patients (During & Spencer, 1992) demonstrate that adenosine accumulation occurs towards the end of a seizure. The mechanism by which adenosine brings about this seizure termination has been proposed to be mediated by adenosine receptors, particularly A_1 (Boison, 2007). However, whether the adenosine accumulation is simply a by-product of energy consumption coinciding with seizure termination is unclear. Nonetheless, the evidence suggesting a key role for adenosine as a messenger in a regulatory feedback loop counteracting seizure continuity is compelling (Van Gompel et al., 2014).

Fitting with observations of adenosine accumulation at seizure termination are theories surrounding depletion of essential precursors required for neuronal firing. During seizures, the excessive synchronous high frequency activity of neuronal cells is highly energy consuming. As a result, energy provision mechanisms may be unable to match the rate of consumption, leading to an inability for the seizure to be sustained (Lado & Moshe, 2008). These metabolic substrates include oxygen (Kloiber et al., 1993), glucose (A. Kirchner et al., 2006) and ATP (Lado & Moshe, 2008; Walker, 2018). Additionally, increases in extracellular K^+, combined with the inability for effective extracellular clearance (requiring ATP) will result in an increased neuronal resting membrane potential. Thus, increasing the likelihood of Na^+-channel inactivation and depolarisation block. As a result, homeostatic balance is disrupted and further neuronal firing cannot be sustained; therefore, promoting seizure termination (Zubler et al., 2014). Intuitively, these could represent plausible mechanisms for seizure termination with evidence supporting this. However, other studies have also revealed that a reduction in precursors such as oxygen and glucose may actually initiate and worsen seizures themselves (Delanty et al., 1998).

Altogether, the role of metabolic substrate depletion and product accumulation in seizure termination remains unclear.

Another hypothesised mechanism leading to seizure termination surrounds extracellular pH. During intense periods of activity, such as generalising tonic-clonic seizures, molecules such as CO_2 and lactic acid are seen to accumulate, which leads to acidification of the extracellular environment. Additionally, pH can decrease through the exocytosis of acidic synaptic vesicle contents. The high concentration of free protons in the extracellular space leads to a state of acidosis marked by a large reduction in pH. An acidic extracellular environment has been shown to have anti-epileptic properties in both patients and brain slices. Several mechanisms have been proposed to mediate this anti-epileptic effect; including pH-induced inhibition of NMDA receptors and pH-mediated increases in extracellular adenosine leading to seizure suppression through the mechanisms mentioned above (Zubler et al., 2014). Compelling evidence also suggests a role for acid-sensing ion channel 1a (ASIC1a) in seizure termination: disruption of ASIC1a activity in transgenic mice revealed exacerbated seizure phenotypes. ASIC1a was shown to have little effect on seizure threshold and onset, however, a clear effect on seizure duration and progression can be observed (Ziemann et al., 2008). Altogether, these findings suggest a role for extracellular proton concentration in the termination of seizures.

Nonetheless, the described mechanisms surround alterations in extracellular environment and are unable to explain the variability seen in seizure durations; as well as cases of a prolonged seizure state seen in status epilepticus. Therefore, it remains unclear as to whether these processes are mechanisms in place to restore tissue homeostasis, or simply contributing factors that coincide with seizure termination.

Intuitively, the aforementioned mechanisms are unable to explain all the observations surrounding seizure termination. Firstly, seizure termination is observed to occur across multiple widespread brain regions rapidly: if seizure termination is determined by the accumulation or depletion of local molecular mediators alone, simultaneous widespread seizure termination would be unlikely. Moreover, these factors alone are unable to account for the variability in seizure duration: one would expect a similar duration of all seizures, determined by the time taken for molecular accumulation and depletion. However, in reality, cases such as status epilepticus exist, wherein a seizure state can be sustained for extensive periods, far greater than those observed during more common seizures. Therefore, it is apparent that other factors and mechanisms must play a role in seizure termination (Zubler et al., 2014). The exact contribution of each mechanism remains elusive and remains a

debated topic of investigation.

Another proposed seizure termination mechanism involves coordinated network communication on a larger scale. Evidence supports the notion that increased synchronisation of neuronal populations leads to seizure termination. Multi-channel electrophysiology, recorded either intracranially or using surface electrodes from epileptic patients, reveaed increased synchronisation towards the end of seizures. Moreover, in cases of status epilepticus, this increased synchronisation was not seen. Furthermore, administration of seizure termination-promoting drugs, such as diazepam, during status epilepticus increased neuronal synchronisation (Schindler et al., 2007). Altogether, the evidence presented by this study provides a compelling argument for the role of overall network synchronisation in seizure termination.

Further evidence supports this role of network synchrony in seizure termination. Non-linear regression analysis to estimate functional connectivity between thalamic and cortical structures revealed greater synchronisation towards seizure end compared to onset. Moreover, the thalamus consistently demonstrated synchronisation at the end of the seizure; suggesting an important role in the restoration of physiological firing (Evangelista et al., 2015). Since the thalamus is known to project to wide areas of the cortex and influence cortical excitability, it appears a likely mediator in the mechanisms leading to seizure termination.

Additionally, frequently observed following generalised clonic seizure termination is a period of activity suppression known as postictal generalised EEG suppression (PGES). PGES is frequently seen to follow convulsive seizures and manifests as a prolonged state of unconsciousness (Figure 16). PGES, commonly associated with respiratory dysfunction, is thought to result from profound cortical and brainstem inhibition (Lhatoo et al., 2010). Moreover, PGES is consistently observed preceding cardiorespiratory arrest and SUDEP; the predominant morbidity of epilepsy. Further strengthening the relationship between PGES and SUDEP are findings of increased PGES duration in SUDEP patients. Studies investigating the events preceding SUDEP have revealed variable heart rate and abnormal breathing, followed by PGES, followed by terminal apnea and lastly cardiac arrest (Kang et al., 2017). In some patients, intervention in a timely manner is able to prevent the terminal consequences of PGES. However, research into the prediction of SUDEP cases is ongoing and will facilitate a reduction in epilepsy morbidity.

Recently, of growing interest is the role of SD and cortical spreading depression (CSD) in seizure termination (Tamim et al., 2021). CSD involves a spreading wave of depolarisation, followed by suppression of subsequent activity due to loss of transmembrane ionic electrochemical gradients (Charles & Baca, 2013). CSD

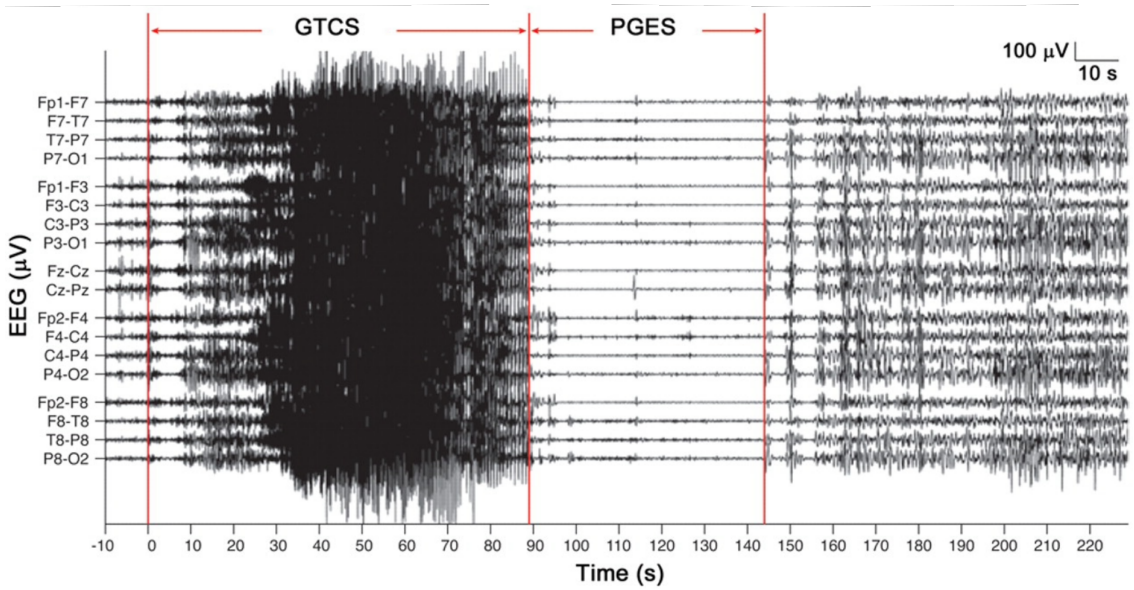

Figure 16: EEG recording of a generalised tonic-clonic seizure followed by post-generalised EEG suppression (PGES) and eventual recovery of brain activity. Adapted from Poh et al. (2012).

has been shown to interact with seizures and the subsequent activity suppression has been hypothesised to play a role in PGES and SUDEP (Jansen et al., 2019). Since, a major focus of this thesis is the investigation of SD and CSD properties, and the role they play in seizure termination, this will be discussed in detail in the forthcoming section titled 'Spreading Depolarisation'.

1.4.6 Prophylaxis of Epileptic Seizures

As mentioned previously, in severe cases of prolonged seizures without recovery, inhibition-enhancing drugs are often administered to induce seizure termination and minimise long-term negative outcomes (Falco-Walter & Bleck, 2016). Nonetheless, these cases are rare and their treatment is reactive as opposed to the more desired methods of predictive and preventative. Depending on the epileptic disorder, interacting medications and drug efficacy in the individual; different drugs are often prescribed to patients to reduce the probability of transition into a seizure (Rogawski & Loscher, 2004). Elaborating on the previous point, often certain drugs are suitable for some patients but not others: an example can be seen in patients receiving drugs from co-morbid disorders where the prescribed drugs are incompatible (Goldenberg, 2010). Other factors relating to the patient must also be considered: an example of this can be seen from recent published guidance recommending the discontinuation of the use of sodium valproate as an anti-epileptic drug in women of

child-bearing age. Sodium valproate has been found to increase the risk of foetal defects and is therefore, unsafe for female patients (Macfarlane & Greenhalgh, 2018). However, sodium valproate remains an effective and viable drug in other patients with epilepsy (Rogawski & Loscher, 2004).

Fortunately for patients with certain drug incompatibilities, a variety of different anti-epileptic drugs are able to act as alternatives. Anti-epileptic drugs typically act to reinstate balance between excitation and inhibition in neuronal networks. This can be seen in the cases of the commonly prescribed drugs carbamezapine and gabapentin; which act on Na^+ channels and Ca^{2+} channels respectively, with indirect effects on GABAergic transmission. Although epileptic disorders display considerable heterogeneity, these different pharmacological agents demonstrate efficacy in reducing seizure frequency and severity in many patients (Rogawski & Loscher, 2004). However, for other patients, this is not the case.

Anti-epileptic drugs are ineffective in up to 30% of patients (Strzelczyk et al., 2017). The drug-refractory epilepsy in these patients is resistant to any available pharmacological intervention. Moreover, epileptic patients frequently exhibit several comorbidities, including gastrointestinal (Harshe et al., 2016), diabetic (Lu et al., 2018), anxiety and dementia-related disorders (Keezer et al., 2016). As a result of these comorbidities, selecting a reliable pharmacological treatment can be difficult due to the contraindication of drugs with limited specificity (Goldenberg, 2010). Firstly, this has resulted in a need for greater understanding of the network alterations that precipitate transitions into an epileptic state. This, therefore, can lead to the development of new therapeutic avenues that are able to target epileptic paroxysms with greater specificity and efficacy. Secondly, understanding the relationship between epileptic seizures and other comorbidities appears essential in improving the quality of life for epileptic patients and providing new pharmacological avenues with minimal side-effects. Therefore, a large focus in epilepsy research is centred on finding novel therapeutic avenues and long-lasting treatments to reduce the sole reliance on pharmacological interventions.

In the case of severe epileptic disorders wherein patients experience multiple daily drug-refractory seizures, surgical intervention is often required (Jobst & Cascino, 2015). As mentioned previously, the success of the surgical intervention is heavily reliant on mapping of the epileptogenic focus, to allow complete resectioning; as well as mapping of nearby 'eloquent' cortex, to minimise damage to essential brain function (Reif et al., 2016a). Novel electrophysiological recordings techniques such as gSGFETs may improve our ability to map these zones (Masvidal-Codina et al., 2019; Garcia-Cortadella et al., 2021; Bonaccini Calia et al., 2021). Addi-

tionally, in this study, I will demonstrate the development of a platform able to provide a greater understanding of seizure dynamics; with the goal of contributing to the body of knowledge assisting drug development and identification for surgical removal.

1.4.7 Migraine

Showing high co-morbidity with epilepsy, migraine is a common paroxysmal disorder seen in approximately 15% of the population (Collaborators, 2018). Migraine manifests through profound electrical and vascular changes, eventually resulting in trigeminal nerve activation and prolonged bouts of a usually unilateral headache. Furthermore, migraine episodes are frequently associated with nausea, sensitivity to light and sound, and visual aura; resulting in the alteration of perceptual experience (Erdener & Dalkara, 2014). Migraine can vary considerably in frequency and severity: some sporadic polygenic forms present with mild symptoms; whereas, other monogenic forms exist with severe debilitating phenotypes.

A migraine episode, similarly to tonic-clonic seizures, can be divided into different phases (Figure 17). The first of these phases is the prodromal phase characterised by mood alterations, fatigue, concentration issues, increased urination and other manifestations. Following this, in some patients, is the aura phase; characterised by sensory disturbances and visual hallucinations. The main phase, known as the headache or migraine attack, is usually characterised by a throbbing head pain; nausea or vertigo; and sensitivity to light, smell and sound. Following this is a postdromal phase characterised by fatigue, altered mood and poor concentration. Migraine attacks typically present in periods lasting for weeks or months. Surrounding these periods, patients are often migraine free for considerable lengths of time. Migraine episodes, depending on the patient, may or may not be associated with the aforementioned stages (Dodick, 2018). For example, cases of migraine with aura are rare and migraine without aura is observed more frequently (Freilinger et al., 2012).

Migraine with aura is complex and a debated topic of research. Evidence suggests that the neurophysiological correlate of the visual disturbances during the aura phase is cortical spreading depression (Tfelt-Hansen, 2010). As mentioned previously, this is a slow wave of SD followed by suppression of cortical activity. CSD properties and evidence suggesting a relationship to migraine aura will be discussed in detail.

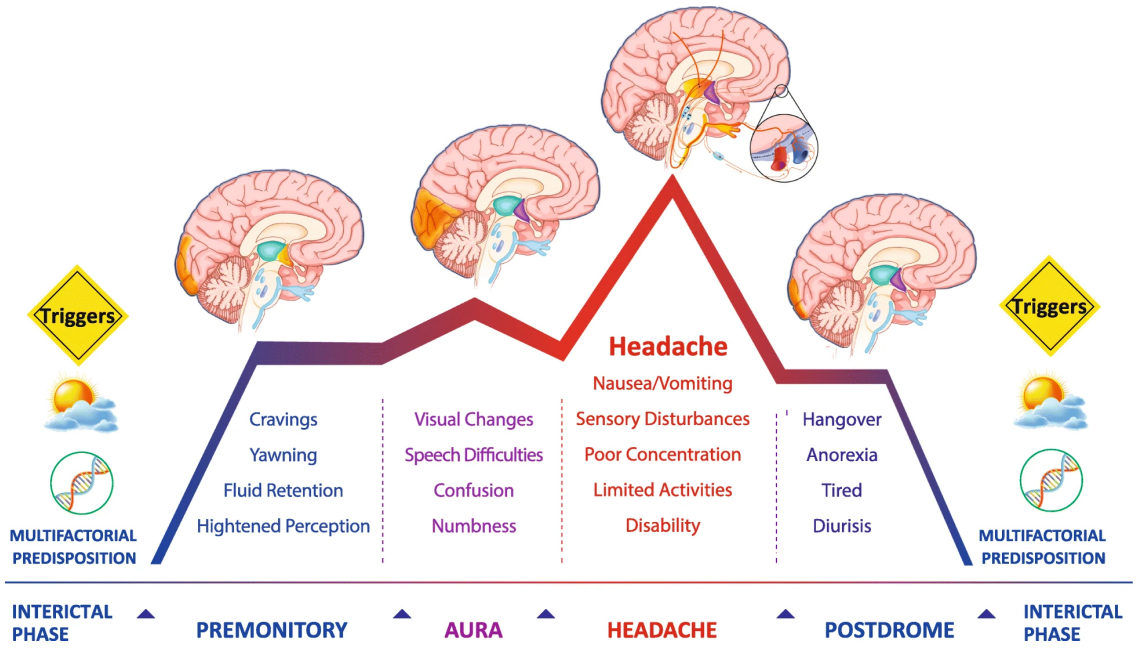

Figure 17: Timeline of the different stages of migraine that may present in patients and the associated symptoms (Andreou & Edvinsson, 2019).

1.4.8 Migraine and Epilepsy

Similar to epileptic disorders, migraine is a paroxysmal disorder occurring in bouts. Due to this paroxysmal nature, understanding underlying network alterations that lead to increased susceptibility is of paramount importance. Evidence suggests a relationship between the underlying network pathology in epilepsy and migraine. Multiple lines of evidence suggest a close interaction between changes in cortical excitability during epilepsy and migraine paroxysms. The most frequently observed manifestation of this is the occurrence of post-ictal migraine, however, pre-ictal migraine with visual aura is also seen (Cianchetti et al., 2017). Rare monogenetic disorders, such as familial hemiplegic migraine (FHM) also offer insight. FHM is a disorder of cortical excitability wherein patients present with migraine episodes combined with epilepsy, ataxia and/or hemiplegia. FHM can be manifest as one of three disorders; FHM1, FHM2 or FHM3; caused by mutations in CACNA1a (P/Q-type/$Ca_v2.1$), ATP1A2 (Na^+/K^+- ATPase) or SCNA1a ($Na_v1.1$) respectively (Haan et al., 2008). The co-occurrence of migraine episodes and seizures in these patients supports the idea of a shared underlying cortical pathology allowing these events to occur.

Further supporting the relationship between epileptic and migraine disorders are pharmacological prophylactic treatments. Frequently, the effective prescribed treatments to reduce the probability of migraine occurrence are also anti-epileptic

drugs. These include sodium valproate, topiramate and gabapentin. Additionally, triggers for migraine episodes are also triggers for epileptic seizures. These include caffeine, stress, powerful sensory stimulation, alcohol and sleep alterations (Oakley & Kossoff, 2014).

Altogether, the evidence presented provides a compelling argument for a similar underlying network pathology between epileptic and migraine patients. Although investigations in this thesis is focused around SD in the context of epilepsy, the developed platforms may be able to simultaneously provide insight into migraine pathology.

1.5 Spreading Depolarisation

CSD is a slow wave of SD that propagates through the cortex at a speed of approximately 2-5mm/min, followed by suppression of subsequent neuronal activity (Charles & Baca, 2013). This slow DC event has long been observed (A. A. P. Leao & Morison, 1945), but its role in disease pathology remains elusive.

Resulting in much confusion and discrepancy, several studies refer to this phenomena as 'spreading depression' and others 'spreading depolarisation'. As mentioned in the above section 'Recording Electrical Activity in the Brain', conventional recording techniques are limited in their ability to provide insight into infraslow activity and DC events due to high-pass filtering and high electrode impedance. As a result, progression of our knowledge into DC events such as CSD has been limited by available technology. Therefore, there have been difficulties in accurately recording both the infraslow activity associated with the spreading depolarisation and the often-associated subsequent suppression of neuronal activity. As a result, the terms spreading depolarisation and spreading depression are often used interchangeably to mean the single spreading depolarising event, with the activity suppression assumed to follow (Dreier, 2011; Cozzolino et al., 2018). However, this is not definitively always the case. To avoid passively complying with these assumptions, I will use the term spreading depolarisation to define the spreading wave of depolarisation seen in all cases; and the term spreading depression to define just the cases of spreading depolarisation that are clearly followed by prolonged suppression of neuronal activity. These phenomena are often observed in the cortex, and therefore, termed cortical spreading depression. However, spreading depolarisation and spreading depression has also been observed in other subcortical structures (Jansen et al., 2019; Loonen et al., 2019; E. Parker et al., 2021); with propagation simply being dominant in the gray matter of the brain. Therefore, throughout my investigations, I will use the

term spreading depolarisation.

1.5.1 Ionic and Molecular Movements during SD

Spreading depolarisation is characterised by a rapid, near-complete breakdown of transmembrane ionic gradients. This breakdown results in the transient formation of a steady state in membrane potential at approximately -10mV. This steady state is formed as a result of the Na^+/K^+-ATPase pump failing to compensate for cation influx (Oliveira-Ferreira et al., 2012).

During initial stages of SD, evidence suggests strong initial neuronal depolarisation results in a large increase in extracellular K^+, as shown by K^+-sensitive electrode recordings (Yao et al., 2015). Moreover, extracellular reductions in Na^+, Cl^- and Ca^{2+} occur as a result of a large ionic influx into the cytoplasm (Pietrobon & Moskowitz, 2014). Glial depolarisation, ineffective K^+ clearance and impaired extracellular buffering further alters neuronal excitability (Bellot-Saez et al., 2017); and when extracellular $[K^+]$ exceeds a threshold of approximately 12mM (Bogdanov et al., 2016), a SD wave will propagate through the grey matter of the brain (Pietrobon & Moskowitz, 2014). This increase in extracellular K^+ can be seen to accompany profound changes in tissue vascularisation, oxygenation, intracellular water content and extracellular volume (Ayata & Lauritzen, 2015). Additionally, SD propagation requires NMDA receptor activation to occur; as shown by studies using potent NMDA blockers to achieve complete inhibition of CSD (Bu et al., 2016; Masvidal-Codina et al., 2021). Therefore, it is clear SD initiation is dependent on glutamatergic synaptic transmission. In addition, glutamate has been shown to play a role in SD propagation: two-photon iGluSNFR imaging has revealed focal abnormalities in glutamate clearance, otherwise known as plumes. These plumes are observed to occur in regions nearby to SD origins prior to SD initiation (P. D. Parker et al., 2021). Altogether, it is clear that SD involves a dramatic perturbation in tissue homeostasis (Figure 18), and as a result, has earned the colloquial term 'brain tsunami' (Bailey, 2019). Understanding the role SD plays in disease pathology is of large importance.

The aforementioned changes have been observed in time periods leading up to, and during, SD. However, the exact contribution of each mechanism to SD initiation remains unclear. Moreover, the mechanisms by which SD propagation is maintained in the tissue remains poorly understood; as well the mechanisms that prevent further propagation and lead to termination. In addition, the mechanisms of SD initiation/propagation/termination may vary depending on the disease-state being investigated; thus, further increasing the complexity of the problem. The

work presented in this thesis aims to further the body of knowledge surrounding these phenomena, specifically in epilepsy-related contexts.

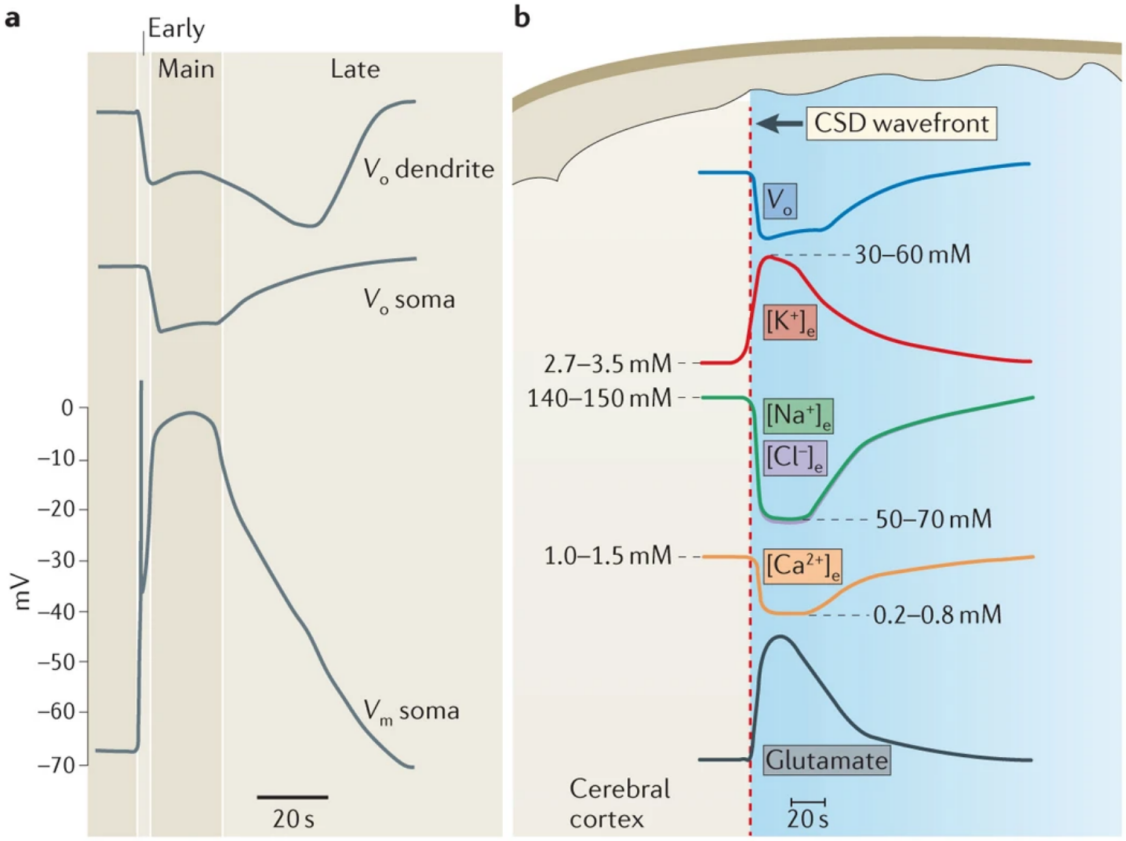

Figure 18: Observations of changes to intracellular potential, extracellular potential, glutamate and various ion concentrations during CSD. **A)** Potentials recorded during a CSD with electrodes recording extracellularly from dendrites (V_o dendrite) and the soma (V_o soma); and intracellularly from the soma (V_m soma). CSD is marked by profound depolarisation of all shown compartments identified by different recording methods. **B)** Depolarisation during CSD is accompanied by a large pathological increases in $[K^+]$ and glutamate. Due to the mass neuronal activation, there is a large reduction in extracellular $[Na^+]$, $[Cl^-]$ and $[Ca^{2+}]$ due to large ionic influx. Adapted from Pietrobon and Moskowitz (2014).

1.5.2 SD in Disease States

SD has been observed in multiple disease states and has frequently been associated with worsened outcomes of pathological events. SD has been investigated in the context of stroke, glioblastoma, traumatic brain injury (TBI), epilepy and migraine (Dreier, 2011).

SD was first discovered by Leao in 1945 following tetanic stimulation of the rabbit cortex. Leao's initial recordings revealed the spreading wave of depolarisa-

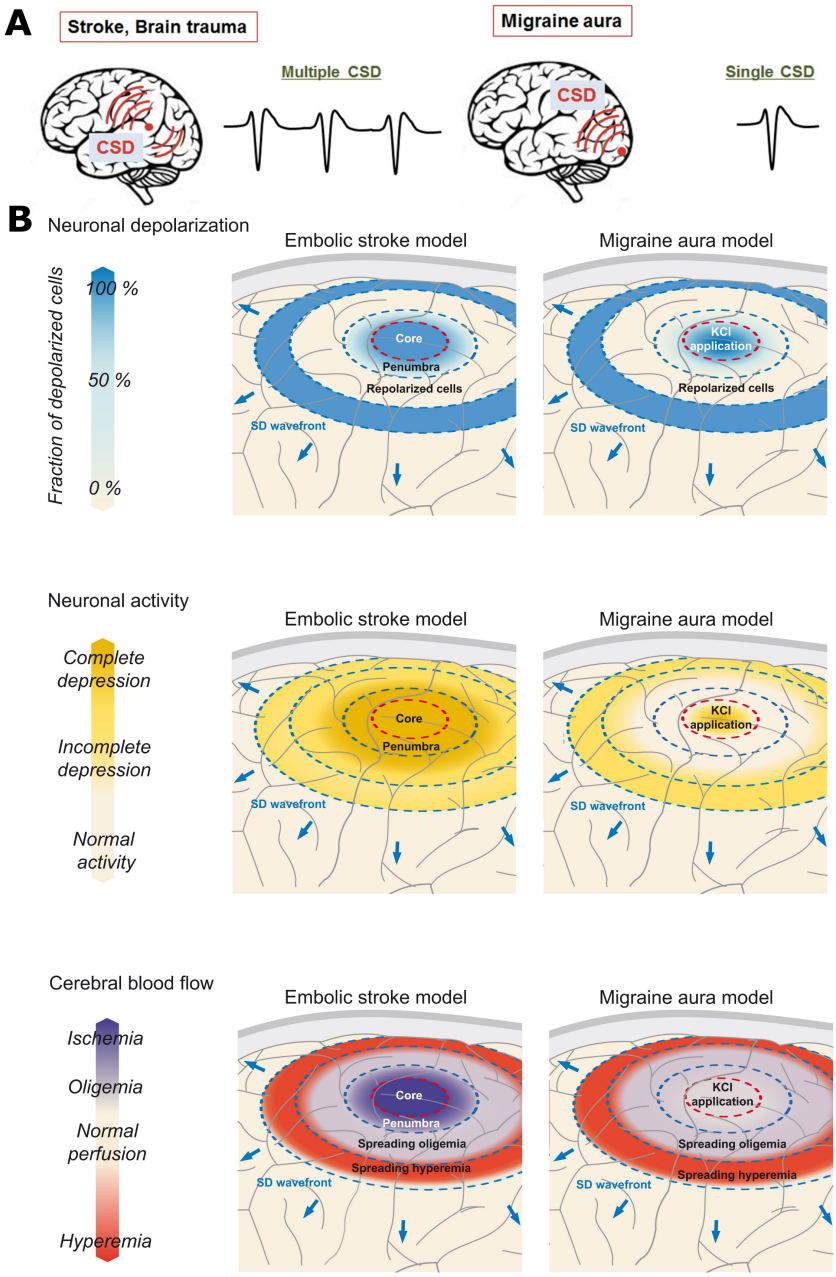

Figure 19: Comparison of SD events associated with migraine and other disease states. **A)** Comparison of CSD observed during stroke or brain trauma and during migraine aura. Migraine-associated CSD often manifests as a single wave, whereas stroke and brain trauma is associated with multiple CSD events in quick succession. Adapted from Shibata and Suzuki (2017). **B)** Comparison of embolic stroke model with migraine aura model. Fraction of depolarised cells, depression of neuronal activity and blood flow alterations shown. For the stroke model, the ischemic core is surrounded by a penumbra with the SD wavefront propagating away from the core. For the migraine model, KCl application results in SD propagation away from the site of application. Adapted from Dreier and Reiffurth (2015).

tion we know as SD (A. A. P. Leao & Morison, 1945). Following this discovery, initial observations first led to the association with migraine. Mapping of the visual disturbances during migraine aura revealed strikingly similar properties to the propagation of SD across the visual cortex (Charles & Baca, 2013). Moreover, SD has been found to lead to prolonged meningeal nociceptor activation (Zhang et al., 2010), trigeminovascular neuron depolarization (Zhang et al., 2011), and as a result, likely the facial pain and headache characteristic of migraine (Bolay et al., 2002; Olesen et al., 2009). Treatments for migraine are seen to reduce SD susceptibility in animal models (Ayata et al., 2006). Additionally, animal models of migraine consistently demonstrate a lower SD threshold (van den Maagdenberg et al., 2010). Therefore, the evidence suggesting a role for SD propagation in migraine pathology is overwhelming. However, the differing SD relationship between migraine with aura and migraine without aura remains elusive.

In recent years, interest into the relationship between SD and other disease states has been growing (Figure 19). One of these disease states is stroke. Ischaemic stroke is characterised by a vascular occlusion leading to reduced perfusion of brain tissue. Surrounding this occlusion, depending on the time taken for reperfusion, the long-term survival of surrounding tissue will be heavily affected. The region immediately surrounding the infarct location is termed the penumbra and spontaneous SDs are seen to arise from this penumbra following ischaemic insult. The penumbra is not fully-damaged tissue as for the core, however, these regions are functionally and metabolically compromised. SD arising from these regions have been termed peri-infarct depolarisations (PIDs) and the frequency of these PIDs have been shown to positively correlate with infarct size. Therefore, SD propagation in an ischaemic state has been shown to lead to worsened outcomes (Mies et al., 1993; Lauritzen et al., 2011; H. T. Zhao et al., 2021a).

Another disease state with a growing interest in SD is glioblastoma. Glioblastoma is an aggressive form of brain cancer with a tumorous growth formed from astrocytic populations. The area surrounding the tumour is termed the peritumoral zone and SDs have been observed to arise from this area. These peritumoral SDs have been hypothesised as responsible for observed neurological defects and may lead to worsened outcomes through influencing the growth of the glioblastoma (Hatcher et al., 2020).

Although lower in incidence, propagating SD waves have also been observed in TBI patients and animal models. These SD waves have been observed both as single waves and in clusters. However, it is unclear whether the occurrence of SD plays a fundamental role in TBI pathogenesis or is simply a byproduct of disturbed ion

homeostasis. Nonetheless, recent evidence from animal models demonstrates that propagating SD waves can lead to alterations in blood-brain-barrier permeability, further exacerbating outcomes (Tas et al., 2019; E. Parker et al., 2021).

The evidence supporting a role for SD in disease pathology is evident, with it clear that a greater understanding of SD mechanisms will lead to improved outcomes in multiple diseases. Additionally, cases of each of these disease states are frequently associated with epileptic seizures. Epileptic seizures, occurring within and outside of these disease states, are also associated with SD events.

1.5.3 Epilepsy and SD

Several studies in both human patients and animal models have revealed epileptic seizure-associated SD (Bastany et al., 2020; Tamim et al., 2021). Recent DC-EEG recordings from human patients with refractory epilepsy revealed a complex interaction between epileptiform high frequency activity and SD events (Bastany et al., 2020). Some studies have revealed SD occurring immediately prior to ictal events (Eickhoff et al., 2014), while others have shown SD occurring during seizures prior to seizure termination (Zakharov et al., 2019; Tamim et al., 2021). Altogether, the relationship between seizures and SD remains enigmatic.

Animal models are able provide insight into the relationship between these two events. Multiple seizure models, including rat tetanus toxin, mouse post-cerebral malaria (Bahari et al., 2020) and mouse flurothyl (Zakharov et al., 2019), have shown seizure-associated SDs (Figure 20). Moreover, mouse models of FHM disorders recapitulate the phenotype seen in human patients and frequently exhibit spontaneous seizure-associated SD (Jansen et al., 2019). As a result, the body of work surrounding investigation of seizure-SD interactions in epileptic animals has grown considerably. This has led to two ideas explaining this relationship; one, that SD may lead to negative outcomes by causing post-ictal generalised EEG suppression (PGES) and sudden unexpected death in epilepsy (SUDEP); and two, that SD results in the termination of epileptic activity which confers a beneficial effect. Here, I will discuss major studies leading to the support for these ideas.

With regard to a negative role for SD in epileptic paroxysms, several lines of evidence support this notion. Firstly, frequently reported are periods of synchronous rebound firing and seizures shortly after SD recovery (Gorji & Speckmann, 2004; Berger et al., 2008; Eickhoff et al., 2014; Rathmann et al., 2020). This had led to the idea that a propagating SD wave will result in increased excitability and lead to an increased probability of seizures. Therefore, these studies suggest that SD may play a large role in the events leading to seizure initiation. Additionally,

DC-coupled recordings from the brainstem further support the notion that SD may lead to negative outcomes. Transgenic mice with the *CACNA1A* S218L mutation present with comorbid seizures and SD, with these SD waves able to propagate to the brainstem. Within the brainstem, these SD waves are able to interact with medullary respiratory centres and lead to apnea, respiratory depression, and in some cases death (Jansen et al., 2019). These events have been proposed as the link between epileptic seizures and SUDEP. Therefore, these findings have led to compelling arguments that seizure-associated SD waves are harmful events leading to undesirable outcomes.

Evidence supporting a positive role for SD in epilepsy pathology stems from the benefits of activity suppression often seen in the period following SD. Several studies have reported seizures terminating with SD and this early termination has been proposed to reduce the long-term consequences of prolonged seizures. A recent study lending major support to an anti-epileptic role for SD characterised this relationship in different mouse-models of seizure (Tamim et al. (2021);Figure 20). Firstly, repeating SD waves were demonstrated to interact with seizures; with successive SDs associated with a gradual reduction in seizure power. Moreover, these seizures were found to originate both nearby to chemoconvulsant application sites and at some distance; suggesting a link to seizure generalisation. Interestingly, exogenous induction of SD through KCl application following seizure induction led to lasting seizure suppression and reduction in ECoG power. Moreover, pre-treatment with KCl before seizure-induction led to inhibition of the emergence of seizure activity. Intrinsic optical signalling (IOS) revealed that inducing SD results in a reduction in seizure generalisation. Additionally, SD prevention using MK-801-mediated NMDA antagonism led to increased seizure generalisation. As a result, these findings prompted the authors to propose SD as an innate anti-seizure mechanism. The proposal can be summarised as follows; in the case of excessive pathological activity where extracellular K^+ levels far exceed homeostatic levels, SD is an evolutionary conserved mechanism to essentially 'reboot' brain activity. However, these investigations were performed under isofluorane anaesthesia, which is known to alter both seizure and SD dynamics (Takagaki et al., 2014).

Combining the information presented by these two opposing theories, the relationship between SD and seizures remains unclear. SD has been shown to exhibit anti-epileptic properties. However, the major study leading to this proposal was performed in anaesthetised animals (Tamim et al., 2021). Moreover, the authors present no plausible explanation for the frequently reported seizures seen to follow SD. Additionally, it remains unclear how the anti-epileptic effect of SD would fit in

the context of both migraine and other debilitating disorders such as stroke; wherein there is clear evidence that SD is pathological. As a result, there is a clear need to further investigate SD in the context of epilepsy, as well as other disorders.

1.5.4 Methods to Study SD

Progression into the understanding of the role of SD in disease pathology has been limited by available recording techniques. Due to SD being a slow DC event, the corresponding activity is dominant below 0.1Hz. As discussed in the above section 'Recording Electrical Activity in the Brain', conventional recording techniques are limited in their ability to capture infraslow activity, and therefore, SD properties. Several studies have presented stable recording techniques able to overcome commonly seen bandwidth and impedance limitations. These methods typically use stable recording interfaces combined with large range amplifiers. Additionally, as described previously, active recording devices, such as gSGFETs, are able to provide insight into SD mechanics at multiple locations with high fidelity (Masvidal-Codina et al., 2019). These investigations take advantage of this technology to provide detailed information on SD properties.

Although the level of detail provided by full bandwidth electrophysiology is unmatched, the spatial information acquired through imaging techniques is able to significantly complement this. Electrophysiological recordings allow SD properties to be recorded in detail due to a high temporal resolution. However, the ability to capture spatial information is limited by the ability to disperse multiple recording sites throughout the tissue of interest. As a result, imaging approaches demonstrate considerable promise in producing recordings with large spatial coverage (Figure 21). Recording infraslow activity over large areas is important in the case of SD investigations, as these waves are known to propagate across large distances; meaning single point measurements are often limited in their ability to provide detailed information into SD properties. Previous investigations of SD dynamics have taken advantage of imaging methods to provide insight: a major example of this is seen through the studies using IOS to track SD propagation. IOS utilises the SD-induced alterations in tissue reflectance and transmittance arising from multiple factors such as cell swelling (Bahar et al., 2000) and hemoglobin oxygenation state (Bere et al., 2014). Several studies have used this technique to investigate SD propagation in both lissencephalic and gyrencephalic brain (Figure 22) to reveal complex patterns of SD propagation, such as spiral waves, reverberations and colliding waves (Shibata & Bures, 1972; Santos et al., 2014). Other imaging investigations take advantage of Ca^{2+} imaging techniques, such as those using GCaMP indicators, to achieve higher

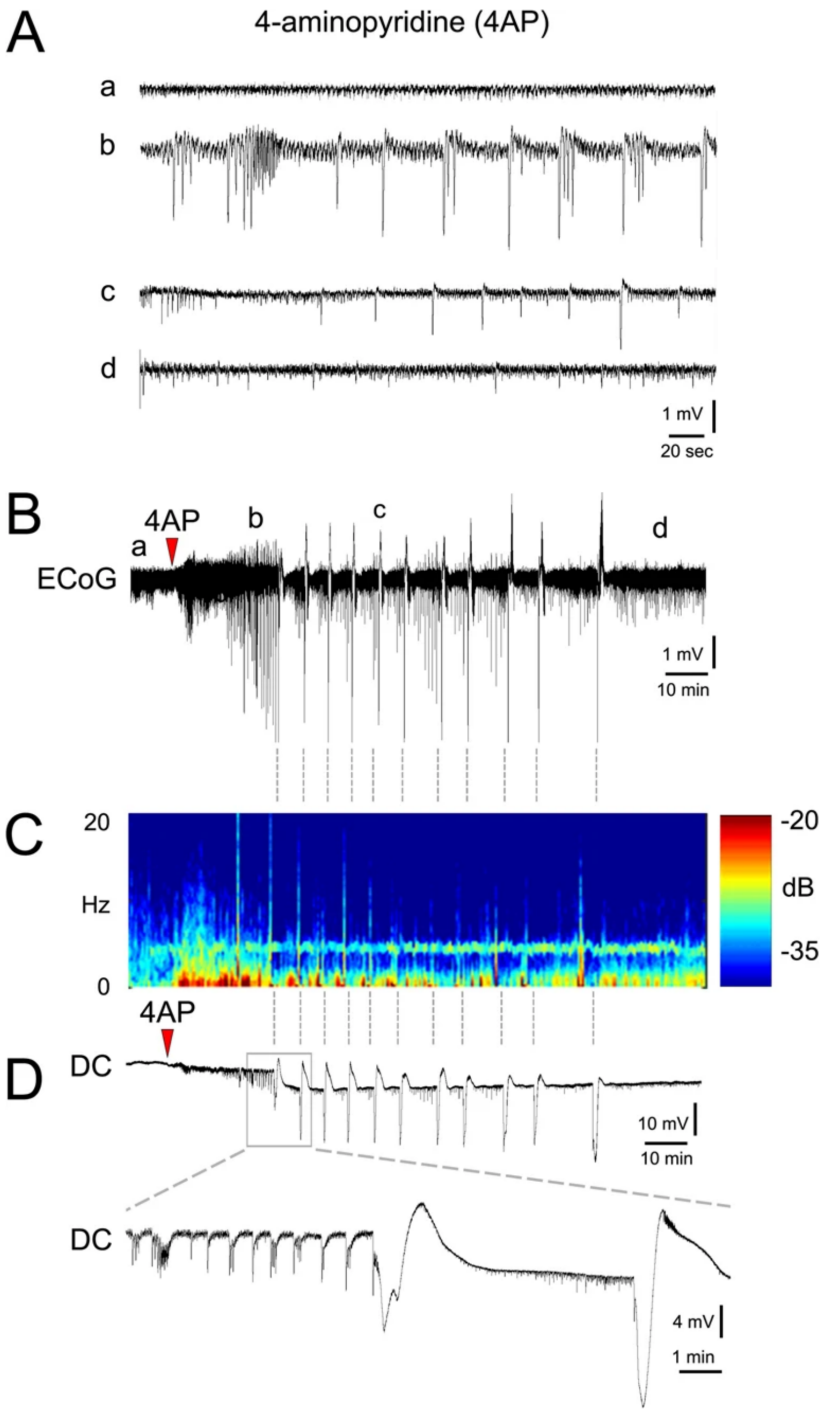

Figure 20: 4-AP-induced seizures and associated SD waves recorded with a glass micropipette and DC-coupled amplifier. **A)** Different periods of activity seen during 4-AP-associated epileptiform activity. Expansion of activity shown in **B**. **B)** Long recording of epileptiform activity with associated infraslow activity. **C)** Time-spectral analysis of trace shown in **B**. **D)** Individual trace with close up showing seizure-associated SD wave. Adapted from Tamim et al. (2021)

.

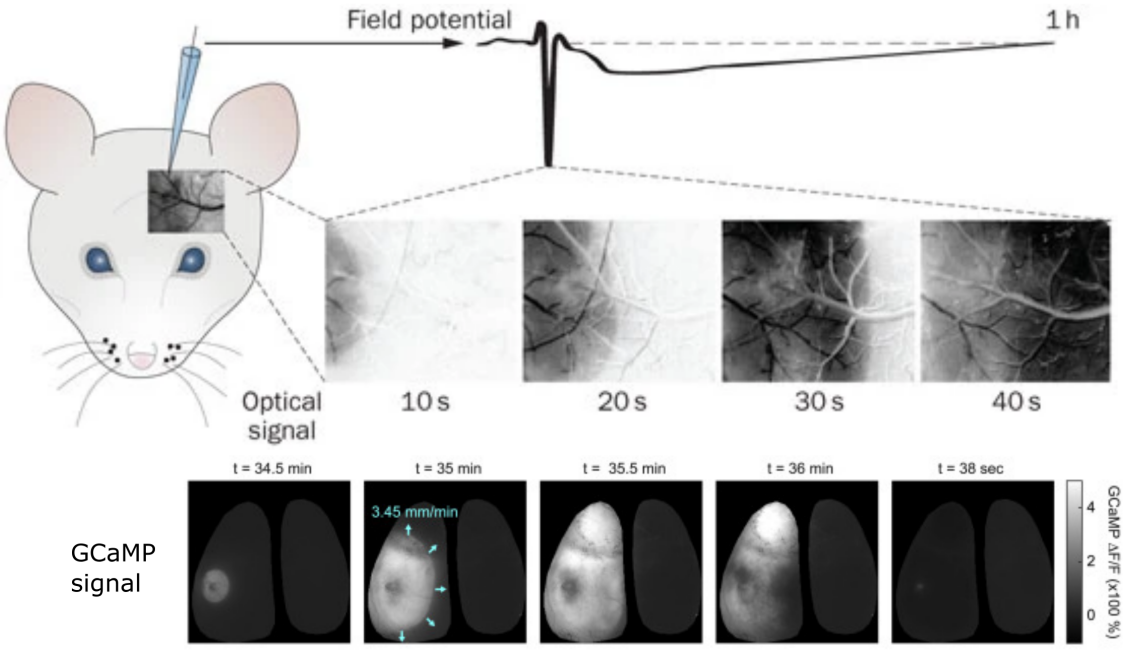

Figure 21: Comparison of methods to investigate SD waveform and propagation. Recordings of KCl-induced SD shown. Top shows glass micropipette-mediated DC-coupled recording. Middle shows intrinsic optical signal of same event over time. Bottom shows a widefield GCaMP recording of a photothrombotic SD. Adapted from Charles and Baca (2013) and H. T. Zhao et al. (2021b)

.

signal-to-noise recordings of SD dynamics and the neuronal firing surrounding this (H. T. Zhao et al., 2021b).

It is clear that both imaging and electrophysiological investigations have their own advantages at providing insight into SD mechanisms. I capitalise on these advantages by using imaging-compatible, full-bandwidth electrophysiological recording devices. Combination of both multi-site electrographic recordings with large scale functional imaging allows recording of SD propagation with both a high temporal resolution and spatial coverage respectively.

1.5.5 Models to Study SD

Several SD models are able to provide insight into SD propagation. SD can be induced in healthy tissue through the application of high concentration K^+ solution, such as 1M KCl (Masvidal-Codina et al., 2021). This allows induction of SD in healthy tissue and investigation of SD properties without the influence of other disease relevant parameters. Another method of SD induction in healthy tissue is ouibain administration which acts to induce SD through destabilisation of ion homeostasis through blockade of the Na^+/K^+ ATPase pump (Balestrino et al.,

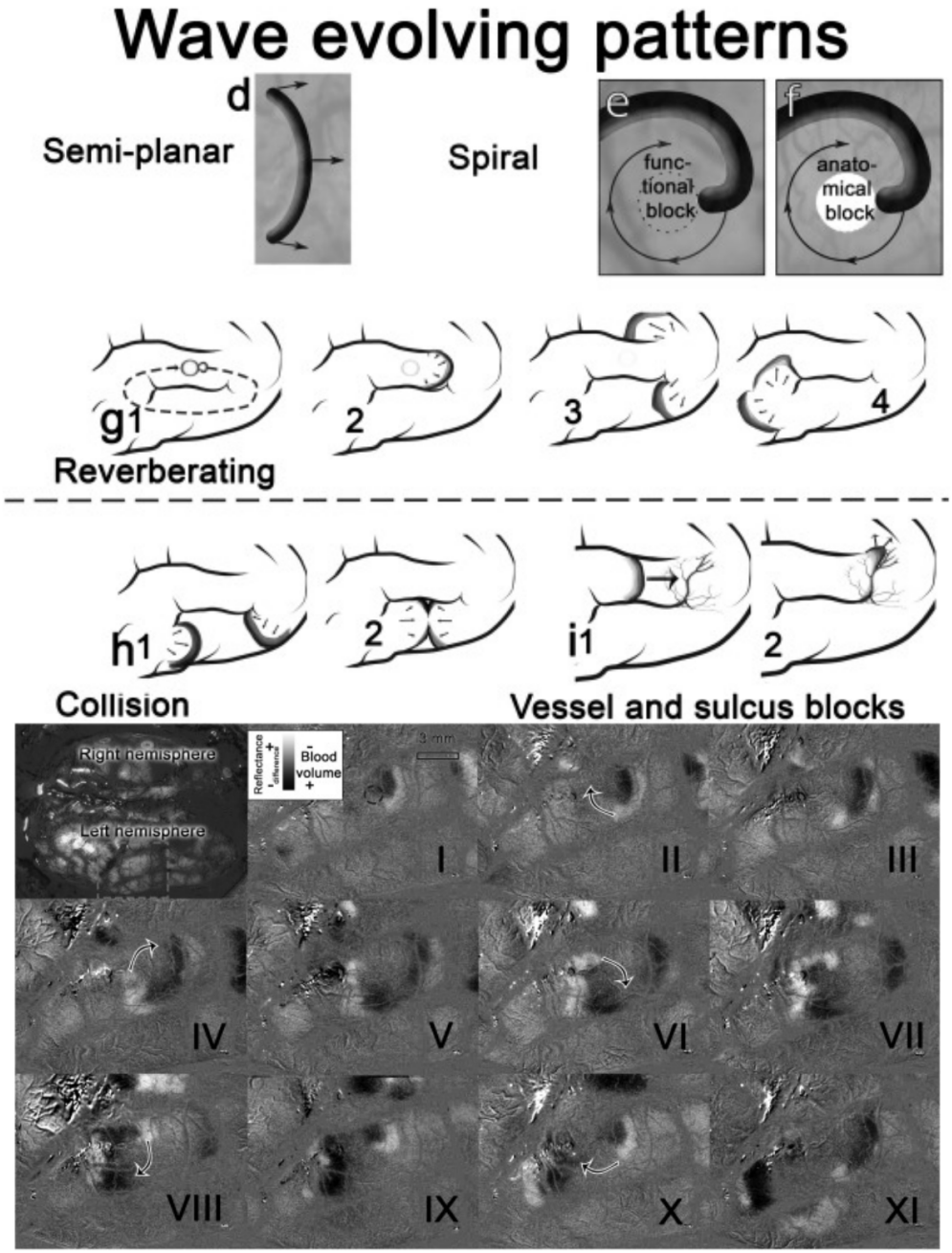

Figure 22: SD events frequently demonstrate complex propagation patterns with imaging techniques able to dissect these properties. Top: Different wavefront propagation patterns shown. Propagation may occur in a semi-planar manner or may exhibit more complex properties. These complex properties include spirals, reverberations and collisions caused by functional or anatomical blockages. Bottom: KCl-induced SD event recorded with IOS showing spiral propagation in porcine brain. Adapted from Santos et al. (2014)

.

1999).

A common method of SD induction in both healthy and diseased tissue is through the administration of a needle pinprick. Mechanical damage to brain parenchyma is known to reliably trigger SD from the site of damage, presumably due to the release of intracellular ions and molecules following tissue damage (Vinogradova et al., 2020). The pinprick method of SD induction is easy to achieve and reliable. However, the ease of induction may lead to accidental SD induction where this is undesirable. Examples of this can be seen in animal studies investigating different phenomena, but requiring insertion of electrodes or cannulae: the damage during surgical implantation will likely lead to SD induction and may confound investigations to a varying degree depending on the process being investigated. Furthermore, during surgical procedures in human patients, tissue penetration is often required for electrophysiological recording, stimulation, or to reach deeper structures. As a result, SD may be induced in the tissue, which may influence the overall outcome from the surgery.

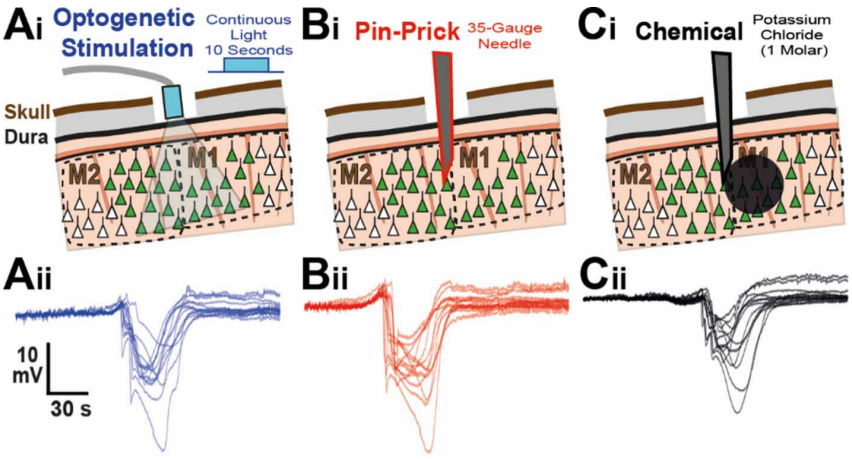

Figure 23: Comparison of different methods able to induce SD in healthy and pathological tissue. **A)** Optogenetic stimulation of motor cortex with continuous illumination leading to propagation of SD wave. **B)** Pinprick-induced SD wave following insertion of 35G needle. **C)** Chemically-induced SD wave following injection of 1M KCl solution into the motor cortex. For each method epicortical full-bandwidth gSGFET-mediated recordings of the propagating SD wave are shown for up to 16 transistors. Adapted from Masvidal-Codina et al. (2021)

.

Another method of SD induction of growing interest uses continuous optogenetic stimulation. These methods build upon classical methods of induction which used tetanic stimulation through a metal electrode, such as in the case of Leao (A. A. Leao, 1947). Metal electrode-mediated induction of SD suffers from limitations that optogenetic induction is able to overcome. One is that the electrode

requires contact with the tissue and insertion of the metal electrode will induce a SD of different origin; the pinprick. Moreover, the physical damage to the brain tissue due to electrode insertion may further alter SD properties through tissue disturbance and physical trauma. Additionally, further tissue damage may be caused by rigid metal electrodes shearing adjacent pulsating brain tissue. As a result, there is a requirement for a less invasive method of SD induction. Optogenetic stimulation is able to overcome this by circumventing the need for invasive insertion of rigid electrodes. Opsin-mediated SD induction can be achieved through delivery of a continuous pulse of light to a population of neurons (Masvidal-Codina et al., 2021). Evidence from electrical (Matsuura & Bures, 1971a) and optogenetic studies (Masvidal-Codina et al., 2021) reveals that depolarisation of approximately $1mm^3$ of tissue will result in SD induction. Opsin expression can be achieved through either virus-mediated methods or using transgenic animals, and interest in this method of SD induction has grown in the past few years. SD induction methods are summarised in Figure 23.

The previously discussed methods of SD induction can be achieved in either healthy or diseased tissue. However, there is evidence to suggest that SD dynamics differ between healthy and diseased tissue, as shown by SD propagation velocity (van den Maagdenberg et al., 2010) and time for local field potential (LFP) band recovery after SD (Dreier, 2011). The aforementioned methods can be induced in pathological tissue. Alternatively, physiologically-relevant, disease states can be induced, and associated spontaneous SD events can be recorded. This has been performed in models of stroke (e.g. after Rose-Bengal induced ischaemia)(H. T. Zhao et al., 2021b), TBI (e.g. after Marmarou weight-drop)(E. Parker et al., 2021), migraine (e.g. in FHM1 transgenic mice)(Jansen et al., 2019) and epilepsy (e.g. after chemoconvulsant administration)(Zakharov et al., 2019).

Transgenic animal models are also able to provide insight into SD properties. A commonly used disease family to study SD mechanics is familial hemiplegic migraine (FHM). As mentioned previously, FHM disorders can be grouped into one of three categories (Figure 24); FHM1, FHM2 or FHM3 which correspond to mutations in CACNA1a (P/Q-type/$Ca_v2.1$), ATP1A2 (Na^+/K^+- ATPase) or SCNA1a ($Na_v1.1$) respectively (Haan et al., 2008). FHM patients often present with a mixture of epilepsy, migraine, hemiplegia, cerebellar ataxia and severe coma following mild head trauma. Rodent models of homologous point mutations found in human patients are often able to provide powerful insight into SD properties in disease-relevant brain networks. For each of the three FHM types, one or multiple animal models have been generated for each (Dehghani & Karatas, 2019). These models

frequently exhibit spontaneous seizure-associated SD events; making these models a powerful tool in investigating the link between single ion channel or pump dysfunction, the mechanism by which this leads to network destabilisation, and the link between network destabilisation and the ensuing SD wave (van den Maagdenberg et al., 2010). These investigations observe these phenomena in a mouse model with a corresponding point mutation found in FHM1 patients.

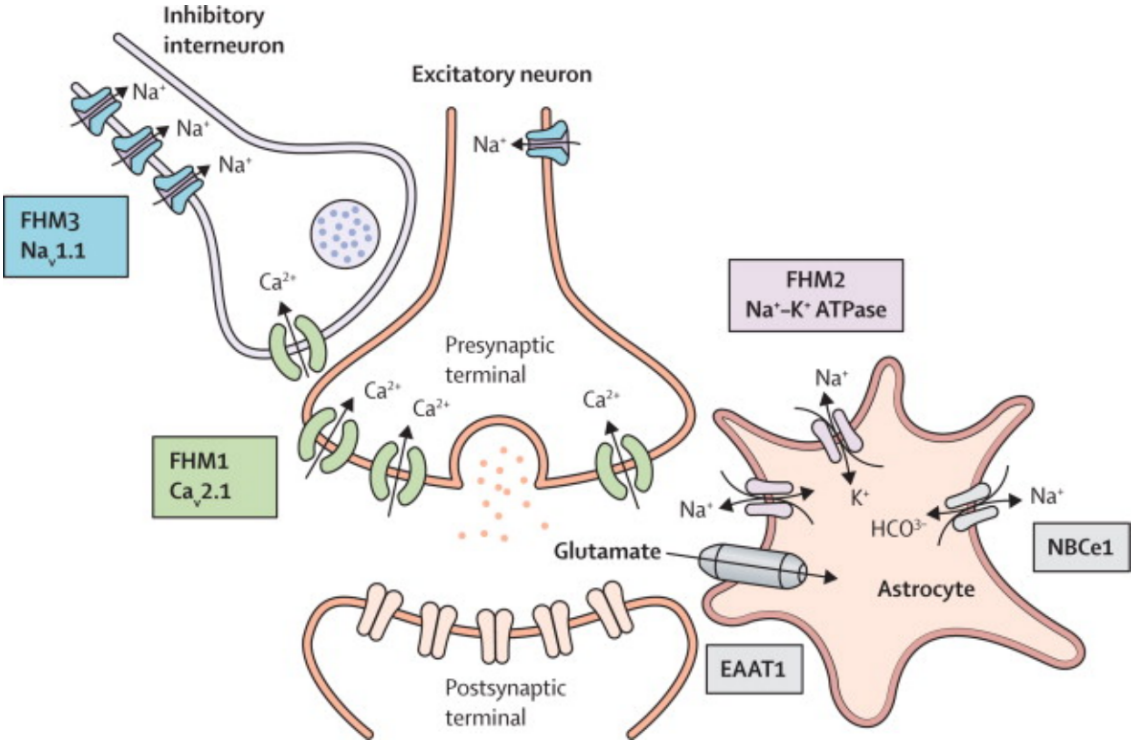

Figure 24: Schematic showing a chemical synapse with pre-synaptic and post-synaptic compartments, along with a local inhibitory interneuron and a neighboring astrocyte. Location of FHM proteins marked with associated molecules of interest. FHM1 disorders are caused by mutations in $Ca_v2.1$ leading to altered Ca^{2+} influx during synaptic transmission. FHM2 disorders result from alterations in Na^+-K^+-ATPase function leading to altered ion homeostasis and increased extracellular K^+. FHM3 disorders result from alterations in $Na_v1.1$ leading to altered inhibitory input and changes to E/I-balance (Russell & Ducros, 2011)

.

1.5.6 CACNA1A S218L

Multiple FHM1 mutations occur in humans with the mutations being located on the pore-forming subunit of the voltage-gated ion channel $Ca_v2.1$ (Figure 25) (Pietrobon, 2010b). This thesis demonstrates the utilisation of a mouse model generated to reflect a small group of patients with the point missense mutation, S218L.

The heterozygous human patients exhibit migraine with aura, seizures, hemiplegia, ataxia and frequently coma without recovery following mild head trauma (Kors et al., 2001; Stam et al., 2009). The mice closely recapitulate these phenotypes (van den Maagdenberg et al., 2010).

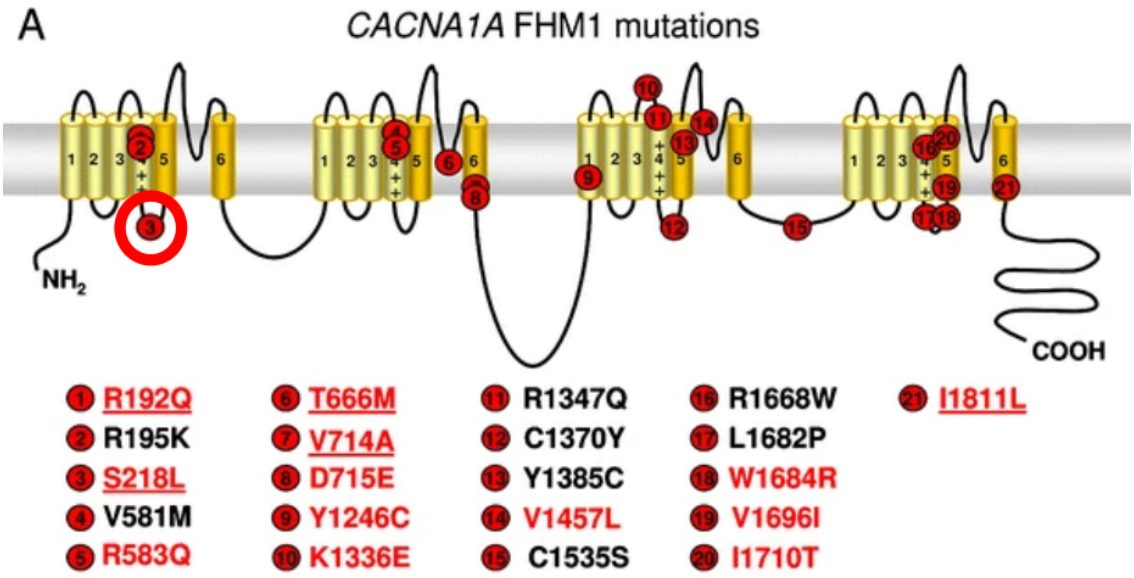

Figure 25: $Ca_v2.1$ channel structure encoded by CACNA1A gene showing locations of FHM1 mutations. Location of the S218L mutation on the pore-forming subunit circled in red. Mutations coloured in red have been studied in recombinant $Ca_v2.1$ channels using heterologous expression systems, and those underlined have been studied in $Ca_v2.1$ null mice expressing the pathological human channel subunit. Adapted from (Pietrobon, 2010a)

.

Investigation of the effect of the S218L mutation on P/Q-type Ca^{2+} channel activation has revealed alterations in the voltage-sensitive activation of the channel (Figure 26). This effect appears to vary between recorded cell types with all mutant cells showing channel activation at more hyperpolarised potentials. Whole-cell recordings from cerebellar granule cells demonstrate a greater channel open probability and peak activation in S218L animals (van den Maagdenberg et al., 2010). This result is also observed in HEK293 cells expressing the S218L channel (Tottene et al., 2005). However, pre-synaptic recordings from the calyx of Held reveal a similar negative shift in activation profile, yet demonstrate a reduction in peak current (Di Guilmi et al., 2014). Altogether, these complex and somewhat contradictory alterations suggest an intricate role for P/Q-type Ca^{2+} channels in a particular neuron's function, and a delicate position in the complex balance maintaining effective synaptic transmission and neuronal excitability.

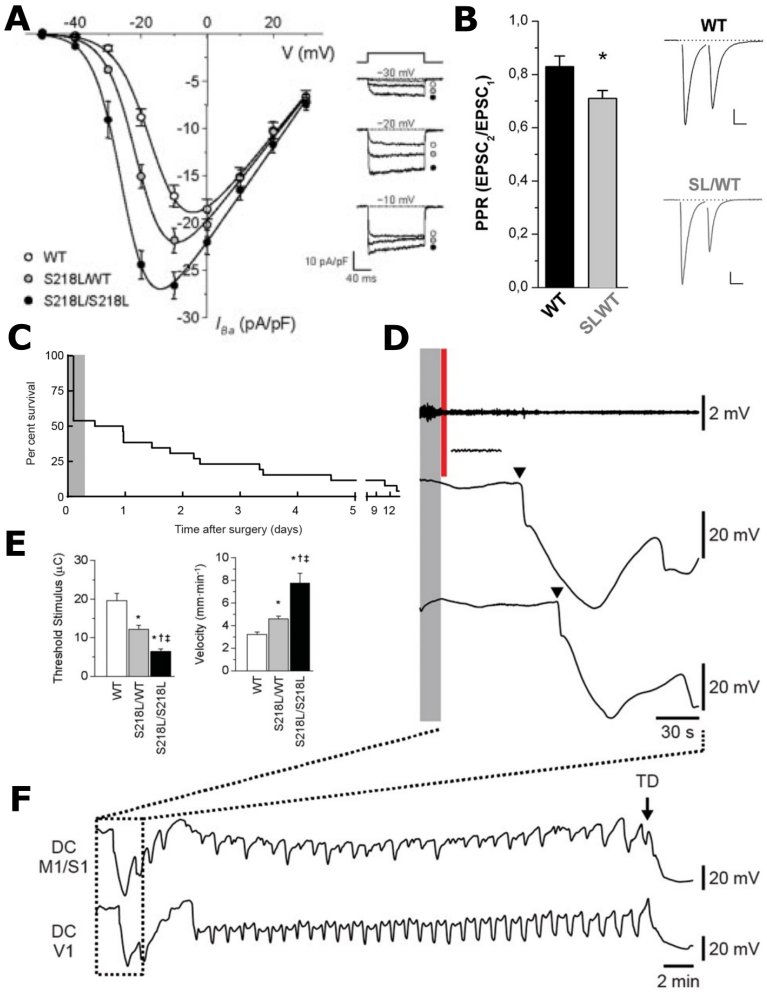

Figure 26: Summary of effects of CACNA1A S218L mutation on both synaptic function and overall phenotype. **A)** I-V curve showing activation of WT, heterozygous and homozygous isolated $Ca_v2.1$ currents at different potentials in mouse cerebellar granule neurons. S218L animals demonstrate a gene-dose-dependent increase in maximum activation with the I-V curve shifting to more negative potentials. Adapted from (van den Maagdenberg et al., 2010). **B)** paired-pulse ratio at 50Hz of heterozygous S218L autaptic pyramidal cells compared with WT. S218L cells demonstrate lower PPR suggesting greater initial release probability (Vecchia et al., 2015). **C)** Survival rate of homozygous S218L mice after surgical implantation. Over 50% of animals fail to survive beyond 24 hours (Loonen et al., 2019). **D)** Recording of terminal depolarisation from homozygous S218L mouse after seizure induction by cortical electrical stimulation. Top trace shows AC-coupled recording from M1/S1, middle trace shows DC-coupled recording from M1/S1 and the bottom trace shows DC-coupled recording from V1 (Loonen et al., 2019). **E)** Plot of electrical threshold to trigger SD in S218L mice (left) and propagation velocity of SD in these mice (right). SD appears easier to induce and propagates faster in S218L mice in a gene-dose-dependent manner (van den Maagdenberg et al., 2010). **F)** Close up of recording from homozygous S218L recording in **D** showing multiple DC events leading to terminal depolarisation (Loonen et al., 2019)

.

Investigations in S218L mice revealed a lower CSD induction threshold and higher propagation speed (van den Maagdenberg et al., 2010). Moreover, spontaneous seizures (Jansen et al., 2019) and poor rotarod performance (van den Maagdenberg et al., 2010), indicative of a motor phenotype (e.g. hemiplegia or ataxia), are also observed. Furthermore, the survival of S218L homozygous mice following invasive surgery is poor with 50% of animals seen to spontaneously die within 24 hours of surgery (Loonen et al., 2019). Investigations into cortical activity using ECoG in these animals has shown large CSD waves propagating to the brainstem, resulting in cessation of breathing: a proposed mechanism underlying SUDEP (Jansen et al., 2019). These prior investigations all suggest the S218L mutation as a suitable model to study the relationship between seizures, SD and CSD.

1.5.7 Contributing SD and Seizure-related gSGFET Studies

Throughout the course of this doctoral research, I have contributed to several studies aiming to further characterise gSGFET technology and demonstrate the superior ability for gSGFET devices to probe infraslow activity and DC events associated with seizures and SD. Data from these studies will be discussed as introductory to the main projects of my thesis.

A significant study supporting the use of gSGFETs to study infraslow activity was recently published in the Journal of Neural Engineering (Masvidal-Codina et al., 2021). Alongside my primary project, I contributed to this study characterising epicortical gSGFET arrays and their ability to investigate CSD propagation across the cortex. Central to these investigations was the development of a novel viral-approach to express ChR2(H134R) in the cortex, and to utilise this to elicit CSD events.

The primary aim of this study was to produce a reliable model of CSD induction, to utilise this model to investigate CSD properties, and to perform pharmacological screens of potentially CSD-modifying drugs in awake head-fixed mice. CSD events were induced through optogenetic stimulation: ChR2 was expressed in all neuronal populations (under a synapsin promotor) through AAV-mediated delivery into the motor cortex. Continuous illumination of the ChR2-expressing motor cortex resulted in profound depolarisation, leading to CSD induction which propagated across the cortex. 16-channel epicortical gSGFET arrays were used to map propagation and investigate the diversity of CSD properties, for example, waveform and duration.

Firstly, successful CSD induction was shown to be dependent on illumination wavelength, addressing concerns that induction may simply be a result of an increase

in brain tissue temperature. Secondly, induction was shown to be dependent on illumination being continuous, as opposed to pulsed; thus arguing that powerful depolarisation without immediate recovery is required for CSD induction. Prior to the original studies demonstrating optogenetic CSD induction (Houben et al., 2017; Donmez-Demir et al., 2020; Masvidal-Codina et al., 2021), the major methods of induction were either mechanical (Gursoy-Ozdemir et al., 2004; Fioravanti et al., 2011; J. Zhao & Levy, 2018), chemical (Fioravanti et al., 2011; Masvidal-Codina et al., 2019; Donmez-Demir et al., 2020), or electrical (A. A. Leao, 1947). To demonstrate that our model generates data consistent with established models, we compared CSD properties between optogenetic, pin-prick (mechanical) or KCl (chemical) induced events. Our results revealed no significant difference in CSD amplitude or propagation velocity.

Following confirmation of the physiological relevance of our model, we developed an assay to investigate CSD properties and drug efficacy in modifying these properties. Firstly, we utilised a custom-built Python library to extract core properties of each recorded CSD. Based on the extracted data, we sorted each CSD waveform into one of four groups; single-peak (SP), double-peak (DP), single-peak with hyperpolarisation (SPh), and double-peak with hyperpolarisation (DPh). SP and DP CSD events were differentiated by the number of peak plateaus before return to baseline. SPh events were those which displayed a positive increase in potential following the CSD. DPh events were those with a positive increase in potential preceding the CSD. Analysis of 633 waveforms from 54 CSD events revealed a large degree of variability with the majority of CSD waveforms being either SP or SPh. However, a single CSD event recorded at multiple sites using a gSGFET array revealed a mixture of the four waveforms. The results from these investigations demonstrated the rich variability in CSD properties, along with the ability of gSGFET arrays to capture dense information regarding this variability.

A large second objective of this study was to demonstrate the power of gSGFET arrays in recording infraslow activity during a pharmacological screen for CSD-modifying drugs. An assay comprising the induction of ten optogenetic CSDs was utilised. Between the second and third CSD events, either a vehicle or drug was intra-peritoneally administered. Various relevant pharmacological agents were investigated and their affect on CSD induction monitored using multiple epicortical gSGFET arrays. MK-801, a potent use-dependent NMDA receptor antagonist was shown to result in complete CSD inhibition, with profound changes observed at the site of stimulation (primary motor cortex). However, due to off-target effects related to psychosis (S. J. Park et al., 2014), MK-801 is not safe for administration to

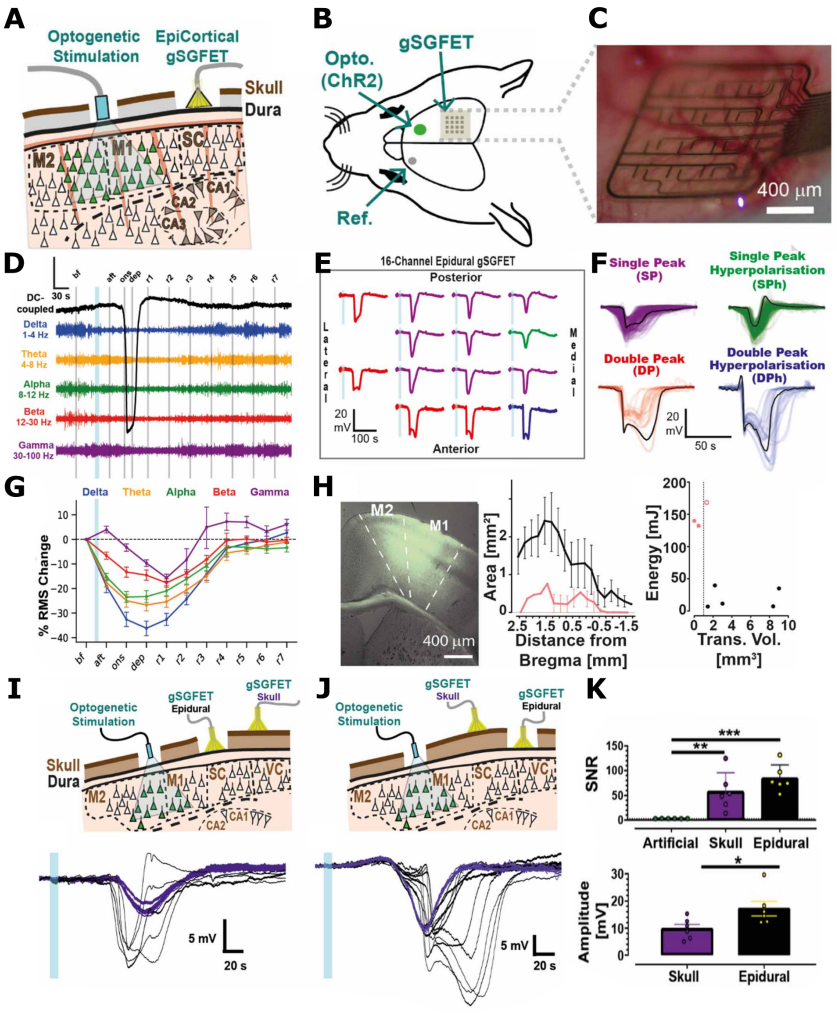

Figure 27: Summary of findings from Masvidal-Codina et al. (2021) showing gSGFET characterisation and investigation of optogenetically-induced CSD. **A)** Diagram showing experimental paradigm. Optical fibre used to induce CSD was placed above the motor cortex and an epicortical gSGFET array was used to record from the somatosensory cortex. **B)** Diagram showing locations of optic fibre, gSGFET and reference electrode in relation to mouse head. **C)** Image of gSGFET array on mouse brain. **D)** Optogenetically-induced CSD with associated changes in physiologically-relevant frequency bands shown. **E)** Example of a single recorded event showing different CSD waveforms on 14 gSGFET channels. **F)** Classification of different observed CSD waveforms. **G)** Percentage change in signal power for each of the relevant frequency bands shown in **D**. **H)** Characterisation of transduction volume of ChR2. Left shows example image, middle shows transduced area relative to bregma, right shows transduced volume against optogenetic CSD induction threshold. Consistent with previous literature, animals with a transduced volume $<1\text{mm}^3$ failed to generate reliable and repetitive CSD. **I)** Experimental paradigm with an added gSGFET array recording through the skull above the visual cortex. Traces for both gSGFETs shown below with through the skull recording (purple) peaking later. **J** As in **I**, but with the skull and epicortical positions reversed. Plotting together reveals an ability to resolve propagation dynamics. **K)** SNR and amplitude plots for epicortical and through-the-skull recordings showing a reduction when recording through bone.

human patients. Therefore, we tested alternative pharmacological agents active in modulating similar pathways. Intraperitoneal ketamine administration resulted in shorter-lasting CSD inhibition when compared with MK-801, thus demonstrating the power of our assay in resolving drug efficacy in an awake animal model.

Investigations using multiple gSGFET arrays revealed the ability to record the profound depolarisation at the site of optogenetic CSD induction, as well as the absence of this depolarisation following MK-801 administration. Moreover, recording of induced CSDs were performed while simultaneously recording on the dura and the skull, allowing inferences to be made regarding the ability for gSGFET arrays to record infraslow activity through bone. Our results indicate that recording through bone, allows successful detection of large DC events, such as CSDs. However, comparing recordings on the dura with those on the skull revealed a reduction in SNR; and the loss of temporal and qualitative information, such as propagation and waveform characteristics. Nonetheless, these investigations revealed the ability for gSGFETs to detect CSDs through the rodent skull; an important step in demonstrating clinical feasibility.

The majority of my contribution to this study was through data analysis. A large part of my work involved the analysis of ChR2 expression profiles in cortices following electrophysiological interrogation. The primary output of this analysis was to understand the volume of transduced neural tissue and to compare this with optogenetic CSD induction thresholds. Our findings revealed that the animals which failed to allow reliable CSD generation had a total transduction volume below $1mm^3$: a finding consistent with the previous understanding that at least $1mm^3$ of brain tissue must be simultaneously depolarised to perturb extracellular potassium sufficiently to trigger CSD induction (Matsuura & Bures, 1971b).

Altogether, this study provided a powerful demonstration of the ability of epicortical gSGFET arrays to record infraslow electrophysiological activity across multiple sites of the cortex in an awake, headfixed animal. Moreover, we present data showing gSGFET compatibility with a pharmacological assay searching for CSD-modifying agents. Lastly, we present data showing successful recording of infraslow activity through the skull. The findings of this study are summarised in Figure 27.

Our findings progress the area of CSD research through providing a non-invasive method to record CSD properties: mechanical damage of nervous tissue through insertion of electrodes has been shown to result in CSD induction (Gursoy-Ozdemir et al., 2004; Fioravanti et al., 2011; J. Zhao & Levy, 2018), potentially modifying the process being investigated. gSGFET arrays are able to circumvent these issues. Moreover, we present an optogenetic model to induce CSD which requires

no transgenic animal colonies; consequentially, reducing experimental cost significantly. Finally, the experimental paradigm presents a powerful method to capture dense information regarding CSD properties, and a platform to examine the physiological significance of each of these parameters. Nonetheless, this study can be developed further, and a large part of this thesis is focused on building upon the findings of these previous investigations.

We have also recently published a study in Nature Nanotechnology further characterising gSGFET technology and demonstrating the applicability in recording epileptiform activity (Bonaccini Calia et al., 2021). This study, which I contributed to through experimental recording of epileptiform activity in rodents, involves the utilisation of gSGFET depth probes to investigate infraslow activity throughout cortical and hippocampal layers. We characterised intracortical gSGFET probes; as done before for gSGFET epicortical arrays. Following this, gSGFET probes were coated in silk fibroin; an insoluble protein that allows stiffening of flexible gSGFET probes. As a result, the gSGFET probes maintain flexibility, yet were able to withstand the force required for insertion into the primary visual cortex. We administered 4-AP into the cortex while recording simultaneously using a glass micropipette and a gSGFET intracortical probe. Intracortical gSGFET probes were able to record both low and high frequency activity with high fidelity and stability. gSGFET depth neural probes were able to reveal active and passive seizure-associated DC shifts, as well as high-frequency oscillations (HFOs). gSGFET correlation to the micropipette signal allowed inferences to be made about the position of the micropipette with the signals showing a high correlation. Altogether, this demonstrated the ability for gSGFET intracortical probes to record a variety of pathological events, including epileptic spikes, seizures and SD across multiple layers of the cortex and the hippocampus.

The next technological advancement demonstrated by this paper involved the utilisation of a chronic, freely-moving preparation in rats to allow us to longitudinally monitor spike-wave discharges in a WAG-Rij model of absence epilepsy. WAG-Rjj rats exhibit pathological thalamocortical oscillations between 8-11Hz that are associated with DC-shifts (Coenen & Van Luijtelaar, 1987). We utilised this model to assess the ability for gSGFET intracortical probes to chronically monitor epileptic activity. Our results showed successful recording of full-bandwidth electrophysiology up to 72 days post-implantation. Lastly, fluorescent labelling of astroglial and microglial activation revealed minimal inflammatory responses following gSGFET probe insertion. The results of this study are summarised in Figure 28.

Altogether, the data presented in this study demonstrates the ability for gS-

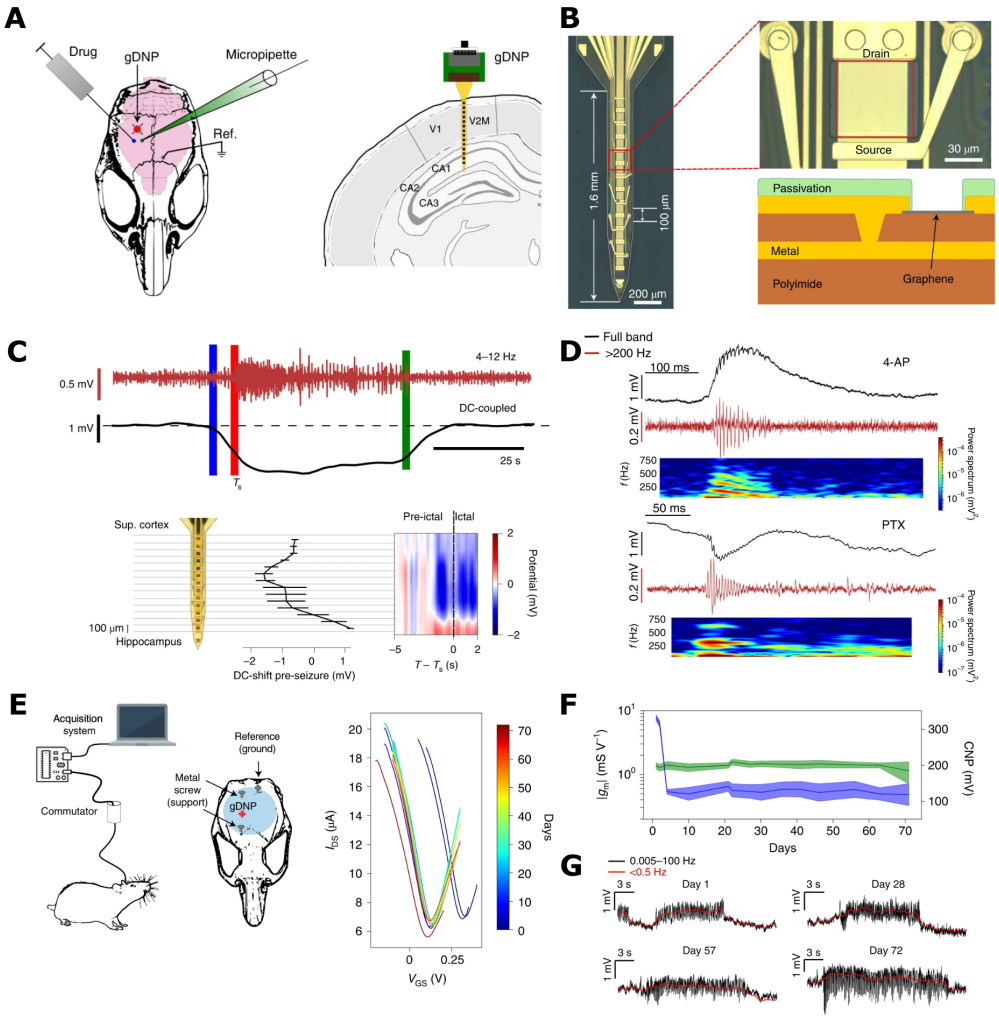

Figure 28: Summary of findings from Bonaccini Calia et al. (2021). **A)** Experimental configuration used for acute **in vivo** mouse recordings. Inserted probe through the visual cortex and hippocampus shown on right. **B)** Microscopy image of gSGFET depth probe. Magnified individual transistor structure shown on right. Similarly to epicortical gSGFET devices, graphene is in contact with the tissue and bridges the source and drain. **C)** Recording of 4-AP-induced seizure in acute mouse experiment. Analysis reveals an active DC-shift preceding the high-frequency onset of seizure. The active DC-shift is greatest in amplitude in deeper cortical layers and has reversed polarity in the hipppocampus. **D)** Examples of HFOs and sharp-wave ripples recorded from the hippocampus of mice following acute picrotoxin or 4-AP administration. **E)** Experimental configuration used for chronic recordings in WAG-Rjj rats. The experimental setup allows recording without movement restriction. Right panel shows high stability of gSGFET probes following implantation. I_{ds}-V_{gs} transfer curves were seen to shift shortly after implantation but stabilised following this. **F)** Plot of charge neutrality point and conductance across time showing gSGFET stability across the recording period following initial stabilisation. **G)** Spike-wave discharges shown at multiple time-points. gSGFET depth probes remained functional for the entire recording duration.

GFETs to be arranged into flexible, biocompatible depth probes. Our study argues that this technology is highly powerful for recording full bandwidth electrophysiology throughout the depths of the cortex and hippocampus. We propose that this will lead to a greater understanding of epileptic paroxysms by allowing greater dissection of activity at the epileptic focus; leading to improved surgical outcomes. Moreover, our chronic implantation studies demonstrate the ability of gSGFET probes to record for considerable periods of time with minimal damage to surrounding neural tissue.

Several studies have speculated whether there is a difference between SD induced in healthy tissue, and between those found to occur during particular disease states, such as epilepsy, stroke and migraine (Lauritzen et al., 2011). The body of work presented in this thesis will attempt to expand upon previous findings by utilising the gSGFET technology presented here to further characterise DC events observed during disease-related paroxysms. Moreover, I will combine this technology with imaging approaches to increase the depth of investigations, and provide the ability to spatially resolve paroxysmal events.

1.6 Proposed Investigations

The work presented in this thesis will utilise novel technology to interface with neural tissue; aiming to increase our understanding of both the efficacy of the technology and the disease-related process being investigated. Following from the previously introduced topics, this thesis presents research utilising combinations of both optical and electrophysiological techniques to stimulate and record from either intact brain tissue in awake headfixed rodents, or in acute brain slice preparations. One major section will be focused on the use of novel technology to investigate single-photon optogenetic stimulation in acute slices. The other major section will build upon previous gSGFET studies, integrate these devices with functional widefield imaging, and demonstrate the potential for these combined recordings to provide insight into epileptic seizures and SD.

1.6.1 Investigation of Single-Photon Optogenetic Stimulation in Acute Slices

Although multiple complex, powerful optogenetic stimulation devices exist, demand still exists for a simple, easy-to-use, commercially available system. Two-photon stimulation is powerful due to the high spatial resolution in all three spatial dimen-

sions. Moreover, combination of these devices with computer-generated holography allows fast stimulation of multiple cells (Shemesh et al., 2017). Nonetheless, these devices are complex, costly, and can be difficult to operate and maintain. Therefore, for simpler applications, there is a requirement for a more compact, affordable stimulation device. This demand led to the development of the Scientifica LASU system. As introduced previously, the LASU system is a single-photon optogenetic laser system which can be mounted directly onto the anti-vibration table of a standard electrophysiology rig. Moreover, the presence of two mirror galvanometers in the light path allows for fine adjustment of laser position at high speed; thus, facilitating the stimulation of multiple regions in quick succession. Although the technology for this system has existed for some time, extensive characterisation of the achievable spatial resolution has not been performed. Here, I characterise the LASU system and the potential for high resolution stimulation in dense cortical tissue.

Since my investigations into the LASU system are focused on the characterisation of spatial resolution in the dense three-dimensional network of an acute brain slice, I investigated multiple spatially-restricted opsin constructs. Traditional channelrhodopsin molecules are expressed throughout the soma and neurites of each expressing cell. Therefore, in a three-dimensional network, as found in an acute slice, the projections of neighbouring neurites may be activated when targeting a soma of interest. To circumvent these issues, I investigate excitatory opsin molecules that are either distributed throughout the entire membrane of transduced neurons (CoChR), or are spatially restricted to either the soma (SoCoChR) or distinct spatially-restricted somatic puncta (PunctCoChR).

To probe the efficacy of the LASU system in producing high resolution optogenetic stimulation, I expressed one of three different opsin constructs (CoChR, SoCoChR, or PunctCoChR) using stereotaxic AAV-mediated transduction. Following expression of the construct in the cortex, acute slices were prepared. An expressing cell, as identified by GFP fluorescence, was recorded from intracellularly using patch-clamp electrophysiology in whole-cell configuration. The patched cell was stimulated with varying pulse duration and laser power to generate an input-output curve. This process was performed for unrestricted, soma-restricted and puncta-restricted opsin constructs. Following comparison of the different constructs and determination of minimal stimulation parameters required to reliably generate a single action potential, LASU spatial resolution was investigated. Using the characterised minimal stimulation protocol, an array of stimulation points were placed across the field of view surrounding the patched cell. The response of the

patched cell was recorded following stimulation at each position in the grid. The data generated by this paradigm was used to characterise the relationship between stimulation distance and response. Therefore, facilitating calculation of the LASU system spatial resolution when stimulating cortical neurons expressing the different opsin constructs. The findings from this study will aid future investigations into network connectivity, and demonstrate the power of spatially-targeted constructs in achieving optogenetic stimulation with high specificity.

1.6.2 Investigation of Seizure-Associated SD Properties

The second major section of this thesis utilises combined optical and novel electrophysiological approaches to investigate the role of infraslow activity and DC events in epilepsy paroxysms. As described previously, understanding of the relationship between epilepsy and SD pathology has been limited by available recording technology. Firstly, electrophysiological recording devices have struggled to capture low frequency events due to poor stability, high electrode impedance and the requirement for a high-pass filter. Secondly, interfaces such as solution-filled glass micropipettes provide limited insight into SD spatial propagation due to difficulties in multi-site arrangement. Thirdly, recording interfaces are often incompatible with functional imaging methods due to high autofluorescence and poor transparency; thus limiting the ability to image nearby brain tissue. Graphene solution-gated field effect transistor arrays are able to overcome these limitations.

These investigations use a new experimental paradigm to provide insight into the relationship between epileptic seizures and pathological SD events. I demonstrate the first use of novel, low-autofluorescence parylene C gSGFET arrays and combine these with widefield Ca^{2+} imaging of the fast fluorescent genetically-encoded Ca^{2+} indicator, GCaMP7f. I optimise surgical procedures to enable maximal spatial coverage through implementation of large bilateral craniotomies. These large craniotomies increase the spatial information acquired relating to SD events and allow access to large areas of the brain for simultaneous gSGFET recording at multiple locations.

I utilise this combination of low-autofluorescence, multisite gSGFET recording with bilateral widefield Ca^{2+} imaging to investigate the diversity of events during epilepsy paroxysms in awake headfixed mice. Firstly, I use this combined approach to investigate SD events and their relationship to epileptic seizures using a picrotoxin seizure model. I demonstrate the feasibility of this paradigm in investigating differences between healthy and chronic pathological networks through recording both spontaneous and picrotoxin-induced SD events in CACNA1A S218L mice.

Moreover, I integrate behavioural imaging into the recording paradigm to increase the physiological relevance of acquired data.

Due to the information-rich data output of this experimental paradigm, a semi-automated analysis pipeline is generated. The presented pipeline processes the widefield imaging movies to achieve stabilisation and normalisation. Following this, events of interest, such as seizures and SD, are extracted along with their properties. These properties include spatial characteristics, such as coverage and velocity; as well as averaged information from all pixels in the field of view, such as amplitude and duration. Extracted event times are then synchronised with gSGFET recordings to allow analysis of relevant time windows from full-bandwidth electrographic recordings.

Together, the information from both widefield imaging and gGSFET recordings is used to examine the spatial and temporal relationship between SD events and seizures; to investigate whether seizures immediately preceding SD exhibit different properties to other seizures; to investigate the diversity of SD events associated with an epileptic network; and lastly, to demonstrate the power of this paradigm in unraveling the complexities of electrographic recordings. I demonstrate that this experimental paradigm and these analysis tools are able to provide insight into the fields of epilepsy and SD research by allowing detailed characterisation of the interaction of these two paroxysms.

Chapter 2

Materials and Methods

2.1 Materials and Reagents

Table of Materials		
Item	Supplier	Details
AAV8-hSyn-CoChR-GFP	Addgene	>1x10^{13}vg/ml
AAV8-hSyn-SoCoChR-GFP	Boyden Lab	>1x10^{13}vg/ml
AAV8-hSyn-PunctateCoChR-GFP	Boyden Lab	>1x10^{13}vg/ml
AAV9-hSyn-GCaMP7f-WPRE	Addgene	>1x10^{13}vg/ml
AAV9-hSyn-SFiGluSnFR.A184V	VectorBuilder	>1x10^{13}vg/ml
Isoflurane	Henry Schein	Surgical Anaesthesia
Sodium Pentobarbital	Animalcare Pentoject	200mg/ml
AP-5	Tocris	Slice NMDA Block
NBQX Disodium Salt	Tocris	Slice AMPA Block
Picrotoxin	Tocris	Slice GABA$_A$ Block
Picrotoxin	Tocris	Slice GABA$_A$ Block
Buprenorphine Hydrochloride	Ceva Vetergesic	0.3mg/ml
Meloxicam	Boehringer Ingelheim	Metacam
Saline	Vetivex	9mg/ml NaCl
Optical Lubricant	Bausch + Lomb	Viscotears
Dexamethasone	MSD Animal Health	Duphacort Q, 2mg/ml
Dental Cement	Kemdent	Simplex Rapid Powder and Liquid
Tissue Adhesive	3M Vetbond	-

Kwik-Cast	WPI	Quick-setting Silicon Polymer
Sylgard	Slow-setting Silicon PDMS Polymer	0.2mm thickness
paraformaldehyde (PFA)	Thermo Fisher Scientific	4% in phosphate-buffered saline (PBS)
PBS tablets	Sigma Aldrich	137mM NaCl, 2.7mM KCl and 10mM phosphate buffer solution
Sodium Azide	Sigma Aldrich	S2002

Table of Surgical Equipment		
Product	Supplier	Item/Info
Stereotaxic Frame	Kofp Instruments	Model 940 with digital display
Homeothermic apparatus	Kofp Instruments	Model 940 with digital display
Surgical Drill	NSK	Volvere i7 with E-type micro-motor
Small Drill Head	NSK	S-Max M95
Large Drill Head	NSK	VR-EB
Small diamond burr drill bit Head	Heraeus Kulzer	B250-012 SF
Large drill bit	Circuit Medic	Ball mill carbide 0.5mm diameter
Injection Pump	WPI	Microinjection Syringe Pump UMP3T
Hamilton Syringe	Thermo Fisher Scientific	Model 95 RN 5μl syringe
Hamilton 33G Needle	Thermo Fisher Scientific	4cm bevelled needle-point style 4
Surgical Support Screw	Plastics One, Bilaney	00-96X3-32

Table of Equipment for LASU Investigations		
Product	Supplier	Item/Info
Vibratome	Leica	Leica VT1200

Filamented Capilary Tubes	Warner Instruments	OD:1.50mm, ID:0.86mm
Pipette Puller	Sutter Instruments	P-97 Horizontal Puller
Peltier Heater	Scientifica	Slice perfusion temperature control
electron-multiplying charge-coupled device (EMCCD)	Photometrics	Evolve 512
LED Driver	Cairn	OptoLED
470nm OptoLED Head	Cairn	Slice GFP
Cool White OptoLED Head	Cairn	Slice jRCaMP1b
470nm MacroLED Head	Cairn	*in vivo* GCaMP7f
495nm Filter	Chroma	T495LP
585nm Filter	Chroma	T585LP
Patch-clamp Amplifier	Multiclamp	700B
BNC Terminal Block	National Instruments	BNC-2090A
Upright electrophysiology rig	Scientifica	Slicescope Pro 6000
4x objective	Olympus	PLN4X 0.1NA
40x objective	Olympus	LUMPLFLN40XW 0.8NA
IR lamp and gradient contrast tube	Scientifica	Dodt Gradient Contrast
LASU System	Scientifica	Laser, Galvanometer, Periscope
Motorised Micromanipulator	Scientifica	PatchStar
Peristaltic Pump	Cole Parmer	Masterflex L/S Economy Pump
Neutral Density Filter	ThorLabs	OD98
Silver Chloride Pellet	WPI	EP1

Table of Equipment for *in vivo* SD Investigations		
Product	Supplier	Item/Info
Headplate	Neurotar	Model 5
Head-fixed Habituation Platform	Neurotar	Multicage Training Arena
Silver Chloride Wire	Warner Instruments	0.25mm diameter

Head-fixed Recording Platform	Neurotar	Mobile HomeCage
1x Objective	Olympus	DF PLAN 1x
16-Channel Epicortical gSGFET Array	Guimera-Brunet Lab	-
gSGFET Amplifier	Gtec Medical Engineering GmbH	g.Hlamp Biosignal Amplifier
Glass Micropipette Headstage	Axon Instruments	CV-7B
Amplifier	Multiclamp	700B
Data Acquisition Unit	Cambridge Electronic Design	Micro1401 mkII
EMCCD	Photometrics	Evolve 512
LED Driver	Cairn	OptoLED
470nm OptoLED Head	Cairn	Slice GFP

Table of Solutions	
Solution	Ingredients
NMDG Slicing Solution	92mM, KCl: 2.5mM, NaH2PO4: 1.25mM, NaHCO3: 30mM, HEPES: 20mM, Glucose: 25mM, Thiourea: 2mM, Na-ascorbate: 5mM, Na-pyruvate: 3mM, CaCl2·2H2O: 0.5mM, MgSO4·7H2O: 10mM, titrated to pH 7.4 with 5M HCl
Artificial Cerebrospinal Fluid (aCSF)	NaCl: 119mM, KCl: 2.5mM, CaCl2: 2.5mM, MgSO4: 1.3mM, NaH2PO4: 1.25mM, NaHCO3: 25mM, Glucose: 10mM
K^+ gluconate intracellular solution	K-gluconate: 97mM, KCl: 38mM, EGTA: 0.2mM, HEPES: 20mM, MgATP: 0.4mM, NaCl: 6mM, NaGTP: 0.3mM, Phosphocreatine: 7mM

Cortex Buffered Saline	NaCl: 125mM, KCl: 4mM, CaCl2: 2mM, MgCl2: 2mM, Glucose: 10mM, HEPES: 10mM, titrated to pH 7.35 with 1M NaOH

2.2 Methods

2.2.1 Functional Characterisation of the LASU System

Here, I will present the experimental and analytical methods employed to investigate the LASU system stimulation resolution in acute slices.

Animals

Experiments conformed to the Animals (Scientific Procedures) Act 1986, and were approved by the ethics committee of the UCL Queen Square Institute of Neurology. Adult C57BL/6J mice were ordered from Charles River and used for acute slice preparation. Animals were housed in individually ventilated cages on 12-hour light-dark cycles with food and water provided ad libitum.

Stereotaxic Viral Injection for LASU Stimulation

Stereotaxic injection of either AAV8-hSyn-CoChR-GFP, AAV8-hSyn-SoCoChR-GFP or AAV8- hSyn-PunctateCoChR-GFP was performed into P26-P35 Male mice. Deep anaesthesia was induced by delivery of 4.5% isoflurane with anaesthesia maintained using 1.5-2.5% isoflurane following head-fixation of the animal in a stereotaxic frame. Small holes (0.5mm diameter) were drilled into the skull overlaying each cerebral hemisphere. 500nl of the selected AAV was injected (200nl/min) into the visual cortex of each hemisphere (coordinates relative to bregma ML= $\pm$2mm, AP=-2.9mm, DV=0.5mm). Following this, a minimum of three weeks recovery was allowed to ensure opsin expression throughout targeted neuronal populations.

Acute Slice Preparation

Mice were deeply anaesthetised using 5% isoflurane and sodium pentobarbital was intraperitoneally administered. Transcardial perfusion with a chilled N-Methyl D-Glucamine-based solution was performed. Following perfusion, the brain was extracted and 300μm thick coronal slices were prepared in the NMDG-based solution

using a vibratome. Slices were warmed to 35°C in the NMDG solution for 10 minutes before recovery at room temperature in aCSF for 1 hour.

Electrophysiology Recordings and Optogenetic Stimulation

Patch pipettes were pulled to a resistance of 3-5MΩ from filamented capillary tubes using a horizontal puller. Following this, the pipettes were filled with a K^+-gluconate-based intracellular solution. The sample was perfused with 32°C aCSF throughout investigations, with the solution containing AP-5, NBQX and Picrotoxin to respectively block AMPA, NMDA and $GABA_A$ receptors. Images of the cell soma were captured (using a Photometrics Evolve 512 EMCCD controlled by Micromanager) and expressing cells were identified using GFP fluorescence. Fluorescent cells with healthy visual properties (intact membrane and no visible opaque irregularities) were patched with a glass micropipette. Prior to the start of the experiment, the liquid junction potential for the K^+-gluconate-based intracellular solution was calculated to be -12mV. This was subtracted from recorded potentials throughout the experiment. Membrane potential was recorded using whole-cell current clamp following bridge balance correction. Healthy cells suitable for further investigation were defined as those with a resting membrane potential below -60mV and healthy action potential firing in response to current injection. Access resistance was regularly recorded during the experiment to monitor seal quality. Recordings were terminated if seal quality was seen to deteriorate. Following this, the Scientifica LASU software was used to control the Scientifica LASU system and deliver pulses varying in intensity and duration to the cell soma. Custom-written LABVIEW software was used for electrophysiology acquisition.

Analysis

Custom written LabView software was used to import the acquired electrophysiology data into Clampfit for analysis of neuronal responses to both light stimulation and current injection. Any transient events (<5ms) exhibiting depolarisation beyond 0mV were classified as action potentials. Custom written MATLAB scripts were used to analyse images and quantify stimulation distance from the soma. Distances from the soma were binned into the following groups $<10\mu$m = Soma; $>10\mu$m and $<30\mu$m = 20μm; $>30\mu$m and $<50\mu$m = 40μm; $>50\mu$m and $<70\mu$m = 60μm; $>70\mu$m and $<90\mu$m = 80μm; $>90\mu$m and $<110\mu$m = 100μm; $>110\mu$m and $<130\mu$m = 120μm; $>130\mu$m and $<150\mu$m = 140μm. Stimulation points falling in the approximate location of the patch pipette were excluded due to scattering. All graphs were plotted using Igor Pro 8.

2.2.2 Investigating the Relationship between Seizures and SD

Here, I will describe the experimental and analytical methods employed during *in vivo* investigations of seizures and SD. The surgical methods remained constant throughout investigations, except for a few modifications (outlined in Chapter 5). However, the analytical methods presented in this section were only used during preliminary investigations. The custom-built Python analysis pipeline used for the majority of analysis is presented in Chapter 6.

Animals

Heterozygous (HET) S218L knock-in mice on a C57BL6/J background were mated with wild-type (WT) C57BL6/J mice (ordered from UCL P-Block). The resulting offspring were ear-notched and genotyped (Post-PCR restriction digest-based method; UCL Biosciences Huxley Building Molecular Biology Facilities) with genetic identity obscured from the experimenter. Male and Female mice aged 2-3 months were initially selected at random from the colony to avoid experimental bias. WT and HET mice were utilised in these investigations. Homozygous (HOM) animals were excluded from investigations due to their high SUDEP susceptibility following invasive surgery (Loonen et al., 2019).

Viral Injection and Headplate Attachment

Stereotaxic viral injections were performed following induction of deep anaesthesia by 4.5% isoflurane and maintenance of anaesthesia using 1.5-2.5% isoflurane. Following head-fixation and stable anaesthesia induction, a combined analgesic containing buprenorphine hydrochloride (0.5mg/Kg; 20%), metacam (15mg/Kg; 30%) and saline (50%) was injected subcutaneously. Dexamethasone (1mg/kg) was injected subcutaneously to minimise inflammation. A temperature-controlled heating pad in a feedback loop with a rectal thermometer was used to maintain stable body temperature throughout each surgery. The scalp was removed with the remaining connective tissue soaked and scraped away. Small burr-holes were drilled above three sites on each hemisphere (only one for initial unilateral recordings) of the cortex (coordinates relative to bregma- ML: ±2.0mm; DV: 0.5mm; AP: 0.9mm, 1.9mm, 2.9mm). 250nl of hSyn-GCaMP7f-WPRE diluted in 250nl filtered artificial cerebrospinal fluid (aCSF) was injected by Hamilton syringe into each of the six aforementioned sites. A small burr hole in the contralateral anterior region of the skull was created to insert a support screw. A headplate was attached via dental

cement and tissue adhesive to the surface of the skull. All exposed regions of skull surrounding the headplate were covered in the dental cement mixture with the inner region left uncovered for the forthcoming craniotomies. Once the dental cement had dried, the inner region was coated in a quick-setting silicon polymer. Once dried, 0.7ml saline was administered subcutaneously and the mouse allowed to recover. During the initial stage of this recovery, the mouse was floor-fed and DietGel was available to combat post-operative dehydration.

Habituation

Following at least a three-week recovery period, the mice underwent their first habituation session. Animals were head-fixed on the training platform and allowed to habituate for 15 minutes. Following a minimum of 20 hours, a second habituation was performed for 30 minutes. Lastly, with the same interval, a third was performed for 60 minutes. If a significant period of time transpired between the final habituation session and recording, a fourth habituation session lasting 30 minutes was added within 2 days of the experiment. Moreover, animals were regularly handled to minimise anxiety during experiments.

Craniotomy

At least four weeks following viral injection, anaesthesia and analgesia was induced and maintained as mentioned previously. Dexamethasone was injected as before. Mice were headfixed in a stereotaxic frame and the silicon covering removed. Excess dental cement was drilled down with a large drill. A small hole in the skull above the left olfactory bulb was drilled to allow later insertion of a AgCl reference electrode. Following this, a diamond-burr drill was used to outline a large bilateral craniotomy over the visual, somatosensory and motor cortices. Periodically, the skull was soaked in cortex-buffered saline (CBS) and any minor bleeding from the skull was halted with haemostatic sponge. Once the skull was sufficiently thinned around the craniotomy site, thin forceps were used to lift the loose skull. Any bleeds were halted using sterilised tissue paper or haemostatic sponge, and the cortical surface prevented from drying by application of CBS. A small piece of previously solidified slow-setting silicon polymer (PDMS) was cut and placed on top of the craniotomy site and fast-setting polymer (Kwik-cast) used to protect the region during recovery. Saline was administered as before and the mouse was allowed 2-4 hours to recover before experimentation. The health status of the animal was assessed by normal, pain-free behaviours and explorative movement before proceeding. The experiment was terminated in cases of major bleeding during craniotomy

surgery or impaired recovery.

in vivo Recording Preparation

Following recovery, mice were head-fixed in the headfixation recording chamber and the silicon removed. A 1x objective was lowered and focused at the cortical surface. A Ag/AgCl wire was inserted into the small craniotomy above the left olfactory bulb. A previously selected and characterised 4x4 16-channel gSGFET array was laid upon the dura above the somatosensory/visual cortex. A custom Simulink model (Gtec; MATLAB) was used to generate an I_{ds}-V_{gs} curve for the gSGFET, with MATLAB code used to obtain the optimal V_{gs} point below the charge neutrality point, signifying the maximum of the mean transconductance across all transistors. All transistors were biased at this calculated optimum throughout the recording period. Multi-channel, full-bandwidth electrophysiology was recorded using a Simulink model and a custom g.HIamp biosignal amplifier sampling at 9.8 or 19.2kHz. More information about the gSGFET acquisition configuration can be found in Masvidal-Codina et al., 2019. A glass micropipette was inserted approximately 500μm into the visual cortex to record intracortically. Images were acquired in 29,000 frame stacks at 49.06Hz (20ms exposure) using Micromanager. Spike2 (Cambridge Electronic Design) software was used to record local field potential (Multiclamp 700B, voltage-clamp) from the glass micropipette (3-5MΩ). All acquisition was synchronised by sweep initiation through the delivery of transistor-transistor logic (TTL) pulses and by recording camera frame times.

Characterisation of Seizures and Spreading Depression

gSGFET and glass micropipette recordings were continuous through the experiment. Initially, two to three 10 minute baseline imaging sweeps were recorded. Following this, injection of picrotoxin (10mM, 200nl, 50nl/s) was performed into the visual cortex. Recording of activity following chemoconvulsant delivery was performed until 2-3 hours post head-fixation. Following this, sodium pentobarbital was injected (i.p.) and a terminal SD recorded using both imaging and electrophysiology (for maximal fluorescence and noise measurements in the absence of brain activity). A final I_{ds}-V_{gs} curve was generated for the gSGFET to assess experimental stability for calibration.

Post-Experiment Fixation

Experiment termination was confirmed by cervical dislocation. Post-experiment, the brain was dissected from the skull and fixed in PFA (4% in PBS) overnight at 4°C. The following day the brain was washed in PBS before storage in PBS + sodium azide (0.02%) at 4°C.

Analysis

The preliminary imaging analysis shown prior to full pipeline creation was generated using custom-written MATLAB scripts. Following subtraction of dark-current, regions of interest (ROI) were manually selected on the image stack. Fluorescence intensity in these regions were averaged among all pixels and a single trace was plotted for each ROI. Custom-written scripts using Python 3.7 packages (Matplotlib 3.2.0, Numpy 1.17.4, Pandas 0.25.3, seaborn 0.9.0, Neo 0.8.0) and the custom library PhyREC (PhyREC4, https://github.com/aguimera/PhyREC) were used to calibrate gSGFET data before traces were plotted. LFP from the glass micropipette was processed using Spike2. The main analysis framework presented in this thesis followed the construction of a comprehensive, semi-automated, combined analysis pipeline. Since the creation of this pipeline comprises a significant body of the work from this research project, these analysis tools will be introduced separately in Chapter 6.

Methods to Reduce Experimental Bias

Throughout this work, several efforts were made to minimise the influence of experimental bias. Initially, genotype blinding was performed prior to recording sessions. However, as detailed in Chapter 5, S218L HET animals demonstrated a clear difference in baseline activity (marked by the presence of spontaneous pathological discharges and SDs). Therefore, experimental blinding to genotype was determined to be ineffective. Instead, since a comprehensive analysis pipeline requiring minimal user input was constructed (detailed in Chapter 6), this allowed data to be processed in a consistent manner with a reduced probability of user bias. Putative events underwent manual screening, however, the benefit of removing false positives outweighed the potential for user bias. Moreover, all event screening during analysis stages was performed blind to genotype. Therefore, analysis of events could proceed with minimal experimenter bias.

Chapter 3

Scientifica Ltd

A large aspect of this collaborative, industry-funded research project involved systematic interaction with multiple departments of the industrial partner- Scientifica UK. Scientifica, founded in 1997, has a focus in developing bespoke novel imaging and electrophysiology tools, tailored to assist neuroscientists in probing both fundamental and translational questions. Scientifica deliver a wide-range of products and associated services, including the manufacture and assembly of complete electrophysiology microscopes, for *in vivo*, *ex vivo* and *in vitro* use. Accompanying these microscopes are accessory devices, specifically developed with the modern-day electrophysiologist in mind: examples of this include large surface-area fan-less cameras, low-vibration micro-manipulators, optogenetic delivery systems and the respective accompanying software. A significant part of this doctoral project has involved developing an understanding of these products and facilitating the development of novel tools.

3.1 LASU Optimisation and Development

As previously mentioned, the development and optimisation of the Scientifica LASU system is a central component to the industry aspect of this PhD project. Due to device finalisation occurring shortly before the start of this project, a considerable amount of work was invested in improving the usability of the LASU system, mainly through guided development of the accompanying LASU software.

The LASU software is a custom-built application, designed to allow easy and efficient interaction between the user and all LASU-associated hardware, including both the photostimulation device and the camera used for visualisation. Constructed using National Instruments LABVIEW, the LASU software allows efficient communication with the laser power supply and the spatially-guiding mirror gal-

vanometers: the end result is the ability to deliver either continuous or pulsed stimulation at user-defined locations in the sample, monitored using the live displayed camera image. Moreover, fine, rapid control of the mirror galvanometers allows the construction of fast, complex stimulation paradigms (e.g. spiral and raster stimulation).

Although, considerable work had been previously invested in the development of this software, during the start of this doctoral project, the LASU software was incompatible for use with our electrophysiology rig configuration. Firstly, integration of a high speed, high sensitivity EMCCD was required (Photometrics Evolve 512). Once integrated, laser calibration procedures required reconfiguration: spatial calibration of the LASU system is achieved through voltage application to the mirror galvanometers, and the resulting position of maximum intensity used to define positions of stimulation for each mirror position. Due to the camera properties differing from those initially compatible with the LASU software, several issues required troubleshooting. These included resetting the galvanometer calibration range and adjusting camera interaction controls. Moreover, several other issues required addressing, including improper spiral and raster stimulation paths, mispositioned grid stimulation and false error messages. Working closely with the Scientifica software development team, we were able to resolve these issues to result in an effectively functioning system; thus leading to wide release of the software to the scientific community.

3.2 Sales

An infrequent, yet recurring aspect of this Scientifica collaboration involved assisting the sales staff in demonstrating LASU functionality. Members of different research institutions interested in acquiring a LASU system for their experiments were invited to our UCL laboratory. Here, I provided assistance through live demonstration of the LASU system configuration, calibration and operation. A large aspect of my contribution involved interpreting individual experimental requirements, and using experimental experience to advise whether the LASU system could be effectively used to achieve the proposed goals. Consequentially, I assisted in the sale of several LASU systems and often the accompanying Scientifica SliceScope.

3.3 Marketing

In recent years, the rapid advancement of technology has progressed information sharing significantly. A large part of this advancement is the ability to find relevant information online to solve a problem of interest. Of course, much of this information is available in peer-reviewed scientific literature. However, much also exists in condensed forms on internet blogs. As a result, a useful method of spreading brand awareness and advertisement can be achieved through the sharing of information relevant to products being sold, delivered under the name of the company. In this case, the company, Scientifica, ask individual researchers to produce relevant research blogs and articles that aim to assist potential customers in solving challenging problems. As a result, more individuals visit the Scientifica website, spend more time understanding the products available, thus, increasing brand awareness.

To assist the marketing department, I have written and published an article on the Scientifica website under the 'NeuroWire' research blog titled 'Planning and Optimising an Optogenetics Experiment'. The article can be found at the following link: https://www.scientifica.uk.com/neurowire/planning-and-optimising-an-optogenetics-experiment

3.4 Research and Development

More recently, Scientifica have invested significant work in the development of a new product. Due to a signed confidentiality agreement, exact details of this work can not currently be disclosed. However, significant work was invested to guide the development of this product. On multiple occasions, individuals from the Scientifica team visited UCL to gain a greater understanding of individual experimental requirements and how experimental equipment could be optimised to streamline experiments and increase usability. This aspect of the collaboration involved the delivery of experimental demonstrations to Scientifica staff as well as several discussions on experimental requirements, hardware compatibility and device interface design.

3.5 Concluding Remarks

Altogether, the Scientifica aspect of this iCASE collaboration; firstly, allowed me to gain experience from multiple different departments of the organisation; and secondly, allowed me to fully understand LASU system functionality through optimisa-

tion, knowledge that proved essential for later investigations of different excitatory opsins and single-photon stimulation resolution.

Chapter 4

LASU Investigations

4.1 Introduction

The industry-sponsored research presented in this section of the thesis has three major goals. Firstly, this work aims to aid future researchers by providing detailed characterisation of the limits of single-photon stimulation in acute brain slices. Secondly, in the process, this work will present data supplementing the LASU system documentation; therefore, aiding future sales by allowing potential customers to identify system suitability in addressing their question of interest. Thirdly, I will characterise novel spatially-restricted excitatory opsins and their ability to improve stimulation specificity. I hypothesise that the combination of soma-targeted opsin constructs with focused laser stimulation will push the limits of single-photon excitation, and lead to high resolution activation of small neuronal populations.

4.1.1 Selection of a Model for Investigation

Since the LASU system is a compact, table-mountable system, the system is compatible with multiple experimental configurations. As a result, this allowed selection from primary neuronal cultures, acute slices, or *in vivo* intact preparations for LASU investigation. Since patch-clamp electrophysiology was required to fully characterise neuronal activation following LASU stimulation, I excluded the *in vivo* paradigm from consideration. Patch-clamp electrophysiology is possible *in vivo*, however, suffers from several limitations. Firstly, neuronal visibility *in vivo* is poor, resulting in difficulties efficiently targeting single neurons. Secondly, since the tissue is intact, the potential for repeated micropipette insertion is limited due to cumulative damage and bleeding (Jouhanneau & Poulet, 2019). Therefore, I focused consideration on primary neuronal cultures and acute brain slices. I performed preliminary in-

vestigations in neuronal cultures, however, I diverted my focus from this model due to two main reasons. Firstly, dense expression in neuronal cultures requires a large volume of AAV (Royo et al., 2008). Secondly, and more importantly, cultured neurons are structured as a monolayer. In order to fully challenge the limits of LASU stimulation, I decided investigation in a sparse monolayer to be simplistic. As a result, acute slices were selected as the model of choice. Firstly, efficient transduction could be achieved in a small area using a small volume of AAV. Secondly, neurons are arranged in a three-dimensional structure and therefore, LASU resolution can be properly challenged. Coronal slices were selected to keep cortical microcircuits intact. Therefore, this work proceeded to investigate LASU stimulation in acute coronal slices.

4.1.2 Optogenetic Actuator Expression

In order to expand the current boundaries of single-photon stimulation, I selected novel spatially-targeted channelrhodopsin constructs for investigation. Targeted stimulation of selected neurons may result in inadvertent stimulation of neighboring neurons if channelrhodopsin is present throughout neuronal processes (see Figure 29). Therefore, I investigated LASU stimulation resolution in acute slices expressing somatic ChR constructs. The spatially-restricted opsin in this case was CoChR, a high photo-current opsin channel enabling generation of large responses even when expression is limited to smaller areas of the membrane. Moreover, for comparison, I investigated the same construct without the spatial restriction. Therefore, this allowed determination of the effect of opsin spatial restriction on LASU stimulation resolution. Moreover, AAV-mediated transduction was used as the method of expression. Firstly, since the selected soma-targeted constructs are novel, no relevant transgenic animal lines exist as of yet. Secondly, AAV-mediated transduction results in dense expression in multiple neurons at the injection site, and therefore, allows proper interrogation of stimulation resolution. Thirdly, the AAV vectors encoding the novel spatially-restricted opsins were previously unpublished and were generated by our collaborators (Dr. Or Shemesh, Prof. Ed Boyden; Synthetic Neurobiology Group, MIT, USA). As a result, I used AAV-mediated transduction of acute coronal slices to investigate three opsin constructs; the soma-targeted SoCoChR (Shemesh et al., 2017); the punctate, soma-targeted construct (manuscript in preparation), Punctate CoChR; and three, the untargeted core construct CoChR (Klapoetke et al., 2014).

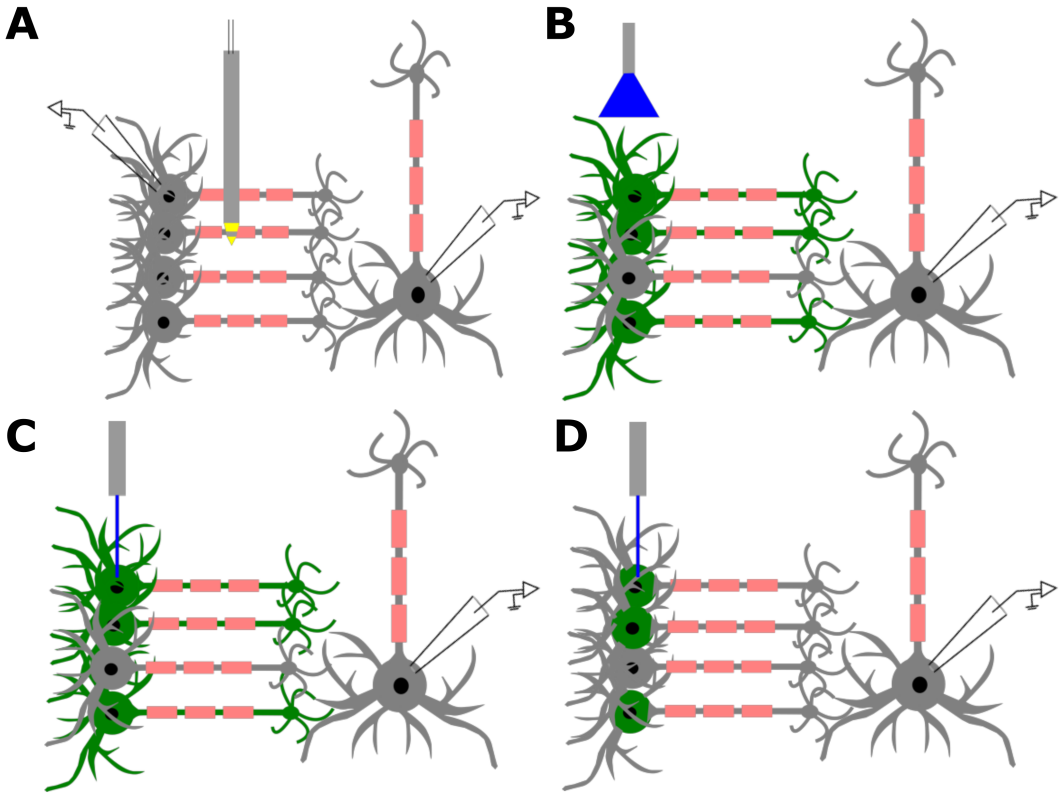

Figure 29: Comparison of electrical and optical stimulation paradigms to investigate cortical network communication. **A)** Electrical stimulation paradigm showing both paired patch clamp recordings and an extracellular stimulation paradigm using a bipolar electrode. **B)** Optical stimulation paradigm showing widefield illumination of a presynaptic population expressing non-targeted ChR. **C)** Optical stimulation paradigm showing LASU stimulation of a presynaptic population expressing non-targeted ChR. Stimilation will result in activation of neighboring cells due to depolarisation of adjacent neurites. **D)** Optical stimulation paradigm using the LASU system to stimulate soma-targeted opsin constructs. Stimulation will result in minimal activation of neighbouring neurites leading to stimulation with a higher spatial resolution.

4.2 Results

4.2.1 Characterisation of Different Opsin Variants

The first stage of these investigations probed the sensitivity of the previously named opsin constructs; and the photostimulation paradigm required to achieve reliable, minimal stimulation. To achieve this, I delivered single pulses to the soma of a patched opsin-expressing neuron using the LASU system (Figure 30B). Simultaneously, I recorded evoked responses and quantified the number of elicited action potentials (Figure 30D). Pulse duration and stimulation power were varied to generate an input-output curve describing the relationship between light delivered and neuronal response. The data revealed that the SoCoChR expression levels in cortical neurons is insufficient to achieve reliable LASU-mediated action potential induction. PunctCoChR-expressing neurons, on the other hand, showed high sensitivity to LASU stimulation: action potentials were reliably induced, with the response to a single pulse modulated by pulse duration and stimulation power (Figure 30E&F). Moreover, reliable induction of pulse trains was also achievable (Figure 31). CoChR expressing cells showed a similar sensitivity to photostimulation as that seen in PunctCoChR-expressing neurons. Action potentials were reliably evoked in CoChR-expressing neurons, however, response modulation by altering pulse duration was not possible (Figure 33A). I utilised this information to guide opsin construct selection for further investigation.

4.2.2 Selection of a Stimulation Paradigm to Investigate LASU Resolution

To appropriately select an opsin construct and stimulation paradigm to investigate the spatial resolution of LASU stimulation, I assessed the input-output curves for CoChR, SoCoChR and PunctCoChR. Due to the inability of SoCoChR-expressing neurons to reliably fire action potentials following LASU stimulation, I excluded this construct from consideration for further use. Both CoChR and PunctCoChR showed a high photosensitivity with reliable induction of action potentials (Figure 30E&F, Figure 33A). However, the response to LASU stimulation in CoChR-expressing cells showed high variability, with somatic stimulation often resulting in multiple action potentials and a slow recovery to back resting membrane potential (Figure 33C). Therefore, going forward, LASU investigations focused on the use of PunctCoChR. Nonetheless, to probe the effect of spatial-restriction on stimulation resolution, I also investigated untargeted CoChR.

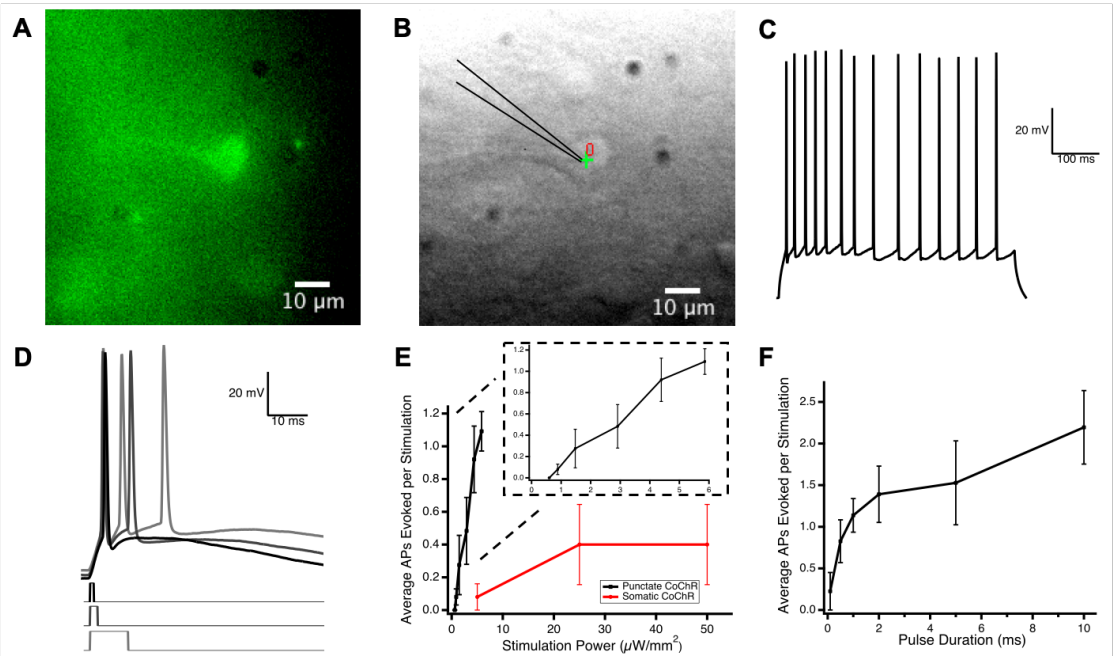

Figure 30: Electrophysiological characterisation of opsin-expressing cortical neurons following LASU stimulation. **A)** Cortical neuron expressing Punctate CoChR, as shown by GFP expression. **B)** Transmitted light image of the same area as in **A** with patch pipette and point of optical stimulation shown. **C)** Response of cortical neuron to current injection (+200pA) for 500ms. **D)** Characteristic traces recorded from a Punctate CoChR expressing cell following stimulation ($5.8\mu W/mm^2$) for 1ms (Black), 2ms (Dark-grey) and 10ms (Light-grey). **E)** Average number of APs evoked following the delivery of a single pulse varying in stimulation power. Evoked responses shown for Punctate CoChR (Black; 1ms) and Somatic CoChR (Red; 10ms) expressing cells. Inset showing expanded responses of Punctate CoChR expressing cells. N=5-16 animals. **F)** Average number of APs evoked in a Punctate CoChR expressing cell following the delivery of a single pulse ($5.8\mu W/mm^2$) varying in duration. N=6-14 WT male mice.

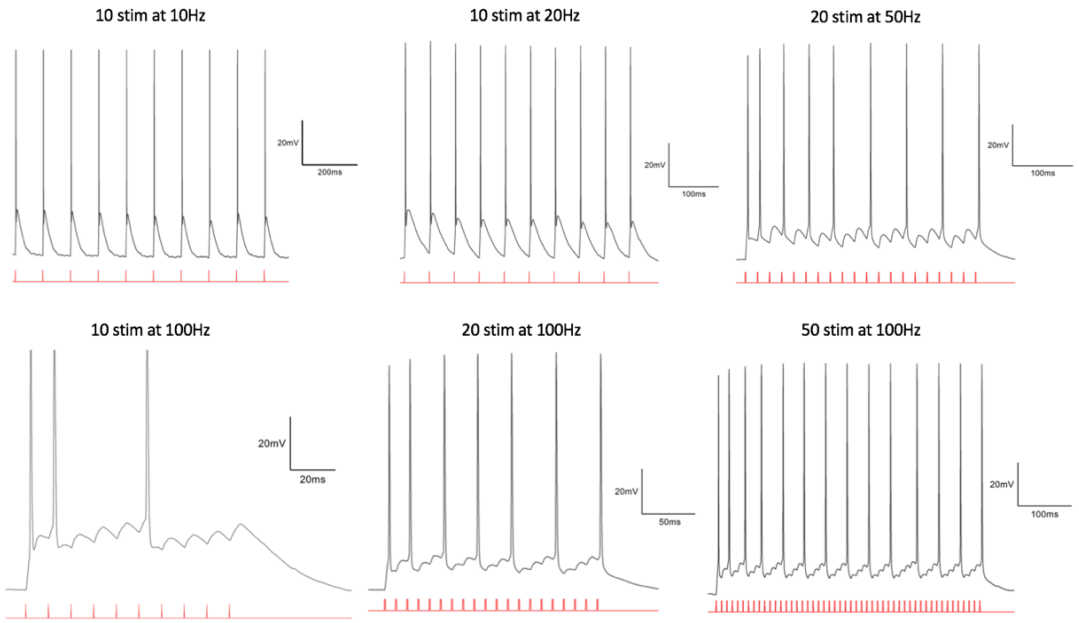

Figure 31: Typical responses from PunctCoChR-expressing cortical neurons following the delivery of pulse trains at different frequencies (5.8μW/mm^2 stimulation power, 1ms pulse duration).

To select the optimal stimulation paradigm for each construct, I selected the lowest stimulation power and pulse duration observed to reliably induce a single action potential. For PunctCoChR, the previously-generated input-output curves indicated a 1ms pulse of power 5.8μW/mm2 as optimal for further investigation (Figure 30E&F). In the case of CoChR-expressing neurons, I selected the minimum power and pulse duration achievable by the LASU system due to the high photosensitivity of CoChR-expressing neurons occasionally resulting in multiple action potentials following somatic stimulation with these parameters (Figure 33C).

4.2.3 Charactisation of LASU Resolution

To achieve the primary goal of assessing the limits of LASU system resolution, I expressed PunctCoChR, and randomly dispersed a 64-point grid across the field of view (Figure 32B). A single pulse was delivered at each point. To confirm a reliable response from the patched cell, each grid stimulation began with somatic stimulation at the same power to confirm an action potential could still be reliably evoked. I plotted average neuronal response for each point in the grid against the binned distance from the nearest edge of the patched soma. As a result, I was able to produce a spatial profile of stimulation resolution. Grid stimulation revealed high resolution stimulation, with the probability of evoking an action potential dropping

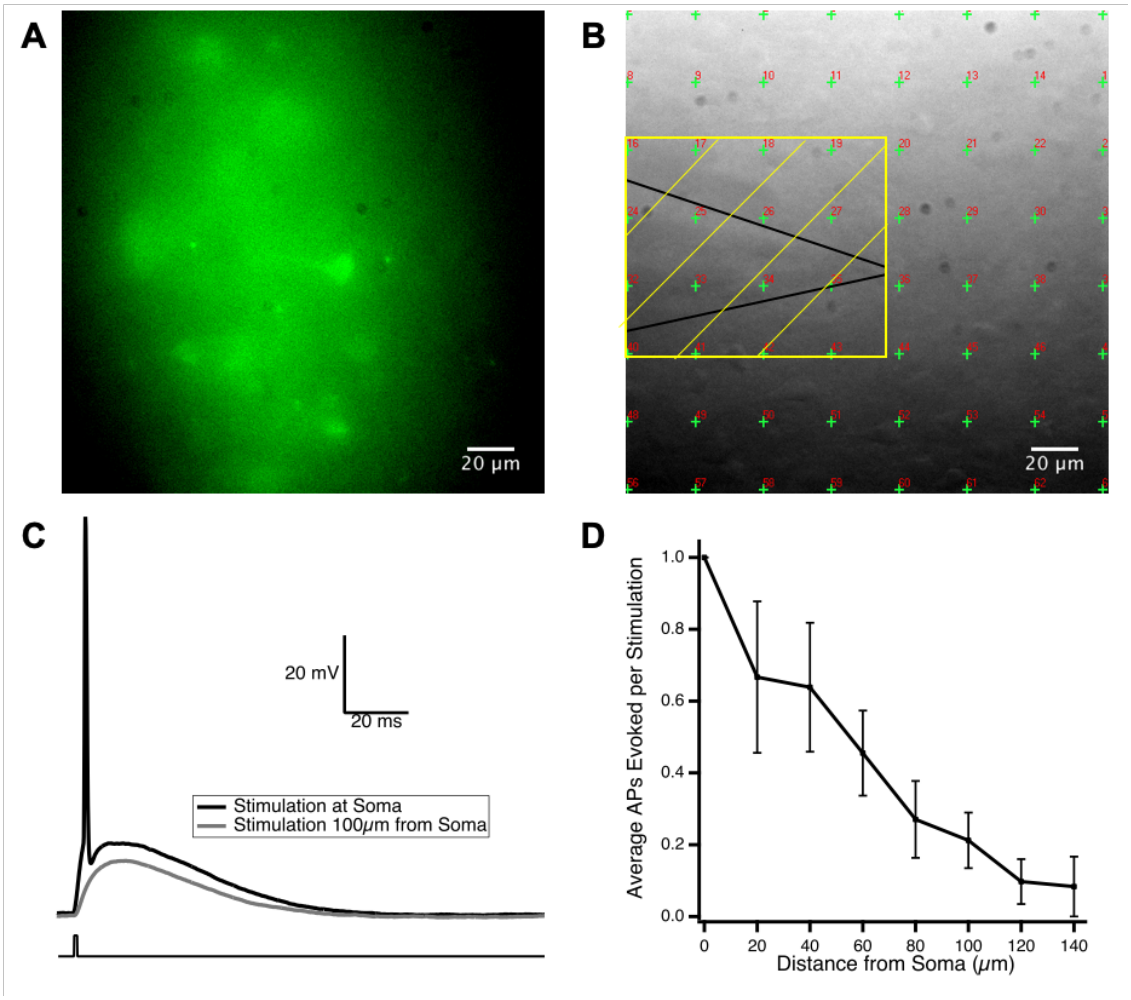

Figure 32: Characterisation of LASU resolution in stimulating PunctCoChR-expressing cortical neurons. **A)** Cortical neurons expressing Punctate CoChR, as shown by GFP fluorescence. **B)** Grid of multiple individual points spread evenly throughout the field of view. Black lines depict the location of the patch pipette and the yellow region indicates points excluded from analysis due to light scattering by the patch pipette. **C)** Characteristic response of cortical neuron to LASU stimulation (bottom) either at the soma (black) or 100μm away from the soma (light-grey). **D)** Averaged responses following stimulation (1ms pulse; 5.8μW/mm^2) at different distances from the soma. Data combined in bins based on the distance from the cell soma. N=6 WT male mice.

below 50% at 60μm from the soma (Figure 32D). Altogether, this demonstrated the generation of powerful control over neuronal dynamics by combining focused laser stimulation with novel targeted opsin constructs.

4.2.4 Investigating the Contribution of Somatic-Restriction on LASU Resolution

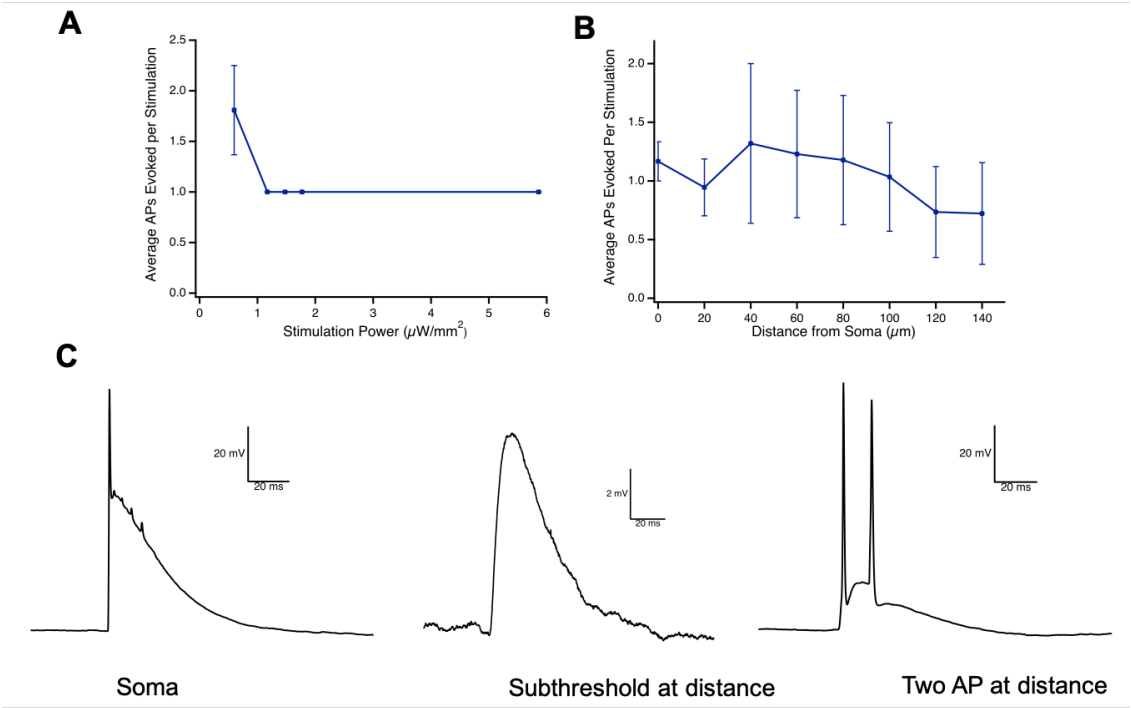

Figure 33: Characterisation of LASU resolution in stimulating untargeted CoChR-expressing neurons. **A)** Average number of action potentials evoked as a function of LASU stimulation power. N=2-4 animals. **B)** Similar characterisation of LASU resolution using the grid stimulation paradigm presented in Figure 31. N=3 animals **C)** Example traces from a single cell showing variable responses with untargeted CoChR.

To investigate the contribution of soma-targeted expression to the observed high stimulation resolution, I repeated the previously described 64-point grid protocol for untargeted CoChR-expressing neurons. CoChR- expressing cells demonstrated unreliable responses following somatic-stimultion (Figure 33C). Moreover, grid stimulation resulted in a mixture of single/multiple action potentials and subthreshold depolarisation. I quantified response to stimulation at different distances from the soma, as before. Quantification revealed a large insufficiency in stimulation spatial resolution, thus preventing targeted modulation of activity in small neuronal populations (Figure 33B). This suggests that along with spatially-constricted light,

spatially-constricted expression is required to maximise single-photon stimulation potential and achieve highly selective control in an intact network.

4.3 Discussion

Using the Scientifica LASU system, I demonstrate the ability to reliably activate cortical neurons in acute brain slices from mice. I tested three opsin constructs, both spatially-restricted and untargeted, to reveal that the punctate CoChR construct was the most effective. I established the stimulation paradigm required to generate reliable responses and characterised the spatial resolution of the LASU system in stimulating punctate CoChR-expressing cells. These results revealed that single-cell resolution stimulation was not possible without the use of a more complex photostimulation system, such as those using multi-photon excitation or holographic pattern generation (Shemesh et al., 2017). However, the presented results support the starting hypothesis that the combination of focused laser stimulation with spatially-restricted opsins will expand the boundaries of what is currently possible with single-photon systems.

Although single-cell resolution stimulation is not possible, the spatial resolution achieved by the LASU system is competitive with top-range single-photon photostimulation devices. Similar devices, although usually custom-built in-house, can be seen. An example of this is the single-photon, galvanometer-guided laser illumination device used by Kätzel and colleagues (Katzel et al., 2011). Kätzel and colleagues aimed to investigate cortical interneuron organisation and connectivity. Their photostimulation device was used to investigate the location of inhibitory inputs onto excitatory cells using a similar grid stimulation approach to ours. Notably, the device used in Katzel et al. (2011) displays a superior spatial resolution in that the distance before spiking probability drops to 50% is lower. However, several key differences to these LASU investigations can be seen. Firstly, interneurons were investigated as opposed to all neurons indiscriminately, as performed here. This would result in a difference in resolution due to the smaller size/membrane area of interneurons compared to pyramidal cells (Krimer & Goldman-Rakic, 2001). Moreover, spike probability is reported as opposed to these LASU investigations which report average action potential counts. Therefore, I am able to differentiate between stimulation causing multiple action potentials and those causing single spikes; which is especially important in the case of interneurons which demonstrate a propensity to burst fire (Golomb et al., 2007).

Another important point is that Katzel et al. (2011) demonstrate considerable

work on the optimisation of transgenic opsin expression at a sufficiently low level to cause selective high expression in interneuron somata without causing high levels throughout the neuropil. As a result, the expression level is also low in the soma and it appears that action potentials can not be evoked as reliably (spike probability at soma < 0.8) as in the data shown here. The protocol presented here shows a simple method to achieve somatic expression of ChR; with the expression level sufficient to consistently generate single action potentials at the soma. Moreover, due to this higher level of somatic expression, the pulse duration used throughout these experiments is considerably lower. Therefore, this allows investigation of the role of high frequency activity; a task important for understanding excitation, inhibition and synaptic integration in cortical circuits.

Altogether, these investigations combining the Scientifica LASU system with novel targeted opsin constructs demonstrate the ability to achieve reliable, high-resolution photostimulation in acute slices, using commercially available tools and software. Moreover, this high-resolution is contingent on the spatial restriction of both photostimulation and the optogenetic modulator. The combination of these novel tools, and the resulting stimulation resolution will be a powerful addition to the modern neuroscientist's toolbox.

4.4 Future Directions

Future work building on these investigations will look to characterise the LASU system in different cellular environments; as well as applying this technology to investigate pathological cortical communication in disease states. The presented paradigm is able to assist with a major problem in slice electrophysiology investigations. Often these studies require paired patch-clamp recordings from multiple neurons in a dense network. However, it is frequently unclear which pairs of neurons form functional connections. Researchers deduce the presence of these functional connections through patching multiple neurons simultaneously, and stimulating and recording from pairs of cells. This is a laborious and difficult method of ascertaining whether two neurons are connected to one-another. Moreover, patching additional cells often causes movement which compromises the seal quality of the previously patched cell. The LASU system combined with PunctCoChR is able to assist with this process. Instead of patching multiple neurons and repeatedly disturbing the tissue of interest, a single neuron can be patched and light delivered to different surrounding regions. When a post-synaptic response is observed on the patched cell, it is clear that the photostimulated neuron forms a functional synapse. Therefore, this

method can be used to either stimulate multiple presynaptic neurons in quick succession; or to identify a connected presynaptic cell to be targeted for paired patch clamp recordings. The overall result is increased experimental efficiency, reduced animal tissue usage, and greater flexibility in investigating integration in neuronal networks. Of course, these powerful advantages come with the caveat of the requirement for stereotaxic injection of the opsin-expressing AAV. Future work will aim to utilise these advantages to construct elaborate investigations of network integration in healthy and pathological cortical microcircuits.

Additional future directions will also characterise LASU stimulation in primary neuronal cultures. Previous work has been invested into this, however, investigations have been limited by the method of expression: plasmid transfection (e.g. calcium phosphate, lipofection, magnetofection) was found to be unable to generate an expression density sufficient to utilise the LASU system's ability to stimulate multiple neurons in succession. AAV-mediated transduction of cultures is possible, however, it is inefficient due to the requirement for delivery of a large volume of the virus per coverslip. As a result, the DNA encoding the PunctCoChR sequence has been subcloned into a plasmid containing lentiviral expression elements. I have produced the virus and preliminary investigations revealed neuronal depolarisation in response to photostimulation. Due to reduced scattering in cultures, the expectation is to see an improved spatial resolution when compared to investigations in acute slices. Future work will aim to optimise transduction parameters and successfully establish targeted photostimulation in vitro, which will more likely lead to single-cell resolution stimulation.

In future studies, it would also be ideal to investigate spreading depolarisation using the LASU system. Several studies have shown SD induction in slices (Tozzi et al., 2012) and in awake animals (Donmez-Demir et al., 2020) using KCl injection. Moreover, multiple recent investigations have shown successful optogenetic SD induction in awake animals (Houben et al., 2017; Masvidal-Codina et al., 2021). Experiments optogenetically stimulating slices using the LASU system to investigate the cellular contributors and depolarisation volume required for SD induction would generate insightful data. Moreover, the investigation of network integration in transgenic epilepsy models, such as CACNA1A S218L mice, may generate insightful data on how spontaeous seizures and SD events arise.

4.5 Conclusion

The research presented in this chapter demonstrates a powerful method to maximise experimental output using a relatively-simple, affordable and commercially-available photostimulation system. The characterisation of cutting-edge, next-generation optogenetic tools reveals the strength of these opsins in increasing stimulation specificity. Moreover, the demonstration of high-resolution, spatially-targeted photostimulation presents a solution to a long-standing technical problem that has afflicted experimental neuroscientists for decades. Therefore, I was able to conclude this work collaborating with Scientifica; with a strong outcome demonstrating the successful development and characterisation of a highly useful tool for the neuroscientific community.

Chapter 5

Optimisation of Experimental Paradigm to Probe Seizure and SD Dynamics in Awake Head-Fixed Mice

5.1 Introduction

To further build upon the theme of novel neurotechnology development and implementation, the focus of this doctoral project shifted towards *in vivo* applications. Since the *in vivo* investigations presented in this thesis involve the novel combination of recently developed technology, several rounds of optimisation were performed to construct an efficient and effective experimental paradigm. Here in this section, I will present the initial experiments performed to probe seizure and SD dynamics, the observed limitations associated with these experiments, and how the experimental paradigm was altered to maximise output. In this introduction, I will outline the rationale behind the parameters selected as a starting point for these investigations. In the following results section, I will present the findings of these initial investigations and the optimisation of experimental parameters to achieve a more efficient and effective, comprehensive paradigm. The end goal is the generation of an experimental paradigm able to provide detailed insight into seizure and SD dynamics, as well as the relationship between these two phenomena in epileptic tissue. Moreover, this paradigm is designed to be flexible and adaptable to different models of epilepsy, both acute and chronic.

5.1.1 Optical Optimisation to Investigate Seizure and SD

To date, previous investigations have utilised IOS techniques to investigate SD propagation in the cortex (Santos et al., 2014; Charles & Baca, 2013; Tamim et al., 2021). These methods have revealed insight into the complexities of SD propagation. However, IOS is limited in that the signal generated is a readout of tissue reflectance and absorbance in the visible light portion of the electromagnetic spectrum. As a result, the recorded IOS is a composite signal generated by multiple factors, primarily oxy- and deoxy-haemoglobin concentrations (Turley et al., 2017). Therefore, the SNR achievable is insufficient to probe seizure dynamics with the level of detail required for this study. Consequentially, this research focused on imaging approaches that generate a more direct output of neuronal activity.

To probe both seizure and SD dynamics with sufficient detail, I utilised fluorescent reporters of Ca^{2+} concentration. Due to DNA-mediated expression, a subset of these are known as genetically-encoded calcium indicators (GECIs). During neuronal depolarisation, voltage-gated Ca^{2+} channels open and conduct Ca^{2+} flux into the firing neuron. Therefore, these reporters allow neuronal dynamics to be probed by using the fluorescent readout of Ca^{2+} concentration as a proxy for neuronal depolarisation. GECIs have been used previously to probe information transmission in the nervous system, making them a well-established tool (Dana et al., 2014, 2019; Deng et al., 2019). However, widefield GECI application to combined seizure and SD research has not been performed previously. Through this work, I optimised the use of GECIs in this context and developed a feasible experimental paradigm to progress the current understanding of seizure and SD paroxysms using widefield Ca^{2+} imaging.

Alteration of neural tissue to enable fluorescence imaging of Ca^{2+} dynamics can be achieved using multiple methods. These include administration of a synthetic dye, viral transduction and use of a transgenic GCaMP model. Although all three methods have powerful strengths, their co-occurring limitations led to the selection of viral transduction as the method of choice. In the case of fluorescent dyes; firstly, the time taken for dye uptake would limit the recording window. Secondly, synthetic fluorescent dyes (such as OGB-1, Tada et al. (2014)) result in small areas of uptake, thus limiting spatial coverage and SNR at areas distal from the site of infusion. Therefore, the use of synthesised dyes was excluded. In the case of transgenic GCaMP-expressing animals, this method allows widespread GCaMP expression with relative ease (Dana et al., 2014; Zariwala et al., 2012). However, the limitation of this method comes when incorporating other transgenic mouse lines, such as the CACNA1A S218L mice investigated in this work. Crossing of two an-

imal colonies, and the associated genotyping, results in greater financial cost and animal usage. Viral transduction, on the other hand, is applicable to any mouse model and can be used to transduce large areas of cortical tissue. Since adeno-associated viruses (AAVs) enable transduction of large tissue volumes, I proceeded to use AAV-mediated transduction in these investigations. In selecting a GCaMP variant, I selected one with a moderate sensitivity to minimise the probability of signal saturation during large amplitude events, such as SD and seizures. Moreover, I selected GCaMP7f, to allow greater dissociation of fluorophore molecules from Ca^{2+} following repeated neuronal discharges (Dana et al., 2019). Therefore, GCaMP7f is more likely to allow resolution of high frequency firing dynamics, as seen during epileptic seizures.

5.1.2 Combined Electrophysiological and Optical Optimisation to Study Seizures and SD

Another point of novelty in these investigations is the combined use of imaging and electrophysiological approaches. Previous studies have combined glass-micropipette recordings with IOS (Charles & Baca, 2013), or used multiple DC-coupled electrodes dispersed across the cortex (D. W. Park et al., 2018). However, no studies have performed simultaneous Ca^{2+} imaging and electrophysiology during seizures and SD. These investigations initially combined the usage of a glass micropipette with GCaMP7f imaging to achieve this. A glass micropipette was selected due to the fine tip leading to minimal tissue damage; an essential requirement to minimise any reduction in the imaging field. Additionally, the transparency of the glass is favourable to allow concurrent imaging from the recording site. However, during the investigations presented in this chapter, several limitations became apparent; prompting the integration of gSGFET technology into the experimental paradigm.

gSGFET technology has been well established to investigate seizures and SD. The ability to capture both high frequency and infraslow activity simultaneously across multiple cortical sites creates a powerful platform to study epilepsy. However, prior to this work, the combined application of gSGFET technology with Ca^{2+} imaging had not been demonstrated. In these investigations, gSGFET devices are optimised for combined imaging. Moreover, the aspects of the gSGFET recording configuration previously shown to be successful were utilised. This includes the signal amplification procedure: throughout these experiments, the custom-built amplifier demonstrated in previous applications was utilised. As a result, separate amplification of low-frequency and high-frequency signals was performed before re-

constitution of the full-band signal and conversion to a field potential using characterised I_{ds}-V_{gs} transfer curves. More information regarding this can be found in the methods section of this thesis and in the following publications (Masvidal-Codina et al., 2019, 2021; Bonaccini Calia et al., 2021).

Nonetheless, due to the recent development of the gSGFET technology, the amplifier and recording software required several rounds of further optimisation. The previously discussed gSGFET-studies utilised a 16-channel amplifier with a Simulink (MATLAB) model able to record from a single amplifier at a time. However, during the course of these investigations, I collaborated with researchers at UCL, Gtec and IMB-CNM to optimise a single Simulink model that can simultaneously communicate with multiple amplifiers; as well as a Simulink model able to communicate with a single 64-channel amplifier. As a result, the work here led to the possibility of simultaneous recordings from multiple gSGFET devices.

When selecting the desired gSGFET recording configuration, I proceeded to use epicortical/epidural arrays. Firstly, since imaging investigations were focused on the cortex, epicortical arrays would allow concurrent imaging and electrophysiological recording from multiple sites simultaneously. Secondly, since the imaging axes are perpendicular to the recording site, straight insertion of an intracortical gSGFET probe is difficult to achieve without the connected printed circuit board (PCB) obscuring the imaging field. Lastly, the invasive nature of the intracortical probe would increase the likelihood of minor bleeding which would lead to a reduction in imaging field. Therefore, I decided the ideal method to proceed with was the previously characterised 16-channel epicortical gSGFET array. I continued with 16-channels as the fabrication procedures were already optimised by collaborators during previous investigations, and the size of the array fit the initial craniotomy size well. However, during the optimisation procedures presented below, considerable work was performed to increase both craniotomy size and array coverage/channel number.

5.1.3 Induction of Epileptiform Activity

Epileptiform activity can be induced using multiple methods. These methods are able to either chronically alter neuronal tissue to induce a long-term state of seizure susceptibility, or are able to acutely induce seizures within a short time frame. Chronic methods include transgenic expression (Loonen et al., 2019), optogenetic/electrical kindling (Cela & Sjostrom, 2020; P. D. Smith et al., 2005), and chronic seizures following status epilepticus induction (Turski et al., 1989). Optogenetic and electrical kindling methods are often lengthy requiring multiple repeated

kindling sessions: therefore, they were excluded due to excessive time consumption, as well as the unnecessary requirement for electrode/fibre implantation. Inducing a chronic epileptiform state following status epilepticus is an effective method of generating a long-term state of seizure susceptibility. However, these methods have several limitations. Firstly, induced seizures may be severe and lead to prolonged status epilepticus, which is especially problematic in the case of already-susceptible transgenic animals (Loonen et al., 2019). Secondly, seizures may be too infrequent to enable successful investigation within a short recording window. Thirdly, the seizures in these models are frequently driven by subcortical structures, and therefore, seizure activity within the cortical field-of-view may be secondary to the focus. Therefore, these investigations recorded spontaneous and induced activity in transgenic and WT animals following acute exposure to different chemoconvulsants.

When selecting the appropriate chemoconvulsant to acutely induce epileptiform activity, several considerations were required. Firstly, since the relationship between seizure and SD dynamics are central to these investigations, I selected a method that is less likely to directly influence SD dynamics. Therefore, since SD is heavily dependent on extracellular K^+ concentration (Pietrobon & Moskowitz, 2014), I avoided chemoconvulsants with a clear dependance on K^+ dynamics. Therefore, this excluded the use of 4-AP which acts upon $K_v1.1$ channels to induce seizures (Smart et al., 1998). As a result, the remaining choice was from molecules acting on GABAergic transmission (picrotoxin and bicuculine), cholinergic transmission (pilocarpine) or glutamatergic transmission (kainic acid). Due to $GABA_A$ antagonism being a well-characterised model to study epileptiform activity and previous imaging studies using picrotoxin (Rossi et al., 2017), I proceeded to build investigations around the picrotoxin model. Picrotoxin was administered through local cortical injection as opposed to topical application; with the aim of creating a more focal onset. Moreover, since acute seizure induction was selected, this allowed construction of a flexible combined paradigm with transgenic CACNA1A S218L animals which are known to have an existing susceptibility to spontaneous seizures and SDs.

Altogether, these investigations were initiated with a small, unilateral imaging field of view. Moreover, a single glass micropipette was initially used as the sole method to electrographically record epileptiform activity induced by picrotoxin injection. Through the course of these optimisations the experimental paradigm was adapted to incorporate a large bilateral imaging field of view with transparent, imaging-compatible gSGFET arrays. Moreover, the picrotoxin application paradigm was adapted to minimise adverse effects in transgenic CACNA1A S218L animals. The result was optimisation and expansion of the recording paradigm to

increase the insight gained from a single recordings session.

5.2 Results

5.2.1 Establishing the Imaging Window

The first objective was to optimise the recording protocol to maximise the likelihood of capturing paroxysmal events at their origin. To perform cortex-wide activity investigations of paroxysmal events, I generated a high GCaMP7f expression level throughout the visual, somatosensory and motor cortex. Imaging with low light intensity allowed the minimisation of bleaching artefacts. Although, at the start of these investigations, the jGCaMP7f expression intensity was high and I reduced the viral titre by 50% ($1x10^{13}$vg/ml to $5x10^{12}$vg/ml) through dilution of the AAV in aCSF before injection. This allowed avoidance of cytotoxicity due to overexpression. Moreover, the initial investigations involved the use of a unilateral craniotomy of limited size, revealing only a small region of one hemisphere (Figure 34A). Brief analysis of these recordings revealed SD events frequently originating outside the field-of-view. Moreover, information regarding contralateral events was missed entirely. Consequentially, I optimised surgical procedures to generate a large, bilateral craniotomy (approximately 3mm x 5mm; Figure 37). I found that this resulted in no change to cortical activity and allowed acquisition of paroxysmal events at their origin more frequently. Therefore, investigation of activity preceding SD initiation was possible; increasing the likelihood of insight into the mechanisms by which seizures precipitate these events.

5.2.2 Optimisation of the Electrophysiological Readout

A large objective of these investigations is the incorporation of electrophysiological recordings into the optimised imaging paradigm. Electrophysiology is able to resolve seizure dynamics in unmatched detail due to a sub-millisecond temporal resolution. Therefore, this task was important to resolve seizure characteristics and understand events leading to SD initiation. Initially, to perform these electrographic recordings, I inserted a glass micropipette close to the picrotoxin injection site. This allowed full-bandwidth electrographic data to be obtained from a location of interest (Figure 35A). However, reliance on this as the sole method of electrophysiological recording suffers from several limitations. Firstly, the glass micropipette is large and only allows recording from a single site. Secondly, insertion of the glass micropipette frequently resulted in minor bleeding at the site of insertion. As a result, concurrent

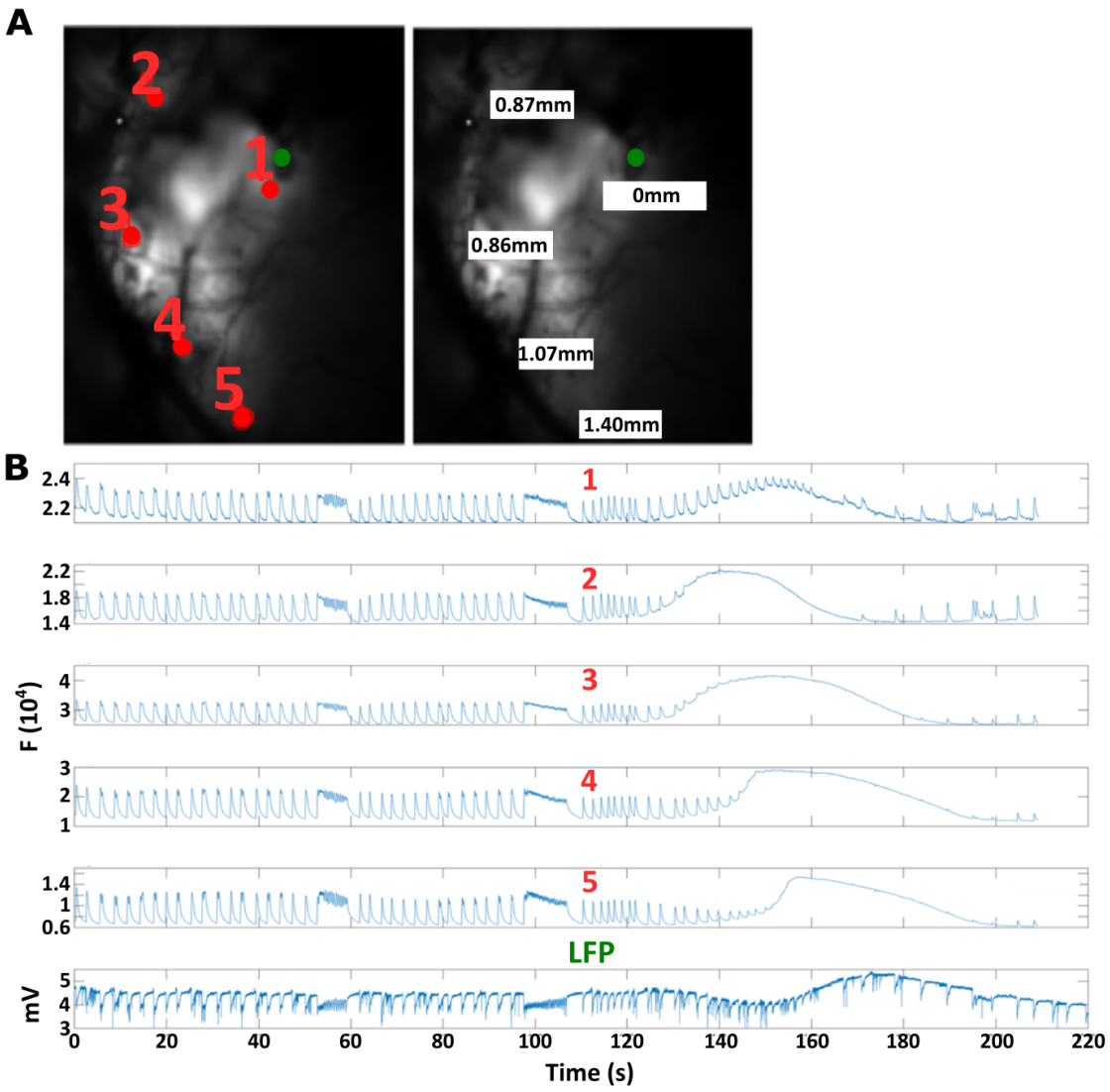

Figure 34: Representative SD associated with picrotoxin-induced epileptiform activity in a WT male mouse recorded using a unilateral craniotomy and glass micropipette. **A)** Images depict unilateral craniotomy with ROIs 1-5 plotted. Right image shows distance from injection site in mm. Micropipette recording site showin in green. **B)** Traces illustrate average activity from ROIs 1-5 plotted in **A**. Bottom trace shows LFP recording from the glass micropipette inserted into the visual cortex adjacent to picrotoxin injection site.

imaging is often not possible at the same location as the insertion site. Therefore, gSGFET epicortical arrays were incorporated into the recording paradigm.

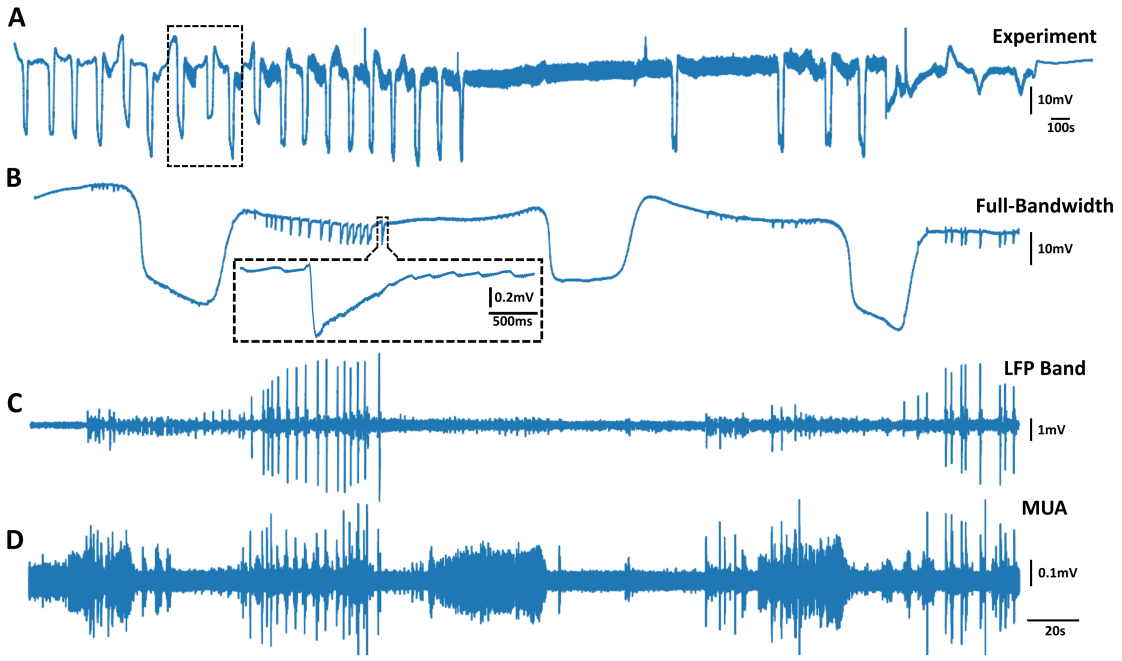

Figure 35: Glass micropipette recording of spontaneous and evoked events from a representative S218L HET animal. **A)** Glass micropipette recording over the course of an entire experiment. Early stages demonstrate spontaneous events before picrotoxin injection. **B)** Expansion of spontaneous activity in dotted box in **A**. Inset shows expansion of a single ictal spike with high frequency oscillations. **C)** Activity shown in **B** filtered between 1-150Hz. **D)** Activity shown in **B** but filtered for MUA band between 1-3kHz. Clear differences in firing populations can be seen during different phases of activity relating to SD.

gSGFET epicortical arrays, as shown in chapter 1, are able to capture full-bandwidth electrophysiological activity with high stability. As a result, these devices are simultaneous able to record both seizure and SD events from multiple cortical sites. Moreover, the gSGFET epicortical arrays are lightweight and do not require penetration of the dura, therefore, this resolves the issue of bleeding at the recording site. However, epicortical recording sites are unable to capture local action potential firing due to the distance from the source. As a result, for a subset of experiments I utilised both gSGFET epicortical arrays and a glass micropipette. The addition of the glass micropipette allowed recording from closer to the picrotoxin injection site. Additionally, this also allowed intracortical recording from nearby to neuronal soma; allowing capture of higher frequency signals, such as multi-unit activity (MUA). These recordings revealed interesting patterns of multi-unit activity,

where different characteristics could be seen with regard to events preceding and following SD (Figure 35D).

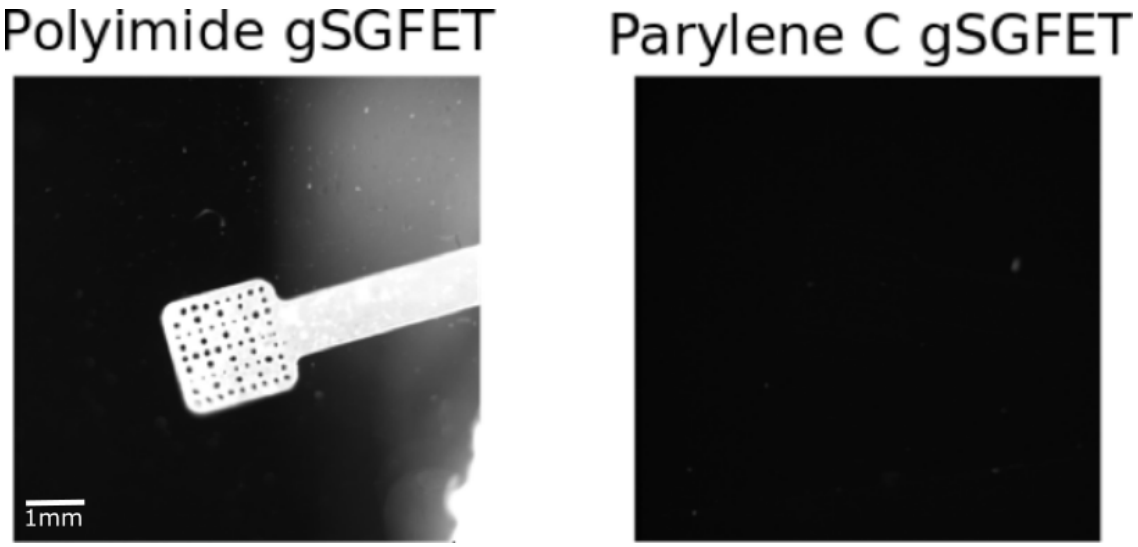

Figure 36: Images showing polyimide and parylene C gSGFET array fluorescence after illumination with a 470nm LED with matched light intensity and camera exposure. Parylene C gSGFETs demonstrate substantially lower autofluorescence.

To date, previous investigations utilising gSGFET technology have recorded with 4x4 (16-channel) transistor arrays coated in a thin layer of polyimide. Preliminary investigations revealed that these arrays display a fluorescence level too high for effective compatibility with live Ca^{2+} imaging. As a result, in order to combine imaging with full-bandwidth electrophysiology, collaborators at IMB-CNM developed novel gSGFET arrays coated in the low fluorescence material, parylene C. Recording GCaMP7f fluorescence through parylene C epidural gSGFETs exhibited a significant reduction in autofluorescence when compared with gSGFETs fabricated using polyimide, allowing conjunctive imaging with improved SNR (Figure 36). However, initial rounds of parylene C-based fabrication resulted in gSGFET arrays with powerful DC-recording capabilities but with limitations recording higher frequency alternating-current (AC) activity. As a result, initial recordings were able to capture DC-events such as SD across multiple transistors, but were unable to capture associated high frequency epileptiform activity (Figure 37C). Following optimisation of parylene C gSGFET array fabrication at IMB-CNM, these investigations were able to fully characterise both AC and DC-coupled activity across multiple sites of the cortex; while allowing concurrent GCaMP imaging.

Building upon initial observations, I designed an experimental paradigm to capture as many details regarding cortical activity as possible. To maximise the likelihood of recording the SD origin, large bilateral craniotomies were created to allow

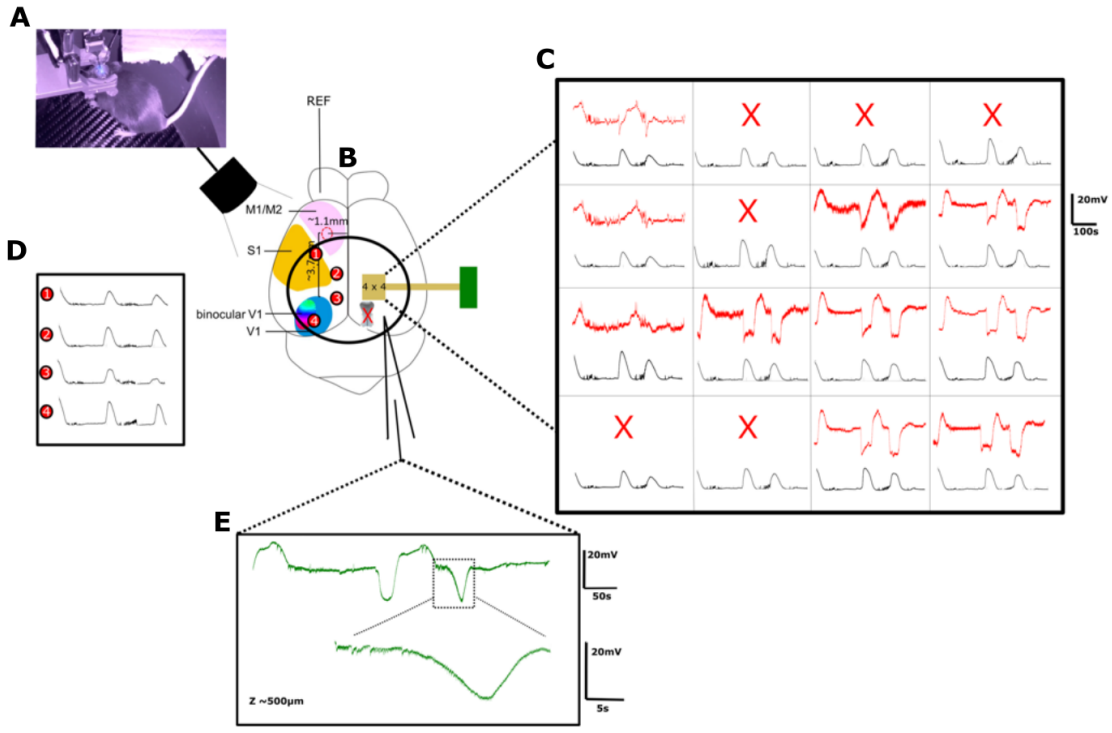

Figure 37: Baseline recording from S218L HET animal showing multiple SDs and synchronous activity. **A)** Image from behavioural movie showing mouse with inserted micropipette and placed array. **B)** Diagram of mouse brain showing primary visual, somatosensory and motor areas. Black circle indicates craniotomy size. Position of gSGFET array and glass micropipette shown. Regions 1-4 correspond to those shown in **D**. **C)** Traces showing activity recorded by each transistor (red) and the corresponding Ca^{2+} trace (black). **D)** Raw Ca^{2+} traces from regions shown in **B**. **E)** Glass micropipette recording of 500μm below the cortical surface showing the same period of activity shown in **C** and **D**. SD shown on smaller timescale to highlight preceding activity.

optical and electrophysiological access to the majority of the cerebral cortex. Furthermore, to maximise the SNR of captured images; low fluorescence, optimised parylene C gSGFETs were utilised throughout the remainder of investigations.

5.2.3 Optimising Chemoconvulsant Dosage

To further optimise recordings, the newly configured experimental paradigm was tested in S218L HET mice. The findings from this prompted alterations in the chemoconvulsant delivery paradigm. S218L animals revealed a highly interesting, strong phenotype. The initial paradigm involved experimental blinding to genotype to avoid any unconscious bias. However, during baseline recording periods, HET mice revealed an active cortical state creating a clear observable difference in activity. In S218L HET animals, I frequently observed the occurrence of multiple, large-amplitude spikes; along with multiple spontaneous SD events that reverberate both unilaterally and bilaterally across the cortical surface (Figure 37). As a result, the baseline recordings from HET mice were considerably different to that seen in WT animals, wherein activity is synchronised to a normal degree with all spike/event amplitudes much lower than those seen in HETs.

Due to the active baseline state of S218L HETs, injection of the selected dose of chemoconvulsant (Picrotoxin, 10mM, 200nl, 50nl/s) into the visual cortex resulted in adverse consequences. Shortly after injection (approximately 10-20 minutes), the first investigated HET animal having received this dosage exhibited frequent high amplitude synchronous events and repeated SDs. This, unexpectedly, led to SUDEP (Figure 38). Due to ethical considerations and animal license restrictions, the protocol was adapted to half the initial dosage of chemoconvulsant (Picrotoxin, 10mM, 100nl, 50nl/s).

For consistency between WT and HET investigations, this protocol was also used for WT animals. However, the reduced picrotoxin dosage was often insufficient to induce seizures in WT animals, and often resulted in focal spiking localised to the injection site. Therefore, depending on the observed behavioural and cortical activity in response to the first dose, either the injection needle was removed or another 100nl of picrotoxin was administered (as before). The result was the prevention of adverse consequences in HET animals, thus allowing recording of the high frequency spiking, seizures and SDs that followed for the entire recording period.

The adaptation of the protocol to deliver a low dose of picrotoxin, although requiring more time within the limited recording window, showed a considerable advantage. In WT animals, the first dose was insufficient to fully synchronise activity in multiple regions across the cortex. However, upon delivery of the second dose,

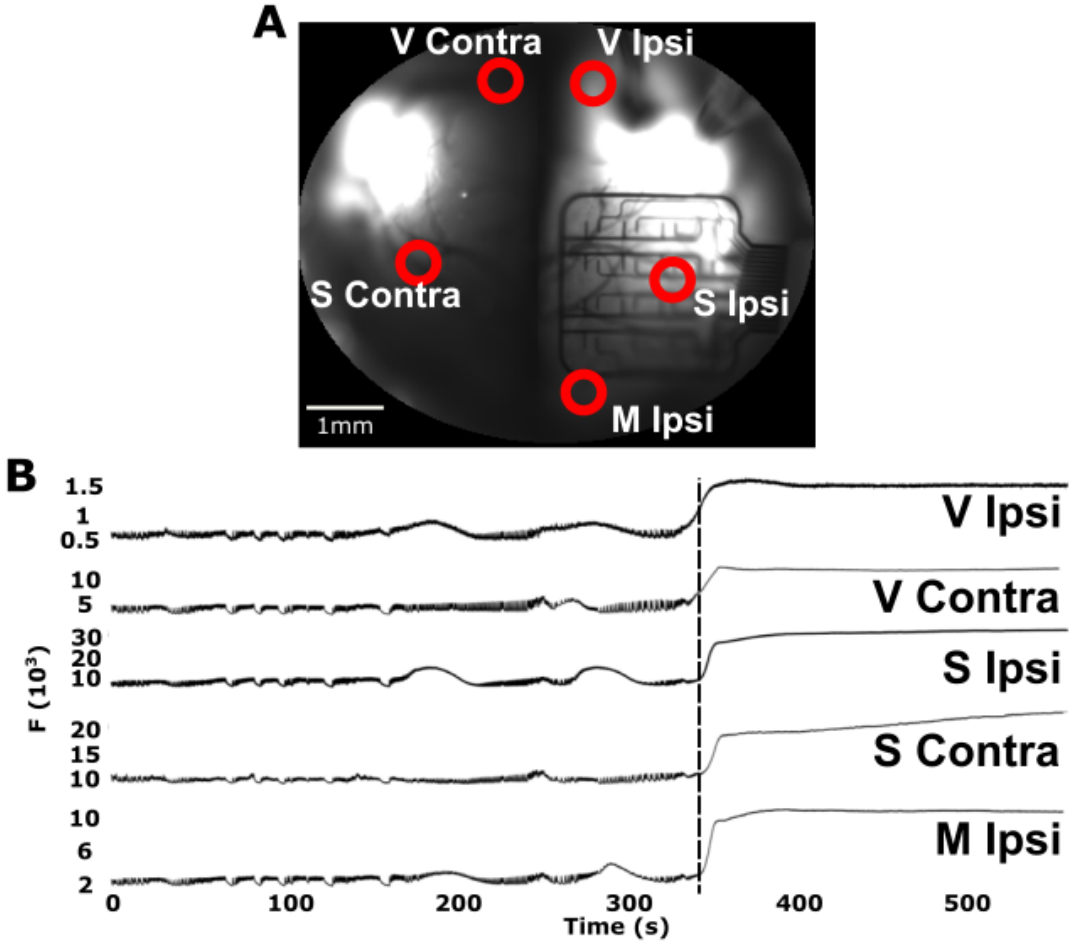

Figure 38: Epileptiform activity with multiple SDs and terminal depolarisation (dotted line) observed in a S218L HET animal following delivery of the pre-optimised dose of picrotoxin. **A** ROIs on the visual, motor and somatosensory cortices of both hemispheres shown on a raw image of the GCaMP fluorescence. Laterality specified in relation to the chemoconvulsant injection site at the right visual cortex. **B** Ca^{2+} traces from the ROIs **A**. Pixel intensities within each ROI were averaged and plotted.

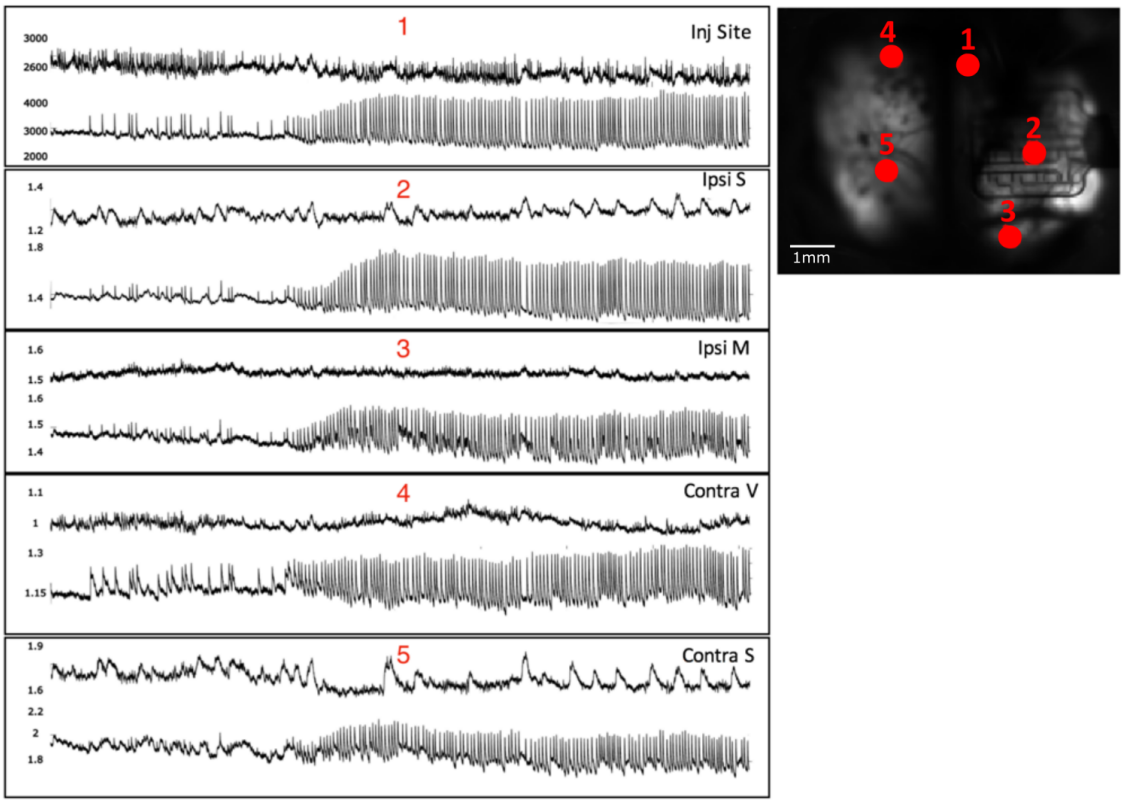

Figure 39: Ca^{2+} traces (left) from different regions (right) showing a representative example of development of epileptiform activity. Top trace for each ROI shows WT activity in response to 100nl picrotoxin. Bottom trace for each ROI shows the same animal 15min after a second dose of 100nl picrotoxin. Injection site is V1 and corresponding regions for other ROIs shown.

the transition from a localised moderately synchronous state to bilateral, cortex-wide discharges could be observed (Figure 39). Further analysis aims to dissect activity patterns during this period to gain insight into seizure development and generalisation.

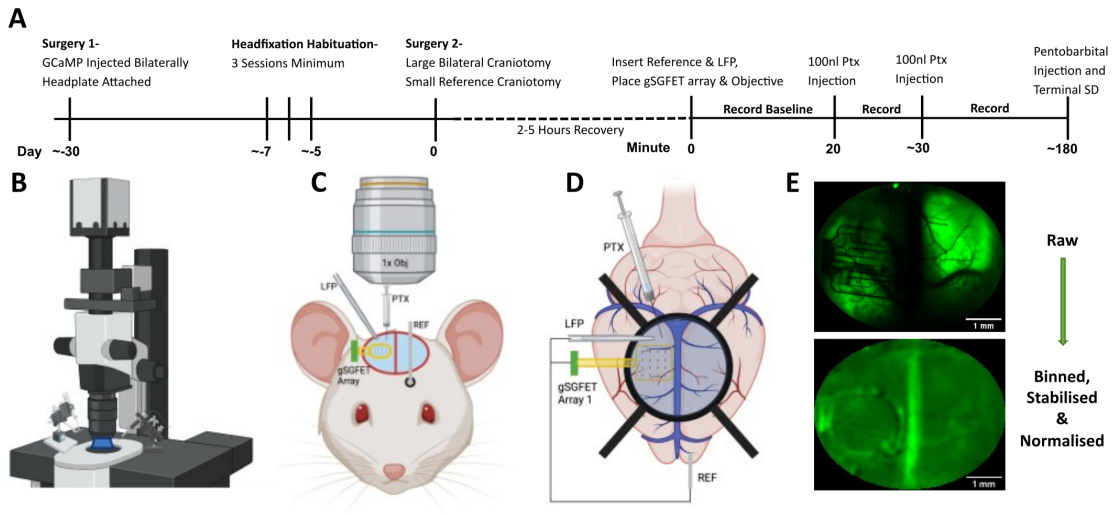

Figure 40: Schematic of final optimised experimental paradigm. **A)** Surgical and experimental timeline showing important events and relative timings. **B)** Image of mesoscope used for widefield imaging. **C)** Image of finalised experimental paradigm showing gSGFET array, glass micropipette, picrotoxin injection site, AgCl reference wire and imaging objective. **D)** Close-up schematic of **C**. Perspective shown from dorsal surface of the brain. Areas of seizure-induction, electrographic recording and fluorescence imaging shown. **E)** Demonstration of widefield imaging preprocessing. Top image shows raw image with heterogenous fluorescence across cortical surface. Bottom image shows normalised image with homogenous fluorescence. Figures **B,C & D** were generated using Biorender.

Altogether, this work established the novel combined usage of Ca^{2+} imaging and multi-site, full-bandwidth electrophysiology recording using gSGFETs. This methodology has been shown to have promise in revealing complex mechanisms during seizure initiation, propagation, termination, and the relation of all these mechanisms to SD occurrence and propagation. Thus, this paradigm is well suited to answer the primary goal of these investigations. Moreover, I have demonstrated the feasibility of this configuration in investigating activity in transgenic chronically epileptic animals. A summary of the final optimised experimental paradigm is demonstrated in Figure 40.

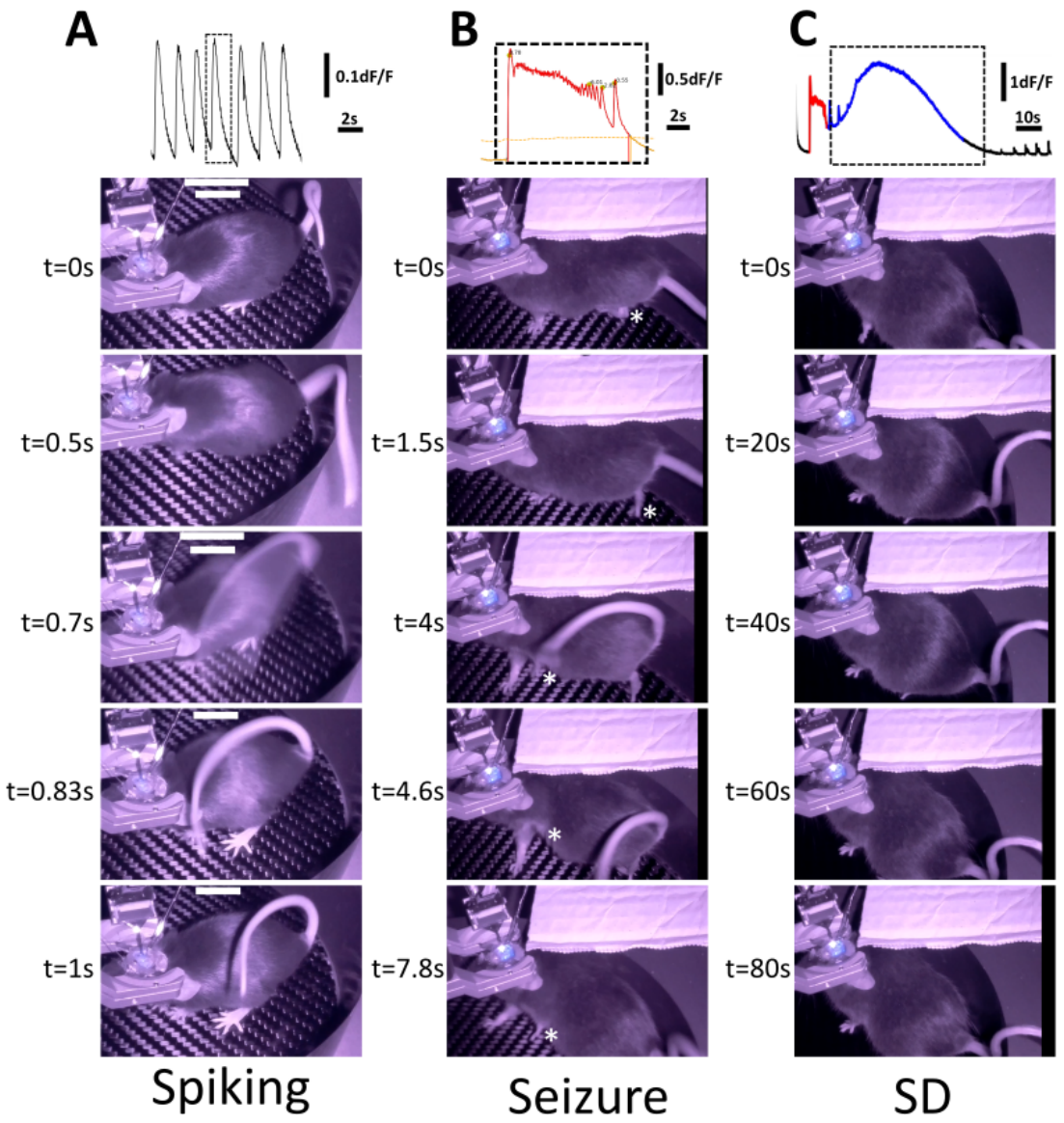

Figure 41: Representative animal-wide behavioural manifestations of different paroxysmal events. **A)** Top shows example trace of ictal spiking seen throughout recording period recorded with widefield imaging. Bottom shows time-lapse images of a brief myoclonic jerk during an ictal spike. **B)** Top shows GCaMP trace of a seizure with seizure highlighted in red. Bottom shows time-lapse images throughout the same seizure. Clonic behaviours are observed originating in the left hindlimb followed by progression to the left forelimb (marked by asterisk). **C)** Top shows fluorescence imaging trace of a SD which failed to propagate to the micropipette. SD highlighted in blue. Time-lapse images of the same SD shown below. During this period, behavioural arrest was observed with minimal movement and absence of myoclonic jerks lasting for over 1min.

5.2.4 Behavioural Manifestations of Epileptic Paroxysms

In order to increase the clinical relevance of the data acquired by the constructed experimental paradigm, simultaneous behavioural recordings were performed. These recordings allowed observation of clear physical manifestations of different fluorescence and electrical activity waveforms. In order to achieve a simple and cost-effective solution to this aim, a Raspberry Pi computer and associated camera were used to acquire the data. This resulted in minimal total cost of the setup. Furthermore, the small size of the camera allowed easy attachment to the recording platform, and therefore, easy integration into the recording paradigm. Additionally, the infrared illumination attachment allowed imaging in the dark experimental setting with no noticeable photo-artefacts on other recording devices. Lastly, behavioural recordings were easily temporally synchronised to other recording devices through capture of the start and end of each imaging sweep by recording the GCaMP imaging LED. Altogether, the result was the ability to record time-locked physical manifestations of recorded electrical activity.

The resulting behavioural imaging configuration was flexible and allowed two possible paradigms. The first, allowed imaging of overall animal-wide behaviours. The second, allowed imaging of pupil diameter during different paroxysms. Animal-wide behaviour recordings revealed clear manifestations of recorded paroxysmal events. Observed single electrical spikes were seen to manifest as brief (approximately 1-2s) myoclonic jerks. These jerks appeared to affect the entire body and result in contraction of all limbs, including the tail (Figure 41A). These myoclonic jerks were consistently observed in all recorded animals. Seizures, on the other hand, were often seen to manifest with profound clonic behaviours. Moreover, this clonic behaviour was seen to spread. In the representative example shown, clonic behaviour originated in the left hindlimb and quickly progressed to primarily affect the left forelimb (Figure 41B). Since picrotoxin was injected in the right visual cortex, this finding is consistent with the anatomical location of motor regions relative to the visual cortex and medullary decussation of the corticospinal tract. These tonic-clonic behaviours were seen associated with all observed seizures, however, the spreading characteristics varied between events. Interestingly, SD events were frequently observed to result in prolonged behavioural arrest marked by an absence of movement or myoclonus for greater than 80s (Figure 41C). However, the extent of this behavioural arrest appeared to correlate with the degree of ictal spiking suppression during SD. Altogether, these findings, allowed observation of important behaviours associated with different paroxysmal events. Moreover, these observations confirmed the pathophysiological relevance of the electrical activity being

recorded throughout these investigations. Lastly, the temporary termination of myoclonic jerks during SD supports the idea of an anti-epileptic role for SD; however, whether this anti-epileptic effect is persistent remains another question.

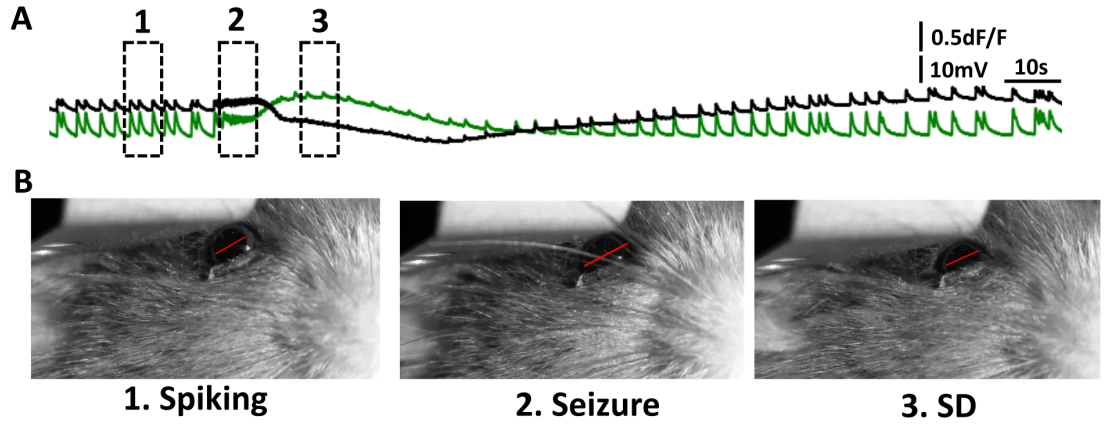

Figure 42: Alterations in pupil diameter during paroxysmal events. **A)** Electrographic (black) recording and fluorescence (green) traces at same site shown during spiking (1), seizure (2) and SD (3). **B)** Still images from pupilometry video acquired during activity recorded in **A**. Red line indicates pupil diameter.

The second possible paradigm accessible through the constructed Raspberry Pi configuration involved imaging of pupil diameter. Pupil diameter has been linked to both overall brain activity and vigilance state, giving these measurements physiological relevance (Larsen & Waters, 2018). These recordings were difficult to achieve due to positioning issues around the recording chamber. However, pupilometry recordings could be successfully acquired during different events. Similarly to animal-wide behaviour acquisition, these movies were time-stamped to other recording devices using the GCaMP LED. Pupilometry responses were somewhat variable. However, typically seen during spiking was rapid pupil dilation followed by rapid constriction (Figure 42-1), as shown by Rossi et al. (2017). Seizures and SD were marked by profound pupil dilation (Figure 42-2&3). Preliminary work has been performed to process these images to allow continuous monitoring of pupil diameter. Difficulties have been seen due to the imaging angle resulting in an elliptical pupil, and therefore, images require circular transformation before pupil edge definition. Nonetheless, these behavioural and pupilometric acquisitions increase the relevance of the electrographic and fluorescence data acquired. As a result, these investigations are also able to capture the greater implications of recorded activity for an organism.

5.3 Discussion

The results presented in this chapter demonstrate the concurrent usage of Ca^{2+} imaging and gSGFET technology to record seizure-SD interactions in awake head-fixed mice. The experimental paradigm optimised through these investigations resulted in advancements to the detail with which epileptic paroxysms can be studied. This research was initiated with a single electrographic recording site within a small unilateral imaging field of view. The work presented in this section developed this paradigm to increase the insight obtained from a single animal. The presented results show the expansion of the imaging window to the contralateral hemisphere, allowing concurrent imaging across a large field-of-view. Moreover, low autofluorescence parylene C gSGFET arrays were optimised and incorporated into this recording window. The result was the powerful ability to simultaneously monitor full-bandwidth electrographic activity at multiple locations while performing Ca^{2+} imaging. The simultaneous recording of LFP using a glass micropipette allowed detailed electrographic recording of activity in the visual cortex, and direct comparison of gSGFET recordings with the 'gold-standard' micropipette. Additionally, the insertion of the glass micropipette, although invasive, allowed detailed analysis of local, high frequency activity (e.g. multi-unit activity; >500Hz). Further to this, I utilised custom-built behavioural imaging equipment to record correlates of different electrical events. Altogether, these optimisations resulted in the powerful ability to record epileptiform activity bilaterally with fluorescence imaging, while simultaneously recording electrographic activity from up to 17 different sites across the cortex. These developments led to the construction of a paradigm able to probe seizures and SD in high detail.

To date, few studies have presented similar technology to the active gSGFETs used here. Notable, is the use of transparent passive graphene electrodes fabricated on a parylene C substrate. Although, these devices have been shown to be compatible with imaging (D. W. Park et al., 2018), the bandwidth and stability is inferior to that shown by gSGFETs due to the superiority of direct DC-coupled transistors. The advantage of using active transistor-based devices surrounds the ability to capture infraslow activity, and therefore, SD events. Without these capabilities, multi-site SD recording would not be possible to the extent presented here. Moreover, the flexibility of gSGFET probes allows versatility when used for recording cortical signals. The current design in use (4x4 16 channel arrays) is easily positioned on the dural surface with it causing minimal disruption to tissue. Furthermore, the flexibility of the device, as well as the high biocompatibility

(Masvidal-Codina et al., 2019), will allow future adaptation of the gSGFET array to expand our recording capabilities (e.g. implantation for chronic investigation or a greater number of sparse cortical sites). I envision this to expand the current understanding of epilepsy paroxysms through the dissection of seizure termination mechanisms and SD initiation.

Previous studies using widefield imaging have utilised a similar approach. However, these studies often record through an intact skull (H. T. Zhao et al., 2021a). In order to allow electrophysiological access to the tissue, a craniotomy was required. Moreover, to allow direct comparison of activity between hemispheres without the skull confounding the signal, the craniotomy used here was expanded to cover both hemispheres. Few studies have demonstrated the use of large bilateral craniotomies such as those shown here (Cha et al., 2020). Therefore, the development of these surgical procedures are an additional point of novelty. Moreover, the majority of studies with large-scale optical access to the cortex are focused on assessing functional connectivity between brain regions (Vanni et al., 2017). Here, this work expands these paradigms to allow investigation of pathological events. The ability to monitor these events both locally and distally from the picrotoxin injection site creates a powerful view into disease-related mechanisms. Moreover, the optical and electrical access to the contralateral hemisphere allows investigation of whole-brain phenomena and the effect of both seizures and SD on wider neuronal networks. Previous studies have revealed interesting contralateral effects in relation to KCl-induced SD (Vinogradova et al., 2021), however, no studies have fully investigated these phenomena in the context of epileptic seizures. The presented paradigm is able to address this absence in the literature.

The ability to record behavioural manifestations of pathological activity while observing the propagation of different events across the cortex is powerful. Further analysis would allow translation of pathological brain activity in different regions to physical behaviours. Moreover, the physiological relevance of acute chemoconvulsant models in studying spontaneous epileptic seizures is uncertain. The integration of behavioural recordings are able to assess this relevance. The findings of clear seizure-like behaviour suggest a strong relevance of the chosen model to study epilepsy. However, it appears important to consider the entire recording window as an ictal period and to avoid referring to the spikes seen between seizures as interictal. Clearly these spikes manifest with myoclonic seizure-like behaviours, and therefore, these events appear distinct to the seemingly 'silent' interictal events observed in human patients. The ability for this configuration to provide insight into these phenomena increases the broader relevance of recorded brain activity.

As a result of the optimisations presented here, I moved forward with an optimised experimental paradigm. This paradigm involved acquisition of bilateral widefield GCaMP7f fluorescence combined with a low-fluorescence 16-channel epicortical gSGFET arrays. Altogether, these developments allowed investigations of seizure and SD dynamics with newfound detail. In the next section, I will present an analysis framework to process the complex recordings generated by this experimental paradigm. Following this, I will demonstrate the strengths of this dual recording modality approach in revealing the complexities associated with epileptic seizures and SD.

Chapter 6

Construction of an Analysis Framework to Probe Seizure-SD Interactions

6.1 Introduction

The previously optimised experimental paradigm yielded an information-rich data-set. In order to fully interact with this data-set, several stages of analysis were required. Moreover, since the imaging field of view has large coverage of the cortical surface, these imaging investigations produce data unmanageable for manual processing. To highlight this point, each imaging sweep lasted 10 minutes, sampled at 49.06Hz, leading to 29,000 frames per image. Moreover, each 5mm by 3mm region-of-interest selected from the EMCCD camera spanned approximately 300 by 200 pixels (conservative estimate). Lastly, the recording period lasted up to 3 hours. Altogether, this resulted in approximately $3x10^{10}$ imaging-related data points per animal. As a result, significant work was invested in the automated processing and analysis of these information-dense imaging stacks.

Initially, I considered using the simpler analytical approach performed in previous studies, to allow a focus on extensive dataset collection. However, this PhD project overlapped with the COVID-19 pandemic. As a result, during a considerable period of this project, the research laboratory was closed, animal colonies were scaled down and data collection was not possible. To fully utilise this closure period, focus was diverted from extensive data collection to novel analytical methodology development. This focus diversion resulted in the caveat of relatively small sample sizes throughout these pilot investigations. However, the advantages well-outweighed this caveat, by allowing efficient use of time and the development

of a powerful, novel analysis pipeline.

The constructed pipeline aimed to surpass the analytical limitations of previous studies using similar imaging methods to study seizures and SD. These previous studies often rely on defined regions-of-interest within the field of view to characterise observed phenomena (H. T. Zhao et al., 2021a; Rossi et al., 2017), or simply characterise events descriptively based on observations (Hatcher et al., 2020). Therefore, previous analysis methods result in limited insight due to the averaging of activity across large regions-of-interest or reliance on human visual interpretation. The analysis framework constructed in this chapter utilised the entire bilateral imaging field of view to characterise and quantify paroxysmal events. Therefore, a readout of activity could be obtained and quantified at each pixel across the entire field-of-view. This development in analytical tools proved to be powerful, especially in the case of propagating events such as SD.

Image processing stages included stabilisation, normalisation, region of interest extraction and event detection. Since these analysis tools have not been previously developed for a Ca^{2+} indicator with the kinetics of the GCaMP7f construct utilised here, considerable work was required to extract both seizure and SD dynamics. Due to the combined novelty of the recording modalities and the events being investigated, these tasks were demanding in both design and implementation. Fortunately, I formed a collaboration with computational experts at the University of Warwick (Adam Smith and Prof. Yulia Timofeeva). This collaboration was instrumental to the construction of this imaging analysis pipeline.

The imaging analysis pipeline was designed collaboratively by Adam Smith and I, with guidance from our PhD supervisors (Prof. Kirill Volynski, UCL; and Prof. Yulia Timofeeva, University of Warwick). Together, we designed the framework to process this data, and Adam generated the Python scripts to perform these tasks and extract event properties. Since these tasks were complex, we collectively performed many iterations and rounds of optimisation to generate the final functional code. This collaborative effort allowed efficient generation of the analysis pipeline and was essential for the processing of imaging data. For stylistic consistency, I will continue to present this work in the first person; however, the analysis stages spanning from preprocessing definitions to event extraction were designed collaboratively and predominantly implemented by Adam Smith. Please refer to the chapter titled 'Acknowledgements' for a detailed description of the contributions of each collaborator.

With regards to gSGFET electrographic recordings, during previous studies, considerable work had been invested by collaborators at IMB-CNM (Dr. Eduard

Masvidal-Codina and Dr. Anton Guimerá-Brunet) to develop analysis tools. I took advantage of these tools, resulting in efficient recording calibration from current to field potentials. However, considerable work was performed to integrate imaging outputs with full-bandwidth electrophysiological recordings.

This section will describe the steps taken to develop the required analysis pipeline and the rationale behind each of these steps. To some degree, the analysis development presented in this section will serve as documentation of the methods applied in later sections.

6.2 Results

Combining a goal-oriented focus with the computational expertise of collaborators at the University of Warwick, I constructed a high throughput, robust, Python-based workflow to allow efficient analysis without continuous user input (see Figure 43 for overview). The outputs of this pipeline were processed images, and an organised database allowing the statistical comparison between characterised events. This results section will proceed to outline the chronological steps taken to process a given widefield imaging stack.

6.2.1 Preprocessing Definitions

Due to some variability between experiments, initial definitions were required to account for small uncontrollable differences between individual experiments, e.g. areas obscured by minor bleeds and exact positions of cranial window edges. Without definition and consideration, in later steps, these inter-experimental variations would result in problematic artefacts that result in false event detections and inconsistencies. Consequentially, I incorporated the manual selection of low SNR regions (where Ca^{2+} dynamics could not be resolved) into the user-input stage of the analysis. This allowed manual exclusion of the corners of each image frame (covered with dental cement due to a circular craniotomy), the regions of cortex underlying the gSGFET ribbon (prone to refraction artefacts) and midline pixels depicting the sagittal sinus (Figure 44B). These regions were graphically defined on the selected reference frame, termed the 'anchor', and were extended to the entirety of the dataset acquired from that animal.

Additionally, at this stage, I define important experimental time-points and other metadata associated with each experiment to allow segmentation and grouping of experiments in time. The main time points of interest in this case are the

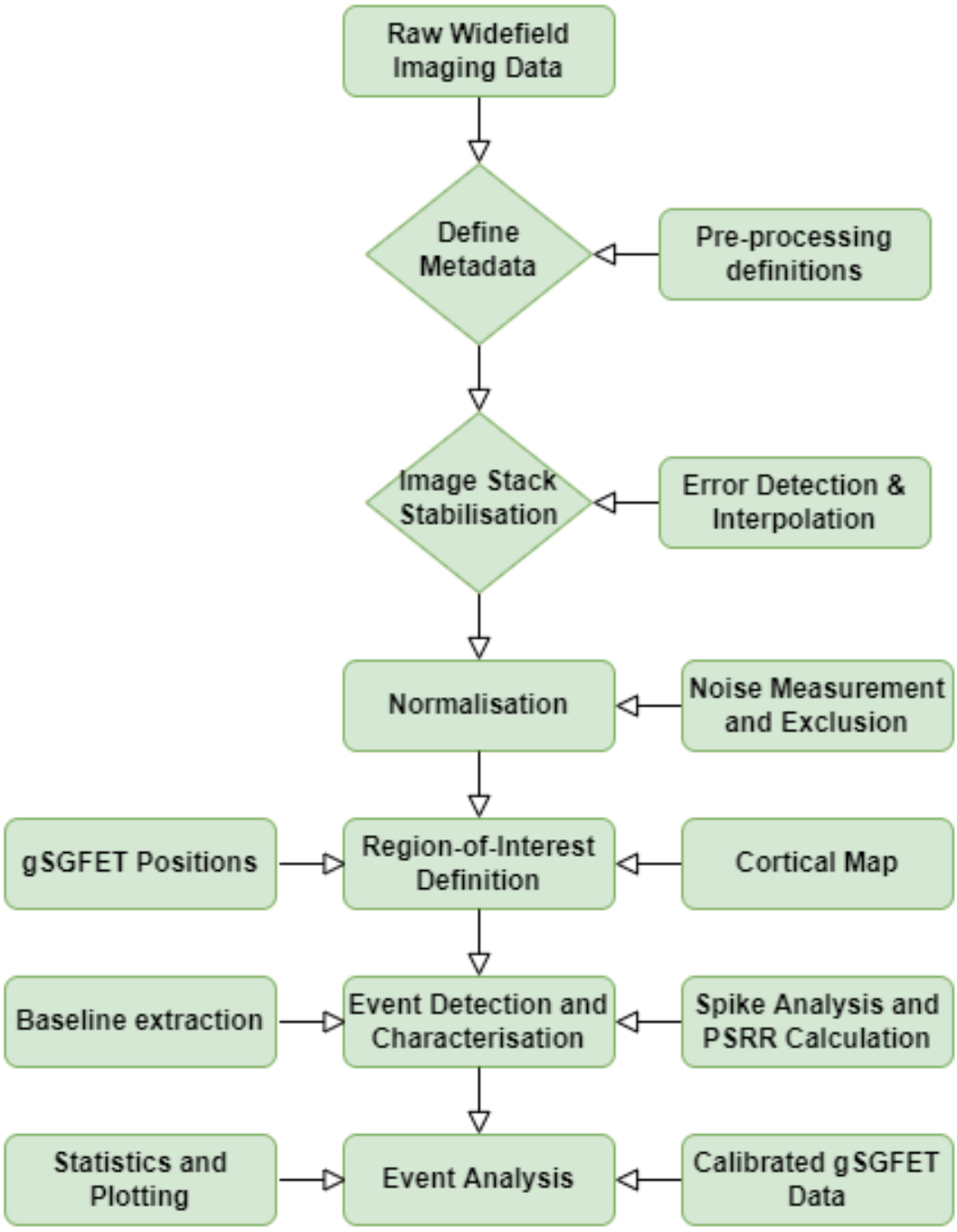

Figure 43: Overview of the constructed Python analysis pipeline to process widefield imaging stacks. Flowchart showing an overview of each stage of the pipeline. Calibrated gSGFET data is integrated into the pipeline at the end to allow comparison of activity between recording modalities.

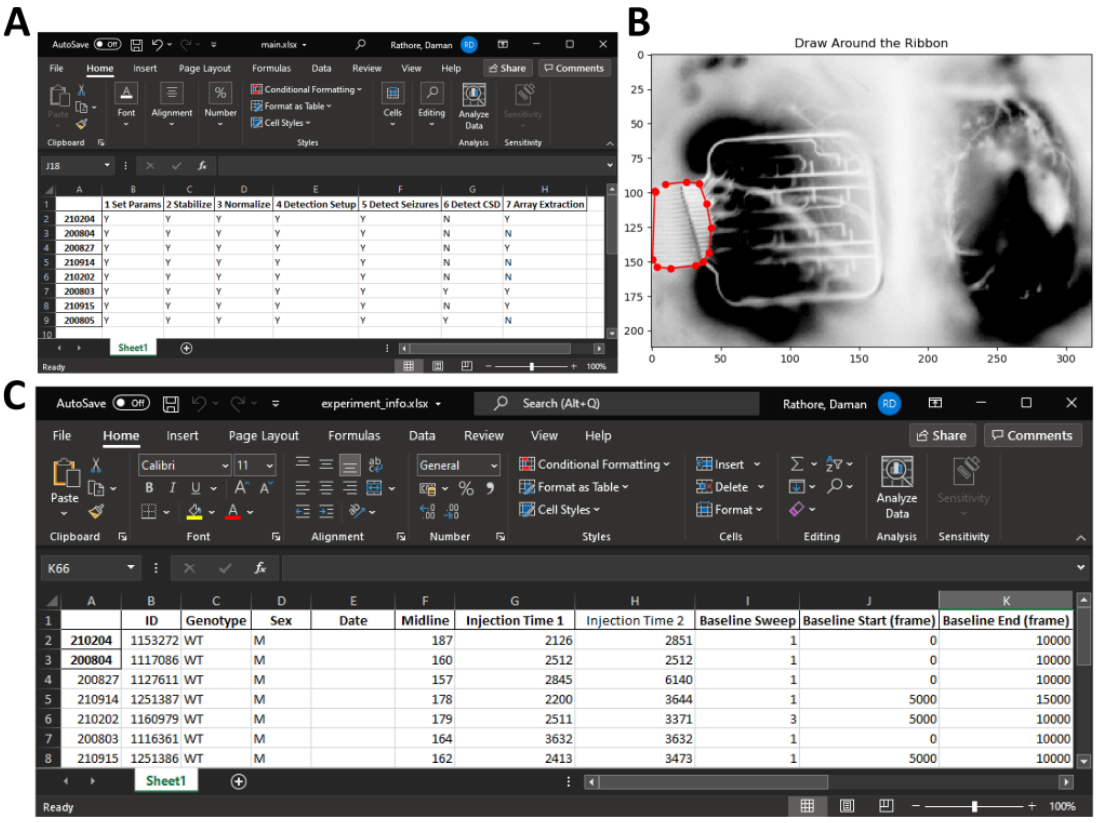

Figure 44: Stages of the pre-processing step of the analysis pipeline. **A)** Excel sheet to track analysis stages for each experiment. Python scripts automatically recognise data and fill values when performing operations. **B)** Graphical interface for marking error prone regions shown. In red marks the area around the ribbon of the gSGFET for exclusion. **C** Excel sheet showing variable defined prior to data processing. Values are accessed by Python script for each analysis stage. E.g. Baseline periods are used for normalisation.

times of chemoconvulsant injection. Occasionally, SD events were observed prior to chemoconvulsant injection due to pin-prick induction by needle or micropipette insertion. Therefore, I defined these time windows to exclude any events not directly associated with epileptiform activity. Altogether, the output of this preprocessing stage is a data structure containing metadata relating to each experiment. This data structure is stored in an Microsoft Excel format, with the variables accessible for later analysis stages (Figure 44C). Moreover, due to the numerous stages of analysis in this pipeline, I generated an Excel interface containing information regarding the analysis stages performed for each experiment (Figure 44A). These were automatically checked and updated by Python when running each stage of the analysis code. Altogether, this resulted in the construction of a user-friendly organised analysis pipeline able to efficiently process large data-sets with relative ease.

6.2.2 Image Stack Stabilisation

In order to allow meaningful information to be extracted from different locations across the cortex, image stabilisation was performed. Firstly, the recording period is lengthy and any gradual drift will result in the quantification of different brain regions when considering a single recorded pixel. Secondly, during natural and pathological activity, brain pulsation occurs on short timescales. To avoid movement artefacts associated with this, I developed the crucial step of image stack stabilisation/registration. All preprocessing (described previously) was performed on a selected frame within each experiment, termed the 'anchor'. This anchor frame, was used as a reference for each subsequent frame to be registered to. Therefore, previously defined low SNR regions were extended to the entire dataset. To generate registered image stacks, I tested the efficacy of various image stabilisation algorithms in generating transformation matrices to allow compensation for any observed movement.

Several of the tested stabilisation algorithms failed due to the complexity of the data and the source of the movement artefacts. One large source of these artefacts is the pulsation of cortical tissue due to changes in water content and haemodynamics. As a result, the two cortical hemispheres may pulsate outwards from the midline. Generation of single transformation matrix for this would result in errors due to opposing movements. Therefore, I separated the cortex into the two hemispheres using the previously defined midline and generated a transformation matrix independently for each. Another issue arising from this source of movement is the transient change in z-dimension focus of the tissue during brain pulsation:

as a result, simple feature tracking algorithms are unable to continually track landmarks during these artefacts. Following thorough testing of multiple algorithms, the phase-correlation based method showed the most effective generation of accurate transformation matrices.

Phase-correlation based stabilisation represents the images in phase-space using a Fourier-based transformation of each frame (skimage.registration.phase_cross_correlation). These frames are then correlated to one another in phase-space and, based on maximal correlation values, a transformation matrix is generated for each frame to the anchor. This matrix is then applied to each corresponding raw image frame to translate these onto the anchor. The result is subpixel-resolution image stabilisation throughout entire recording periods.

Although this method was found to work well for baseline periods and seizures, SD events were found to be problematic. This was due to the SD being of such high amplitude that the stabilisation algorithm detected these spreading events as large movement artefacts in the image stack. Consequentially, when trying to correct for real, slight movement during these SDs, large amplitude movement was falsely detected and wrongly corrected for; resulting in overcompensation and the generation of even greater movement artefacts. To circumvent this issue, I applied a spatial high-pass filter in both X and Y dimensions of each image frame (Figure 45). After several rounds of optimisation, I selected an appropriate filter cutoff frequency (signal.butter; cutoff frequency=130) to highlight key spatial features on the image, while removing homogenous areas of tissue that confound detection. I used these spatially-filtered images and the phase-correlation stabilisation method to generate a transformation matrix that is applied to the raw unfiltered images. As a result, it was possible to reliably stabilise small movements in image stacks with sub-pixel resolution. Moreover, this stabilisation was robust to influence by coinciding brain activity. Altogether, the result is the ability to track activity in multiple small cortical regions over the lengthy recording period with minimal movement-induced error.

6.2.3 Error Detection, Correction and Exclusion

In case of any errors during acquisition or stabilisation, contingencies were in place to minimise ongoing effects. To detect errors either in the camera or in the previously presented stabilisation steps, each pixel intensity was compared to the intensities of the same pixel at the immediately following time point. Using a high-threshold gradient-based approach, sudden changes in pixel intensity were detected

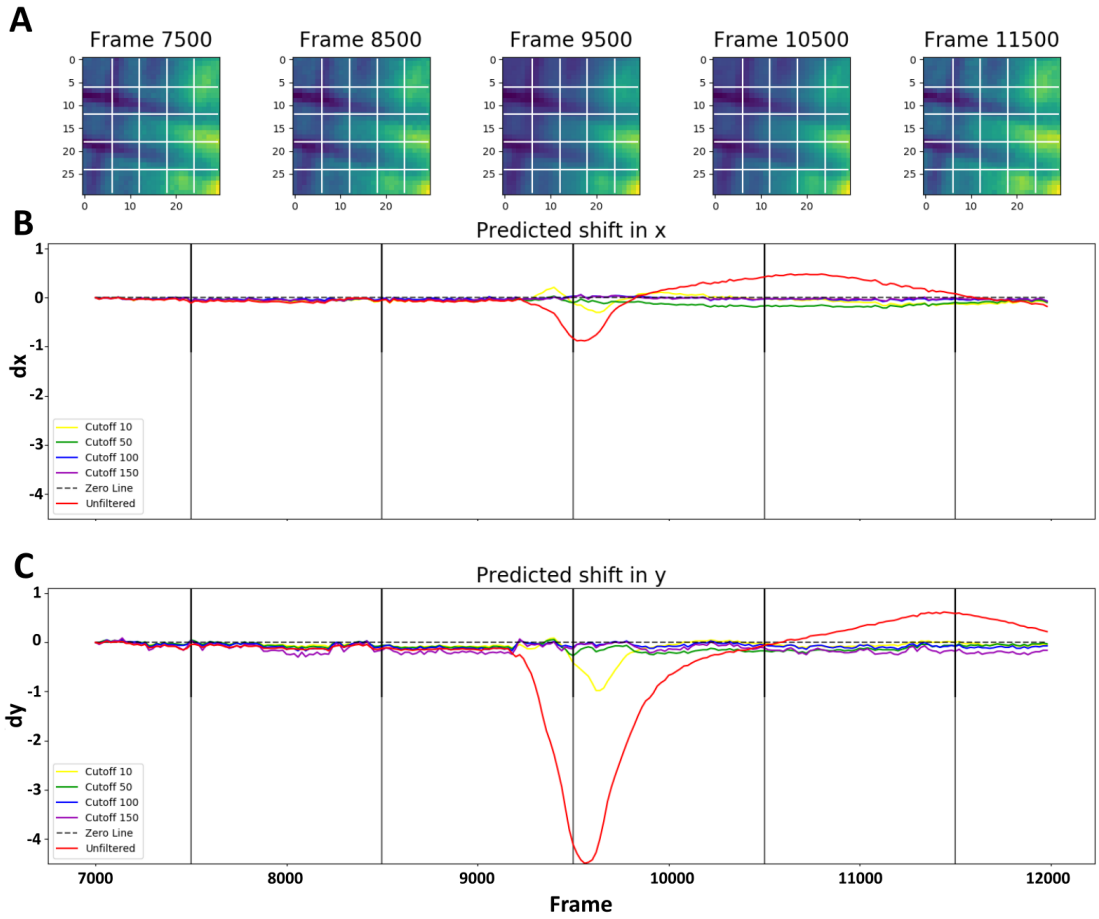

Figure 45: Testing of the phase-correlation stabilisation algorithm during a SD event. **A)** Time series images of a cropped region nearby the gSGFET array during a seizure-associated SD. X and Y axis represent pixel coordinates. Noticably there is minimal movement. **B)** Predicted shift calculated using phase-correlation in X direction for time points in **A**. Different traces plotted after a spatial high-pass filter was applied with different cutoff frequencies. **C)** As in **B**, for the Y direction. A large movement of over 4 pixels is detected on the non-filtered movie due to the SD. Spatial filtering resolves this false predicted shift.

as potential errors. If these errors are isolated and last few frames, interpolation over these values was performed to avoid unnecessary exclusion of data points. If these intensity artefacts are prolonged over tens or hundreds of frames, these time points are added to the previously generated experimental metadata file and are later referenced for exclusion from further analysis.

To investigate the ability of the imaging camera in reliably capturing Ca^{2+} fluorescence without becoming desynchronised from other recording modalities, the time of each camera exposure pulse was recorded. I investigated the number of these pulses for each recorded imaging sweep, as well as for testing sweeps of different frame lengths. Although, cameras used for scientific imaging are highly reliable, they are prone to frame skipping, whereby the camera outputs an exposure signal but no image is captured. As a result, these skipped frames can be detected by counting the total number of exposure pulses compared to those actually acquired. In all cases of recordings presented here, the maximum number of skipped frames did not exceed two frames. This suggests that only mild desynchronisation occurs over the time course of each imaging sweep (40.77ms over 591s or 0.0069%). Altogether, this suggest a reliable ability to temporally compare imaging and electrophysiological modalities for events of interest which occur over time scales orders of magnitude greater than the error observed.

6.2.4 Normalisation

To allow valid comparison between the amplitudes of different cortical regions, dark current subtraction and normalisation was required to generate comparable values. Due to the viral approach to GCaMP expression, Ca^{2+} indicator expression was seen to differ across the cortical surface. This was due to GCaMP injection occurring at discrete stereotaxically defined sites; with the AAV diffusing outward through the tissue from these injection sites. As a result, the concentration of GCaMP is highest near these injection sites and lower in distal regions. Therefore, for each pixel, either $F_{0.1}$ or F_{max} normalisation was performed (Figure 45). For $F_{0.1}$ normalisation, each pixel value intensity was divided by the intensity during a baseline period. However, due to the baseline often containing spontaneous pathological activity, particularly in the cases of S218L HET animals; I selected the averaged minimum 10% value of intensity over the baseline period as the denominator for our $F_{0.1}$ normalisation. As a result, $F_{0.1}$ normalisation was robust, with minimal influence from spontaneous activity.

F_{max} normalisation was performed using the final sweep of each recording. This sweep was recorded following injection of sodium pentobarbital which results in

a terminal SD event. During this event, ion homeostasis is fully lost and a large Ca^{2+} influx is seen to occur into all neurons. As a result, the maximum level of fluorescence achievable at each pixel could be recorded, giving a strong readout of the quantity of Ca^{2+} indicator within each region.

The subsequent analysis has mainly been utilising $F_{0.1}$ normalised recordings instead of F_{max}, due to F_{max} normalised recordings being more susceptible to artefacts that arise during the experiment, e.g. minor bleeds during chemoconvulsant injection. These were found to be problematic and $F_{0.1}$ was found to be more robust; therefore, these investigations proceeded with the $F_{0.1}$ method. Moreover, at this stage, images were binned by 2 (16μm pixel to 32μm pixel size) to reduce the size of image stacks and improve processing speed. Due to inherent light scattering and diffraction limitations, this binning had minimal effect on the spatial information content in recordings. Altogether, following these previous stages, an image stack was generated that has been sufficiently processed to allow automated data extraction from homogenously fluorescent imaging pixels, with it now possible to compare different brain regions to one another.

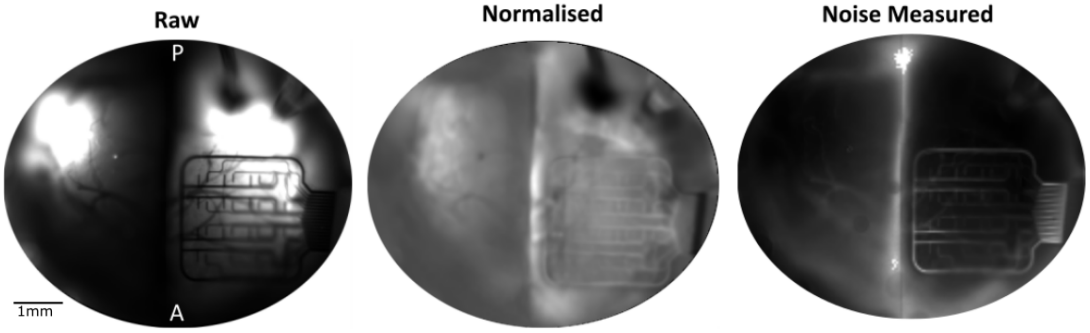

Figure 46: Examples of raw, normalised and noise measured widefield images. Raw images illustrate varying basal fluorescence levels that is resolved using the $F_{0.1}$ normalisation method. Noise measured image shows intensity based on regions with the highest noise levels, which is used for automatic exclusion from further analysis. A and P marked on raw image refer to anterior and posterior.

To further minimise error during later automated detection stages, image stack normalisation was combined with noise measurement processes. These were performed in addition to the previously described manual low SNR exclusion stage. Following normalisation of each 29,000 frame recording sweep, a custom noise measurement function was used to calculate the SNR at each pixel using median averages during baseline periods (Figure 46). Based on the calculated SNR values, a threshold was set to exclude high noise pixels. This was especially important for later seizure detection steps, whereby high-frequency noise can easily be mistaken

as epileptiform activity. Therefore, these SNR values were used to generate a binary mask for each sweep. Each binary mask was summed for all sweeps across an entire experiment, and low SNR areas were excluded across the entire experiment. This resulted in the automated detection being robust against unpredictable events during recordings, such as minor bleeds. Additionally, this allowed exclusion of areas with low GCaMP expression, or those obscured by the needle used to deliver chemoconvulsant.

Altogether, the previously defined stages of stabilisation, error correction, normalisation and SNR-based exclusion led to the generation of error-free, high SNR image stacks; with a homogenous Ca^{2+} signal across spatially-stable regions of the cortex. Therefore, I was able to proceed to stages of trace extraction and event detection.

6.2.5 Imaging Region-of-Interest Definition and Extraction

The previously mentioned stages of stabilisation and normalisation were crucial to allow extraction of meaningful Ca^{2+} fluorescence data from different pixels and regions-of-interest. Stabilisation allowed each region to remain constant and represent the same area of brain tissue throughout the lengthy recording period. Normalisation allowed each defined region-of-interest to be compared to one-another both at the same time point and during different periods of activity. Therefore, I was able to confidently proceed with region-of-interest definition and extraction. The two main goals identified to be of interest were; one, to allow the definition of different cortical areas on functional imaging stack; and two, to allow extraction of fluorescence traces from regions surrounding gSGFET recording sites.

Addressing the first aim, I utilised currently available data on stereotaxically defined brain regions (Allen Brain Atlas) and information regarding cortical boundaries on the dorsal brain surface from the powerful tool, the Allen Brain Explorer 2 (Figure 47A). During the craniotomy surgery, the stereotaxic coordinate of the posterior edge of the craniotomy was noted (Bregma -4mm). Combining this information with the camera pixel size (32μ after 2x binning), the stereotaxic coordinate of the anterior edge of the visual cortex (Allen Brain Atlas), and a to-scale map of the dorsal surface of the brain; I was able to fit a map of the different cortical regions to these functional imaging stacks. Lastly, the Allen Brain Atlas tool was used to define the cortical region marked by each boundary. As a result, I was able to broadly define which cortical region each imaged pixel belongs to (Figure 47C). Therefore, this allowed spatial definition of later detected events and comparison of different cortical regions with relevance to the functional role they play in animal

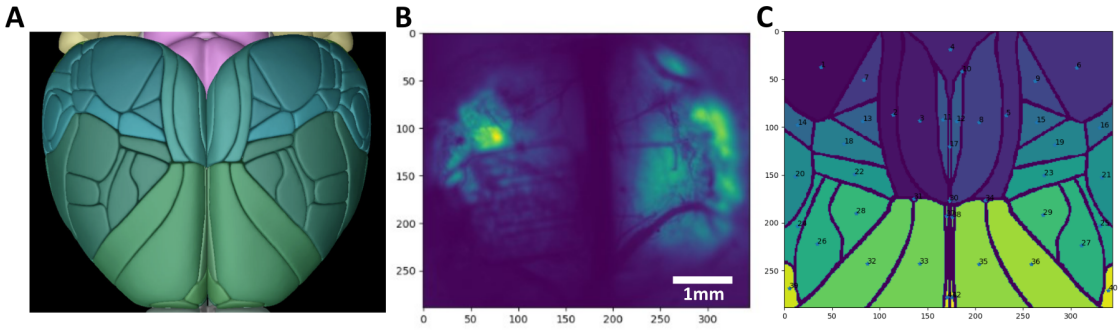

Figure 47: Process to map cortical regions onto the imaging field-of-view. **A)** Image from Allen Brain Explorer 2 used to generate a mask of cortical regions. **B)** Still image showing field-of-view with pixel numbers on X and Y. **C)** Cortical map generated using **A** cropped, transformed and translated to fit field-of-view shown in **B**. Each color represents an automatically identified distinct cortical region detected using mask segmentation.

physiology.

For the second aim of extracting Ca^{2+} fluorescence from gSGFET recording sites, each site was defined manually on a single frame from the stabilised and normalised stack (Figure 48A). I initially was able to define a single transistor position and automatically generate the position of other recording sites based on known gSGFET spacing. However, I selected a method of manual definition for each transistor for two reasons. Firstly, curvature of the gSGFET array on the cortical surface can skew the observed spacing between the transistors on the imaging. Secondly, in some cases, I performed bilateral dual gSGFET array recordings, and therefore, the channel order of the contralateral array was reversed. To account for these cases and minimise any chance of error, I manually defined the position of each transistor by visually selecting co-ordinates using a graphic interface; similar to that used for craniotomy definition. Following gSGFET position definition, traces for each sweep were automatically extracted and stored for later use. A circle with a radius of 4 pixels (128μm) was centred on each previously defined coordinate. All pixels falling with the defined circle for each gSGFET were averaged at each time point. Therefore, the data stored contained an array of 16 traces (one for each transistor) sampled at 49.06Hz (50Hz cycle rate) for each 10 minute imaging sweep (Figure 47B). These traces were used for later comparison with gSGFET activity.

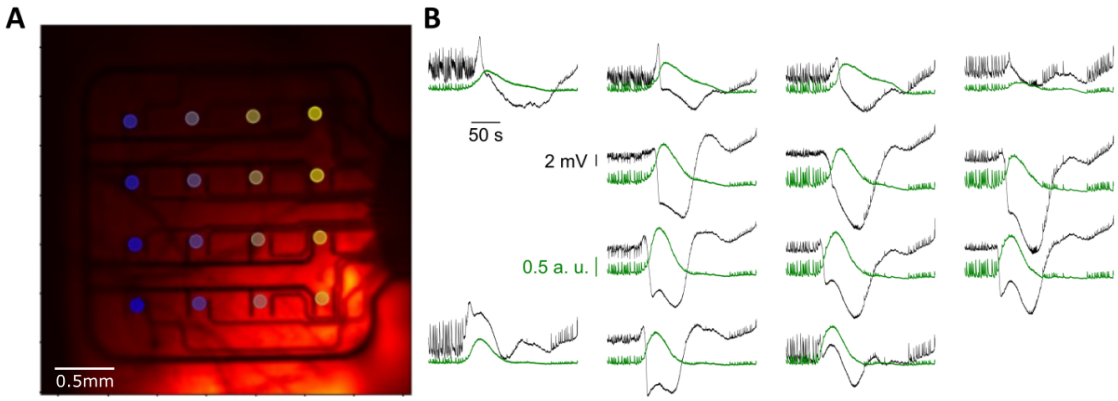

Figure 48: Extraction of Ca^{2+} fluorescence at gSGFET recordings sites during a representative seizure-associated SD recorded from a WT male mice. **A)** Extracted image of gSGFET with labelled transistor sites using the developed graphical labelling interface. **B)** Plotting of gSGFET traces with Ca^{2+} fluorescence at each functional recording site during SD.

6.2.6 Imaging Event Detection

One of the major objectives of the work presented in this thesis is the analysis of SD and seizures using novel imaging techniques. Few previous studies have fully investigated the spatial characteristics of SD propagation. Moreover, to my knowledge, no studies have attempted to characterise the spatial relationship between seizures and SD with the level of detail presented in this thesis. To extract meaningful, quantifiable information regarding these paroxysms, significant work was invested to develop event detection modules to allow extraction of seizure and SD core properties from each single pixel within the field-of-view. Both SDs and seizures showed considerable diversity in event properties, thus leading to difficulty in their separation: seizures are often observed to have high amplitude, infraslow components; and SDs are observed to occur with low amplitudes and persistent spiking. Therefore, it was difficult to resolve these events based on the presence of spiking, or the amplitude of infraslow waves alone. Consequentially, several rounds of optimisation were required to generate a robust and reliable method able to correctly classify the diverse plethora of observed events.

Spiking Detection

The developed imaging event detection algorithms underwent several rounds of refinement and optimisation. This analysis stage was highly complex to orchestrate. For simplicity, I will only present the final optimised workflow. In order to achieve accurate and reliable SD and seizure detection using this optimised workflow, spike

detection was essential. Each pixel was processed with various filters to achieve this. Firstly, the traces were baseline filtered (pybaselines library; Figure 49A) to remove any baseline fluctuations that would result in changing spike detection thresholds relative to the spike height. Following this, a spike detection algorithm was performed (Signal.findpeaks library; Figure 49A) to detect the times of all spikes, along with their amplitudes. The recording sweep was then segmented into 6 sections (each lasting approximately 100s), and the spike heights within each window were assessed. Based on these spike heights, each recording segment was attributed an amplitude value, with this value interpolated across 100s segments to allow dynamic definition within time windows (Figure 49C&D). The generated information regarding spikes, each recording segment and the baseline was stored for use in subsequent analysis stages.

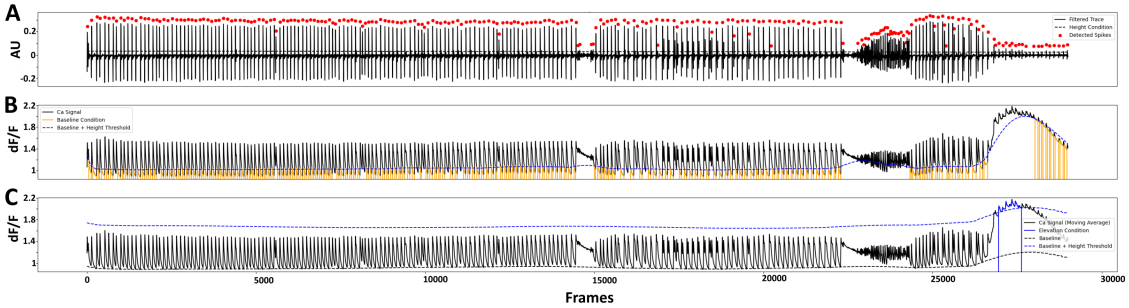

Figure 49: Spike detection and parameter extraction during initial stages of the imaging event detection algorithm shown for a single pixel. **A)** Filtered trace used for spike detection with red markers showing detected spikes. Spike detection threshold shown by dotted line. **B)** Conditions for detecting baseline periods. Baseline threshold shown by blue dotted line and any time periods at baseline indicated in yellow. **C)** Criteria for detecting putative SD events. Blue dotted line shows elevation condition which is dynamically calculated based on spike amplitude. Putative SD event highlighted in blue; which will be accepted if other conditions are met. Representative recording sweep from a WT male animal.

SD Detection

Using the previously-generated windowed spike amplitude information, a dynamic upper threshold was defined. This threshold was consistently defined as a proportion of the spike amplitudes within the segmented window for that pixel. If the baseline-filtered Ca^{2+} trace crossed this threshold, the event was identified as a putative SD event. To minimise false detection of events, known SD properties were incorporated into the required criteria for acceptance as an SD. Firstly, SD is known to propagate and will not occur at a single pixel in isolation. Therefore,

if the putative event displayed insufficient coverage (25% of each hemisphere), the event was discarded from consideration. Since preliminary investigations revealed the occasional occurrence of focal, localised SD events, this coverage criteria was lenient (Figure 50). To further refine detection, if SD propagation velocity was outside the likely range of 0.1-100mm/min, the event was likely a high amplitude seizure. However, to accept this putative SD event as a seizure, the event was required to pass the seizure detection criteria defined in the following section.

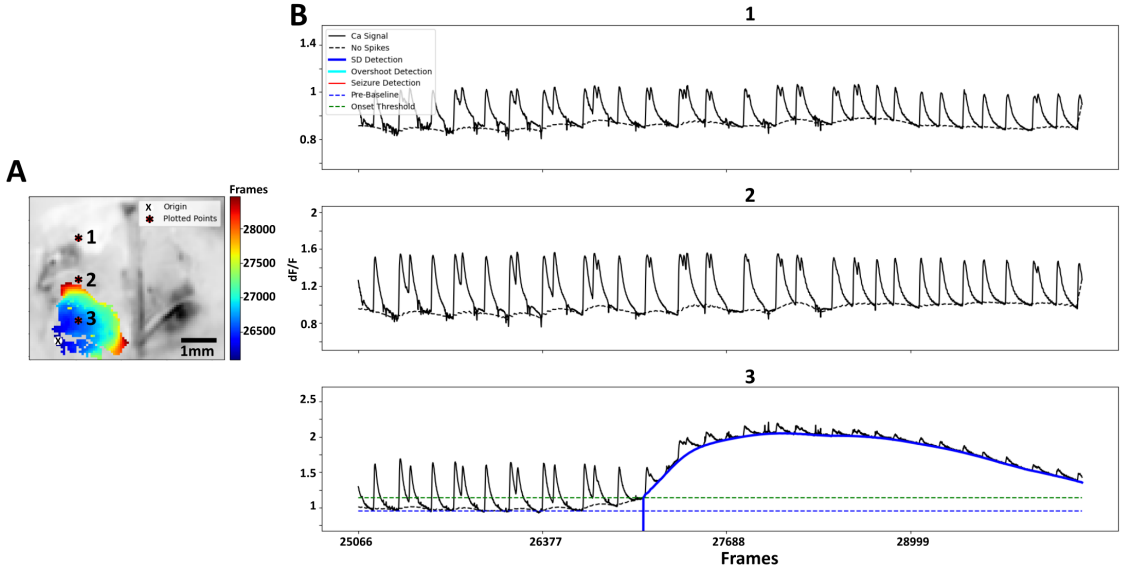

Figure 50: Accepted SD event after additional detection conditions were met. Detection is robust and able to detect small focal SD events. **A)** Widefield image with area of SD coverage shown. Origin shown as black 'X', and plotted points 1-3 in **B** shown with asterisks. Colour map depicts frames taken for propagation to other areas. 500 frames represent approximately 10s. **B)** Plotted traces corresponding to the positions of the asterisks shown in **A**. A SD can be seen in only the bottom trace that falls within the mask shown in **A**. Dotted blue line shows baseline prior to SD and green dotted line shows the SD onset threshold.

For each detected SD event, several properties were calculated. Since SD can not propagate between hemispheres contiguously across the cortical surface, detection was performed independently for each hemisphere. The extracted SD properties were SD origin, calculated as the first pixel with SD detection; hemisphere relative to chemoconvulsant injection; total event duration, calculated as time from first pixel detected to recovery of the last pixel; median duration, calculated as the median time for each pixel to return to baseline after crossing the SD threshold; median amplitude, calculated as the median of peak amplitudes for all detected pixels; area covered, calculated as the number of SD pixels scaled by pixel size; total area under the curve, calculated as the sum of SD integrals in all pixels; and, mean area

under the curve, calculated by the mean of SD integrals in all pixels. Information regarding SD velocity was also calculated by performing phase-correlation (skimage.registration.phase_cross_correlation) of SD waveforms along different linear axes from the origin. This allowed dynamic investigation of SD propagation velocity in all directions from the origin. These parameters were exported into the database, which is fully described below.

The outcome of this section is the ability to dynamically track SD propagation across the entire field of view. Each pixel was attributed a binary value of SD or not for each entire recording sweep. This was used to define windows of interest to extract relevant SD properties. The ability to track SD dynamics with this detail and investigate these SD properties is novel, and expands the current boundaries of SD analysis.

Seizure Detection

Seizure detection using widefield functional imaging is a relatively unexplored area. Notably, Rossi et al. (2017) developed a bespoke method to detect and track seizure propagation. Rossi et al. (2017) measured the peak fluorescence during a seizure at the focus and defined the onset for each pixel as the time when 30% of this fluorescence intensity is exceeded. For ease, I investigated this method using the recordings acquired with this experimental paradigm. However, due to differences in expression methods (transgenic animal vs. viral expression) and construct kinetics (GCaMP3/GCaMP6f vs. GCaMP7f), the previously characterised method was unsuccessful in tracking seizure propagation for these recordings. Therefore, a new method was required. Initially, for simplicity, methods frequently employed for seizure detection in EEG studies were investigated. These included spike frequency, coastline and signal power. However, these methods alone were insufficient to distinguish seizures from high frequency spiking activity coinciding with SD events. As a result, a novel custom-built method was generated using the previously-extracted spiking information.

Each previously detected spike was investigated for each pixel. A novel measure termed post-spike recovery ratio (PSRR) was defined for each spike. This measure was a ratio of the amplitude following a spike to the amplitude preceding the spike. The amplitudes preceding and succeeding each spike were defined by subtracting the previously generated baseline filtered traces, and these values were normalised to the spike amplitude for each event. A threshold was then set for the PSRR value (0.25, where 0 indicates complete post-spike recovery), and if the PSRR exceeded the threshold, the event was considered as a putative seizure. The rationale behind

this measure was built upon findings from Rossi et al. (2017), wherein it was discovered that seizures initiate with a spike identical to those observed to occur between seizures, however, the activity that follows differs. Therefore, the developed algorithm detected these spikes and searched for the signature of a seizure immediately following; marked by the absence of immediate recovery to baseline. This absence of immediate recovery to baseline resulted in a high PSRR value, indicating a putative seizure.

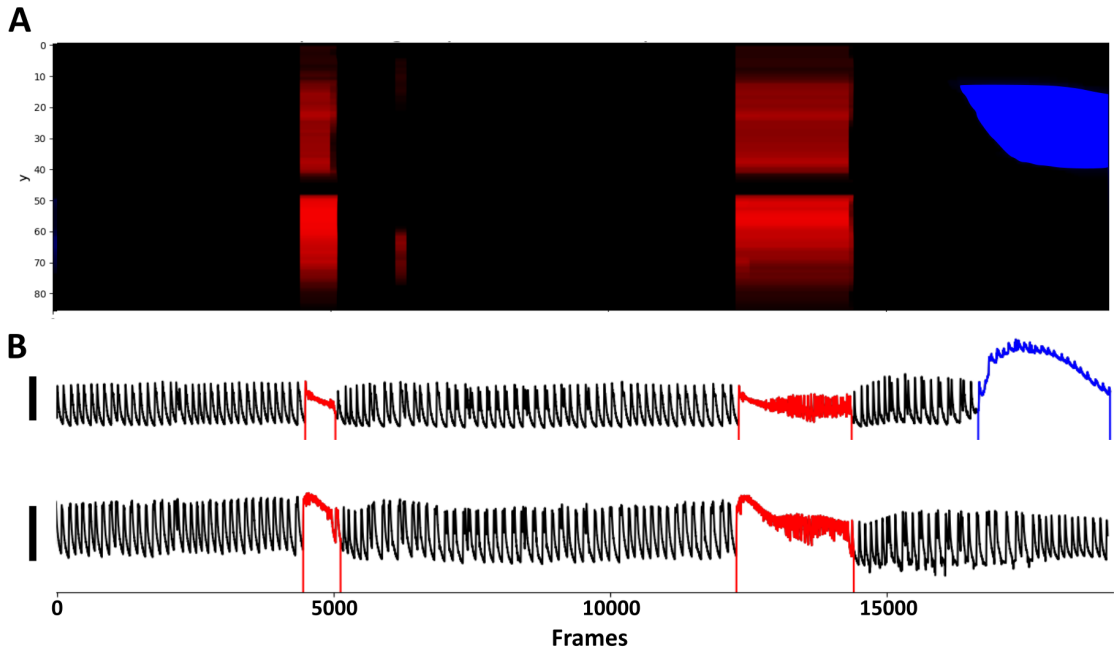

Figure 51: Successfully detected and spatially-discriminated seizures and SDs from widefield imaging data acquired from a WT male animal. **A)** Projection in the X-dimension showing detected events across different Y-coordinates of the image for an entire 10min imaging sweep. Seizures are shown in Red and SD in Blue. **B)** Traces of the activity shown in **A**. Top trace falls within the SD zone and the bottom trace does not. Similarly, seizures are shown in red and SD in blue. Amplitude scale bar is for 0.5dF/F.

Putative seizures were then further screened using several conditions. Firstly, if the spatial coverage of the event footprint was restricted to few sparse pixels (<20% of the hemisphere), the event was excluded from consideration. This removed false positives occurring in isolated pixels. Secondly, if the duration of the event was below 4s, it was not considered to be a seizure. This allowed clear distinction between seizures and complex spikes. Thirdly, if the pixel exceeded the upper amplitude threshold for the window defined previously using spike heights, the event was considered as likely to be a SD instead. The end of the seizure was defined either as the point where the amplitude returned to baseline, or as the point where

the amplitude crossed the upper threshold and transitioned directly into an SD state. Altogether, this method allowed extraction of time points and broad cortical regions that were involved in seizure activity.

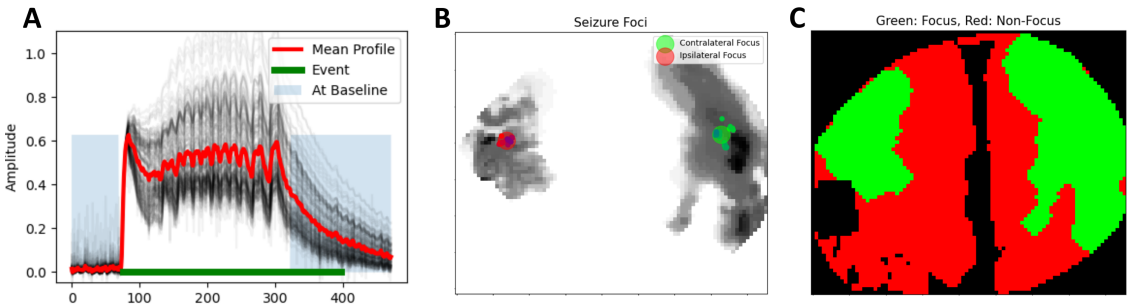

Figure 52: Further analysis of seizure activity to highlight spreading core. **A)** Detected seizure with overlay of waveforms at all pixels across the accepted field-of-view. Pre-event baseline subtracted from seizure. Mean profile of all waveforms shown in red; black traces represent each pixel; blue regions indicate period of baseline consideration; green bar indicates length of accepted event. Clear variability in waveform can be seen with some pixels showing a far greater increase in amplitude during the seizure compared to others. **B)** Areas accepted as the seizure core based on further amplitude increase beyond initial interictal amplitude. Red shows the focus ipsilateral to picrotoxin injection. Green shows the secondary focus on the contralateral hemisphere. Interestingly, the focuses are mirrored across the midline with seizures originating at homotopic locations nearby to the site of injection. **C)** The detected areas in **B** were used to generate binary masks of areas recruited to the seizure focus (green). These were compared to those that had a signature of a seizure but showed no further amplitude increase beyond the initiating interictal spike; and were therefore, accepted to have a passive role in seizure dynamics (red).

Initial findings revealed a similarly large footprint in imaged seizures compared to that presented in the literature for EEG recordings. Outputs revealed diversity in seizure waveforms for a single event: on one end of the spectrum, there was a clear increase in amplitude beyond the initiating interictal spike; on the other, the amplitude fell and remained slightly above baseline until the entire seizure had terminated (Figure 52A). These two waveforms were identified as two different signatures of seizure activity. The first, wherein fluorescence continues to increase above the interictal amplitude was considered to be a region driving the seizure through additional neuronal discharges. The second, wherein fluorescence falls considerably, yet remains above baseline, was considered to be synaptically activated by the seizure core, but with no local excessive neuronal firing. The areas actively participating in seizure propagation were defined by subtracting the initiating spike amplitude from the remainder of the seizure and binarising any remaining values. Visual examination of the generated areas revealed propagation dynamics consistent with current

knowledge of seizure characteristics. These areas were seen to expand from a focus at the start of the seizure and spread to multiple regions, before contracting back to the focus at seizure termination (Figure 52B&C). Moreover, these regions were often mirrored between hemispheres, consistent with the literature regarding preferential propagation between areas showing strong functional connectivity (Rossi et al., 2017). Altogether, this method allowed delineation of areas actively participating in seizures and those showing seizure activity due to passive synaptic input from elsewhere.

Several properties regarding seizures were extracted. These included mean and total duration, as defined for SDs; and mean and total area under the curve, once again, defined using the event intregral at each pixel. Multiple different properties relating to seizure coverage were also extracted. These included total area covered by the seizure; marked by the pixels displaying any seizure waveform. Information regarding the seizure focus was also extracted, including the origins of different foci and the maximum area covered by the seizure focus. In addition to the extraction of these properties, binary masks for each seizure were stored, as for SD events. The end result was the ability to readout seizure activity across multiple cortical regions, with it possible to distinguish between areas actively participating in seizure dynamics and those being passively influenced by the seizure core. These many properties and binarised events were extracted and stored in databases for later use.

Event Outputs and Screening

The previously outlined algorithms allowed detection of spiking, seizures and SD events; along with their propagation across large regions of the cortex. From these detected events multiple outputs were generated. Firstly, a binary mask was created for each event. This was used for later methods to track spatial propagation and extract information to allow classification of different gSGFETs during different events, e.g. gSGFETs recordings from inside and outside seizure core. Moreover, two excel databases were generated, one for seizures and another for SD. Within each database, every detected event was represented as a column. For SDs, each column contained the extracted properties previously mentioned, along with metadata such as event sweep, start frame and end frame. Moreover, several example waveforms were plotted to allow screening of detected events. False positive events were rare and were simply deleted from the Excel database. Similarly, seizure events and their properties were stored in a similar database. Event waveforms were also stored and screened, with falsely detected events similarly removed. The screened

and modified Excel databases were then loaded back into a Python script, converted to a dataframe (Pandas library) and analysis was performed on extracted seizures and SD events.

6.2.7 Event Timeline Generation

To automatically generate a timeline of event relationships without any bias from user input, the extracted SD and seizure properties were processed. Each SD event was examined and the nearest seizure before and after the SD in the same imaging recording sweep were selected. Since these events had been spatially classified, the start and end times used referred to the entire cortical event as opposed to emergence at a single point. Therefore, the constructed timeline took full advantage of the spatial coverage of widefield imaging recordings, and allowed greater dissection of the seizure-SD temporal relationship. Each entire event from start to finish was plotted for each SD to allow examination of interactions and temporal overlap between seizures and SD. Moreover, a histogram was generated using the difference between event start times. These histograms were generated with multiple permutations centring either seizure or SD. To generate adequate controls, data from sweeps without SD were manipulated. The result was a control timeline plot with temporal relevance to experimental timepoints. These controls were used to compare the probability of seizures occurring within certain time-windows relative to the time of SD. The end result is the ability to characterise the temporal relationship between seizures and SD in newfound detail due to the incorporation of spatial information. These tasks were all achieved through manipulation of stored Python Pandas libraries.

6.2.8 Spatial Characterisation of Events

Acquisition of widefield imaging data led to the powerful ability to spatially dissect event properties. SD origins were defined as the first area in which a pixel was observed to meet the previously defined SD criteria. This information was used to investigate patterns in SD propagation in the cortex. Propagation of SD events was examined using the generated binary masks relating to SD initiation at each pixel. These were used to generate maximum intensity projections of total SD coverage. Spatial information regarding seizures were similarly processed. Initial readouts of all seizure waveforms showed coverage across the entire field-of-view and rapid propagation. However, the previously described methods to track the seizure core were used to identify an origin. The detected seizure core was used to generate a binary

mask localising regions driving observed epileptiform activity. These masks and spatial origins were combined with the previously described brain mapping functions to allow investigation of event origins with relation to the functional properties of different brain regions.

6.2.9 Statistical Analysis

Several statistical modules have been generated to analyse the outputs of the presented pipeline. These have been fully integrated into the workflow of the pipeline. Outputs relating to different SD and seizure properties were plotted in relation to one-another (matplotlib.pyplot), to allow investigation of mechanisms of SD induction and to probe SD properties. To allow correct comparison between these variables, their properties had to be explored in detail. Firstly, histograms of all event properties were inspected to enable visual examination of different distributions (Pandas and Seaborn). Secondly, to enable justified comparisons of events using the correct statistical tests, a statistical workflow was generated. These tested data for normality (scipy.stats.normaltest) and homoscedasticity (scipy.stats.levene). Depending on whether data passed these tests, parameteric (scipy.stats.ttest with or without Welch correction) or non-parametric (scipy.stats.mannwhitneyu) statistical tests were employed. For comparison of SD property relationships, since the relationships are relatively uncharacterised, linearity and normality could not be assumed. Therefore, Spearman correlation (scipy.stats.spearmanr), Pearson correlation (scipy.stats.pearsonr), data ranking and linear regression (sklearn.linearmodel.LinearRegression) modules were integrated. Altogether, this demonstrates the efficient integration and implementation of statistical modules into the presented Python analysis workflow to allow easy comparison of different event properties. As mentioned previously, due to COVID-19-related disruptions, complete datasets could not be collected. Therefore, many sample sizes are insufficient for proper use of these statistical tests. Nonetheless, the development of these methodologies enables the efficient expansion of current datasets.

6.2.10 gSGFET Processing

Prior to the work presented here, several gSGFET-related analysis tools had been developed and employed in multiple studies (PhyREC library; Guimera-Brunet Lab; CNM-CSIC). These tools were utilised as a starting point for my investigations. The first step of gSGFET processing is loading the Simulink (MATLAB) output files

containing low and high frequency current traces, processing the I_{ds}-V_{gs} transfer curves, and reconstructing the field potential signal (Figure 52). Previously generated Python code was used for this procedure. Moreover, previously optimised tools such as signal filtering and plotting methods was also utilised. For more information regarding these tools, please refer to Masvidal-Codina et al. (2021).

The major developments to gSGFET processing tools surrounded the incorporation with imaging outputs. Firstly, during acquisition, the recording configuration was adapted to allow TTL inputs to the gSGFET amplifier. This TTL pulse was used to signify the start of each imaging recording sweep during continuous gSGFET acquisition throughout the experiment. During analysis, this pulse was used to segment the gSGFET recording into relevant time windows corresponding to imaged periods. Following this, previously extracted imaging traces from gSGFET locations, and the associated channel-related metadata, were used to plot the signals together (matplotlib.pyplot). SD and seizure masks were also used to define whether each gSGFET was recording from a region within, or adjacent to each paroxysmal event. These definitions were used to group gSGFET recordings to allow detailed electrophysiological analysis of events that had been spatially characterised using Ca^{2+} imaging.

Extracted time points from imaging were used to segment gSGFET recordings into relevant event-related time windows. This allowed investigation of detected SDs and seizures using the greater detail and temporal resolution of electrophysiology. To achieve this, each event time window was extracted from the imaging and matched to a time on the gSGFET recording. Each gSGFET seizure trace was filtered into relevant frequency bands of interest (PhyREC library). These frequency bands included; infraslow (0.001-0.1Hz), slow (0.1-0.5Hz), delta (0.5-4Hz), theta (4-8Hz), alpha (8-12Hz), beta (12-30Hz), low gamma (30-50Hz) and high gamma (50-100Hz). The band 'slow' has not been used until now: infraslow activity has an upper limit of 0.1Hz, and delta a lower limit of 0.5Hz. Therefore, the slow band was created to bridge this frequency interval. The root-mean-square of filtered traces was then calculated using a sliding window of 500ms and a median filter of 500ms. The mean of different time windows relative to seizure initiation were then calculated. These were calculated as pre (-10s to -5s), active (-5s to 0s; reflecting the active-DC shift described in Bonaccini Calia et al. (2021)), onset (0s to 1s), mid (1s to t_{end}-1s), end (t_{end}-1s to t_{end}) and post (t_{end} to t_{end}+5s). Activity at different time points was normalised to a baseline period of activity for that transistor and to the pre time window value at each recording site. Electrographic seizure recordings were separated into groups based on their association to SD and their

spatial relationship with regard to the seizure core. Additional investigations used similar methods to extract a value for LFP power (1-150Hz) before the seizure (-70 to -10s) and to investigate the time taken for the LFP power to return to this value after a seizure with or without SD. Altogether, these modules allowed easy integration of imaging analysis outputs into gSGFET analysis streams; thus, allowing the spatial power of widefield imaging to be combined with the temporal resolution of electrophysiology.

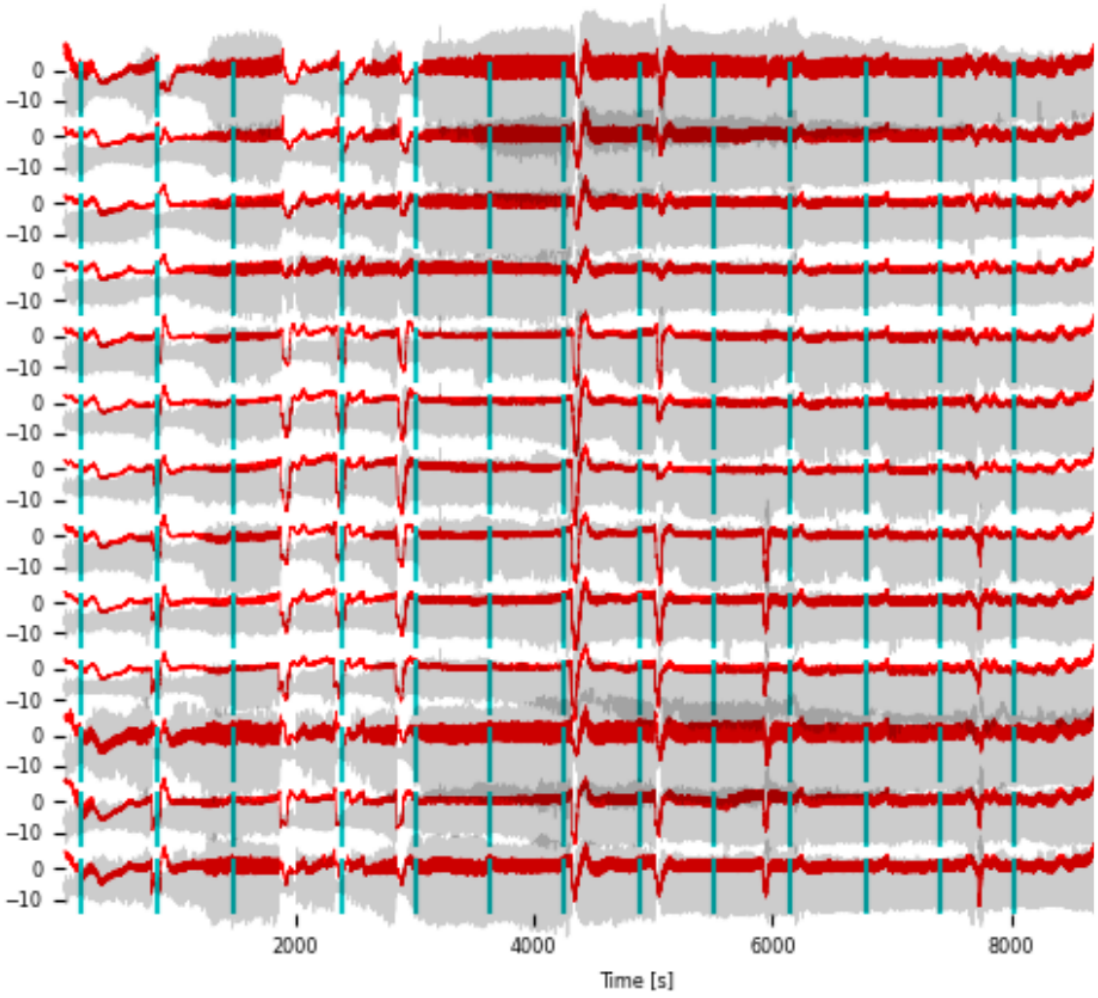

Figure 53: Entire recording period plotted for one animal showing 13 of 16 functional and calibrated gSGFETs. Multiple SDs and seizure observed. Stable, high SNR, full-band electrophysiology shown for each trace in red. Grey shows the same signal filtered to illustrate the LFP band. Each blue line indicates the start of a new 10min imaging sweep and was used to time-stamp different recording modalities to one-another.

Other analysis modules were also investigated such those probing signal correlations between the two recording modalities, seed pixel correlations and those investigating phase-amplitude coupling. Examples of the results of this analysis

have been generated, however, full integration is still underway.

6.3 Discussion

The results presented in this section demonstrate the successful construction of a complex, organised analysis pipeline able to process and quantify the optimised information-rich experimental paradigm. I presented several modules, that when combined, are able to access the dense information generated by widefield imaging investigations with a newfound level of detail. These steps included stabilisation, normalisation, error detection, trace extraction, event detection, gSGFET calibration and imaging-gSGFET incorporation. Due to the multiple analysis modules, several files allowing easy tracking of analysis stages and experimental metadata were generated. Moreover, each analysis stage generated multiple outputs and interactable objects; allowing manual correction in the rare event of any errors. Altogether, these presented analysis tools were essential to allow full access to the information contained within these recordings. Therefore, this allowed meaningful insight to be gained into seizure-SD dynamics, as well as the power of the constructed experimental paradigm. The analysed outputs of this pipeline will be discussed in detail in forthcoming sections.

To my knowledge, no similar tools have been previously generated. The majority of studies imaging seizure and SD dynamics either use IOS (Houben et al., 2017; Santos et al., 2014), or in some cases two-photon microscopy (Wenzel et al., 2019). The previous studies that have used widefield Ca^{2+} imaging simply sample from few selected regions of interest across the field-of-view (H. T. Zhao et al., 2021a; Rossi et al., 2017); similarly to the preliminary data presented in Chapter 5. Moreover, these widefield SD investigations have been performed in the context of other disease states (such as stroke and glioblastoma) (Hatcher et al., 2020; H. T. Zhao et al., 2021a), but have not included concurrent investigations of seizure dynamics. As a result, the presented analysis allows tracking of both seizure and SD activity continually across the large field-of-view. Moreover, the presented tool holds considerable promise in assisting the wider neuroscience community. The ability to easily and robustly detect SD events across an entire field-of-view is a powerful method; useful for all pathological contexts where SD is observed (e.g. epilepsy, migraine, stroke, glioblastoma).

Therefore, the presented development of a tool to simultaneously investigate widefield Ca^{2+} fluorescence during seizure and SD dynamics is novel and powerful. The initial stages of image stack stabilisation have been performed previously.

However, not specifically in the context of SD with this precision. Moreover, the ability of this pipeline to extract information automatically across the entire field of view without reductive ROI selection and averaging leads to full access to the spatial information in these recordings. Additionally, the extraction of properties relating to detected seizures and SDs across the large field of view generates a detailed dataset able to provide powerful insight into these paroxysms. Lastly, the incorporation of novel full-bandwidth electrophysiological recording methods into the widefield imaging paradigm has not been previously demonstrated; and creates another point of novelty. Altogether, the constructed experimental paradigm to simultaneously study SD and seizures using optical and electrophysiological methods shows great novelty; and to match this, a powerful, novel analysis pipeline was constructed. Together, the combination of the experimental configuration and the developed analysis tools leads to a powerful ability to probe paroxysmal events.

6.4 Future Directions

Although several major developments have led to the optimisation of the presented analysis pipeline, minor additions are still required. These additions will follow the work presented in this thesis to allow finalisation of outputs.

Firstly, validation of imaging detection will be performed by using an established method of seizure and SD detection on gSGFET recordings. Cross-validation between recording modalities will be a powerful tool demonstrating the accuracy and reliability of the presented image analysis pipeline. Due to currently performed manual event screening, it is evident events are being detected correctly. However, quantification of the accuracy of the pipeline without this manual screening would be a powerful development.

Secondly, further work into spike characterisation will be performed. The presented stage of spike detection combined with PSRR measurements allowed classification of single spikes, complex spikes and seizures. These complex spikes demonstrate diversity in their waveform as well as spatial properties. Further investigation of these events may lead to a greater understanding of alterations in network excitability leading to the increased probability of transitioning into a seizure or SD state. Currently in development are tools to characterise the properties of these different complex spikes. Once characterised, these spikes can be sorted into various groups using principal-component analysis. Since, the imaging recordings are, to some extent, electrographic recordings with reduced dimensionality, these sorted imaging spikes can be used to group electrographic spikes. This may lead to an

increased understanding of electrophysiological signatures of epileptiform activity which would lead to a greater understanding of the network alterations precipitating seizures and SD.

In general, the presented analysis pipeline is powerful, reliable and robust. Therefore, the major future developments will be in the application of this pipeline to different disease-related contexts, as opposed to further pipeline development itself. However, to allow long-term flexibility, the pipeline has been designed to allow easy integration of additional modules. Here I conclude the section describing this analysis framework, and move forward to demonstrate applications in investigating pathological paroxysmal events.

Chapter 7

Synergistic Investigation of Neuronal Network Dynamics using Combined Imaging and Electrophysiological Recordings

7.1 Introduction

Both imaging and electrophysiology have separately been shown to provide insight into seizure and SD dynamics (Rossi et al., 2017, 2018; Hatcher et al., 2020; Bonaccini Calia et al., 2021). Imaging techniques are able to provide this insight through utilisation of high spatial resolution. Electrophysiological techniques, on the other hand, are able to provide insight through an unmatched temporal resolution. Nonetheless, each method alone presents with limitations and the other method is often able to overcome these limitations; leading to an information-rich combined paradigm able to probe paroxysmal events in high detail. This chapter will use the experimental paradigm and analytical tools described in previous sections to explore simultaneous electrophysiological and optical readouts of pathological events in WT mice.

Imaging techniques are able to spatially dissect activity by revealing complex dynamics of signal transmission (Rossi et al., 2018). Depending on the desired scale of investigation, imaging techniques are able to provide insight from the subcellular level to entire brain regions. The investigations presented here focus on capturing information from large cortical areas, hence the use of widefield imaging. Therefore, this leads to the requirement for a fast scientific camera able to capture a large field of view. Considerable advancements have been performed in recent

years in the manufacturing of charge-coupled device (CCD)-based and complementary metal-oxide semiconductor (CMOS) cameras. However, the rate of acquisition still remains limited. This acquisition rate ceiling is primarily a result of current technological limitations. Imaging acquisition rate is also limited by the dimensions of the recording field due to larger images requiring a longer time to clear charge from the photosensitive array between frames. Additionally, since I utilise Ca^{2+} dynamics as a readout of neuronal activity, temporal resolution also depends on the kinetics of the fluorescent reporter. As a result, a clear constraint of such studies solely relying on widefield fluorescence Ca^{2+} imaging is a limited temporal resolution. The inclusion of electrophysiology into the recording paradigm is able to overcome these temporal limitations and increase the insight gained. To further increase this insight, DC-coupled recording devices (gSGFETs) also allow simultaneous investigation of the role of infraslow activity and ultraslow potential shifts.

Nonetheless, gSGFET arrays and other full-bandwidth recording techniques present other limitations. Firstly, the number of recording sites on the tissue is far lower than pixels within a widefield imaging window. Secondly, the area sampled by a single recording site is uncertain. Electrical footprints of epileptiform activity are known to be present well-beyond the generating source due to factors such as volume conduction (Viventi et al., 2011). As a result, electrophysiological recordings are limited in their ability to spatial resolve pathological activity when compared to imaging methods. In addition to these spatial limitations, epicortical gSGFET arrays are also limited in that they record from a distance relative to neuronal soma. Therefore, the frequency range of the recording has an upper limit below multi-unit activity, and recorded potentials are dominated by synaptic activity. I investigate these spatial limitations through simultaneous fluorescence Ca^{2+} imaging at recording sites; with the aim of increasing the current understanding of both fluorescence and electrophysiology signal contents.

Altogether, it is empirically evident that combining optical and electrical approaches to probe paroxysmal events is advantageous. Each of the methods are able to overcome limitations of the other, and the synergistic combination of these two methods will create a platform able to unravel complex mechanisms surrounding paroxysmal disorders. Here in this section, I will further delve into the notion of this advantageous synergism and demonstrate clear advantages of the discussed combined approach.

7.2 Results

The first and primary aim of the results presented in this section is the demonstration of the strengths of combined widefield imaging and multi-site full-bandwidth electrophysiology. Due to previous gSGFET optimisation leading to low autofluorescence, transparent devices; I was able to successfully extract GCaMP fluorescence traces from the sites of electrophysiological recording. Firstly, previously described stages of stabilisation and normalisation were performed to enable accurate comparison both spatially and temporally. Secondly, the previously described extraction algorithm was used to enable averaged fluorescence traces correctly corresponding to gSGFET recording sites. The result was the ability to investigate normalised Ca^{2+} dynamics with full-bandwidth electrophysiological activity during different paroxysmal events.

To initially investigate this relationship, I first selected one of the observed seizure-associated SD events. Calibrated gSGFET recordings and corresponding Ca^{2+} fluorescence were visually displayed together (Figure 54). Since fluorescence is commonly observed spatially, and electrophysiology is commonly observed using time-series plots, I represented both recording modalities using both methods of visualisation. The aim of this was to reveal differences in signal properties with minimal bias from the method of displaying the data. Therefore, in one instance, gSGFET recordings were represented graphically, as seen for Ca^{2+} fluorescence. Each gSGFET was represented as a single point and the neighbouring regions between transistors were attributed a magnitude through bicubic interpolation of surrounding transistor recordings. The result is a graphical representation of the activity recorded by the gSGFET array in an image stack similar to that acquired for Ca^{2+} dynamics. To allow comparison, a region-of-interest was placed around the gSGFET array on the imaging stack and the imaged array was cropped and rotated to match the area and orientation of the transistor map. Multiple time points with an interval of 16s were displayed to allow comparison of the abilities of gSGFETs and GCaMP in capturing different stages of spiking, seizures, and SD (Figure 54A).

Initial observations revealed clear bidirectional information from gSGFET recordings and unilateral information from GCaMP recordings. During different depolarising events such as spiking, seizure and SD, GCaMP fluorescence only displayed a clear increase from the baseline level. However, gSGFET recordings clearly presented more information which was conveyed through the polarity of recordings: spiking and seizure-associated depolarisation clearly manifest as both negative/downward and positive/upward spikes. However, the depolarisation dur-

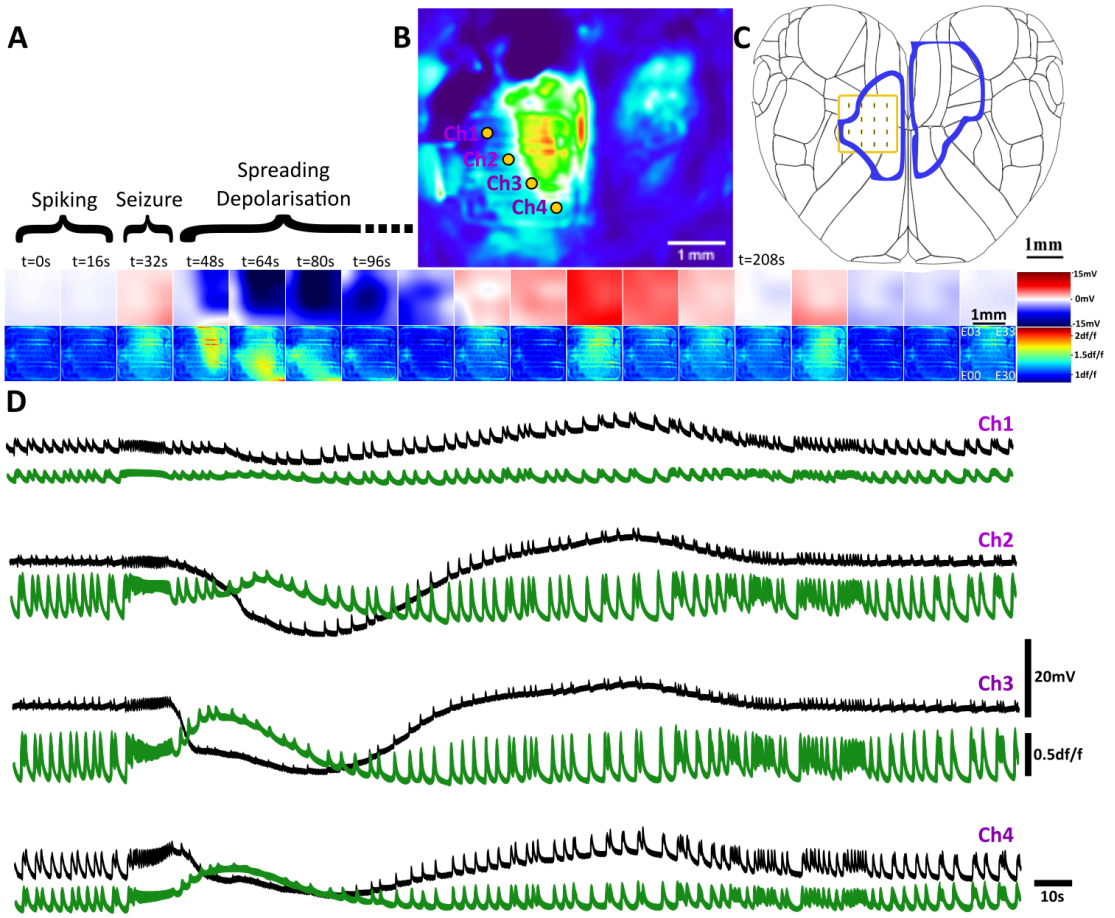

Figure 54: Concurrent calcium imaging and full-bandwidth electrophysiological recording of a representative seizure-associated SD event in a WT male animal revealing clear differences in event signatures. **A)** Time-lapse images of gSGFET recording represented as a map using bicubic interpolation between transistors (top). Time-matched time-lapse images of normalised GCaMP fluorescence under gSGFET array. Spiking, seizures, SD and SD-recovery shown. Activity corresponding to each still image shown directly below in **D**. **B)** Imaging field-of-view during bilateral SD, with 4 gSGFETs plotted in **D** annotated. **C)** Map of cortical regions on dorsal surface of the mouse brain. Location of gSGFET array and each transitor marked, along with outline of maximum area covered by SD (blue). **D)** Traces of recording in **A** for 4 of 16 gSGFETs (black) and corresponding GCaMP fluorescence (green) averaged over a radius of 128μm around each transistor. gSGFET annotations match those shown in **B**.

ing SD is represented as a negative/downward event (Figure 54D). Moreover, during later stages of SD, a clear upward overshoot can be observed on gSGFET recordings, with this activity absent from GCaMP recordings (Figure 54A). Therefore, it can be seen that the differing polarity in gSGFET recordings highlights clear differences in signal generation mechanisms and the information these two recording modalities represent. Further dissection of the causes of gSGFET signal polarity differences may reveal interesting insight into dominant synaptic pathways during these events. Nonetheless, imaging methods provide clear advantages in resolving events spatially: the previously presented SD detection method allowed mapping of the spatial coverage of SD events, revealing bilateral characteristics and propagation to areas beyond the coverage of the gSGFET array (Figure 54C). Therefore, this creates a compelling argument for a combined approach, where each recording modality provides information absent from the other.

To closer examine these differences in signal contents, individual traces were expanded. Three spatially-separated transistors and corresponding Ca^{2+} traces were selected for close examination. Investigation of seizure-associated SD recordings from these different modalities at different locations revealed striking differences. The Ca^{2+} fluorescence amplitude of the SD was seen to differ largely between GCaMP recordings extracted from gSGFET locations (leading to classification of some regions within the SD mask and some outside; Figure 55A). However, the observed GCaMP waveform was similar across all locations within the mask (Figure 55B; Ch2 & Ch3- green traces). With regard to this same event recorded from gSGFETs at the same locations, the different transistors showed diversity in waveform. Firstly, the properties of the depolarisation phase during the SD were seen to vary considerably: some gSGFETs showed biphasic SD waves with more prominent dual-peaks (Figure 55B; Ch3- black trace) than others (Figure 54B; Ch2- black trace). Moreover, the gSGFET recordings showed clear lasting upward deflections lasting long after the SD depolarisation (Figure 55B; black traces). This upward deflection is seemingly absent from GCaMP recordings (Figure 55B; green traces). To examine the gSGFET-GCaMP difference closer, the time-period surrounding the spikes preceding a seizure was expanded. Similarly to as described for the SD wave, the GCaMP traces showed similar spike waveforms across the investigated sites (Figure 55C; green traces). However, gSGFET recordings of the same period of activity revealed clear diversity in spike waveform (Figure 54C; black traces). Sharp spikes were observed in some transistor recordings but not others. Moreover, in one case, this sharp spike was followed by an upward deflection (Figure 55C; Ch1- black trace), in another, the sharp spike was negative and followed by a upward deflection

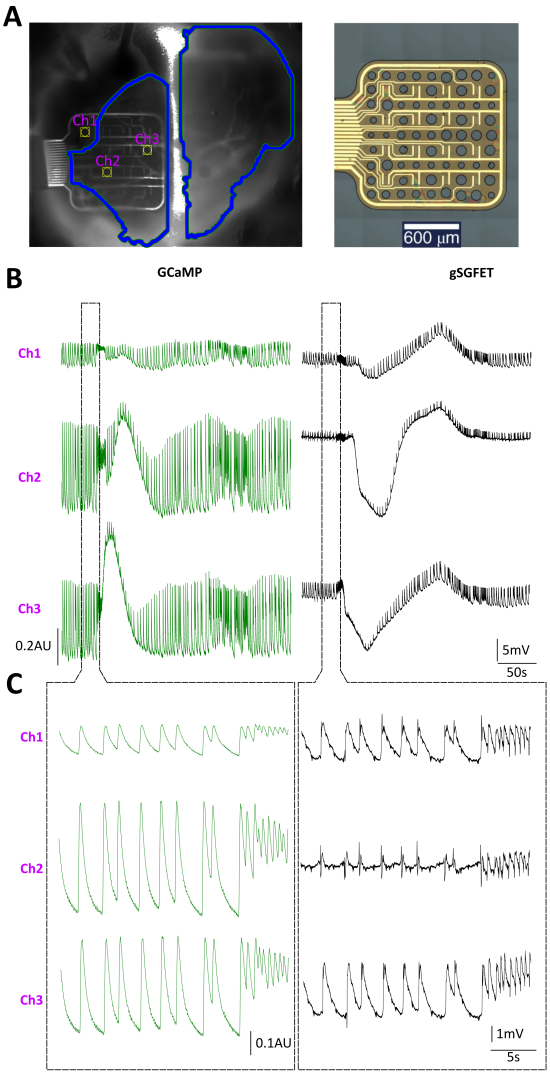

Figure 55: Investigative comparison of gSGFET and GCaMP signal contents during a representative seizure-associated SD in a WT male mouse revealing greater event resolution using gSGFET recordings. **A)** Imaging field of view with relevant transistors marked and SD maximum area covered shown (left). Image of gSGFET array also shown (right). **B)** Traces for the 3 marked transistors in **A** shown. GCaMP fluorescence (left) shows similar waveforms across multiple locations with minimal SD signature seen outside of SD area (Ch1). Full-bandwidth gSGFET traces (right) demonstrate diversity in SD waveform and illustrate clear signatures of upward DC deflection during SD recovery away from SD area (Ch1). **C)** Expansion of highlighted activity in **B** at transition from ictal spiking to seizure. GCaMP fluorescence (left) displays similar spike waveforms and properties across different locations. Corresponding gSGFET traces (right) demonstrate diversity in waveform properties with complex spikes of mixed polarity and spike-wave complexes shown at some transistors (Ch2) but not others (Ch3).

(Figure 55C; Ch2- black trace; observationally similar to a spike-wave discharge), and in a third, the spike and wave/deflection were seemingly merged with the trace looking similar to the GCaMP recording (Figure 55C; Ch3- black trace). Altogether, this close view of gSGFET and GCaMP recordings revealed a high level of detail on gSGFET recordings that GCaMP is unable to capture. Moreover, the difference in signal polarity between electrographic recording sites demonstrates an ability to capture complex phenomena that Ca^{2+} dynamics are unable to convey.

To further highlight this difference in signal content, a Fourier-based method was used to investigate the frequency components of the gSGFET and GCaMP signals during the previously presented period of activity. gSGFET (Figure 56A) and GCaMP (Figure 56B) recordings were resolved into different physiologically-relevant frequency bands. For gSGFET recordings, all relevant frequency bands could be clearly resolved (Figure 56A). However, for GCaMP recordings, frequencies above 24Hz could not be resolved (Figure 56B). This was due to the limited imaging sampling rate (49.06Hz) resulting in a Nyquist limit of 24.5Hz. Therefore, the beta band upper limit was reduced from 30Hz to 24Hz. Moreover, no information in the low-gamma to high-gamma range could be acquired. Furthermore, by the alpha and beta ranges, the ability to resolve these frequencies can be seen to drop considerably. Of course, due to these being local fluorescent measurements and not widespread electrical oscillations, the signal content within these frequency bands would differ considerably between modalities: however, the comparison highlights differences in temporal resolution between the two recording techniques.

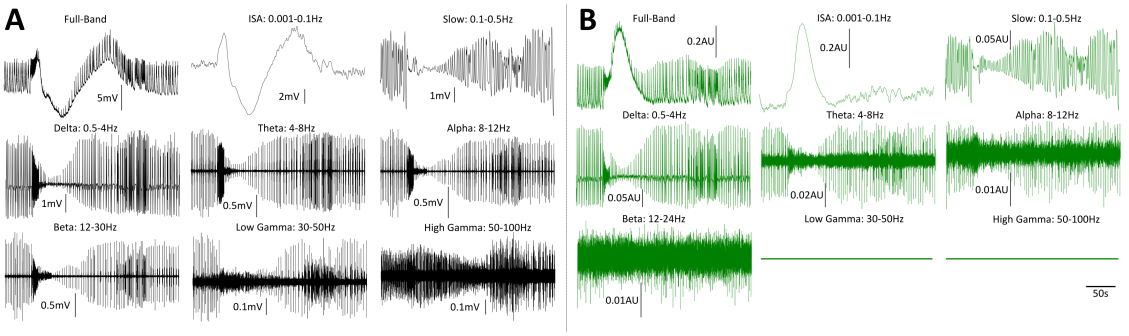

Figure 56: Examination of the bandwidth capabilities of gSGFET and GCaMP recordings. gGSFET arrays demonstrate greater temporal resolution and ability to resolve high frequency activity. **A)** gSGFET recording of a representative seizure-associated SD from a single transistor. Full-band, ISA, Slow (to bridge ISA and Delta), Delta, Theta, Alpha, Beta, Low Gamma and High Gamma traces shown. **B)** Traces as shown in **A** for GCaMP fluorescence traces at the same location. Inability to resolve frequencies above 24Hz due to Nyquist limitations shown. Representative traces from a WT male animal.

To further probe differences in the events underlying gSGFET and GCaMP signal generation, the recording configuration was expanded to incorporate a second gSGFET array on the hemisphere contralateral to chemoconvulsant injection (Figure 57A). The activity surrounding a series of seizures leading to a unilateral SD was investigated. gSGFET activity from ipsilateral and contralateral hemispheres was compared (Figure 57B&C). The results interestingly revealed a similar amplitude for electrographic seizures recorded both ipsilaterally (Figure 57D; black traces) and contralaterally (Figure 57D; orange traces). However, this was not the case for GCaMP recordings. For imaging traces, ipsilateral sites (Figure 56E; green traces) showed far greater amplitudes than contralateral sites (Figure 57E; teal traces). Altogether, this finding suggests either a difference in signal generation mechanisms, a large contribution of volume conduction to distally recorded gSGFET signals, or both. Therefore, it is clear that combined gSGFET and GCaMP recordings are able to provide insight into the complexities of electrographic signal generation.

7.3 Discussion

To summarise, the data presented in this chapter reveals the powerful ability for gSGFET arrays and GCaMP imaging to complement one-another, therefore leading to increased potential insight into epileptic paroxysms. Firstly, graphical representation of gSGFET recordings revealed clear variability in signal polarity during different events; a finding that is absent from GCaMP recordings. Closer examination of these events revealed more variable waveform properties from gSGFET recordings compared to GCaMP. This increased ability for gSGFETs to resolve waveform properties was present for both SD events and epileptiform spiking. The frequency range of recorded signals revealed the ability of gSGFET devices to capture high frequency activity dynamics far beyond that capable by GCaMP imaging. Bilateral dual gSGFET and GCaMP recordings revealed clear differences in the spatial footprint of ictal activity between the two modalities. These results consistently demonstrate the ability for GCaMP imaging to spatially resolve SD propagation dynamics as either unilateral or bilateral; overcoming a major limitation of purely electrophysiological studies.

The variability in gSGFET signal waveforms, while GCaMP signal waveforms remain consistent, raises further questions. Understanding the mechanisms underlying optical and electrical signal generation is essential to interpret these waveform differences. Based on the current understanding of electrographic signal generation, gSGFET recordings will be primarily dominated by activity of superficial cortical

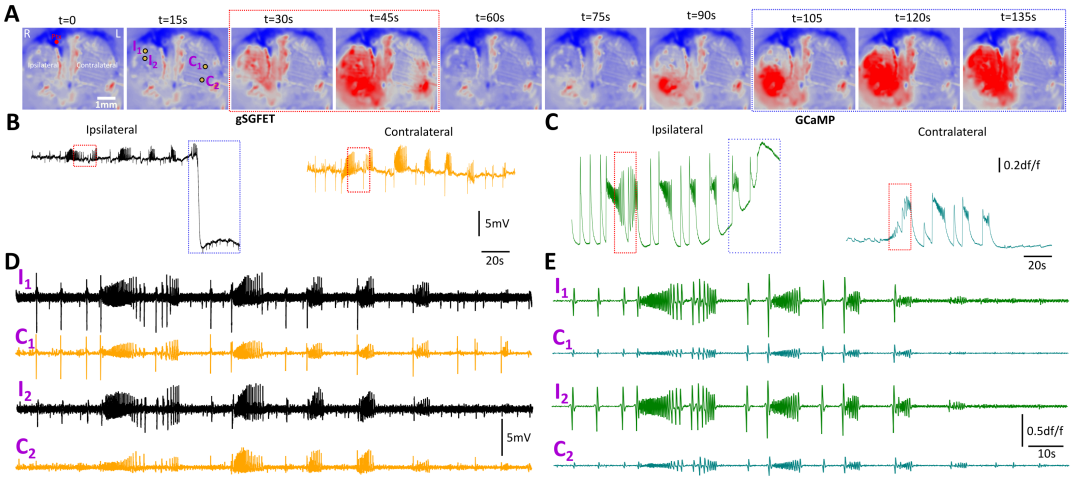

Figure 57: Representative comparison of bilateral GCaMP and bilateral gSGFET recordings revealing differences in signal localisation. **A)** Time-lapse images of GCaMP field-of-view showing two 16-channel gSGFET arrays, each recording from a different cortical hemisphere. Ipsilateral (R) and contralateral (L) hemispheres, along with picrotoxin injection site, labelled on first panel. Recording sites plotted in **DE** shown on second panel. **B)** Full-bandwidth gSGFET recording for activity shown in **A** for a gSGFET ipsilateral to picrotoxin injection (black) and contralateral (orange). **C)** As in **B**, for full-band GCaMP recordings at the same site. **D)** gSGFET traces high-pass filtered above 1Hz for 2/16 recordings sites from each hemisphere. Contralateral recordings (orange) are shown with ipsilateral recordings (black) and reveal a strikingly similar amplitude during seizures. **E)** GCaMP traces for locations plotted in **D**, processed as in **D**. Overlayed contralateral traces (teal) display far lower amplitudes than ipsilateral traces (green) suggesting differences in spatial resolution and signal generation between gSGFETs and GCaMP fluorescence. Representative traces shown for a WT male animal.

neurons with dipoles perpendicular to the cortical surface. Therefore, the acquired gSGFET signal will be a composite of synchronised synaptic activity, dendritic Ca^{2+} spikes, after-hyperpolarisation potentials and intrinsic currents (Buzsaki et al., 2012a). Action potentials are likely absent from epicortical gSGFET recordings due to extensive spatial filtering by the extracellular space. GCaMP signals, on the other hand, will readout any events leading to Ca^{2+} influx in superficial cortical neurons: these events primarily include action potentials and synaptic activity. Therefore, if the GCaMP waveforms are dominated by action potential firing in local neuronal populations, simultaneous variability in gSGFET waveforms at the same locations may be due to differences in location and constituents of synaptic inputs. Previous findings in the literature support this idea by demonstrating differences in epicortical signal polarity in response to excitatory and inhibitory inputs arriving at either superficial or deeper layers. Superficial excitatory and deep inhibitory inputs have both been observed to result in negative EEG deflections; whereas deep excitatory and superficial inhibitory inputs are seen to result in positive deflections (Beniczky & Schomer, 2020). Therefore, the simultaneous acquisition of both optical and electrical signals holds promise in providing detailed insight into epileptic network dynamics by allowing concurrent readouts of neuronal spiking and synaptic activity across large areas of tissue.

The demonstration of interhemispheric amplitude differences between recording modalities further highlights differences in electrical and fluorescence signal generation mechanisms. Since the investigated model involves induction of epileptiform activity at a single, unilateral cortical site; epileptiform activity is expected to be dominant in the injected hemisphere. According to GCaMP recordings, this is the case. However, according to gSGFET recordings this is unclear. Once again, this difference may be a result of GCaMP signals containing a large contribution from action potential-mediated Ca^{2+} influx; whereas gSGFET recordings are dominated by synaptic activity. This theory appears plausible due to the likelihood of synchronous action potential firing in the hemisphere ipsilateral to picrotoxin injection. However, in contralateral regions, synchronous action potential firing is less; yet synaptic activation is still occurring due to long-range projecting axons from the ipsilateral hemisphere and affected subcortical regions. Therefore, these mechanisms could explain the similar bilateral amplitude of gSGFET recordings (synaptic) and the differing amplitude of GCaMP recordings (local spiking and synaptic).

Another plausible explanation for interhemispheric amplitude differences between modalities surrounds the volume conduction of electrical activity. If epilep-

tiform activity is primarily driven by neuronal firing in areas ipsilateral to the injection site, contralateral gSGFET recording sites may record these large neuronal population discharges due to electrical conduction through the small tissue volume of the mouse brain (Viventi et al., 2011). Since GCaMP signals rely on local fluorescence measurements, there would be no contribution of volume conduction. Therefore, this may result in larger amplitude contralateral gSGFET signals when compared with GCaMP recordings at the same sites. The ability to simultaneously record activity with (gSGFET) and without (GCaMP) the contribution of volume conduction holds promise in dissecting the spatial complexities of ECoG signal generation.

Another interesting observation presented in this chapter is the presence of slow positive DC deflections on gSGFET traces following SD depolarisation recovery. These are absent from GCaMP recordings which raises questions. These slow electrographic deflections typically have a small electrical field, and can be explained by a few mechanisms. One of these potential mechanisms is that SD is followed by widespread hyperpolarisation, which Ca^{2+} fluorescence is unable to convey. A second possible explanation surrounds widespread SD-associated haemodynamic and osmolarity changes. SD is strongly associated with lasting vascular changes and extracellular shrinkage (Ayata & Lauritzen, 2015), and the influence of these on recorded DC potentials has not yet been fully characterised. Therefore, these changes may lead to the recorded positive DC event through alterations of cellular architecture and neuronal density. A third possibility when interpreting these positive deflections is the contribution of activity at the site of the reference electrode. Although the AgCl reference wire was selectively inserted into the olfactory bulb, a structure notoriously difficult for SD induction, SD propagation is still possible in these structures (Amemori et al., 1987). SD propagation to the olfactory reference would result in the slow positive polarity wave observed on gSGFET recordings following downward depolarisation at the reference site. This mechanism, although possible, appears unlikely: the time taken for SD propagation to the reference site would be in the order of minutes, which is greater than the recorded interval between negative and positive DC events during SD. Therefore, it appears likely that these positive deflections reflect widespread post-SD phenomena related to vascular changes, tissue swelling or widespread hyperpolarisation. Investigation of these phenomena, and the pathological changes following SD, will likely lead to an improved understanding of how SD events are able to result in lasting activity suppression, whether this suppression is beneficial or harmful, and the mechanisms by which this may lead to SUDEP (Loonen et al., 2019).

Previous studies have examined the relationship between optical and electrical recordings during physiological brain activity and sensory stimulation in mice. Notably, some of these studies use two-photon imaging, and therefore, have a limited field of view (X. Liu et al., 2019). Others have focused electrophysiological investigations on single-spike analysis (Xiao et al., 2017). Since the goal here is to observe how activity on the wide macroscale appears electrographically and optically, the use of multi-site epicortical devices with widefield imaging is clearly advantageous. Additionally, the ability to interpret infraslow electrographic signals in conjunction with Ca^{2+} dynamics provides novel insight that bandwidth-restricted devices are unable to capture. The work here presents a platform to investigate electrographic and optical activity readouts in physiologically compromised tissue. Further investigation would lead to a greater understanding of cellular and synaptic contributors to pathological discharges, and may aid interpretation of both experimental and clinical data that rely on only a single recording modality.

Several advantages of incorporating gSGFET recordings into a widefield imaging paradigm have been presented throughout this chapter. The ability to spatially resolve SD events as either unilateral or bilateral provides powerful insight into the diversity of SD propagation dynamics, and highlights clear limitations of previous SD studies using only single- or dual-point electrophysiological measurements. Fortunately, multi-site gSGFET arrays are able to overcome some of the limitations of single-point measurements. However, the coverage of these arrays is still limited and the incorporation of widefield Ca^{2+} imaging clearly provides greater insight into the areas invaded by SD. Moreover, the use of widefield imaging combined with gSGFETs is also powerful due to the ability to simultaneously capture both spiking phenomena (imaging) and synaptically-driven activity (gSGFET). Additionally, since imaging recordings are not influenced by reference electrode artefacts and volume conduction, combined recordings hold considerable promise in unraveling the complexities of electrographic signals. Insight into these electrographic signals would advance the meaningful interpretation of experimental and clinical recordings, where imaging recordings are often not possible. However, imaging recordings suffer from limitations of their own, primarily due to sampling frequency limitations, and supplementation with full-bandwidth gSGFET arrays resolves these.

7.4 Future Directions

Future studies will aim to further investigate the signal contents of gSGFET and GCaMP recordings. Since Ca^{2+} imaging is not possible in human patients, dissect-

ing contributors to electrophysiological signal generation in animal models could lead to an improved ability to interpret patient data. Electrographic techniques are frequently employed to diagnose epileptic disorders and aid pharmacological or surgical intervention. Future work to further dissect electrographic signals could aid interpretation of these recordings.

Additionally, volume conduction is a large issue in all electrophysiological recordings; both in animal models and patient studies. The recording of activity distal to the source, and the inability to locate this source, often leads to difficulty interpreting electrographic traces. To improve this ability, researchers and clinicians often employ montaging techniques to aid source localisation (Acharya & Acharya, 2019). However, this may result in several artefacts and the contribution of volume conduction is persistently uncertain. The experimental configuration presented here is able to provide insight into the contribution of volume conduction to electrographic signals. Future work will probe these phenomena further through the closer examination of bilateral electrophysiological and imaging recordings. This future work will aim to further characterise this relationship by investigating the instantaneous phase of signals separated over large distances. Since activity from a single electrical source will propagate quasi-instantaneously, signals recorded over large distances (e.g. from different hemispheres) will demonstrate phase synchronisation if they represent a readout of a single source. Therefore, these measurements, combined with concurrent imaging at the same locations, will allow calculation of the contribution of volume conduction and aid interpretation of future electrophysiological studies (Vinck et al., 2011).

In recent years, the availability of different fluorescent indicators has grown considerably (Dana et al., 2019). As a result, several voltage-sensitive fluorescent indicators have been developed (Abdelfattah et al., 2019b; Bando et al., 2021). Although these constructs still suffer from SNR limitations, they are often able to provide a direct readout of cellular depolarisation or hyperpolarisation; with the ability to readout subthreshold fluctuations. Combination of these constructs with transparent gSGFET arrays will allow a greater understanding of the differing polarities of different phases of paroxysmal events, therefore, aiding further dissection of electrographic signal generation.

To further aid this dissection of the cellular contributors to electrographic signal generation, GCaMP can be conjugated to different fusion proteins, resulting in targeted expression in specific cell types. The presented investigations probe activity in neuronal populations indiscriminately (synapsin promoter). However, specific investigation of activity in both excitatory and inhibitory cells separately may provide

further insight into signal generation mechanisms. As mentioned previously, positive and negative ECoG deflections can be caused by either superficial inhibitory or deep excitatory inputs and vice versa respectively (Beniczky & Schomer, 2020). Specific investigation of particular neuronal populations during epileptic paroxysms would lead to an increased understanding of the dominant contributors to electrographic signals seen prior to seizure and SD transition. This may lead to an improved ability to predict the occurrence of paroxysmal events in epileptic patients.

These proposed studies surrounding electrographic signal dissection are currently outside the scope of this PhD project. However, the data presented here demonstrates an experimental platform able to provide strong insight into both epileptic paroxysms and electrographic activity. Further work following this PhD project will aim to implement the ideas discussed, and utilise these to aid interpretation of experimental and clinical electrophysiology datasets. However, for the remainder of this thesis, the focus will be directed at utilising this experimental paradigm to probe epileptiform paroxysms, such as spiking, seizures and SD, as well as the relationship between these different phenomena.

Chapter 8

Characterisation of the Seizure-SD Relationship using Combined Imaging and Electrophysiology

8.1 Introduction

As discussed previously, a large cloud of ambiguity surrounds the temporal relationship between seizures and SD. Several studies have revealed that SD leads to a period of increased excitability, thereby promoting the occurrence of epileptiform discharges (Gorji & Speckmann, 2004; Berger et al., 2008; Eickhoff et al., 2014; Rathmann et al., 2020). However, other studies have proposed a converse relationship. Specifically, these studies have supported the notion that SD following epileptiform activity leads to activity suppression and reduces subsequent seizure frequency and propagation (Tamim et al., 2021). These two contradicting theories result in ambiguity regarding the relationship of seizures and SD. Moreover, this ambiguity has led to two theories regarding the role of SD in brain tissue. The first idea is that SD is a pathological event associated with abnormal brain activity, leading to worsened outcomes (Loonen et al., 2019). The second is that SD exists as an evolutionary mechanism to allow a 'reset' of pathological activity in an attempt to return brain conditions to within homeostatic limits (Tamim et al., 2021). Here in this section, I will address these hypotheses and provide insight into the nature of this seizure-SD relationship.

SD involves the slow propagation of a DC potential through the grey matter of the brain (Pietrobon & Moskowitz, 2014). Investigation of the temporal relationship between seizures and SD using single-point electrographic measurements can be limited in the insight achievable. If the origin of activity cannot be ascertained

to a reasonable degree, it is unclear which paroxysmal event preceded which. To elaborate, investigations of SD-seizure temporal relationships using recordings from only a few sites may draw false conclusions due to the difference in time taken for propagation from origin to each recording site. Therefore, for temporal classification, this study uses the large bilateral imaging field of view to define event onset and end times. As a result, I am able to simultaneous record electrographic seizures while observing SD events initiating and propagating from various locations in the tissue (for more details see Chapter 6- analysis pipeline development). Moreover, the large bilateral field of view allows investigation of the laterality of events, and therefore, allows inferences to be made regarding generalisation and propagation to subcortical structures.

In addition to investigating the temporal relationship between seizures and SD, this study probes the events leading to SD initiation. Specifically, the presented work probes what differentiates seizures that are associated with SD from those that are not. Several changes may lead to SD initiation. These changes may be directly related to the seizures themselves, or may involve alterations in network activity leading to both seizures and SD. To gain a readout of these pathological alterations leading to SD-induction, seizures surrounding SD periods were assessed in detail. Moreover, electrophysiological data is used to gain more detailed insight into different seizures and their potential influence on subsequent brain activity.

Altogether, the investigations presented in this section utilise the large spatial coverage of widefield imaging to investigate the diversity of seizure-associated SD events. The experimental platform is then used to determine seizure and SD origins and onsets, leading to an improved ability to study the temporal relationship between these different paroxysmal events. These extracted time windows are then matched to gSGFET traces and used to extract information regarding each paroxysm in greater detail. Moreover, this combined approach is utilised to investigate different SD events and the effect they exert on subsequent neural activity. This work demonstrates a platform to unravel the elusive relationship between seizure and SD events in awake, headfixed WT mice.

8.2 Results

The first objective of the investigations presented in this section was to probe the diversity of seizure-associated SD events. To achieve this, I manually inspected different paroxysmal events, detected using the previously presented detection algorithm. This was firstly performed to confirm the algorithm was correctly de-

tecting all events. Secondly, this manual inspection was used to investigate the diversity of SD events. Seizure-associated SDs revealed considerable variability in event characteristics. SDs were frequently observed in WT animals. However, the exact properties of these events were seen to vary considerably. Frequently observed were single SD events following an epileptic seizure (examples shown in previous sections). However, alongside these events, other SD event signatures were observed.

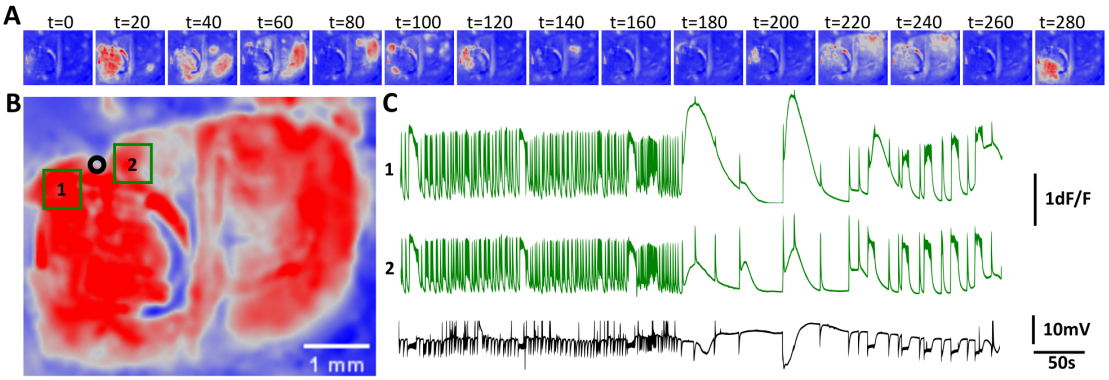

Figure 58: Large diversity in seizure-associated SD events showing a case of multiple reverberating SDs in quick succession in a male S218L HET animal. **A)** Time-lapse images with a 20s interval showing propagation of 12 distinct seizure-associated SD events within a single 10 minute window. **B)** Maximum intensity projection of activity in **A** showing coverage of all SD events. ROIs 1 and 2 represent imaging selections and black circle marks micropipette recording site. **C)** Fluorescence and electrographic traces extracted from the regions marked in **B**. Traces illustrate multiple seizures and SD events within a short time window.

In few cases, multiple repeating SD events were observed that reverberated and spiralled across the dorsal cortical surface. In one case, visual inspection of the SD events revealed 12 seemingly-independent SD origins in the cortex within a single 10 minute sweep. These events often originated simultaneously from multiple locations before the SD waves converge, collide and terminate (Figure 58A). Investigation at multiple locations revealed limited propagation of these events, with some failing to leave a clear electrographic footprint on an adjacent recording micropipette. Moreover, inspection of both image stacks and plotted traces revealed a high amplitude spike at the onset of each SD event (Figure 58C). This SD waveform showing clear initiation with a spike was not seen associated with the more frequently-observed classical single SD events. Lastly, inspection of activity after this recording sweep revealed a status epilepticus transition, suggesting these abnormal recurrent SD waves may be associated with a failure in seizure termination mechanisms, therefore leading to worsened outcomes. Although this case was rare compared to more commonly observed single SD waves, the occurrence of these complex phenomena

suggest that the relationship between seizures and SD may be more complex than initially predicted.

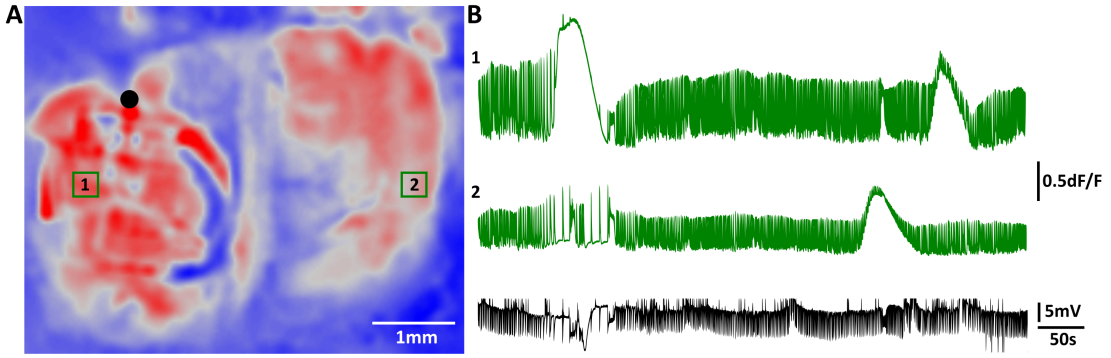

Figure 59: Large SD event diversity observed within a single imaging sweep. SD exerts mixed effects on coinciding ictal spiking. **A)** Maximal projection of GCaMP fluorescence during the imaging sweep shown in **B**. Black circle marks micropipette recording site. 1 and 2 indicate ROIs at the same cortical region on each hemisphere. **B)** Plotted traces from regions shown in **A**. Differential effects of SD on surrounding epileptiform activity shown. Unilateral SD followed by bilateral SD observed. The first unilateral SD has a clear effect on surrounding neuronal spiking. However, ictal spiking is persistent throughout the second SD. Second SD shows minimal propagation to micropipette recording site, highlighting the power of gSGFET incorporation. Representative traces from a WT female animal.

To further examine SD diversity, more conventional SD waves were also investigated. These events also demonstrated considerable variability. A single recording sweep is able to illustrate this variability through the demonstration of differential effects of SD propagation on coinciding epileptiform activity. Inspection of an example recording sweep revealed two SD events, one unilateral and the other bilateral. The first SD of the presented sweep propagates unilaterally and halts spiking during the SD, with apparent quick recovery and subsequent resumption of spiking. However, the second SD within this 10 minute recording sweep, displayed propagation in both hemispheres. Moreover, this second SD event appears to exert a minimal effect on epileptiform spiking, with spiking observed throughout the SD (Figure 59B). These two events would result in different EEG signatures, with the first SD causing far greater activity suppression than the second event. Altogether, these findings demonstrate the considerable diversity in SD events within a single time window recorded from a single animal. Moreover, these results demonstrate that even on a short timescale, each SD may have variable properties and interact with epileptiform activity differently.

This diversity in seizure-associated SD events was also captured using gSGFET

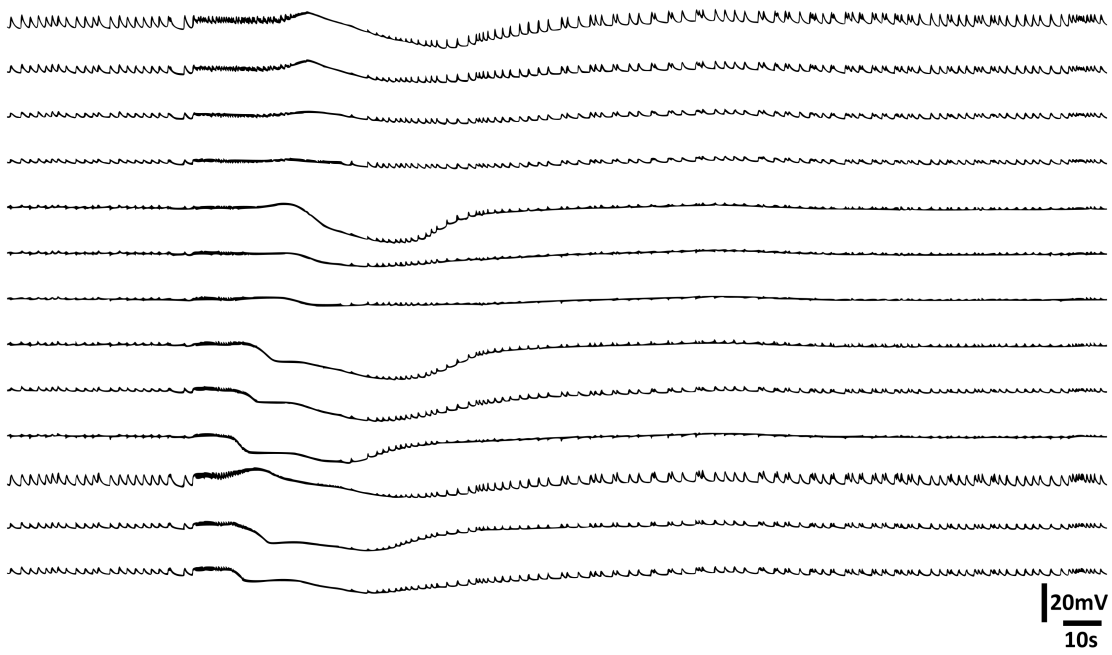

Figure 60: Representative seizure-associated SD event recorded across 13 of 16 gSGFETs from a WT male animal. Full-bandwidth signal shown. SD shows clear signature across all gSGFETs with an induced reduction of ictal spiking.

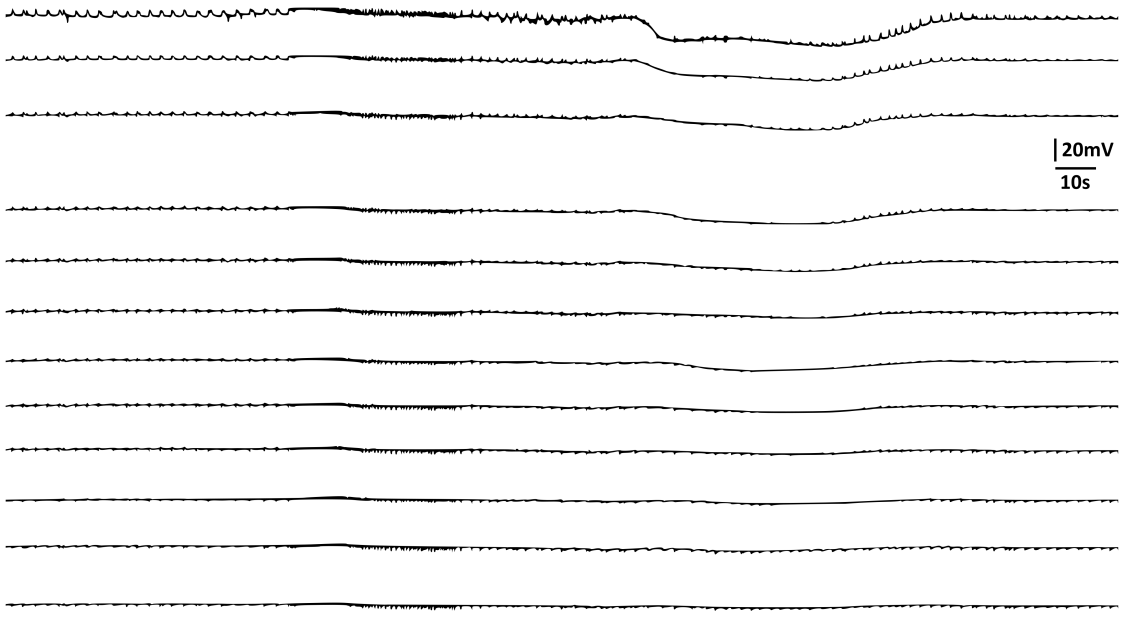

Figure 61: Seizure-associated SD event recorded across 12 of 16 gSGFETs from a WT male animal. Full-band signal shows partial SD propagation across gSGFET array with minimal influence on ictal spiking.

arrays. Different SD events could be clearly observed electrographically. In some cases, a seizure could be seen to result in direct transition into SD; with this SD wave propagating across the entire gSGFET array (Figure 60). However, in other cases, a seizure can be seen to terminate, followed by periodic spiking (as seen throughout the experiment) and after a delay, a SD event is initiated and terminates before propagation across the entire gSGFET array (Figure 61). These two event types were commonly observed and may indicate different mechanisms of SD induction. Nonetheless, the use of the gSGFET array alone limits the spatial insight attainable, and therefore, may lead to false inferences about the temporal and spatial interactions of seizures and SD. As a result, I continued to use events detected during widefield Ca^{2+} imaging to define seizure and SD onset times for temporal comparison.

Using the previously described imaging-detection algorithms, SD and seizure events were ascribed a start time and end time for the entire event (Figure 62B). Each detected event was manually inspected to confirm minimal error. Based on the previously defined criteria, the start time for each event was defined as the timing of entry of the first detected pixel into the seizure or SD mask. The end time, on the other hand, was defined as the last time point for the final imaging pixel within the mask. Therefore, the generated timeline incorporates information across a large area of the cortex. As a result, the seizure-SD relationship can be characterised as a cortex wide phenomenon, enabling more accurate temporal characterisations of seizures and SD.

Since the initial question was whether SD more often precedes or follows seizures, seizure onsets were aligned at time=0s. All sweeps with an SD within 400s before or after each seizure onset were included (Figure 62C; top). SD events, both unilateral and bilateral, were plotted around these seizure onset times as a bar spanning the SD duration (Figure 62C; top- blue bars). These SD events were each plotted according to the time difference from the nearest seizure onset. Based on these time differences, a histogram was generated and the probability density of SD at each 100s time bin relative to seizure onset was calculated (Figure 62C; bottom). Clearly observed is a large increase in SD probability within the 100s following seizure initiation (Figure 62C; bottom; 0 to 100s bin). This approach is clearly advantageous due to the precise determination of cortical paroxysm onset times, as well as the ability to define a simultaneous state of both SD and seizure.

In order to generate a more comparable and compatible dataset with forthcoming controls, the previously described timeline plot was generated in reverse. Therefore, SD onsets were centred at time=0s and the nearest seizures within 400s

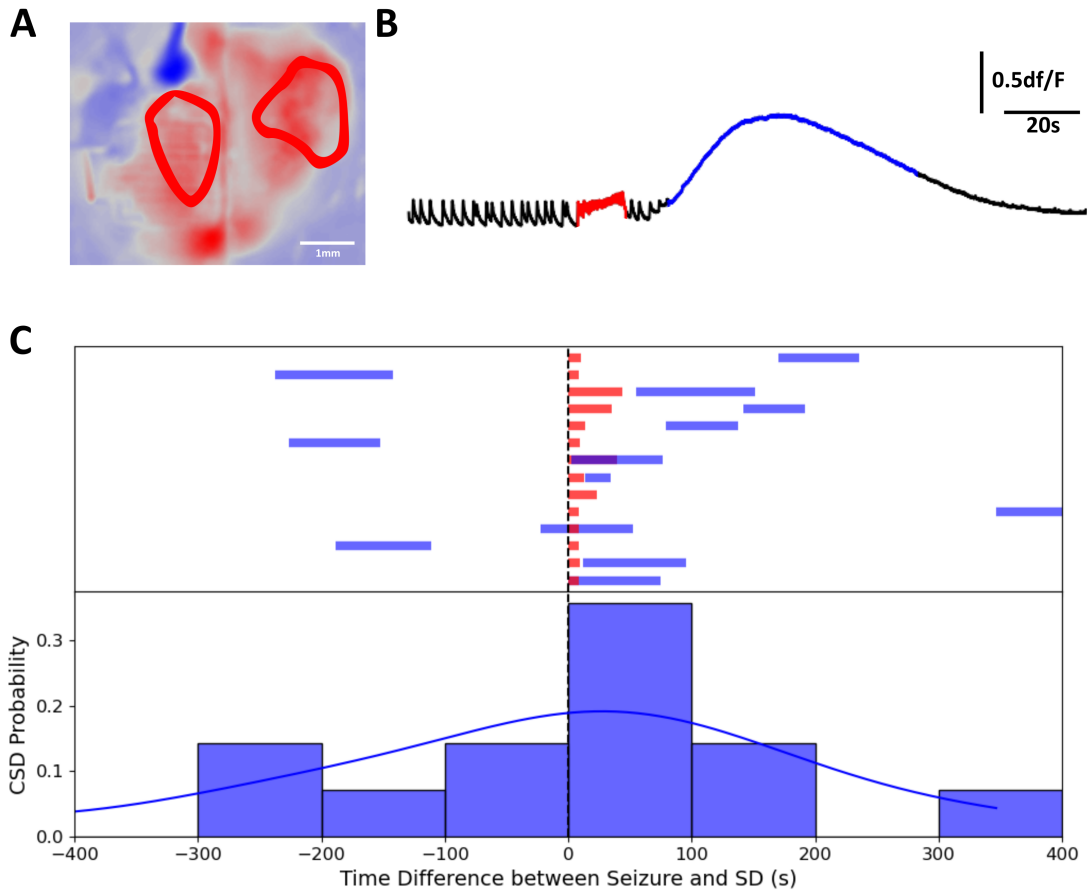

Figure 62: Examination of the temporal relationship between seizure and SD using GCaMP fluorescence information extracted from across the field-of-view. A clear increase in SD probability is observed in the 100s following a seizure. **A)** Fluorescence image during seizure, with seizure core maximum size marked in red. **B)** Fluorescence traces of seizure followed by SD. Red indicates a seizure and blue indicates an SD; both automatically detected using the previously presented event detection tools. **C)** Timeline of seizure and SD events. Top: seizure events shown in red and SD events in blue. Seizures aligned at t=0 and each SD plotted relevant to the entire event observed across the field-of-view. Bottom: histogram of SD events shown in top panel. Kernal density estimate plotted for each 100s time-window reveals a far greater probability of SD immediately following a seizure. Data shown for 4 WT male animals.

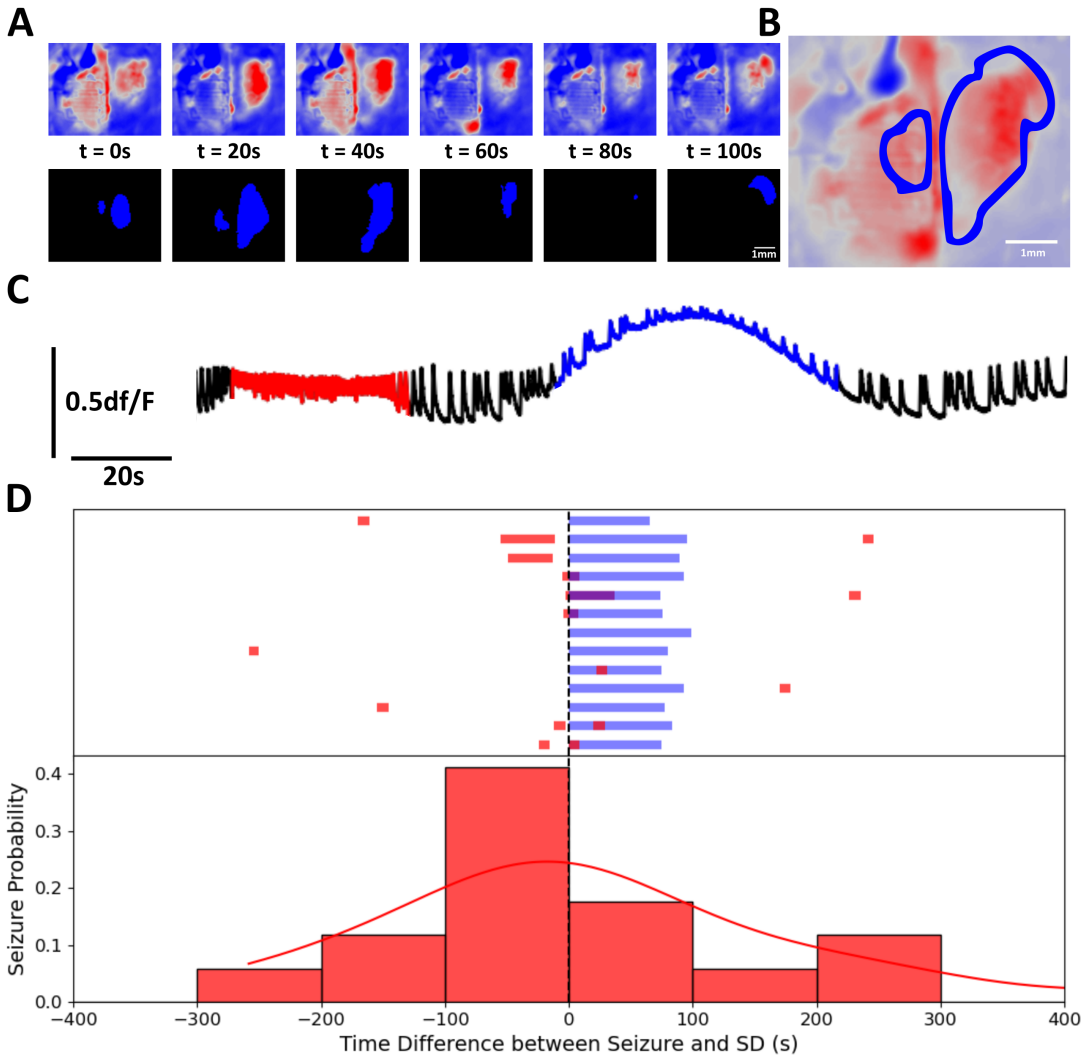

Figure 63: Timeline of seizure-SD relationship calculated using widefield fluorescence imaging across the field-of-view. SD events are centred at t=0 to enable easier comparison with subsequent controls. **A)** Time-lapse images of a bilateral SD event. Bottom images depict the automatically-generated SD mask with regions of SD marked highlighted in blue. **B)** Fluorescence image with overlay of maximum area covered by SD mask. **C)** Single fluorescence traces from within SD mask. Seizure followed by SD shown. **D)** Timeline plot of all observed SD events and the nearest seizure. Top: clear overlap of SD and seizures seen with seizures clustered at timepoints preceding SD initiation. Bottom: histogram of seizure times relative to SD at t=0s. Kernal density estimation used to estimate seizure probability relative to SD time. High probability of seizure seen immediately preceding SD. Data shown for 4 WT male animals

were plotted around this (Figure 63D; top). Similarly to as observed before, a high seizure probability can be seen immediately preceding SD initiation (Figure 63D; bottom; 0 to -100s bin). To enable future statistical comparisons (following dataset expansion) of event probabilities with matched-controls, two complementary plots were generated. In one control plot, all recorded seizures without SD in the same sweep were randomly plotted around a randomly-generated SD time. The probability distribution was then generated for this dataset, revealing a seemingly random seizure distribution around the SD time (Figure 64B). Secondly, a control consisting of a shuffled dataset was generated (Figure 64A). This was performed to account for other potentially-confounding variables such as time from picrotoxin injection. In this second control plot, the time from picrotoxin injection for each SD was extracted and used to ascribe a pseudo-SD time in all other animals without an SD in this recording period (591s window). Seizures surrounding this false time point were then plotted and probability density calculated relative to this. Similarly, a low probability of SD was consistently seen throughout the sweep; confirming that the observation of a high seizure probability prior to SD initiation in the unshuffled dataset is likely true.

Based on these observations, subsequent focus shifted to the seizures immediately preceding SD. Seizures were attributed the characteristic of pre-SD or not. Pre-SD seizures were defined as those with an onset that preceded the SD onset by 30s or less. This window was selected to allow inclusion of associated events while minimising the influence of repeatedly counting the same seizure during cases of multiple successive SD events. Once each recorded seizure had been attributed different characteristics, different seizure groups could be compared. The first performed comparisons used the outputs of the imaging detection algorithm to compare seizures from the two groups.

Following classification of each seizure event as pre-SD or not, plots were generated comparing properties of the two event groups in an attempt to reveal seizure properties that lead to increased probability of SD. Firstly, the frequency of seizure-associated SD occurrence was examined. Of 79 recorded seizures (from 4 WT male animals), 91% were seen to terminate without SD. In the other 9%, a SD event was observed within 30s of seizure termination (Figure 65B). To compare the properties of these two groups of seizures, median seizure duration and seizure area under curve were examined (Figure 65C). Median seizure duration appeared to reveal no clear difference in seizure duration between seizure groups. Area under the curve for each seizure was examined in two ways: the first, used a mean of area under the curve for each pixel within the seizure area; the second, used the total area under

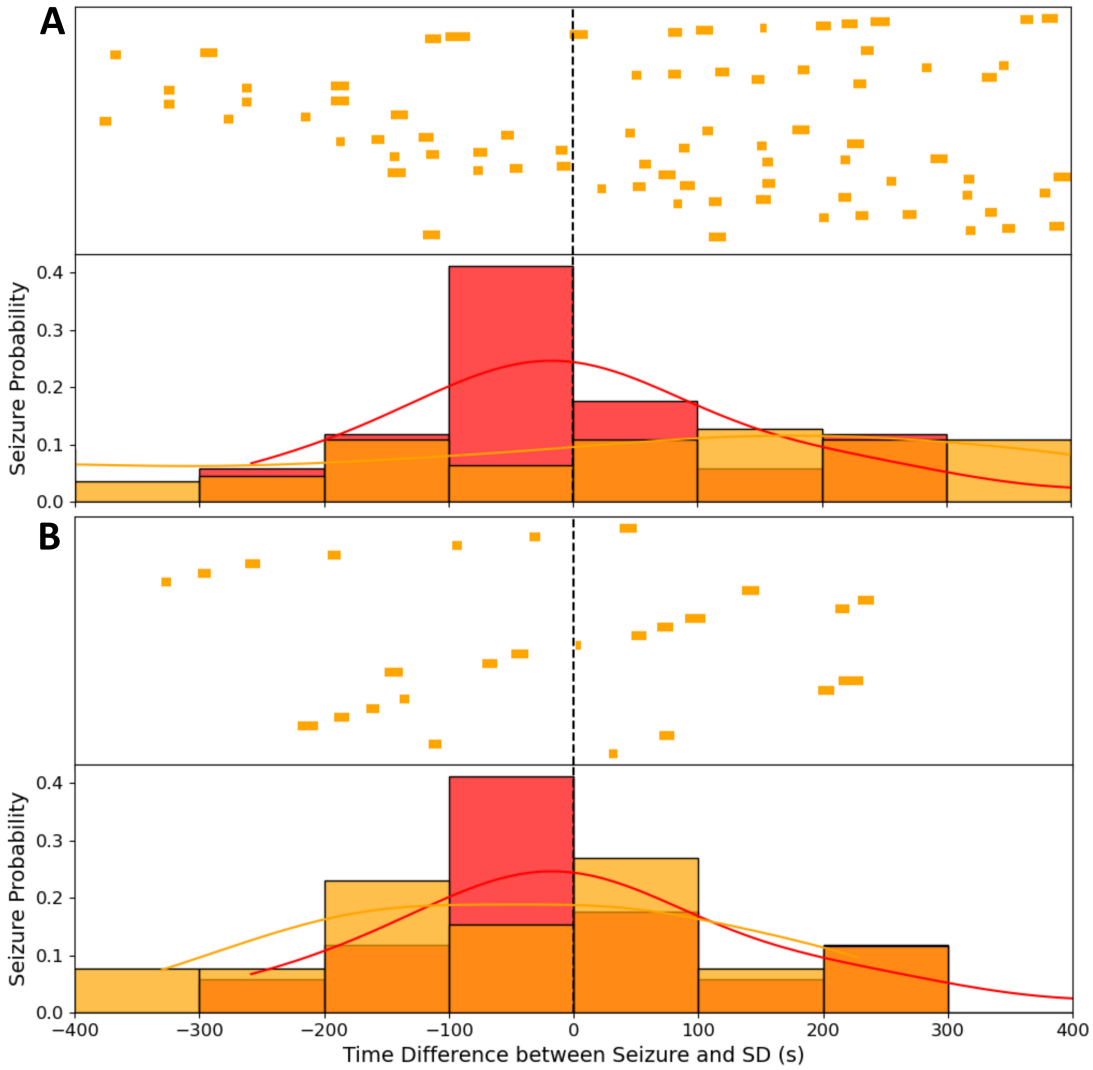

Figure 64: Control timeline plots for comparison, generated by shuffling event times. No clear difference in seizure probability with reference to pseudo-SD time at t=0s. **A)** Control timeline plot of all seizures not associated with SD. Time from picrotoxin injection was calculated for real SD times. These times were used to generate pseudo-SD events in animals without SD at these time points. The distribution of seizures around these events was then plotted. Shuffled distribution (orange) compared against real dataset (red). **B)** Simpler approach to generate control timeline revealing similar random seizure distribution. All seizures not associated with SD were given a random time difference relative to a SD time. Data displayed as in **A** and incorporates recordings from 4 WT male animals.

the curve for all pixels within the seizure area, and therefore, also took into account spatial coverage. Averaged results from 4 animals revealed a tendency for seizures preceding SD to have a larger integral; which can be indicative of greater Ca^{2+} influx and neuronal depolarisation during the seizure. However, a larger sample size is required to fully resolve an effect.

Following investigation of differences in seizure properties that may trigger SD, widefield imaging was used to probe seizure properties and their interaction with SD properties (Figure 65D). For all seizures followed by SD, different properties of both seizures and SD were plotted against one another. These properties were examined in detail by pooling data from up to 40,000 pixels for each recording. Since the distribution of these properties is uncertain, data was ranked prior to correlation calculations. All extracted event properties (see Chapter 6, analysis pipeline description for details) were compared and investigated. Notably, seizures with a longer duration were found to result in SD events of a lower amplitude (N=17 event pairs from 4 animals, SC=-0.47, $p<0.05$). Moreover, longer seizures were found to lead to SD events with a higher median propagation velocity (N=13 event pairs from 4 animals, SC=0.57, $p<0.05$). SD velocity was also found to significantly positively correlate with the area covered by the seizure focus (N=5 event pairs from 4 animals, SC=0.97, $p<0.01$). Lastly, the mean area under the curve (using all pixels within the mask) was seen to positively correlate with the amplitude of the subsequent SD (N=17 event pairs from 4 animals, SC=0.72, $p<0.01$). Since this somewhat contradicts the previous result of negative correlation between seizure duration and SD amplitude, the correlation between seizure median duration and seizure area under the curve was also examined. This revealed a significant positive correlation (N=79 seizures from 4 animals, SC= 0.52, $p<0.01$), suggesting disparity in results is not simply due to longer seizures having a lower profile. Altogether, it appears there is clear interaction or co-modulation of both seizures and SD during epileptic paroxysms. Nonetheless, these comparisons were limited in that they solely relied on imaging techniques to provide information regarding seizure properties. To provide further insight, these different seizure groups were used to extract time-matched gSGFET traces.

In order to increase insight into seizures, the electrographic recordings were separated into time windows relative to the seizure onset and end calculated using widefield imaging (Figure 66B). Since seizures are variable in length, for consistency, time windows were selected around the seizure start and end, with a variable length middle window bridging this. Within each window, a power value was calculated for each physiologically-relevant frequency band (Figure 66E). This value was

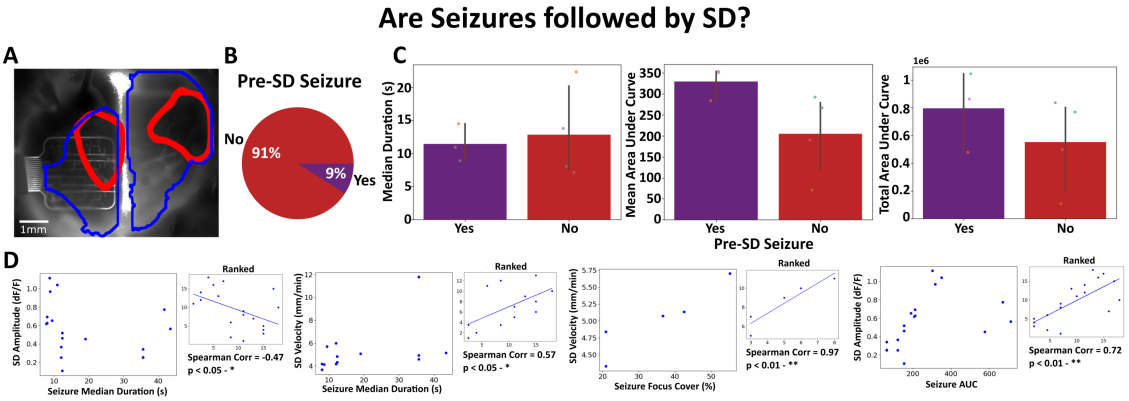

Figure 65: Examination of seizure properties using widefield imaging. A platform to investigate differences in seizure properties that precipitate SD is shown. **A)** Widefield image showing masks for SD propagation (blue) and seizure core (red) generated using automated analysis pipeline. **B)** Proportion of seizures followed by a SD event. Examination of 79 seizures from 4 animals revealed 9% were followed by SD. **C)** Investigation of seizure differences that lead to SD initiation. Seizures occurring 30s prior to SD were classified as a Pre-SD Seizure. All detected pixels were averaged to calculate a median or mean for each event, and each event was averaged for each animal. Each data point represents a different animal. Seizure AUC calculated by the integral of each pixel, either averaged (mean) or summed (total). **D)** Investigation of correlation between seizure properties and SD properties. Clear modulation of SD properties can be observed either by seizures directly, or co-modulation by co-occurring cortical network alterations. Other property relationships were investigated but found not to be significant. Data recorded from 4 WT male animals.

calculated by applying a bandpass filter to each trace, applying a median filter over a sliding time window and averaging the resulting values within the time window of interest. This method could not be performed for slower oscillations due to a single oscillation outlasting the length of the sliding window. However, for oscillations in the frequency range of delta and above, this was a viable method.

Interestingly, considerable variability was observed in the different physiological frequency bands. Since the high-performance gSGFET devices required to resolve these frequency bands were only recently fabricated, the sample size was insufficient to allow meaningful statistical conclusions (N=3 animals). Therefore, data was plotted for each animal separately (Figure 66F). Each recording of each seizure incorporated data from up to 16 gSGFETs. The power of each frequency band was calculated for each transistor recording (Figure 66E), before averaging for each seizure. Each seizure was then averaged for each time point for each animal. Interestingly, all three animals showed a higher power in the high gamma band during seizure onset for seizures that led to SD compared those that did not. The other frequency bands appeared to demonstrate variable responses, with some animals showing lower power in cases of SD and others showing higher power in the same conditions.

To add to the richness of data incorporated into this combined paradigm, each gSGFET recording site was allocated a descriptive value. This value was determined by the location of the transistor relative to the previously determined seizure focus (Figure 67A; red region). This allowed further grouping of gSGFET recordings, allowing comparison of electrophysiological activity inside and outside of areas actively participating in seizure propagation. Altogether, this allowed detailed investigation of electrical activity during seizures that preceded SD, from areas both within the seizure focus and outside.

Following the investigation of events preceding SD, analytical focus shifted to the consequences of SD on subsequent epileptiform activity and the potential role SD plays in modulating following epileptiform activity. To investigate this, the LFP band (1-150Hz) across classified gSGFETs was isolated (Figure 67B). Following each seizure classified as pre-SD or not, the time taken for LFP recovery to pre-seizure levels (median of -70s to -10s) was calculated. Similarly to before, up to 16 gSGFET recordings were processed with the outputs averaged for each detected event. Events from each animal were then averaged to allow comparison. Consistent with previous literature, seizures followed by SD had a longer LFP recovery period (Figure 67C). Moreover, this recovery appeared to be influenced by location relative to seizure focus. Clear differences could be observed for gSGFET recording sites

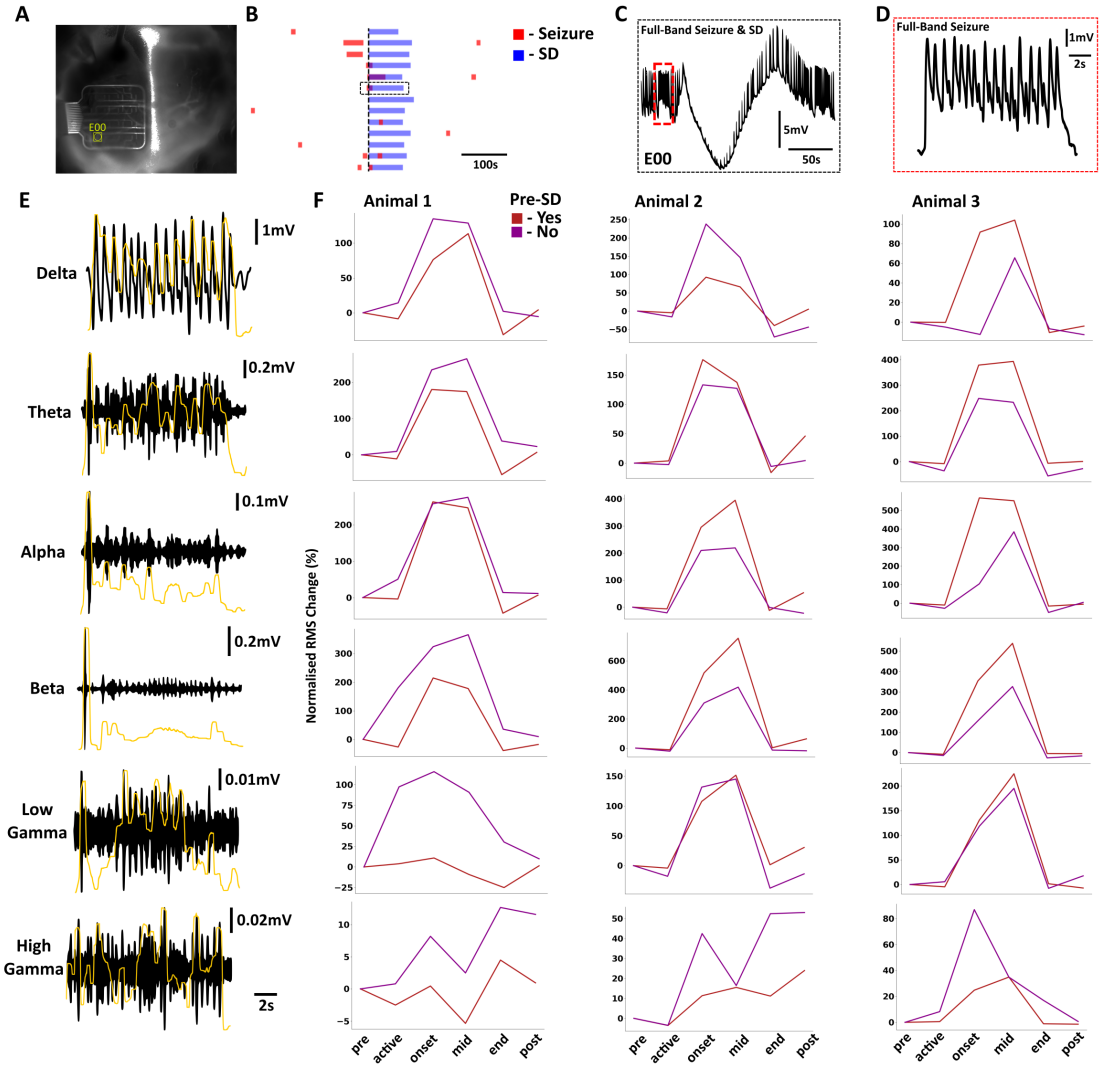

Figure 66: Investigation of differences in pre-SD seizures using electrophysiological analysis of gSGFET arrays. Clear variability is observed with greater sample sizes required to fully reveal differences. **A)** Widefield image showing gSGFET array with location of gSGFET E00. **B)** Section of seizure-SD timeline showing selected event for representative trace generation. Cortex-wide event windows identified from widefield imaging were used to define timepoints of interest for electrophysiological analysis. **C)** Full-band activity highlighted by black dotted line in **B** for gSGFET highlighted in **A**. **D)** Full-band expansion of seizure highlighted by red dotted box in **C**. **E)** Seizure shown in **D** resolved into physiological frequency bands (black). Bands were defined as delta (1-4Hz), theta (4-8Hz), alpha (8-12Hz), beta (12-30Hz), low gamma (30-50Hz) and high gamma (50-100Hz). root-mean squared for each band shown calculated with a 500ms window (yellow). **F)** Quantification of activity in different frequency bands using normalised RMS change relative to pre-seizure value. Each series of vertical plots shows data pooled from each recorded animal. Data shown for 916 recordings of 65 seizures from 3 WT male animals.

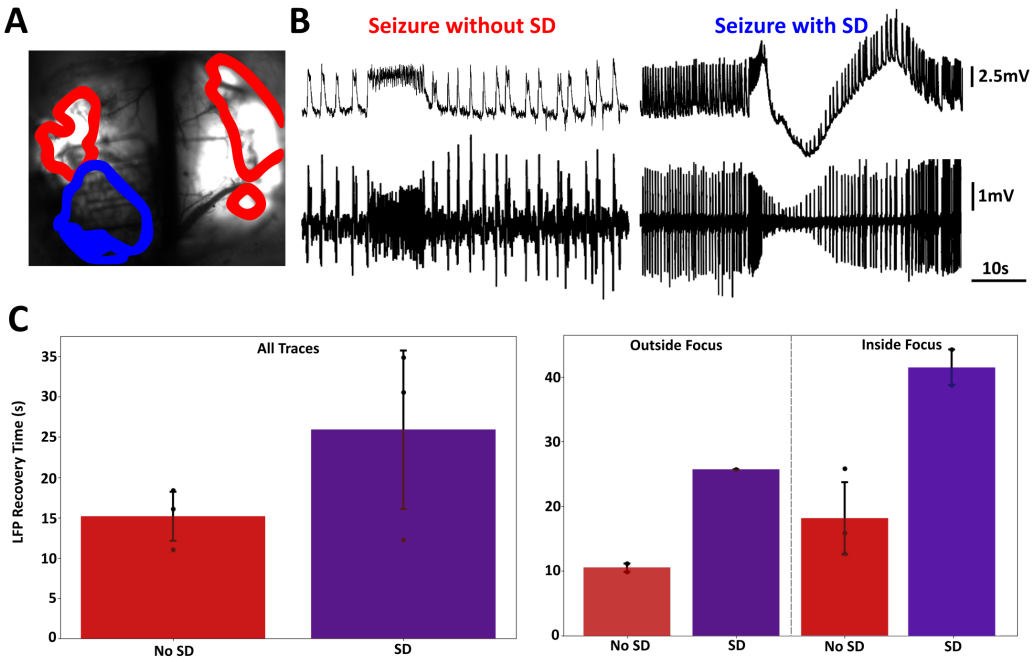

Figure 67: Investigation of the effect of SD on subsequent brain activity. Time taken for recovery of LFP band following seizures with and without SD shown. **A)** Widefield image showing detected SD mask (blue) and seizure core (red), with gSGFET array. **B)** Example gSGFET trace of full-band recording (top) and LFP band filtered trace (>1Hz; bottom). Example shown for both seizure with and without SD. **C)** Time taken for recovery of LFP band to pre-seizure values. Electrophysiology time points were extracted according to detected events using widefield imaging. Recovery threshold calculated as median LFP value of -70 to -10s prior to seizure initiation. Recovery time calculated by time for LFP RMS to return to this value after seizure initiation. Left: all gSGFETs are grouped based on whether the seizure is followed by SD or not. Right: same data with gSGFETs classified according to spatial position relative to detected seizure focus from widefield imaging. Average and standard deviation calculated for each animal. 916 recordings of 65 seizures from 3 WT male animals.

located inside and outside the seizure focus for both seizures with and without SD. Firstly, seizures that were followed by SD consistently showed a longer LFP band recovery time. Secondly, cortical regions invaded by the seizure focus displayed a longer LFP recovery time compared to those outside the seizure focus. Therefore, it is clear that seizures accompanied by SD have a longer-lasting impact on subsequent brain activity. Moreover, this recovery appears to take longer for regions actively participating in seizure activity. The ability for this experimental paradigm and the developed analytical tools to unravel these complex relationships is a powerful demonstration of the strengths of the developed approach.

8.3 Discussion

The work presented in this section demonstrates a practical application of the constructed experimental paradigm in probing seizure-SD interactions. To summarise, the large imaging field of view was used to characterise events temporally, utilising the ability for imaging to accurately determine events onsets. Temporal relationships were used to classify seizure events in relation to SD occurrence. Seizure properties for each group were examined using both imaging and electrophysiology. To supplement this, corresponding gSGFET traces were investigated. Physiological frequency bands and LFP band recovery was investigated for each extracted event. Moreover, each gSGFET recording site was classified according to location relative to the seizure focus. Altogether, these investigations highlight potential differences in seizures that may precipitate SD. Additionally, the results demonstrate a clear relationship between seizure and SD properties; showing support for a strong interaction. Moreover, these findings raise questions surrounding the notion that SD occurrence leads to lasting alterations in epileptiform activity.

Interpreting the findings from this chapter highlights several interesting points. Firstly, the variability in SD properties highlights the complexity of the task at hand. These different SD types may behave differently or have distinct origins leading to a need for further classification before analysis. Moreover, since the occurrence of a seizure-associated SD during each experiment is slim (less than 10% of seizures), large quantities of data would be required to fully unravel this relationship. This can also be seen from variability in frequency band analysis of different seizure time windows. Fortunately, the analysis tools constructed here allow efficient, high-throughput information extraction, quantification and comparison. Therefore, the means to unravel the seizure-SD relationship are in place.

Investigation of the temporal relationship between seizures and SD confirmed

previous findings in the literature that describe seizure-associated SD events. Two notable previous studies have attempted to characterise this relationship in detail. One, used a single DC silicone depth probe to generate a seizure-SD timeline following acute fluorothyl-induced seizures (Zakharov et al., 2019). Therefore, information from only a single location was considered. The other, characterised seizure-SD relationships in different chemoconvulsant models using either IOS or few electrical point measurements. In this case, the authors only generated a timeline in relation to chemoconvulsant application time and did not fully characterise this relationship with seizures themselves (Tamim et al., 2021). Therefore, the work presented here is able characterise this relationship in greater detail due to continuous sampling from a bilateral field-of-view with direct classification of seizure-SD interactions. Moreover, a state of simultaneous seizure and SD can be recorded, wherein one location is in a seizure state and another in SD.

Although the work presented here demonstrates an increase in seizure probability prior to SD initiation, the exact temporal relationship between these two events is seen to vary. One would assume that if seizures were directly triggering SD, the time taken for this to occur would remain relatively constant. Moreover, it would also seem likely that SD would be triggered before the seizure terminates and ictal spiking returns. However, the presented data appears to contradict this direct seizure-SD transition. In some cases, seizures were observed to directly transition into SD, with cortex-wide seizure termination at the time of SD onset. However, in other cases, seizures terminate, and following a short interval of ictal spiking, the SD is observed. Lastly, seizures can also be seen to initiate elsewhere in the cortex after a SD event has already started to propagate. Therefore, it is unclear whether seizures are directly triggering SD. Previous studies have not fully characterised these phenomena due to recording limitations, and therefore, this variable relationship is open to interpretation in one of few ways.

Firstly, it is entirely plausible that previous studies draw the false conclusion that the seizure is the sole cause of the SD. The observed variability in temporal relationships could be explained by the fact that an underlying network pathology leads to an increased propensity for both seizure and SD to occur, with these events coinciding due to a third shared causative phenomenon. Therefore, the observation of SD following seizures may simply be due to an overall change in network activity that leads to a simultaneous increase in both seizure and SD probabilities. The variable time difference between these two events could be explained by random occurrences during a small period of increased susceptibility. In the case of repeated seizures and SD events in succession, this could be indicative of a pro-

longed state of susceptibility; and this severely pathological network state could explain the status epilepticus transition that was observed to follow these repeated SDs. These ideas relating to the role of underlying network state are relatively unexplored. Further support for these notions would advance the interpretation of these paroxysms. However, to fully reveal these differences, greater sample sizes are required to account for event variability.

Another possible mechanism explaining the variable seizure-SD temporal relationship surrounds the accumulation of intermediate factors. Seizures may lead to extracellular accumulation of metabolites and ions due to excessive firing. If clearance mechanisms are disrupted and homeostatic balance can not be restored, SD will be initiated. In some cases, these mechanisms may be more intact and can temporarily postpone SD initiation, leading to an interval of ictal spiking. In other cases, for example following extensive energy depletion or metabolic compromise, seizures may be able to directly trigger a transition to SD without a delay. This theory fits closely with ideas related to the role of underlying network pathology.

Another interpretation is that subcortical structures are playing a major role. Observed variability in the time difference between seizures and SD could be explained by the time taken for propagation from subcortical structures. Seizures may always directly trigger SD without an intermediate interval, but this may occur in different brain structures beyond the reach of the recording view presented here. As a result, by the time one event propagates to the cortex and an origin is detected, the other event may have already terminated elsewhere. This would contribute to the variability of observed temporal relationships. Moreover, this could also result in the observed electrophysiological variability due to the relevant pathological oscillations occurring beyond the reach of epicortical recording sites. Previous studies have examined these subcortical structures during seizure-associated SD to reveal SD initiation in both superficial layers of the cortex and in the hippocampus (Zakharov et al., 2019; Bonaccini Calia et al., 2021). Therefore, a role for subcortical structures is entirely plausible.

Regardless of the variability between seizure end and SD onset, it was clear that seizures had a tendency to cluster around SD onset. Therefore, a large section of the results in this chapter focused on investigating seizure properties and their ability to influence SD propagation. Several different significant correlations were observed between seizure properties and the properties of SDs that were seen to follow. Whether the observed correlations between these event properties can be explained by direct modulation by the preceding seizures or co-modulation by the underlying network state remains unclear. However, the observed relationships raise

several interesting questions.

Firstly, the significant negative correlation between seizure duration and SD amplitude could be explained by several different phenomena. One explanation is that a seizure gradually leads to depolarisation block of sub-populations of neurons. Therefore, upon SD initiation, fewer neurons are able to depolarise further, leading to a SD with lower amplitude. Another possibility fitting with current literature (Tamim et al., 2021), is that the SD is an active mechanism to terminate the seizure: the longer and more severe the seizure is, the greater the impairment of seizure termination mechanisms, and the less effective the SD is at counteracting the seizure: therefore, the observed SD amplitude is smaller. These two potential mechanisms provide plausible explanations for the observed correlation.

Another intriguing result is that seizure area under the curve is positively correlated with subsequent SD amplitude. The controversy of this result comes from the contrast of SD amplitude being negatively correlated with seizure duration. A possible explanation for this is a negative correlation between seizure duration and seizure area under the curve: however, seizure duration was compared with seizure area under the curve to reveal a significant positive correlation. Therefore, it is evident that there are more complex mechanisms involved. A possible explanation could stem from the idea that there are mixed groups of seizure waveforms. This idea is supported by previous literature demonstrating different seizure onset patterns, e.g. low-voltage fast and hypersynchronous (Lisgaras & Scharfman, 2022). These different seizure types have different waveforms which may lead to differing relationships between seizure properties and SD amplitude. Separating these different seizure waveforms may reveal insight into these seemingly contradictory seizure-SD relationships.

With regard to the positive correlation between seizure duration and SD velocity, this could also indicate a role for shared underlying cortical pathology. SD velocity has been shown to be closely linked to the severity of network pathology; as clearly shown by SD propagating faster in diseased tissue compared to healthy (van den Maagdenberg et al., 2010). Therefore, the occurrence of faster propagating SD events following longer seizures may indicate co-modulation by a greater severity of pathology in the underlying network. Another possible explanation for this result is that longer seizures are more likely to propagate further, and therefore, a greater body of cortical tissue is directly affected by the seizure, leading to faster propagation in a higher number of neuronal populations. This is consistent with the observed positive correlation between SD velocity and seizure focus coverage. Both scenarios of SD velocity modulation by the underlying network and seizure

coverage appear plausible and one does not necessarily exclude the other.

The use of imaging to define events, and electrophysiology to perform detailed analysis is a clear demonstration of how this study utilises the strengths of both recording modalities. Electrographic analysis comparing seizures preceding SD with others highlighted interesting ideas for further investigation. Of interest is the consistent increase in high gamma activity during the onset of seizures that lead to SD. High gamma in healthy tissue is linked to higher functions such as cognition and memory (Mably & Colgin, 2018). However, in epileptic tissue, pathological high gamma oscillations have been linked to regions actively participating in seizure propagation. Moreover, resection of these areas results in improved patient outcomes (Weiss et al., 2015). Therefore, it is clear that pathological high gamma activity plays a role in driving epileptiform activity. As a result, greater high gamma activity during seizures preceding SD may indicate a link between SD and seizures of greater severity; a finding fitting with previously characterised event property correlations. Further work will aim to characterise these alterations further through inclusion of more animals and different epilepsy models.

In addition to investigating seizures preceding SD, this chapter probed the effect of SD on subsequent epileptiform activity. These investigations revealed a greater delay in the recovery of the LFP band following seizures that terminate in SD, when compared to all other seizures. Although this lends support to the notion of an anti-epileptic effect for SD, this idea is also accompanied by caveats. The observed time taken for recovery of the post-SD LFP band to pre-seizure levels was consistently under 60s. Therefore, if an anti-epileptic effect is exerted, it does not appear persistent. Moreover, ictal spiking is often seen throughout SD events raising questions about the extent to which this suppression occurs. One could argue that acute epilepsy models such as the investigated picrotoxin model delivers a continual pro-epileptic effect; and therefore, recovery may not fully reflect that seen following spontaneous seizures. However, lasting activity suppression post-SD has been demonstrated in acute seizure models by a previous study (Tamim et al., 2021). The primary difference between the work presented here and previous studies is that this work is performed in awake mice in the absence of anaesthesia. Therefore, these findings support the requirement for an awake *in vivo* experimental preparation to fully probe the effect of seizures and SD on network activity. Additionally, these findings collectively build support against the idea of a lasting anti-epileptic effect of SD.

Altogether, this section has demonstrated powerful insight into the potential mechanisms linking seizures and SD. The presented experimental and analytical

platform allowed detailed characterisation of the seizure-SD temporal relationship. Moreover, the diversity of events and relationships between different event parameters seem to suggest a complex relationship between the two phenomena. Previous studies have tried to explain this relationship, however, the findings here build a complex picture suggesting these studies are employing a reductive approach focused on seizure-SD links as opposed to incorporating studies of underlying network pathology. Considerable future work will be performed to complete this picture and fully utilise the strengths of the platform presented here.

8.4 Future Directions

Future work will primarily focus on increasing the size of the investigated dataset and repeating these investigations in different models of epilepsy. Firstly, SD events are more variable than initially expected, requiring larger samples to characterise relationships. Secondly, due to COVID-19-related disruptions, data collection was interrupted. Thirdly, analysis pipeline completion was ideal before collection of an entire dataset to ensure compatibility of the experimental paradigm with feasible analysis tools. Since data collection can be resumed, and analysis pipeline compatibility has been demonstrated, additional recordings can be acquired to further characterise seizure-SD relationships.

Another area of progression will be the further development of seizure focus detection algorithms. This will increase the success rate of focus identification and allow greater inferences to be made regarding seizure activity. In line with the development of these tools, analysis modules will be created to probe underlying alterations in cortical network activity. Considerable evidence presented in this section suggests a possible role of underlying network pathology in simultaneously precipitating both seizures and SD. Further work to explore this notion may bear fruitful results. Recent work has allowed identification and isolation of every individual event, such as single spikes, complex spikes and high frequency burst firing. Investigation of these events and their properties may reveal interesting information regarding underlying network pathologies. Moreover, the examination of spiking events during time periods surrounding SD may lead to a better understanding of whether SD does, in fact, exert an anti-epileptic effect.

With regard to electrophysiology, the analysis presented in this chapter shows limited insight into low frequency activity. Power calculation using a window of 500ms for frequencies below 1Hz during short seizures would produce invalid results. Since a major strength of gSGFET devices is the capture of full-bandwidth activity,

investigation of infraslow activity during different seizure types is of interest. Future work will investigate this using raw DC values. Moreover, MUA recorded with the glass micropipette will look for simultaneous local differences in neuronal spiking at the chemoconvulsant injection site.

To further address ideas regarding a subcortical role in seizure-associated SD, depth gSGFET probes would be a powerful addition. Preliminary data using these devices has been acquired following optogenetic SD induction; showing successful integration into the experimental paradigm with widefield imaging and epicortical recordings (see Appendix). Moreover, recently, alongside collaborators at UCL and IMB-CNM, I have assisted in the design of extended depth probes capable of recording from the cortex, hippocampus and thalamus simultaneously. These devices have been designed to incorporate a long transparent ail leading to the PCB, and therefore, are more compatible with simultaneous imaging. Future work will aim to incorporate these devices to gain an understand of the subcortical role in seizure-associated SD initiation.

Additionally, by working with our collaborators at the IMB-CNM, I have designed a 64-channel gSGFET array that is currently being fabricated (see Appendix). In the meantime, I am optimising a novel 64-channel gSGFET amplifier with collaborators at Gtec (Austria). The result will be the ability to record full-bandwidth activity across large areas and with greater coverage. The additional recordings sites would lead to greater electrophysiological characterisation of events across both hemispheres.

Future work will aim to progress the findings from this section considerably. Clear insight has been gained into seizure-SD relationships using the developed methodologies. However, important questions have been raised and remain unanswered. This work clearly demonstrates the advantages and strengths of this approach. Next steps will prioritise the expansion of these pilot datasets, the investigation of subcortical structures, the analysis of underlying network activity and gSGFET DC analysis.

Chapter 9

Insight into Seizure-Associated SD Events using Widefield Imaging

9.1 Introduction

Previous studies to date have attempted to investigate SD properties in different preparations, including both healthy and diseased tissue (Houben et al., 2017; Masvidal-Codina et al., 2021; H. T. Zhao et al., 2021a; Tamim et al., 2021). Of these, several studies have attempted to characterise SD properties in epileptic tissue through the use of both acute (Tamim et al., 2021) and chronic models (van den Maagdenberg et al., 2010). The findings from these studies are insightful, yet often lacking in acquired detail due to technological recording limitations. Since the investigations presented throughout this thesis make use of novel technology that has not been applied in this context, the constructed paradigm was employed to provide insight into SD properties.

Several previous studies have used imaging techniques to probe SD propagation. Most frequently employed is IOS (Santos et al., 2014; Houben et al., 2017; Tamim et al., 2021). IOS is a powerful tool able to track SD propagation. Moreover, the fact IOS does not require expression of any indicators and can be recorded without tissue perturbation, increases the power of the method (Santos et al., 2014). Nonetheless, the IOS signal is generated as a composite of multiple factors and provides a less direct readout of neuronal activity than GCaMP. Therefore, GCaMP reporters are able to capture information regarding SD propagation in greater detail with greater SNR. Previous investigations have used GCaMP to generate insight into seizure (Rossi et al., 2017) and SD properties (Srienc et al., 2019; H. T. Zhao et al., 2021a). However, no previous studies have used these methods to investigate SD-associated with epileptic seizures. Moreover, due to the constructed imaging analysis pipeline

and the large field of view, this study has the novelty of avoiding reductive ROI-based averaging. As a result, both seizure and SD propagation can be tracked and quantified continuously throughout the majority of the cortex. Therefore, the experimental framework optimised throughout this thesis is able to advance the current understanding of SD dynamics in epileptic tissue.

The work presented in this section is focused around investigating seizure and SD properties in awake male WT mice using widefield GCaMP imaging. Due to the use of a large bilateral field of view, and continuous sampling across the entire field, each event is captured in detail; allowing detailed spatial classification. The result is the ability to extract a large amount of information regarding each paroxysmal event. This will, therefore, generate detailed insight into epilepsy-associated SD properties. In conjunction, novel aspects of the generated analysis pipeline are assessed.

9.2 Results

The first objective of the work in this section was to utilise the spatial information generated by the previously presented experimental and analysis paradigm. Cortical origins of both seizures and SD were investigated (Figure 68A). As described previously, SD origin is defined as the first pixel in the cortex to transition into a SD state. The seizure origin was defined as the centre of mass of the first area identified within the seizure focus ipsilateral to chemoconvulsant injection. For these spatial comparisons, secondary seizure foci appearing during the event were ignored. The resulting data showed considerable variability in event origins.

Investigation of the laterality of events revealed a consistent footprint of seizure in both hemispheres (marked by the presence of a pathological seizure waveform). Interestingly, bilateral SD events were frequently observed with multiple ipsilateral and contralateral events occurring (Figure 68B). These were often observed to occur together with a short delay, in bilateral events; or separately, in distinct unilateral events.

Inspection of the cortical boundaries that these event origins fell under revealed the majority of seizures were originating in visual areas nearby to picrotoxin injection (Figure 68C). Seizures were also observed to initiate in other cortical locations. The first emergence of seizures from these additional foci suggests the eventual ability for these locations to initiate and drive seizures independently. Moreover, several seizures showed secondary foci in the contralateral hemisphere. These secondary foci were often present in the same functional regions contralateral to the primary

focus.

These same spatial investigations of SD origins revealed a large proportion of events originating from retrosplenial areas of the cortex (Figure 68C). Moreover, these events of retrosplenial origin were frequently found to occur bilaterally; with a second retrosplenial origin in the contralateral hemisphere. SDs were also observed to originate in other brain regions. However, few SDs originated in the visual cortex ipsilateral to injection; suggesting a propensity for SD generation in locations distal to the seizure focus.

Spatial information was then utilised to investigate interhemispheric differences relative to picrotoxin injection (Figure 68D). Since picrotoxin is delivered unilaterally, one hemisphere is compromised to a greater extent than the other. These investigations sought to probe whether this interhemispheric difference leads to differences in SD properties. SD amplitude, duration, area and velocity were investigated and revealed no statistically significant result between hemispheres (N=27 SDs from 4 animals, $p>0.05$). Therefore, this raises interesting questions about the state of the underlying tissue in influencing SD propagation dynamics. Nonetheless, the emergence of contralateral secondary foci suggests the contralateral cortex may become rapidly compromised following initial epileptogenesis.

Following this, the relationship between SD properties was investigated (Figure 68). SD area covered (Figure 69A), velocity (Figure 69B), duration and amplitude (Figure 69D) were calculated for each event as before. Each measurement incorporated data from tens of thousands of imaging pixels across the field of view. Interestingly, a significant positive correlation can be seen between SD area covered and SD amplitude (Figure 69E; N=27 SDs from 4 animals, SC=0.69, $p<0.01$). SD area covered was also positively correlated with SD duration (Figure 69F; N=27 SDs from 4 animals, SC=0.83, $p<0.01$). Moreover, SD duration and amplitude were also seen to positively correlate (Figure 69G; N=27 SDs from 4 animals, SC=0.71, $p<0.01$). The relationship between other extracted properties was also investigated (see Chapter 6- analysis pipeline for details), however, these were found not to be significantly correlated. Therefore, it appears that average SD amplitude, SD area covered and average SD duration are related to a common phenomenon.

In order to investigate the insight attainable with few point measurements, and the ability to extrapolate beyond the field-of-view, the relationship between average event duration and total event duration was compared (Figure 70). Average event duration was calculated by using either the mean or median of the event in all pixels within the detected region (Figure 70A). Total event duration was calculated as the time from the first pixel to entire the event mask to the last pixel to recover

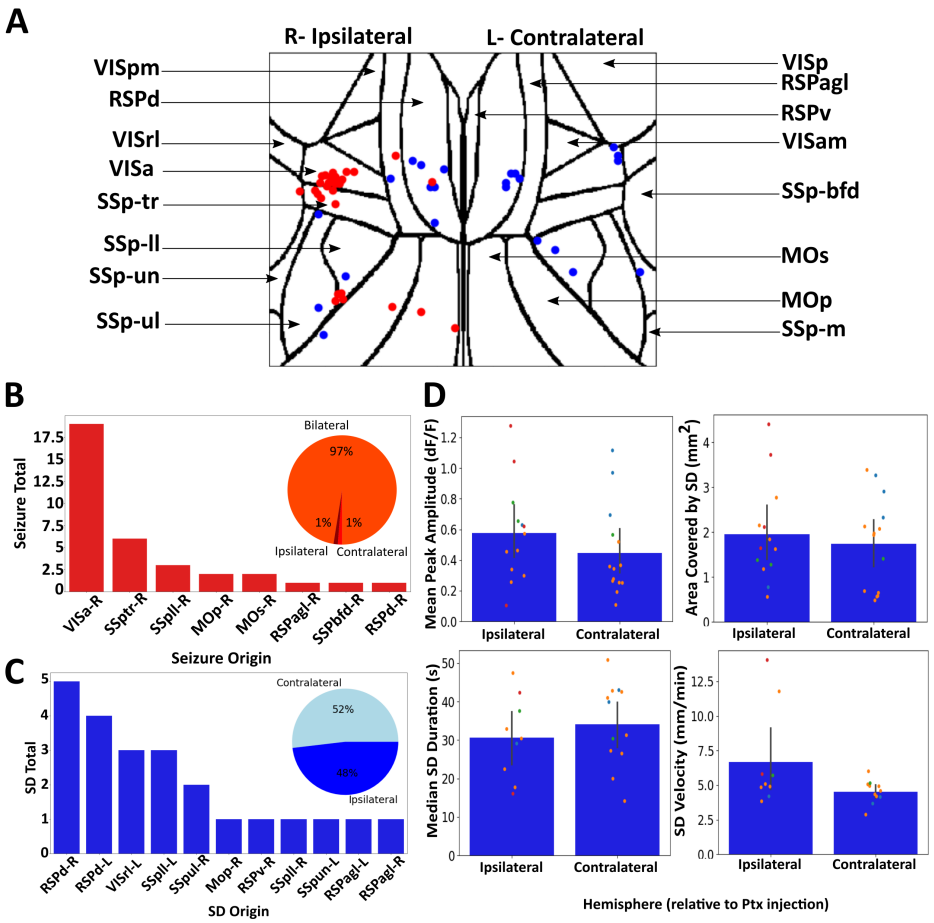

Figure 68: Investigation of seizure and SD spatial properties using widefield imaging. **A)** Map of cortical regions showing locations of seizure (red) and SD (blue) origins. Image labeled with all cortical regions within imaging field of view. VISp:primary visual cortex; VISpm:posteromedial visual area; RSPagl:lateral agranular retrosplenial cortex; RSPd:dorsal retrosplenial area; RSPv:ventral retrosplenial area; VISam:anteromedial visual area; VISrl:rostrolateral visual area; VISa:anterior visual area; SSp-bfd: somatosensory barrel field; SSp-tr:somatosensory trunk; SSp-ll:somatosensory lower limb; SSp-un: somatosensory unspecified; MOs:secondary motor area; MOp: primary motor area; SSp-m:somatosensory mouth. **B)** Barplots of seizure origin location plotted against number of events. Seizures are seen to cluster in visual areas close to picrotoxin injection. Inset shows pie chart with laterality of seizures shown. **C)** As in **B**, for SD. SDs tended to originate from retrosplenial areas. Inset shows pie chart showing SD laterality. **D)** Comparison of SD properties recorded in hemispheres ipsilateral or contralateral to chemoconvulsant injection. SD properties were defined as before averaging data from approximately 40,000 pixels for each data point. Data point hue reflects events recorded from different animals. No significant difference was found between hemispheres for any of the investigated parameters. Data recorded from 4 WT male animals.

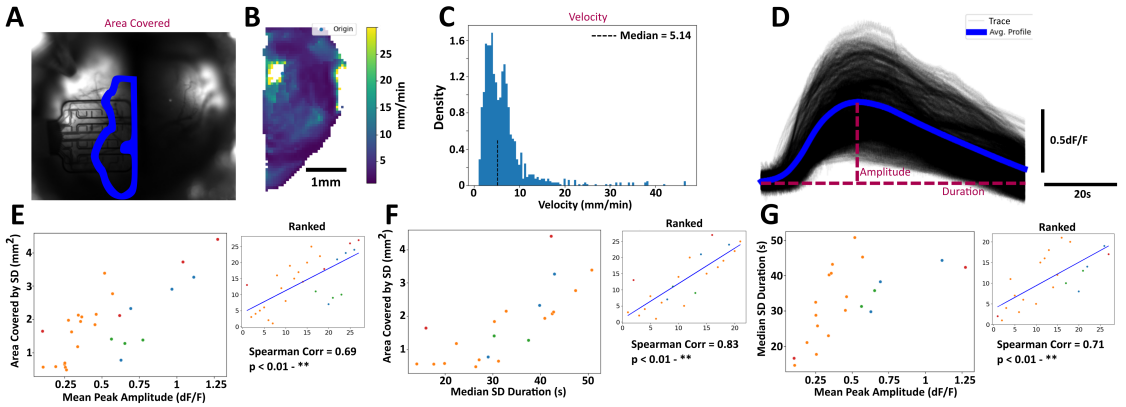

Figure 69: Investigation of the relationships between different SD properties. **A)** Widefield image with area of maximal SD coverage shown (blue). This strategy was used to calculate SD area covered. **B)** Quantification of SD velocity across the entire field-of-view, calculated using phase-correlation methods. **C)** Histogram of SD velocity for a single event. Few outliers can be seen, hence the selection of a median representative. **D)** Overlay of SD traces from all pixels in the SD mask (grey). Average SD profile shown in blue. Windows used for peak amplitude and duration calculation shown. **E)** Plot of SD amplitude against SD area covered. Data was ranked with Spearman correlation performed due to uncertainty regarding distribution. Linear regression was plotted on ranked data. **F)** As in **E** for median SD duration against area covered. **G)** As in **E** for peak amplitude against SD duration. Data shown for 4 WT male animals.

from the event mask. The results demonstrated a high positive correlation for both SD events (Figure 70C; N=27 SDs from 4 animals, SC=0.86, $p<0.01$) and seizures (Figure 70D; N=79 seizures from 4 animals, SC=0.93, $p<0.01$) when comparing duration at individual pixels to entire events. Therefore, this supports the idea that measurements from small areas can be extrapolated to draw inferences about propagation dynamics on a greater scale.

In line with this previous approach, the validity of investigations using seizure focus-related information was assessed. Since this is a novel method, further confirmation that these regions accurately reflected the seizure focus was required. To achieve this, area covered by the seizure was plotted against median seizure duration. Intuitively, the longer the duration of a seizure, the further it is likely to propagate. Therefore, this relationship was used to probe the validity of the generated measures of seizure area. Total area was defined as the total area displaying any seizure-like waveform. Initial observations suggested the majority of these waveforms arose from synaptic activation away from the seizure focus. Investigation of correlation with seizure duration confirmed that this was likely the case: no significant correlation was observed (Figure 71D; N=79 seizures from 4 animals

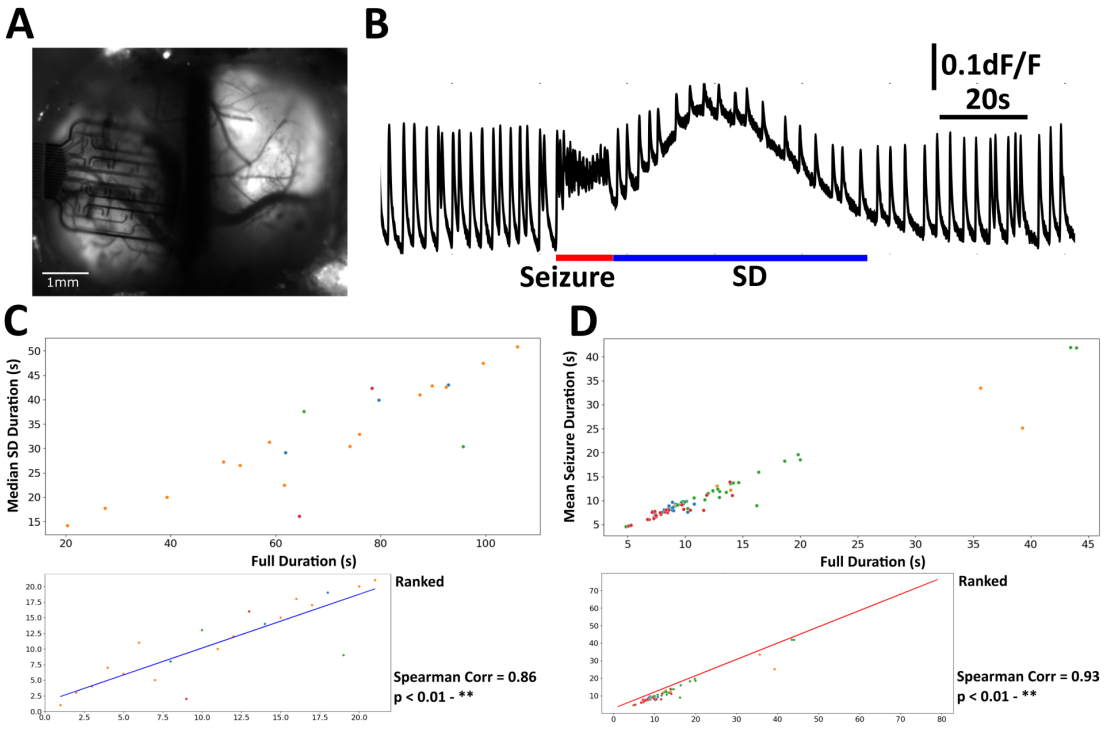

Figure 70: Investigation of the ability of single point recordings to predict whole-event phenomena. **A)** Widefield image showing GCaMP fluorescence. **B)** Example GCaMP trace of a seizure-associated SD. Red line marks the time used to calculate mean seizure duration, and blue line marks the time used to caculate median SD duration. **C)** Characterisation of the correlation between median duration at individual pixels and entire SD duration across the entire cortical hemisphere. Data was ranked before Spearman correlation calculation. Linear regression shown. **D)** As in **C** for seizure duration. Data shown for 4 WT male animals.

, SC=0.2, p>0.05). However, when investigating the seizure focus (as defined by a further fluorescence increase beyond the initiating ictal spike; see Chapter 6- analysis pipeline for details), this was found to significantly positively correlate with seizure duration (Figure 71E; N=34 seizures from 4 animals, SC=0.41, p<0.05). Therefore, this data supports the validity of the presented method to track the spreading seizure focus, and supports the use of this novel analysis method.

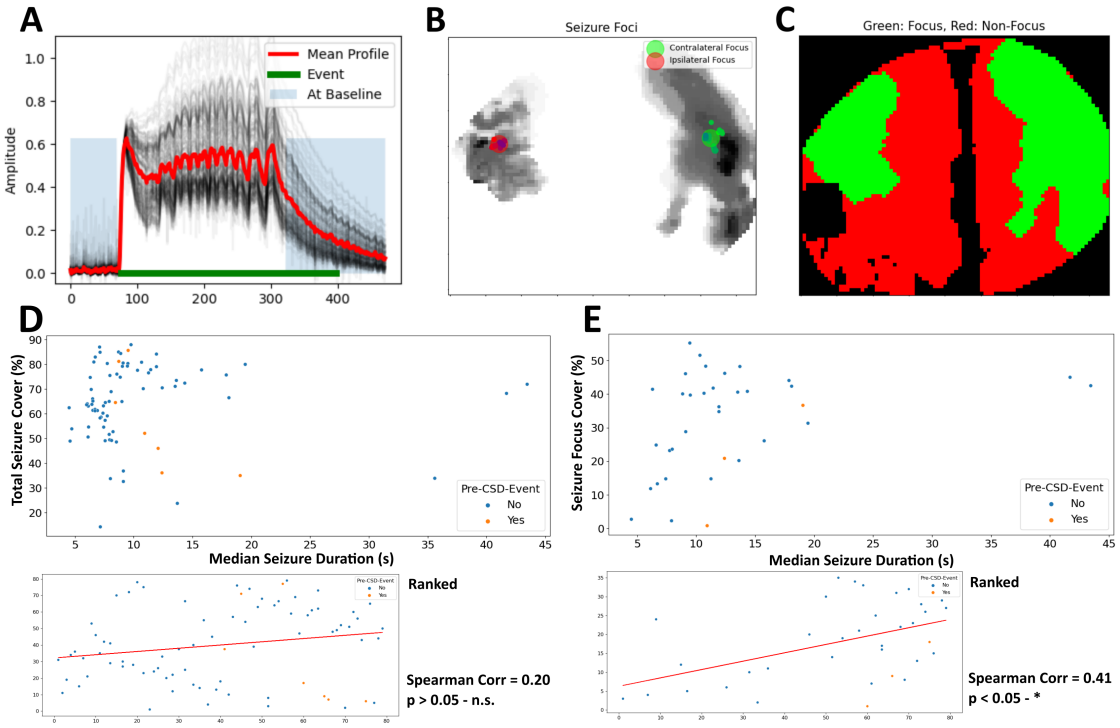

Figure 71: Comparison of seizure properties confirming the validity of the presented method for seizure focus extraction. **A)** Overlay and mean profile of seizure event showing clear differences in waveform between pixels. **B)** Ipsilateral and contralateral seizure focus with origin plotted. **C)** Areas found within the seizure focus (green) and outside (red). **D)** Total area showing a seizure footprint plotted against median seizure duration from approx. 40,000 pixels. No significant relationship observed when ranking data and calculating Spearman correlation. **E)** As in **D**, but comparing the relationship of seizure focus cover with median seizure duration. Calculated seizure focus coverage shows a significant correlation with seizure duration supporting the strength of this approach. Data shown from 4 WT male animals.

9.3 Discussion

The work presented in this section is focused on using the full spatial information contained within widefield imaging recordings to gain insight into seizure and SD paroxysms in awake mice. The findings here incorporated information from across

the field-of-view, to reveal interesting phenomena related to the spatial properties of paroxysmal events. The extraction of event properties from across the field-of-view allowed investigation of commonalities between parameters, therefore highlighting common properties that may interact or undergo co-modulation. Moreover, this platform is expanded to gain insight into studies lacking the spatial information presented here; and to assess their ability to extrapolate beyond the field-of-view. Lastly, the presented platform is also used to confirm the validity of novel approaches to investigate seizure focus propagation.

Of interest is the data describing the laterality of seizure-associated SD events. To date, no studies have spatially characterised seizure-associated SD with this level of detail. The presented findings revealed a high probability of SD in the contralateral hemisphere. These findings somewhat contradict existing literature that points to SD typically being a unilateral phenomenon (Vinogradova et al., 2006). Nonetheless, SD events in the contralateral hemisphere have been reported in other models. For example, a recent study employing similar techniques to study ischaemia-induced SD revealed the occasional occurrence of contralateral SD events with smaller amplitude (H. T. Zhao et al., 2021a). Therefore, data has started to suggest that consideration of SD as a bilateral phenomenon may be required; as opposed to assuming unilateral propagation based on migraine-related findings (Cozzolino et al., 2018).

The bilateral propagation of seizure-associated SD raises interesting questions. Firstly, unlike ischaemia-induced SD (H. T. Zhao et al., 2021a), seizure-associated SDs were found to have a similar amplitude in the contralateral hemisphere compared to those ipsilateral to picrotoxin injection. Therefore, this may suggest a pathological alteration of tissue properties in an area well beyond the location of chemoconvulsant delivery. This would be fitting with the presented results describing secondary generalisation of focal seizures, and previous observations of this in human patients (Blumenfeld et al., 2009).

Nonetheless, the presence of SD events in the contralateral hemisphere may not necessarily be a direct result of secondary generalisation. The presented findings also reveal a consistent footprint of seizures in the contralateral hemisphere. However, this footprint is distinct from areas actively participating in seizure propagation and is likely a result of widespread synaptic activation. Therefore, SD in these contralateral areas may be a result of long-range synaptic input from regions nearby to chemoconvulsant injection. It is unclear whether synaptic activation alone is sufficient to trigger SD in distal areas. However, NMDA receptor inhibition studies build a compelling argument for the strong role for synaptic activation in

SD initiation (Masvidal-Codina et al., 2021).

SD events were seen to originate in one hemisphere (often in retrosplenial areas), and followed by a short delay, a second origin was seen in the contralateral hemisphere. The time difference between the emergence of these bilateral SD events was too large to be explained by simple contiguous propagation across the midline. Therefore, one of few possible mechanisms seem likely. The first is that the SD originates in the ipsilateral hemisphere, propagates ventrally to subcortical regions (e.g. the hippocampus or thalamus), which then directs SD propagation to the contralateral hemisphere. The second hypothesis is that the seizure generalises to subcortical structures, and triggers an SD event that propagates and emerges on both hemispheres. This would explain the similarity in SD properties across both hemispheres but would struggle to explain any time delay observed between emergence in different cortical hemispheres. A third theory is that the seizure is generalised and a SD event is initiated independently in both hemispheres. This could explain the observed similarities in SD properties between hemipsheres (due to a common precipitating event). Lastly, SD may be initiated in one hemisphere and propagate across the corpus callosum to the other hemisphere. This propagation across the corpus callosum has been demonstrated to be possible following SD induction using tetanic stimulation (A. A. P. Leao & Morison, 1945). These theories all seem entirely plausible, and there is no clear evidence to suggest that observed recordings are not a mixture of all of these phenomena. To gain conclusive insight into these mechanisms, incorporation of a depth recording interface would be required.

With regard to the locations of event origins, these appear relatively widespread across the cortical surface. Initial seizure foci predictably clustered around visual areas, nearby to the picrotoxin injection site. However, additional seizure foci were observed distal to the injection site. This observation supports the idea of generalisation of epileptiform activity and the generation of secondary foci through widespread alterations in network physiology in this epilepsy model. Notably, a previous study employing similar methods reported seizure activity remaining focal to the injection site. However, this study utilised a shorter recording window with a smaller field-of-view, limiting the ability to capture these phenomena (Rossi et al., 2017). Moreover, the method of delivery throughout this thesis is intracortical bolus injection as opposed to passive diffusion out of a micropipette. Therefore, the delivery of picrotoxin is concentrated and may overload homeostatic mechanisms faster and to a greater extent. These differences in experimental paradigm could explain the emergence and observation of these additional epileptogenic zones.

With regard to SD origins, events frequently originated from retrosplenial areas of the cortex. The clustering of SD to these locations raises interesting questions about the propensity for these specific regions to generate SD. A plausible explanation surrounds the properties of the retrosplenial areas themselves. Interestingly, in Leão's original studies characterising SD, they reported a greater difficulty in electrically-inducing SD in the retrosplenial cortex (A. A. P. Leao & Morison, 1945). The findings presented in this epilepsy model somewhat contradict these initial observations. Several explanations can account for this disparity. Firstly, considerable literature supports a role for retrosplenial areas in visual processing of landmarks (Fischer et al., 2020). Therefore, since seizures are induced in the visual cortex, and visual areas are functionally connected, pathological input from the visual cortex may trigger SD in these retroplenial areas. Contralateral SDs of retrosplenial origin could be explained by the same mechanism. A second hypothesis explaining the retrosplenial origin of SD relates to subcortical propagation. Several rodent studies highlight strong connections between the retrosplenial cortex and subcortical regions. Evidence suggests the retrosplenial cortex acts as a hippocampal gateway to the cortex (Wyss & Van Groen, 1992). Moreover, the retrosplenial cortex also receives considerable input from the thalamus (Sripanidkulchai & Wyss, 1986). The hippocampus is known to play a role in seizure dynamics (Chatzikonstantinou, 2014); while the thalamus is known to have a large number of reciprocal connections with multiple widespread cortical regions (Adams et al., 1997). Seizures that have generalised to these subcortical structures may result in profound synaptic activation of neurons in the retrosplenial cortex, leading to SD initiation. Moreover, perhaps tetanic electrical stimulation of these cortical regions alone is insufficient for SD induction due to the dependence of initiation on subcortical synaptic input. Therefore, this would explain the contrast to previous investigations (A. A. P. Leao & Morison, 1945). A third possible explanation surrounds the excitability of neuronal populations in superficial layers of the retrosplenial cortex. Recent work has characterised populations of small, hyperexcitable pyramidal retrosplenial neurons. Neurons in this region are able to fire at higher frequencies than typical pyramidal neurons (Brennan et al., 2020). Therefore, this may lead to the rapid accumulation of extracellular K^+, overloading homeostatic clearance mechanisms and triggering SD. This idea seems entirely plausible as it highlights an increased propensity for SD to originate in retrosplenial areas while maintaining the possibility for SD initiation at other locations in the cortex. Altogether, it seems likely that these multiple factors all interact, with the excitable and interconnected properties of the retrosplenial cortex leading to a high probability of SD initiation following seizure induction

in the visual cortex. Depth recordings from hippocampal and thalamic structures would allow definitive characterisation of the temporal sequence of propagation events and allow assessment of the feasibility of these different hypotheses.

The work presented in this chapter also probed properties relating to SD and their relationship to one-another. Many of these relationships were found not to be significant. However, a significant positive correlation was observed between SD area covered, amplitude and median duration across pixels. These relationships highlight interesting points regarding SD properties. One explanation is that a characteristic of the preceding seizure simultaneously determines these three SD parameters and scales these together. Alternatively, these SD properties may be linked to one-another due to the fundamental properties of an SD event. In the case of correlation between SD amplitude and median duration, if the SD has a higher amplitude, a greater number of neurons have entered depolarisation block and homeostasis is disrupted to a greater extent. Therefore, it is plausible that the duration of SD at each pixel will last longer. This would be due to an increased time for homeostatic balance to be regained, as a result of more energy and time required to restore electrochemical gradients. This seems an entirely plausible and simple explanation for observed correlation. One the other hand, the relationship between these SD properties and SD area covered seems more complex to interpret.

The mechanisms halting spatial SD propagation in cortical tissue are currently unclear. Fortunately, the work presented here is able to provide insight into these mechanisms due to the ability to track SD propagation across the cortex. Findings here demonstrate a strong correlation between SD area covered and both average SD amplitude and duration across all pixels. The positive correlation between area and amplitude supports the notion that SDs leading to greater widespread homeostatic disruption, as signified by average SD amplitude, lead to further SD propagation. Moreover, the positive correlation between area covered and average SD duration suggests that SD recovery at each pixel may not be a locally-determined phenomenon, but may be linked to recovery of large-scale networks, as marked by the absence of continued SD propagation. This hypothesis is fitting with previously demonstrated electrographic recordings of lasting abnormal positive DC events in areas beyond the observed area invaded by SD depolarisation. Future work to dissect these phenomena will spatially investigate SD properties as a function of distance from the origin. This may highlight whether the boundaries of SD propagation are determined at the SD origin or dynamically in the tissue as the SD propagates.

In addition to providing insight into SD parameters, this section also delved

into the strengths of different experimental paradigms. The field-of-view presented here allowed investigation of paroxysmal events across a large area of the cortex. However, due to the requirement for a craniotomy, the field of view did not span the cortex in its entirety. Moreover, previous studies have relied on measurements from few-point measurements or a limited field-of-view. To provide insight into the accuracy of extrapolated information from few point-recordings, event duration at individual pixels were compared with overall observed event duration. The positive correlation between these durations for SDs and seizures suggests that event duration at a single pixel is an accurate reflection of overall event duration across the entire cortex. Therefore, studies recording from small areas are able to make accurate inferences about widespread event propagation duration by investigating duration at restricted locations. Nonetheless, the ability to directly capture these events across larger areas without making inferences, as demonstrated here, is clearly advantageous.

The final work in this section aimed to confirm that observations relying on the novel method of seizure focus detection are reliable and accurate. Since no previous study has developed these tools in this experimental context, this is an important task. Sole reliance on the presence of a seizure-like waveform can be misleading due to this seizure signature being present across the majority of the cortex, likely due to synaptic connectivity. The results here demonstrate that the novel measure of seizure focus coverage (using further fluorescence increases during the seizure) correlates with seizure duration, however, the simple presence of a seizure waveform does not. Therefore, this increases confidence in the previously presented work characterising seizure origin based on the detected seizure focus.

Altogether, the research presented in this section provides powerful information regarding SD and seizure spatial relationships in the cortex. Several likely novel mechanisms explaining these spatial relationships are proposed and discussed in the context of past literature. The work here provides insight into multiple areas. Firstly, this study provides insight into the generalisation of epileptiform activity in chemoconvulsant models. Spatial information is used to characterise the locations of seizure-associated SD onsets. This revealed the increased propensity for SD to initiate in retrosplenial areas, and several mechanisms are proposed to explain this. However, other SD origins are also seen suggesting this increased propensity is due to increased probability resulting from network architecture and cellular properties. Examination of SD properties with regard to one-another highlights the importance of considering the role underlying network alterations in SD dynamics and how SD recovery could involve widespread network activity. Moreover, this

section investigates local activity readouts compared to entire events in order to aid the interpretation of both past and future studies. Lastly, confirmation of novel seizure focus tracking methods is demonstrated. To summarise, these findings further highlight the importance of widespread network analysis and the insight achievable into epileptic paroxysms using these comprehensive imaging methods.

9.4 Future Directions

The work in this section, as in others, would benefit considerably from simultaneous depth neural probe recordings to understand the role of subcortical structures in SD initiation and propagation. These additional recordings would elaborate upon the presented findings regarding event origin locations, and allow greater understanding of propagation characteristics. Nonetheless, a powerful strength of this study is the ability to track paroxysmal events across multiple regions of the cortex with a readout from thousands of individual pixels. Further analysis will work to characterise different properties spatially, with relevance to cortical SD origin locations. Investigation of SD parameters as a function of distance from the origin will lead to considerable insight regarding SD propagation dynamics and the role of the underlying tissue state. Moreover, tracking of activity at the SD origin prior to SD initiation may reveal interesting results about the events leading to SD induction. Lastly, confirmation of these findings in multiple epilepsy models, both acute and chronic, would confirm the validity of these findings and demonstrate that they are not a direct result of picrotoxin-mediated $GABA_A$ block. Forthcoming future developments to this work are discussed in greater detail in the following chapter.

Chapter 10

Outlook and Conclusions

In this concluding chapter, I will summarise the findings of the presented investigations. Moreover, I will discuss the greater implications of these findings; along with how future work will endeavor to build upon this research. Lastly, I will draw from the strengths and weaknesses of the presented pioneering tools to speculate upon the future of novel recording techniques, and how a similar thesis may look in 20 years after further technological developments.

10.1 LASU Investigations

A large proportion of this industry-sponsored thesis involved interaction with Scientifica to develop and characterise the LASU system. Here I will summarise these findings and discuss the implications of this work.

10.1.1 Summary of Findings

The primary goal of the LASU-related work in this thesis was the investigation of the limits of single-photon optogenetic stimulation in cortical slices. The LASU system was tested due to it being a compact, commercially available system accessible to any researcher worldwide. Moreover, these investigations incorporated novel opsin constructs with spatially-restricted expression. These spatially-restricted constructs allowed more reliable neuronal stimulation with greater spatial resolution. Nonetheless, although high resolution optogenetic stimulation was demonstrated, single-cell resolution stimulation was not possible. This is likely due to the three-dimensional structure of an acute brain slice and the lack of single photon stimulation spatial resolution in the z-dimension. However, high-resolution stimulation is possible in acute slices and this research demonstrates a powerful tool that would benefit the

neuroscientific community.

10.1.2 Discussion and Future Developments

The work presented relating to LASU-mediated single-photon stimulation can be developed in multiple directions. Firstly, the LASU system remains a powerful tool in investigating neuronal communication in acute slices. This instrument holds considerable promise in quickly dissecting functionally connected cell populations to allow paired recordings with greater ease. Moreover, the LASU system could also allow investigation of synaptic integration at a single patched neuron following optogenetic activation of multiple different presynaptic neuronal populations in quick succession. Lastly, this paradigm could also allow insight to be gained into SD initiation mechanisms through focused optogenetic stimulation of small neuronal populations. The work presented here lays the groundwork for several interesting future investigations that could either reveal interesting disease mechanisms directly, or optimise current electrophysiological experimental paradigms.

There is also a potential for the LASU system in studying activity in neuronal cultures. Since the neurons are organised in a monolayer, single-cell resolution would likely be possible. Considerable work has been invested in investigating the feasibility of this, and the required vectors to achieve this have been generated. This would allow control over neuronal dynamics in a more-controlled culture environment.

The use of novel spatially-restricted opsin constructs is another powerful aspect of these LASU studies. The continual development of these optical tools regularly updates the toolbox available to neuroscience researchers. As a result, researchers are gradually able to study disease processes in more detail. The Synthetic Neurobiology Group (MIT, USA) is at the forefront of the development of these tools and provided the opsin constructs used in this doctoral thesis. The presented data comparing LASU stimulation of these opsin constructs will be incorporated into a larger collaborative publication (Dr. Or Shemesh and Prof. Ed Boyden) demonstrating the strength of these targeting strategies in unlocking new insight into nervous system communication.

10.2 Combined gSGFET Recording with Imaging to Study Paroxysmal Events

A large proportion of the work presented in this thesis involved the construction of an experimental configuration to probe the seizure-SD relationship in awake head-

fixed mice. Novel gSGFET arrays were used to record multi-site, full-bandwidth electrophysiology. The transparent nature of gSGFETs allowed concurrent functional imaging from recording sites. Moreover, the optimisation of surgical procedures also allowed imaging of activity bilaterally across both cortical hemispheres. To access the information contained within these recordings, a powerful automated analysis pipeline was generated. The result was the ability to investigate seizure-associated SD with a newfound level of detail. Moreover, the ability to simultaneously record electrical and optical readouts of neuronal population activity raised interesting questions regarding electrographic signal generation mechanisms.

10.2.1 Summary of Findings

The initial stages of these investigations demonstrate how a seemingly simple experimental paradigm can be optimised to increase the depth of information gained from a single animal, and to allow the flexibility to investigate different animal models. The optimised experimental paradigm has revealed several interesting phenomena. Firstly, the electrographic and optical readouts of neuronal activity deliver different information regarding the neuronal population being investigated. The dominant contribution of synaptic activity to the electrographic signal results in a large footprint of epileptiform discharges. Imaging techniques appear able to resolve these discharges with greater resolution due to the large contribution of action potential-mediated Ca^{2+} influx to recorded fluorescence. The construction of an automated analysis pipeline to complement this experimental paradigm led to a toolset with the potential to reveal insights into seizure and SD related-mechanisms, and their relationship to one another. The use of this pipeline to analyse acute seizures in WT animals revealed interesting phenomena relating to SD initiation, and the interaction with epileptiform activity. Altogether, this work has potential in two main areas. The first surrounds insight into paroxysmal events and their relationship to one another. The second is to unravel the complex mechanisms of electrographic signal generation during epileptiform discharges. Future work will further delve into these two areas.

10.2.2 Discussion and Future Developments

The majority of the work presented in these investigations was focused on WT male animals. The same experiments have been performed in multiple WT female, S218L HET male and S218L HET female mice. Future experiments will perform the experimental paradigm in a larger sample size. Since SD events showed greater variability

than initially expected, more experiments are required to perform meaningful statistical comparisons between genotypes. These comparisons will probe differences between evoked events in WT animals and evoked or spontaneous events in HET mice. These events in HET mice may hold greater physiological relevance due to widespread alteration of neuronal networks. These investigations may also make it easier to highlight and pinpoint specific network alterations leading to SD initiation through shared commonalities.

The presented study has considerable strengths that create a potential platform to unravel the seizure-SD relationship. Additional to the insightful combination of novel technology, this study also has several other advantages. Importantly, investigations were performed in awake headfixed mice as opposed to under anaesthesia. Anaesthesia has been shown to have an influence on both seizure and SD dynamics (Veronesi et al., 2008; Takagaki et al., 2014). Therefore, disparity in the literature may arise due to these effects. Moreover, the anaesthesia used during surgery prior to recording was isofluorane, an inhaled anaesthetic known to have a short half life (Wyrwicz et al., 1987). The recovery period in this recording paradigm was sufficient to enable near-complete elimination of anaesthetic from the brain. As a result, animals were recorded in the absence of any anaesthetic agents; and therefore, findings may hold greater clinical relevance.

Nonetheless, several limitations of this study can be observed. Firstly, analgesic was required to minimise post-operative pain. In this case, buprenorphine was used due to high efficacy in delivering rapid analgesia. However, unlike isoflurane, buprenorphine has a longer halflife and will remain in the system throughout the experiment (Kendall et al., 2014). Nonetheless, the effect of buprenorphine on SD dynamics has not been demonstrated and these effects can not be avoided due to animal-related ethical concerns. Moreover, a wide range of studies have used buprenorphine-mediated analgesia with this resulting in no clear influence on activity (Jansen et al., 2019; Loonen et al., 2019; Masvidal-Codina et al., 2019).

Another major limitation of these investigations is the invasive nature of the experimental paradigm. Since, SD can be induced by a simple pinprick of the cortical parenchyma (Vinogradova et al., 2020), surgical procedures are likely to inadvertently induce SD. Moreover, SD is seen to alter subsequent brain activity (Gorji & Speckmann, 2004). As a result, the generation of a large bilateral craniotomy and cortical insertion is not ideal. These events may have an influence on the processes being studied and this should be considered when interpreting results. Nonetheless, these limitations were justified by the accompanying strengths. A craniotomy was required to enable electrophysiological access to the tissue for gSGFET devices. To

enable comparison of activity between cortical hemispheres without the presence of the skull confounding observations, the craniotomy needed to be expanded to encompass the other hemisphere. Otherwise, without the need for craniotomy, a thinned-skull preparation would have been used (demonstrated in Appendix).

Another limitation of this study surrounds the acute nature of the recording paradigm. Each recording session was performed in an acute session with each animal culled after recording. This was required due to the large bilateral craniotomy being too large for coverslip fixation. Moreover, fixation of a coverslip results in optical phenomena such as reflectance and refraction, and leads to loss of photons and worsened SNR. As a result, the absence of a sealed recording site requires a terminal experimental paradigm. Future work will aim to overcome these limitations and expand time windows of investigation. This would be especially interesting in the cases of S218L animals where observed spontaneous events may differ according to animal age, and an intact preparation would allow longitudinal imaging of a single animal and how these events change across time. This would be especially important in the context of migraine-related SD, where events in humans are shown to have age dependency (Victor et al., 2010).

An additional limitation of this study is the absense of haemodynamic correction. During widefield imaging of large populations, haemodynamic responses result in alterations in fluorescence due to the light absorbing properties of oxy- and deoxy-haemoglobin. These responses may lead to an increased difficulty in interpreting fluorescence signals and relating these to neuronal activity. To circumvent these issues and simultaneously investigate haemodynamic responses during SD, several studies remove these signals from the recorded Ca^{2+} signal. To achieve this, GCaMP illumination is often interleaved with illumination using a longer wavelength outside the GCaMP spectral range. As a result, this second frame can be used to correct the fluorescence signal and algorithms such as the modified Beer-Lambert law can be used to resolve Ca^{2+} dynamics with greater precision (H. T. Zhao et al., 2021a). When constructing the presented experimental paradigm, these factors were considered. However, they were not incorporated primarily due to the sacrifice in temporal resolution required to interleave different wavelengths. This would considerably reduce the temporal level of detail acquired regarding paroxysmal events. Moreover, the recorded signals with GCaMP7f provide a powerful readout of activity in absence of this correction. As a result, it was justified to proceed without haemodynamic correction of recorded GCaMP signals.

A final major limitation of this experimental paradigm is the lack of information acquired regarding event propagation in the Z-dimension. These investigations, like

several others, are focused entirely at the cortical surface. However, it is clear that propagation of both SD and seizures to subcortical structures may play an important role in disease pathogenesis. The view into paroxysmal activity presented here is highly comprehensive with regard to cortical activity, but lacking in detail regarding other structures. Techniques such as magnetic resonance imaging (E. Parker et al., 2021) and functional ultrasound imaging (T. Kirchner et al., 2019) are able to image event dynamics throughout the depth of the tissue simultaneously. However, the level of detail acquired relating to the activity of each area is limited compared to GCaMP. Therefore, the selection of fluorescence Ca^{2+} imaging appears justified.

Several future developments will be able to overcome the presented limitations. To maintain the level of detail acquired into cortical activity while capturing greater information about subcortical structures, other gSGFET configurations can be utilised. Imaging is limited in this regard due collection of photons from a single focal plane. gSGFET devices, however, are available in intracortical configurations. Throughout this work, these were avoided due to several limitations. Firstly, the depth probe substrate is polyimide (Bonaccini Calia et al., 2021), and has not been optimised for combined imaging; as for the epicortical arrays presented here. Secondly, these devices require insertion perpendicular to the imaging objective which would reduce the imaging field of view. Thirdly, these devices are invasive and can alter activity dynamics. Therefore, epicortical arrays were the focus of these investigations. However, future work would be interested in supplementing the techniques presented here to gain greater insight in the subcortical role of paroxysmal events. In recent months, by working with collaborators at UCL and ICN2, we have designed imaging compatible gSGFET intracortical probes able to record from multiple sites in the cortex, hippocampus and thalamus simultaneously. These devices have been designed with a long flexible tail to allow diagonal insertion through the tissue with minimal effects on simultaneous GCaMP imaging. Incorporation of these devices into the presented paradigm will lead to a more detailed understanding of the seizure and SD relationship. Although difficult to incorporate into an already dense recording paradigm, preliminary data has been generated recording optogenetically-induced SD events with GCaMP, epicortical and intracortical gSGFETs (see Appendix). Therefore, the combination of this technology, although difficult, is possible.

In order to circumvent limitations of the invasiveness of the presented paradigm, preliminary investigations were performed through the intact skull. This would also facilitate a greater understanding of the influence of anaesthesia and analgesic on recorded events. These preliminary investigations revealed a high SNR and

ability to resolve paroxysmal events (see Appendix). Of course, this preparation does not allow electrophysiological access to the brain. However, this would allow construction of complex longitudinal imaging paradigms in chronic epilepsy models. These investigations have not yet been performed repeatedly in the same animal due temporary facility restrictions. However, this will be addressed in forthcoming investigations.

Altogether, the weakness of this study appear well outweighed by the strengths; and the alterations to mitigate these weaknesses in future work will lead to an even more comprehensive and robust experimental view into paroxysmal events. Since the results have displayed compatibility between the experimental paradigm and developed analytical tools, further work will focus on completing datasets to enable statistical comparisons between results obtained from WT male and female animals with CACNA1A S218L HET animals. Previous studies, using similar methodologies to this, report observed phenomena descriptively. The power of the methods shown here surround the ability to quantify these phenomena across the entirety of the imaged cortex and investigate them in greater detail than that demonstrated previously.

Regarding the analysis pipeline, the presented tools have undergone several rounds of development and optimisation. The construction of the presented pipeline is currently undergoing the final round of optimisation. Following this, the accuracy of this pipeline will be validated by comparison to electrophysiologically-detected events. Moreover, simultaneous electrical and optical measurements will be used to dissect electrographic signal contents.

The forthcoming outputs of this work will lead to multiple novel avenues of investigation and developments. Firstly, the novel widefield analysis tools can be shared with other researchers to allow efficient detection and analysis of paroxysmal events in different settings, e.g. stroke and glioblastoma. Secondly, the experimental paradigm and analysis tools will be used to probe the seizure-SD relationship and investigate changes in cortical network activity leading to an increased propensity for SD occurrence. Thirdly, the presented paradigm extracts SD properties in detail and these can be investigated to gain insight into SD dynamics. Lastly, the combined recording of electrical and optical readouts of a multiple neuronal populations simultaneously will lead to a greater understanding of electrographic signal generation mechanisms.

These avenues will be the focus of any forthcoming work. In order to finalise the pipeline, the accuracy of detection algorithms will be investigated as mentioned previously. Moreover, this will be investigated in transgenic animals and other epilepsy

models to ensure sufficient flexibility to adapt to multiple experimental configurations. The seizure-SD relationship will be probed in more detail by increasing sample sizes. Additionally, the data from transgenic animals and other epilepsy models will be used to confirm findings are not specific to picrotoxin-injected animals. To this end, considerable data has already been acquired from male and female S218L HET. SD properties will be investigated in concurrence with these objectives using the previous presented analysis code. Electrographic signatures of epileptiform activity will be investigated in detail using this combined paradigm with additional recordings. Moreover, additional alterations in experimental configuration will be performed to gain further insight into these signatures. This will include GCaMP targeting to different neuronal subpopulations (e.g. pyramidal cells and interneurones). Moreover, incorporation of a beam splitter will allow these excitatory and inhibitory populations to be resolved separately and imaged simultaneously during paroxysmal events. This would be a powerful development and lead to considerable advancements in the literature surrounding seizures and SD. Additionally, investigation of the relationship of electrographic discharges to the activity of other fluorescent reporters would provide insight. These would include neurotransmitter reporters (such as iGluSnFR and iGABASnFR), and voltage reporters. Preliminary work has investigated iGluSnFR activity in the above experimental paradigm (see Appendix). Future work will investigate glutamate dynamics further. Moreover, investigation of fluorescent voltage indicators would provide a more direct readout of local neuronal activity and subthreshold alterations, allowing insightful comparisons with recorded full-bandwidth activity. These next steps will develop the tools shown here to further progress our understanding into recording techniques and epileptic disorders.

Following these developments, significant work will be invested into modeling the seizure-SD relationship using computational methods. The collaboration formed with University of Warwick will be developed by incorporating the outputs of these investigations into a computational model. This model will aim to replicate any findings observed in animal models and investigate paroxysm-modifying parameters, such a extracellular K^+ concentration. This model will also perform in-depth modelling of seizure-SD relationships in different spatial configurations, that are inaccessible in the presented experimental paradigm. For instance, these presented investigations all focus on characterisation in the lissencephalic mouse brain. However, to understand seizure-SD interactions in humans, it is important to consider the gyration of the cortical surface. Therefore, the incorporation of data generated by this experimental paradigm into a model able to simulate different spatial

tissue properties would allow greater relation of these findings to human patients. These computational investigations will comprise a considerable body of work for a forthcoming doctoral thesis (Adam Smith) from collaborators at the University of Warwick.

10.3 Future of Neural Interfaces and Recording Techniques

Since the title of this doctoral thesis is 'Novel tools to Investigate Cortical Activity in Paroxysmal Disorders', the outcomes of this thesis are tightly interlinked with the current stage of technology and neuroscientific tools. It is entirely feasible that in coming years, these tools will progress and be developed. As a result, a thesis with a similar title that is produced in later years may yield different results. Here I will speculate what this future thesis may characterise and the technological advancements that may lead to this.

With regards to single-photon optogenetic stimulation in slices, clearly there are limitations in the intrinsic properties of light that lead to difficulties probing neuronal populations with single-cell resolution. To circumvent these limitations, developments are proceeding in two major areas. The first is the development of novel, spatially-restricted optogenetic probes; such as those presented here. Further development of these tools will result in reliable optogenetic stimulation in desired cells with minimal activation of neighboring populations. Moreover, these tools may lead to reduced variability in trans-synaptic investigations; wherein observed responses are a result of somatic depolarisation leading to action potential-mediated neurotransmission, as opposed to direct ChR-mediated depolarisation of synaptic terminals leading to exocytosis. The work presented in this thesis demonstrates a clear major step in the development of these tools.

Nonetheless, in order to full utilise these spatially-restricted opsin constructs, developments in stimulation technology are also required. In recent years, several developments have been performed in this sphere. To overcome diffraction limitations and achieve high spatial resolution, two-photon systems are often employed. However, these experimental configurations typically suffer from common limitations. The first is that the field of view is typically small, allowing investigation of only a single neuronal population at a time. Secondly, the activation of opsin molecules is limited by the ability for the mirror galvanometers to rapidly switch position. This can, therefore, limit the number of neurons that can be stimulated in quick succession, and the number of photosensitive channels activated

within a given time window. To overcome these limitations, computer-generated holography-based methods are being employed more frequently (Shemesh et al., 2017). Although complex, these methods allow light to be sculpted to occupy specified volumes. The result is the ability to stimulate single neurons in quick succession in a complex three-dimensional tissue structure. Simplification of these devices into a user-friendly, cost-effective, commercially-available system will lead to the next generation of control over neural dynamics being available to a greater number of researchers. Additional developments have increased the number of photons required to activate a photoreceptive molecule from two to three, or even more in some cases (Zipfel et al., 2003). These increase the spatial resolution of stimulation even further. These devices are useful for targeted stimulation of small structures and may be unnecessary for fast activation of multiple soma. Nonetheless, the use of longer wavelengths in these cases allows photostimulation of deeper structures with reduced photon-scattering. Therefore, increasing the number of photon energies combined for stimulation may be advantageous for these purposes.

Altogether, the future of optogenetic stimulation in three-dimensional tissue structures will clearly benefit from developments in opsin-tool spatial restriction. Moreover, the affordable availability of complex, expensive technology such as multi-photon microscopes with patterned light generators, will advance the ability for neuroscientists to probe neural networks in high detail.

With regard to *in vivo* investigations of paroxysmal events, advancements can be predicted in multiple areas. The first would surround imaging and the ability to image large areas of the cortex, with higher spatial resolution. The work presented here trades the ability to resolve activity in individual cells for the ability to image multiple brain regions simultaneously. The development of novel tools to enable imaging from widespread cortical regions with sufficient spatial resolution to localise fluorescence to individual cells would be powerful. Moreover, complex devices able to image multiple populations of neurons at different depths simultaneously would further increase the power of these investigations. This would allow high resolution optical interrogation of cells in multiple brain regions simultaneously, without the need for electrophysiological depth probe insertion.

Another area of potential development and optimisation is the method of transduction used to generate GCaMP expression. The work presented here uses multiple neocortical AAV injections. However, this is not ideal as it requires lengthy surgical procedures that can lead to complications due to a prolonged state of anaesthesia. Moreover, each injection site has the potential to cause damage which result in a reduction in imaging field-of-view, or may alter local neuronal behaviours. In re-

cent years, of growing interest are AAV-PHP.eB vectors which are able to achieve efficient neuronal transduction following intravenous administration. GCaMP sequences have recently been incorporated into these vectors, with this holding potential in transducing large areas of tissue with relative ease (Dana et al., 2019). Nonetheless, additional factors should be considered such as off-target effects and GCaMP fluorescence of cells outside the cortical region of interest.

With regard to electrical measurements using gSGFET devices, it appears likely that considerable progression will occur in this sphere. Commercialisation of this technology will lead to use in a greater number of research facilities. Therefore, this would allow more researchers to investigate the role of low frequency oscillations in their field of interest. Thus far, the role of these slow potentials have been overlooked due to technical limitations; and insight into this may lead to the development of novel therapeutic avenues.

Moreover, with relation to the strengths of gSGFET devices, the flexible nature of these devices builds a strong case for use in chronic settings. Since these devices are able to adapt in shape to the surrounding tissue, they result in minimal brain damage when implanted over long periods (Bonaccini Calia et al., 2021). As a result, these devices would be powerful in chronic implantation studies where a pathological process is to be investigated and minimal confounding effects from the invasive electrical interface is required.

The combination of these factors also make gSGFET devices suitable for clinical applications. SD is easily induced by mechanical disruption of brain tissue, and this commonly occurs during surgical procedures. However, the effects of these induced SDs are uncertain. Clinical translation of gSGFET devices for use during surgical procedures holds potential in minimising long-term surgical complications and ensuring healthy outcomes for patients. Future developments will require optimisation of fabrication materials to ensure compliance with regulatory authorities.

In line with the work presented here, it is clear that recorded electrographic signals contain information regarding a complex mixture of different phenomena. A greater dissection of electrographic signals will lead to a greater understanding of different cell types driving pathological activity in human patients. This will therefore likely lead to a greater ability to diagnose epileptic disorders and target areas for surgical resection. As a result, research combining gSGFET devices with functional imaging holds promise in leading to improved outcomes for epileptic patients by unraveling the constituents of electrographic signals recorded at a distance from sources.

Stepping away from gSGFET devices and examining electrophysiological inter-

faces as a whole, it would seem a major problem is the localisation of sources of activity. Somatic action potentials can only be recorded locally due to the filtering properties of the brain parenchyma. Often this is not feasible in human patients and can lead to additional damage. Novel technologies to allow greater localisation of electrical sources and to directly record neuronal spiking from multiple populations will lead to a greater understanding of cellular contributors to pathological events. This may reveal novel therapeutic targets.

Several other developments in recent years have led to increased insight into pathological brain states. One of these surrounds data storage and computing capabilities. In recent years, the act of reading, writing and processing large quantities of data has become far easier and more accessible. This now allows the generation of more complex and complete experimental paradigms, with a lower need to minimise the complexity of recording configurations. Previously, the ability to store and manage large datasets was limited, and this resulted in a trade-off between constructing comprehensive experimental paradigms and generating manageable quantities of data. Today, due to rapid access storage devices, large memory drives and cloud storage, these considerations are less important. Therefore, more comprehensive paradigms can be constructed; such as those shown here which incorporated continuous behavioural imaging using the compact Raspberry Pi to enable physiological readout of electrical events.

Along these lines, another major advancement surrounds the complexity of analysis tools. Previous studies employing similar widefield imaging methods simply average ROIs and quantify activity within these. These analysis methods to allow continuous monitoring of events across the entire field-of-view are complex and required considerable work to construct. The ability for more researchers to perform detailed investigations such as these will expand our current understanding of disease mechanisms. Often, simpler analysis methods are selected to generate quicker results. However, the ability to perform comprehensive and complex analysis at high speeds will lead to greater uptake in the neuroscience community. Over time, more researchers will develop these analytical skills due to the slowly unraveling 'coding revolution'. Moreover, the availability of online services (e.g. GitHub) to enable sharing of analysis tools between researchers results in more collaborative efforts. Therefore, more researchers will have access to complex analysis tools, such as those presented in this thesis. These tools will maximise the information gained from a given animal and experimental paradigm.

There is a growing interest in recent years in the application of machine learning. Thus far, applications have been limited due to complex tasks typically requiring

powerful graphical processing units to accomplish tasks in a reasonable time window. However, as technology has progressed, these methods have been employed more frequently. Although no machine learning analysis has been presented in this thesis, one can not ignore the future potential these methods hold in unraveling complex disease-related paroxysms; especially in cases of complex experimental paradigms such as those presented here. The availability of these tools with easy to use interfaces will advance our understanding of disease states by increasing the depth in which a given dataset can be analysed. Future work will take this into consideration.

Another consideration is the extent to which animal models will be used. Animal models currently exist as the only viable, detailed method of experimentally studying disease-related processes in intact tissue. This has resulted in a clear road-map from findings in animal models to clinical translation. However, drugs often fail clinical translation (Percie du Sert & Rice, 2014); raising serious questions about the relevance of data collected from animal models to human patients. Firstly, the discussed approach of using animal models to advance the interpretation of clinically-acquired data is a feasible path for the future. However, studies involving screening for drug efficacy in modifying disease processes clearly require a model of investigation. As technology advances and computation modelling progresses, perhaps these complex dynamic models can reduce the need for animal models. Nonetheless, to create a computational model sufficient to fully mimic biological systems, considerable computational power would be required. Additionally, to construct such a model, a deep, comprehensive understanding of biological systems would be needed. Therefore, this raises the question of whether the knowledge required to generate such a powerful computational model would render any further investigations futile. Nonetheless, regardless of whether computational modelling will ever full replace animal models, the growing use of computational methods provides a powerful additional view into disease mechanisms.

Compiling these individual points, it can be speculated that future investigations into neurological disease will be able to study larger populations of neurons in greater detail. As the availability of novel tools increases, more researchers will be equipped with the powerful ability to interrogate widespread circuitry in high detail. Moreover, the concurrent development of targeted optical tools will allow more precise activation and perturbation of activity. In line with this, electrophysiological brain interfaces and recording equipment will also progress. Interest in the use of gSGFET devices to record full-bandwidth multi-site electrical activity has grown in recent years. This technology demonstrates phenomenal stability,

with clear room for commercialisation and clinical translation. Concurrently, technological advancements will advance the ability to interpret and extrapolate from these datasets. The availability of technology allowing storage of large datasets will reduce limitations on what can be acquired within an experimental window. Moreover, advances in data analysis will increase the insight gained from a given dataset. Computational advances will lead to the generation of more powerful models able to extrapolate experimental findings beyond our current capabilities. Lastly, combination and detailed analysis of different recording modalities together is likely to progress the understanding of electrographic signal contents; leading to more detailed interpretation of clinical recordings.

10.4 Concluding Statements

Throughout this thesis, the development, optimisation and implementation of novel technology is presented. These tools clearly demonstrate potential in revealing insight into complex neurological disease-related phenomena. The application of these tools to investigate cortical dynamics during epileptiform activity is demonstrated. Moreover, the work presented here provides a powerful view into SD dynamics. Additionally, the developed experimental platforms and analytical tools demonstrate flexibility, allowing their potential application in studying multiple other neurological disorders.

To summarise, the research presented here demonstrates a large step forward in the optimisation and employment of novel experimental neurotechnology. The developed analytical tools allow the information contained within complex datasets to be fully unlocked, allowing the full potential of this technology to be explored. Future work will use these experimental and analytical tools to perform high-throughput investigations of different models of neurological disease, to provide newfound insight into disease mechanisms, and to highlight novel therapeutic avenues.

Chapter 11

Appendix

In this section I will discuss recent developments and present additional investigations that will be pursued in the future. A considerable proportion of this work was performed in parallel to the main investigations in the body of this thesis to guide novel technology development.

11.1 Introduction

Considerable work throughout this thesis has demonstrated the effective use of Ca^{2+} imaging and multi-site gSGFET-mediated full-bandwidth electrophysiology. Future work will expand upon these findings in multiple ways.

A major aspect of this expansion will be to increase the size of datasets to account for observed SD variability. Moreover, the majority of data presented in this thesis has characterised seizures and SD in WT male animals. However, considerable work will be performed to characterise these phenomena in WT female mice, as well as S218L animals of both sexes. Several animals have already been recorded from for each of these groups to confirm compatibility of the experimental paradigm with the increased SUDEP susceptibility of S218L mice and the smaller skull size of female mice. These datasets will be completed and analysed in conjunction with the WT data presented previously.

Another major development will involve the use of different models of investigation. As mentioned previously, several chemoconvulsant models exist and future work will utilise these to demonstrate findings are general to the epileptic state and not simply a direct result of the chosen chemoconvulsant. Additionally, SD can be induced by prolonged optogenetic stimulation of small tissue volumes: this would be a powerful method to perform controlled investigations of SD propagation in healthy (WT) and pathogenic (S218L) networks. Preliminary work has been per-

formed to record 4-AP and ChR2-evoked SD from WT animals. Further work will build a complete dataset characterising paroxysmal events in an alternative model of epilepsy.

Other preliminary investigations have probed different fluorescent reporters of activity. In recent years, interest in fluorescent reporters of neurotransmitter concentration has grown considerably (Marvin et al., 2013). Preliminary investigations were performed to investigate the optical readout of glutamate concentration (iGluSnFR) during seizure and SD. Glutamate, the primary excitatory neurotransmitter in the brain, is known to play a considerable role in epilepsy pathology. The extracellular concentration of glutamate is tightly controlled under physiological conditions to allow effective synaptic transmission. However, during pathological firing, glutamate can exceed physiological levels and spillover outside if the synaptic cleft. The use of widefield imaging to probe these glutamate levels provides a unique view into interesting phenomena related to glutamate concentration regulation. Preliminary results demonstrate a powerful ability to capture these glutamate dynamics.

Another powerful forthcoming development will involve the repetition of experiments in a non-invasive preparation. Throughout these investigations, craniotomies are required to allow electrophysiological access to the tissue. However, the generation of a craniotomy may confound SD-related results due to physical disruption of brain tissue. Although this effect is minimised by ensuring minimal disruption to the dura, there is still possibility for contribution to observed phenomena. Moreover, the generation of open craniotomies results in the need for acute experiments; thus, preventing longitudinal studies of spontaneous events in chronic models. Therefore, preliminary investigations were performed using an intact-skull preparation.

Lastly, considerable recent developments have been made with regard to gSGFET devices. The devices presented here have a coverage of 1.6x1.6mm. However, the craniotomies optimised through these experiments are far greater in size. To increase the spatial coverage of gSGFET devices, novel 64-channel devices were designed with specific dimensions to fit the craniotomies presented here. Although fabrication of these devices is still underway, considerable work has been performed to optimise recording hardware for these purposes. Moreover, to pilot investigations of intracortical depth recordings, depth gSGFET probes have been combined with epicortical gSGFET arrays and Ca^{2+} imaging to investigate SD propagation.

Here in this chapter, I will discuss the progress made into these multiple areas of interest and present pilot data which will guide future developments.

11.2 Results

The investigations presented throughout this thesis are able to characterise cortical activity during seizures and SD with a high level of detail. However, this work suffers from the limitation that subcortical structures are somewhat overlooked. The potential role of these subcortical structures in SD and seizures is discussed in detail. However, without direct recording of temporal sequences of SD propagation in the cortex and subcortical structures, a degree of ambiguity remains. Fortunately, gSGFET depth probes are able to address this.

Preliminary recordings were acquired incorporating 14-channel intracortical gSGFET probes into the previously described experimental paradigm. For more information regarding the gSGFET intracortical probes see Bonaccini Calia et al. (2021). These experiments performed unilateral GCaMP imaging with an epicortical 16-channel gSGFET array. Moreover, diagonal insertion of a intracortical gSGFET probe was performed into the somatosensory cortex (Figure 72A). To investigate SD dynamics, AAV9-CaMkII-ChR2(H134R)-YFP was expressed in the ipsilateral motor cortex. 10s continuous 470nm illumination was used to illicit an optogenetic SD event. More details regarding the expression and induction protocol can be found in Masvidal-Codina et al. (2021). Five distinct regions of interest were placed across the field-of-view to characterise SD propagation (Figure 72B&C) with ROI 1 furthest anteriorly, and therefore, closest to the motor cortex (site of SD induction). Two of the ROIs were selected for visualisation (Figure 72D&E). SD events are visible on full-band intracortical and epicortical electrographic recordings. Moreover, these are also clearly visible on simultaneous GCaMP recordings. Therefore, this recording paradigm demonstrates the successful combination of epicortical and intracortical gSGFET devices with GCaMP7f imaging to record optogenetically-induced SD.

These results demonstrate the ability to successfully incorporate intracortical gSGFET devices into the recording paradigm. Another development to gSGFET recording capabilities is the expansion of the epicortical array to allow a greater number of recording sites. These novel gSGFET epicortical arrays were developed to allow recording from 64 different sites, instead of 16 (Figure 73C). These were designed to fit the specifications of the optimised craniotomy size presented previously in this thesis (Figure 73B). Therefore, the spacing and arrangement of transistors is optimal for integration into the paradigm presented throughout this thesis. The gSGFETs are arranged to place maximal wiring around the midline. This maximises the ability to simultaneously record GCaMP as the midline predominantly

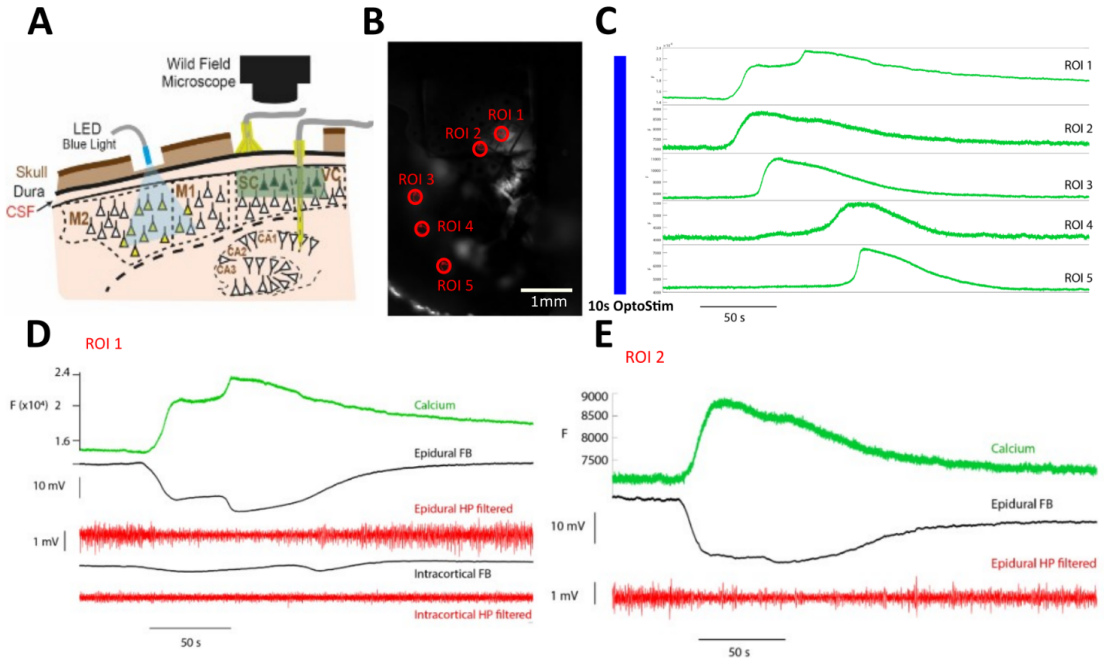

Figure 72: Combined GCaMP, epicortical and intracortical gSGFET recordings of an optogenetically-induced SD in a WT male mouse. **A)** Schematic illustrating the recording paradigm. ChR2(H134R) was used for optogenetic SD induction in the motor cortex. A 1x objective was used to image GCaMP concurrently with intracortical and epicortical gSGFET devices recording from somatosensory and visual areas of the cortex. **B)** Widefield GCaMP image showing location of ROIs plotted. **C)** 10s optogenetic stimulation followed by SD propagation through the ROIs shown in **B**. **D)** Activity at ROI 1 shown for GCaMP and both gSGFET configurations. Intracortical full-bandwidth recording shown for a site deep within the cortex. High-pass filtering (>1Hz) impairs the ability to record SD in both gSGFET devices. **E)** Activity plotted for ROI 2 shown in **B**. GCaMP and epicortical activity shown for the region.

depicts the sagittal sinus. Moreover, these devices were fabricated using the low-autofluorescence substrate, parylene C. Therefore, concurrent imaging with high SNR is possible.

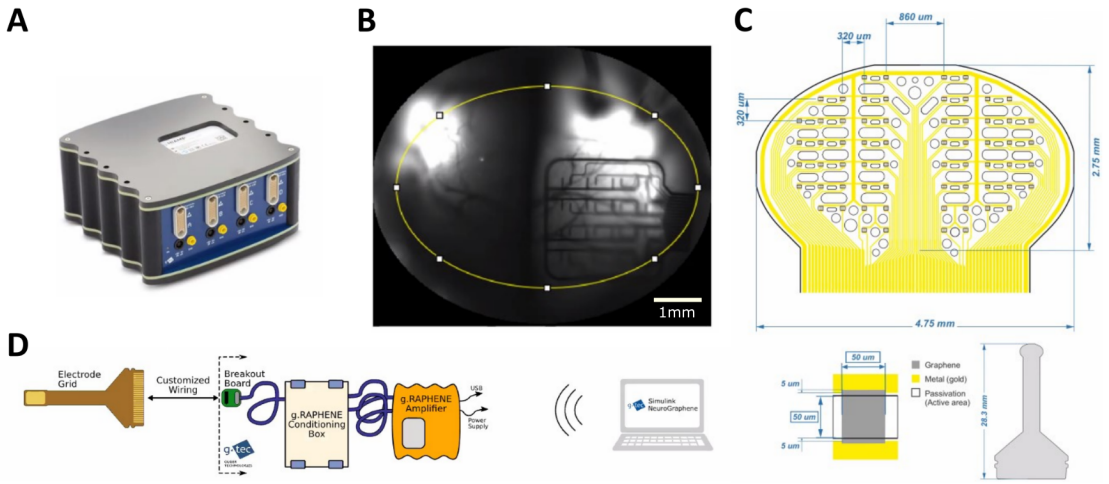

Figure 73: Recording configuration for upcoming 64-channel epicortical gSGFET experiments. **A)** Gtec recording amplifier that allows full-bandwidth acquisition from 64-channels and 4 independent V_{gs} bias points. **B)** Widefield image of field-of-view with 16-channel array shown and target array of 64-channel array marked by gold circle. **C)** Current 64-channel gSGFET epicortical array currently undergoing fabrication. Transistor size (bottom) and spacing (top) shown. **D)** Recording configuration for acquisition from 64 gSGFET channels.

Morevoer, to enable acquisition from these devices, considerable work was invested to optimise a 64-channel amplifier (Figure 73A&D). Since, gSGFETs are active devices that require a potential to be set between the gate and source (V_{gs}), these new amplifiers were developed (Gtec) to allow selection of four different V_{gs} points for groups of 16 transistors at any given time. Therefore, each transistor could be biased optimally to enable high SNR recordings. Considerable optimisation of hardware and recording software was required to achieve this. Both system optimisation and 64-channel array fabrication is still underway. However, these devices will soon be available for integration into the presented experimental paradigm.

In concurrence with developments to gSGFET recordings, imaging developments have also been pursued. One of these is the recording of activity non-invasively through the intact skull. To investigate this, animals were prepared as before. Half of the skull was left unaltered, while the other was thinned using a coarse drill. This allowed comparison of recording SNR from different skull thicknesses in the same animal (Figure 74A). To investigate this, ictal spiking following picrotoxin injection (as before) through a burr hole was examined (Figure 74B). Since these

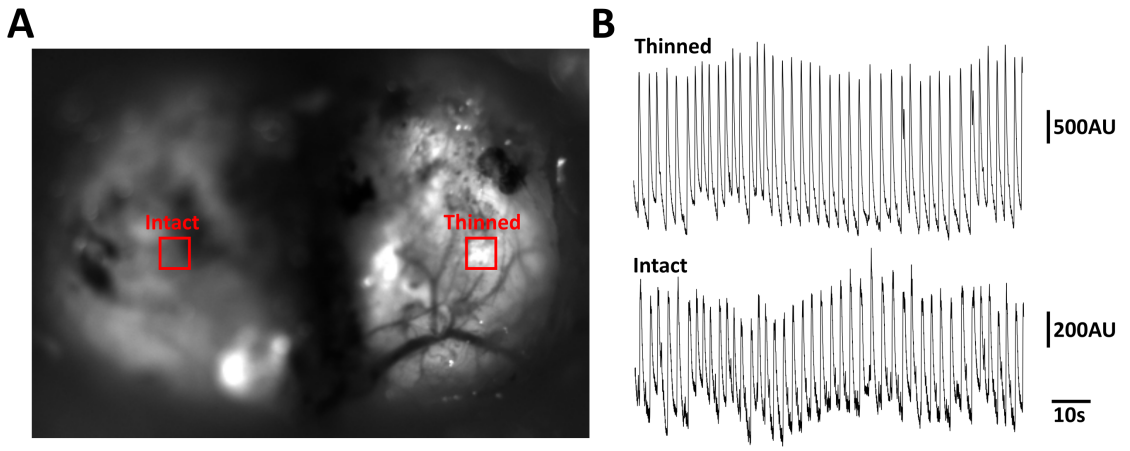

Figure 74: Pilot experiment investigating GCaMP7f imaging through the intact and thinned skull of a WT male mouse. **A)** Widefield image of intact (L- Left hemisphere) and thinned skull (R- Right hemisphere). **B)** Comparison of myoclonic spiking between the regions shown in **A**. Thinned skull clearly provides higher SNR recordings, however is prone to artefact.

events are typically generalised and occur simultaneously across both hemispheres, these allowed clear observations of the effect of skull thickness. A ROI was placed on either hemisphere and revealed a greater SNR in the thinned skull preparation compared to intact. Nonetheless, both hemispheres allowed readout of GCaMP dynamics with sufficient SNR to resolve events. However, occasional artefacts are observed on the images. These include autofluorescent spots or regions with blood; likely due to the presence of the skull. Therefore, it is clear the use of a craniotomy allows more GCaMP recording with greater clarity. Additionally, this also allows electrophysiological access.

Another method in which the imaging paradigm was developed was through the investigation of different fluorescent indicators. To test this, the previously defined paradigm was investigated, with the injected GCaMP AAV exchanged for an AAV vector containing iGluSnFR (Figure 75A). iGluSnFR allowed fluorescence imaging of glutamate dynamics while recording electrographic activity using gSGFETs. The observed signal shows clear differences to GCaMP during SD (Figure 75B). Glutamate dynamics during SD onset shows a sharp rapid increase. Moreover, waveforms are diverse and frequently demonstrate intermediate plateaus during SD initiation and recovery; indicative of a glutamatergic role in observed electrographic double peak SD events. ROIs were selectively placed on both gSGFET recording sites and wiring tracks to demonstrate the ability to sample from across the entirety of the gSGFET array and not just at transparent transistor sites. gSGFET recording for the entire experiment is shown (Figure 75C). Spontaneous and picrotoxin-evoked events

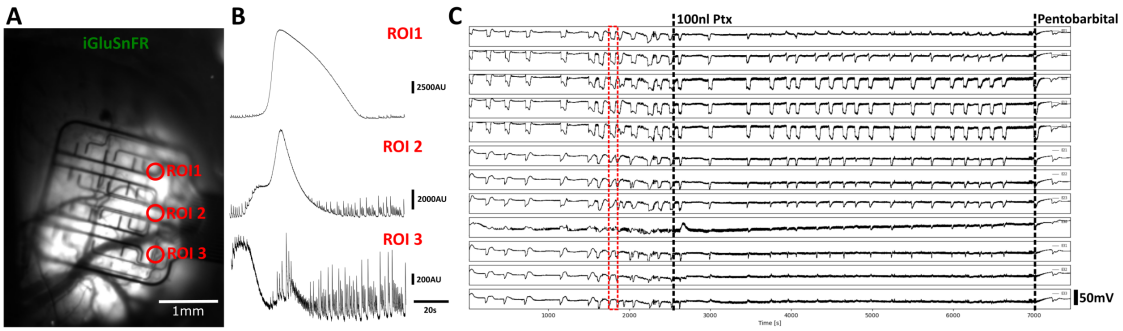

Figure 75: gSGFET recordings combined with simultaneous widefield iGluSNfR imaging during spontaneous and picrotoxin-evoked seizures and SDs in S218L HET male mice. Large amplitude, high frequency SD events can be seen. **A)** Widefield image of iGluSnFR fluorescence showing plotted ROIs in **B**. **B)** Glutamate fluorescence from ROIs shown in **A**. ROIs were sampled from both gSGFET sites and array gold tracks. **C)** gSGFET recording for entire recording period acquired with 12 of 16 transistors. Large amplitude spontaneous and evoked events shown. Time periods of data plotted in **B** (red), picrotoxin injection, and experiment termination shown.

were recorded from S218L mice. These investigations were performed in S218L HET mice to further demonstrate the flexibility of the experimental paradigm.

Altogether, both electrical and optical developments have been incorporated into the presented experimental paradigm. This demonstrates the ability for the novel experimental paradigm presented here to be developed even further and therefore, provide even greater insight into paroxysmal disorders.

11.3 Discussion

The work presented here demonstrates the ability for intracortical gSGFET devices to be incorporated into the recording paradigm. Alongside this, optogenetic SD induction is demonstrated as a possible model for investigation. Moreover, expansion of the epicortical gSGFET arrays to 64-channels is demonstrated. This presents the future design that will allow even greater characterisation of electrographic activity across large areas. Moreover, associated hardware developments are presented. Alongside these electrographic developments are imaging developments. These have been progressed to allow both non-invasive recording through the skull and recording of glutamate dynamics in transgenic animal models. These results clearly demonstrate the room for further progression of the experimental paradigm. Further development will lead to greater insight into seizure and SD mechanisms, which will build-upon the research presented in this thesis.

The demonstration of the efficient incorporation of intracortical gSGFET probes demonstrates the ability for the experimental paradigm to be adapted to gain insight from subcortical structures. Although the demonstrated depth probes were only able to reach within the cortex, new devices are currently being fabricated to record from the cortex, hippocampus and thalamus simultaneously. Incorporation of these devices without compromising GCaMP imaging will allow investigation of the role of subcortical structures in seizure-associated SD initiation. This will build upon the work demonstrated previously, and allow more definitive answers to be obtained regarding the mechanisms by which epileptiform activity is able to precipitate SD. This expanded recording paradigm will be utilised in future work.

Considerable work in this thesis has explored differences in electrographic and optical readouts of epileptiform activity. As mentioned previously, this method holds promise in decoding the electrographic signal and leading to improved interpretations of both experimental and clinical data. In order to increase the insight attainable, novel gSGFET devices were designed to allow recording from a 4-fold greater number of sites (64 instead of 16). This would firstly, improve the ability to spatially resolve epileptiform activity with high temporal resolution. Moreover, this would also allow more continuous electrographic sampling across the cortex; thus, aiding interpretations of electrographic signal contents and the contribution of volume conduction when performing simultaneous fluorescence imaging. These devices would be a powerful addition to the experimental paradigm and demonstrate the potential for future expansion of the work presented in this thesis.

With regard to developments in imaging, the ability to perform non-invasive fluorescence imaging is powerful. Firstly, this would be a useful control to demonstrate that the generation of a craniotomy is not drastically altering observed phenomena. Secondly, this is a powerful method that will allow detailed forthcoming investigations of SD dynamics in chronic epilepsy and migraine models. Considerable work will be performed to use the previously optimised experimental paradigm to investigate activity in FHM1 CACNA1A S218L mice. However, these investigations will also be expanded to incorporate longitudinal SD studies. Migraine is known to display age-dependent phenomena, where attacks are more frequent during certain developmental periods (Victor et al., 2010). The ability to perform repeated imaging from the same animal will be used to image for a given time period from S218L animals throughout different developmental stages. This will allow an improved understanding of spontaneous SD events, and how factors such as age and sex can modulate these.

Another piloted development of the presented experimental paradigm is the in-

corporation of different fluorescent reporters. As described previously, the ability to generate simultaneous optical and electrical readouts of activity at the same location is a powerful method; with potential to reveal insight into complex signal generation mechanisms. The successful integration of functional glutamate imaging into this paradigm is a powerful development. Firstly, this demonstrates the flexibility of the constructed paradigm to be adapted to particular questions of interest. Moreover, the ability for low autofluorescence gSGFET devices to be combined with novel imaging tools is shown. GCaMP constructs have been optimised for high SNR for considerable time, however, the ability for novel neurotransmitter reporters to be integrated demonstrates the flexibility of this paradigm going forward. Furthermore, the ability to alter optical readouts while obtaining electrical recordings is powerful and will aid future deconstructions of electrographic signals.

11.4 Future Directions

The pilot data presented throughout this appendix will contribute to future avenues of investigation. These developments clearly demonstrate the flexibility of the novel experimental paradigm optimised in this thesis. The pursuit of these additional investigations holds promise in complementing the research presented throughout this doctoral project. These developments would allow both increased understanding of the seizure-SD relationship, as well as greater deconstruction of pathological electrographic signals.

Chapter 12

References

References

Abdelfattah, A. S., Kawashima, T., Singh, A., Novak, O., Liu, H., Shuai, Y., ... Schreiter, E. R. (2019a). Bright and photostable chemigenetic indicators for extended in vivo voltage imaging [Journal Article]. *Science*, *365*(6454), 699-704. Retrieved from https://www.ncbi.nlm.nih.gov/pubmed/31371562 doi: 10.1126/science.aav6416

Abdelfattah, A. S., Kawashima, T., Singh, A., Novak, O., Liu, H., Shuai, Y., ... Schreiter, E. R. (2019b). Bright and photostable chemigenetic indicators for extended in vivo voltage imaging [Journal Article]. *Science*, *365*(6454), 699-704. Retrieved from https://www.ncbi.nlm.nih.gov/pubmed/31371562 doi: 10.1126/science.aav6416

Acharya, J. N., & Acharya, V. J. (2019). Overview of eeg montages and principles of localization [Journal Article]. *J Clin Neurophysiol*, *36*(5), 325-329. Retrieved from https://www.ncbi.nlm.nih.gov/pubmed/31490449 doi: 10.1097/WNP.0000000000000538

Adams, N. C., Lozsadi, D. A., & Guillery, R. W. (1997). Complexities in the thalamocortical and corticothalamic pathways [Journal Article]. *Eur J Neurosci*, *9*(2), 204-9. Retrieved from https://www.ncbi.nlm.nih.gov/pubmed/9058041 doi: 10.1111/j.1460-9568.1997.tb01391.x

Adler, A., Zhao, R., Shin, M. E., Yasuda, R., & Gan, W. B. (2019). Somatostatin-expressing interneurons enable and maintain learning-dependent sequential activation of pyramidal neurons [Journal Article]. *Neuron*, *102*(1), 202-216 e7. Retrieved from https://www.ncbi.nlm.nih.gov/pubmed/30792151 doi: 10.1016/j.neuron.2019.01.036

Aihara, M., Hatakeyama, K., Koizumi, K., & Nakazawa, S. (1997). Ictal eeg and single photon emission computed tomography in a patient with cortical dysplasia presenting with atonic seizures [Journal Article]. *Epilepsia*, *38*(6), 723-7. Retrieved from https://www.ncbi.nlm.nih.gov/pubmed/9186256 doi: 10.1111/j.1528-1157.1997.tb01243.x

Akerboom, J., Carreras Calderon, N., Tian, L., Wabnig, S., Prigge, M., Tolo, J., ... Looger, L. L. (2013). Genetically encoded calcium indicators for multi-color neural activity imaging and combination with optogenetics [Journal Article]. *Front Mol Neurosci*, *6*, 2. Retrieved from https://www.ncbi.nlm.nih.gov/pubmed/23459413 doi: 10.3389/fnmol.2013.00002

Akula, K. K., Dhir, A., & Kulkarni, S. K. (2008). Nitric oxide signaling pathway in the anti-convulsant effect of adenosine against pentylenetetrazol-induced seizure threshold in mice [Journal Article]. *Eur J Pharmacol*, *587*(1-3), 129-34. Retrieved from https://www.ncbi.nlm.nih.gov/pubmed/18457833 doi: 10.1016/j.ejphar.2008.03.038

Albuja, A. C., & Khan, G. Q. (2021). Absence seizure [Book Section]. In *Statpearls.* Treasure Island (FL). Retrieved from https://www.ncbi.nlm.nih.gov/pubmed/29763042

Amemori, T., Gorelova, N. A., & Bures, J. (1987). Spreading depression in the olfactory bulb of rats: reliable initiation and boundaries of propagation [Journal Article]. *Neuroscience*, *22*(1), 29-36. Retrieved from https://www.ncbi.nlm.nih.gov/pubmed/2442664 doi: 10.1016/0306-4522(87)90195-3

Andrasfalvy, B. K., Zemelman, B. V., Tang, J., & Vaziri, A. (2010). Two-photon single-cell optogenetic control of neuronal activity by sculpted light [Journal Article]. *Proc Natl Acad Sci U S A*, *107*(26), 11981-6. Retrieved from https://www.ncbi.nlm.nih.gov/pubmed/20543137 doi: 10.1073/pnas.1006620107

Andreou, A. P., & Edvinsson, L. (2019). Mechanisms of migraine as a chronic evolutive condition [Journal Article]. *J Headache Pain*, *20*(1), 117. Retrieved from https://www.ncbi.nlm.nih.gov/pubmed/31870279 doi: 10.1186/s10194-019-1066-0

Arenkiel, B. R., Peca, J., Davison, I. G., Feliciano, C., Deisseroth, K., Augustine, G. J., ... Feng, G. (2007). In vivo light-induced activation of neural circuitry in transgenic mice expressing channelrhodopsin-2 [Journal Article]. *Neuron*, *54*(2), 205-18. Re-

trieved from https://www.ncbi.nlm.nih.gov/pubmed/17442243 doi: 10.1016/j.neuron.2007.03.005

Asrican, B., & Song, J. (2021). Extracting meaningful circuit-based calcium dynamics in astrocytes and neurons from adult mouse brain slices using single-photon gcamp imaging [Journal Article]. *STAR Protoc*, *2*(1), 100306. Retrieved from https://www.ncbi.nlm.nih.gov/pubmed/33554141 doi: 10.1016/j.xpro.2021.100306

Auzmendi, J., Buchholz, B., Salguero, J., Canellas, C., Kelly, J., Men, P., ... Lazarowski, A. (2018). Pilocarpine-induced status epilepticus is associated with p-glycoprotein induction in cardiomyocytes, electrocardiographic changes, and sudden death [Journal Article]. *Pharmaceuticals (Basel)*, *11*(1). Retrieved from https://www.ncbi.nlm.nih.gov/pubmed/29462915 doi: 10.3390/ph11010021

Avoli, M. (2012a). A brief history on the oscillating roles of thalamus and cortex in absence seizures [Journal Article]. *Epilepsia*, *53*(5), 779-89. Retrieved from https://www.ncbi.nlm.nih.gov/pubmed/22360294 doi: 10.1111/j.1528-1167.2012.03421.x

Avoli, M. (2012b). A brief history on the oscillating roles of thalamus and cortex in absence seizures [Journal Article]. *Epilepsia*, *53*(5), 779-89. Retrieved from https://www.ncbi.nlm.nih.gov/pubmed/22360294 doi: 10.1111/j.1528-1167.2012.03421.x

Avoli, M., Louvel, J., Kurcewicz, I., Pumain, R., & Barbarosie, M. (1996). Extracellular free potassium and calcium during synchronous activity induced by 4-aminopyridine in the juvenile rat hippocampus [Journal Article]. *J Physiol*, *493 (Pt 3)*, 707-17. Retrieved from https://www.ncbi.nlm.nih.gov/pubmed/8799893 doi: 10.1113/jphysiol.1996.sp021416

Ayata, C., Jin, H., Kudo, C., Dalkara, T., & Moskowitz, M. A. (2006). Suppression of cortical spreading depression in migraine prophylaxis [Journal Article]. *Ann Neurol*, *59*(4), 652-61. Retrieved from https://www.ncbi.nlm.nih.gov/pubmed/16450381 doi: 10.1002/ana.20778

Ayata, C., & Lauritzen, M. (2015). Spreading depression, spreading depolarizations, and the cerebral vasculature [Journal Article]. *Physiol Rev*, *95*(3), 953-93. Retrieved from https://www.ncbi.nlm.nih.gov/pubmed/26133935 doi: 10.1152/physrev.00027.2014

Bahar, S., Fayuk, D., Somjen, G. G., Aitken, P. G., & Turner, D. A. (2000). Mito-

chondrial and intrinsic optical signals imaged during hypoxia and spreading depression in rat hippocampal slices [Journal Article]. *J Neurophysiol*, *84*(1), 311-24. Retrieved from https://www.ncbi.nlm.nih.gov/pubmed/10899206 doi: 10.1152/jn.2000.84.1.311

Bahari, F., Ssentongo, P., Liu, J., Kimbugwe, J., Curay, C., Schiff, S. J., & Gluckman, B. J. (2020). Seizure-associated spreading depression is a major feature of ictal events in two animal models of chronic epilepsy [Journal Article]. *bioRxiv 455519*. Retrieved from https://www.biorxiv.org/content/biorxiv/early/2020/05/20/455519.full.pdf doi: 10.1101/455519

Bailey, D. M. (2019). Oxygen and brain death; back from the brink [Journal Article]. *Exp Physiol*, *104*(12), 1769-1779. Retrieved from https://www.ncbi.nlm.nih.gov/pubmed/31605408 doi: 10.1113/EP088005

Balestrino, M., Young, J., & Aitken, P. (1999). Block of (na+,k+)atpase with ouabain induces spreading depression-like depolarization in hippocampal slices [Journal Article]. *Brain Res*, *838*(1-2), 37-44. Retrieved from https://www.ncbi.nlm.nih.gov/pubmed/10446314 doi: 10.1016/s0006-8993(99)01674-1

Bando, Y., Wenzel, M., & Yuste, R. (2021). Simultaneous two-photon imaging of action potentials and subthreshold inputs in vivo [Journal Article]. *Nat Commun*, *12*(1), 7229. Retrieved from https://www.ncbi.nlm.nih.gov/pubmed/34893595 doi: 10.1038/s41467-021-27444-9

Baraldi, S., Farrell, F., Benson, J., Diehl, B., Wehner, T., & Kovac, S. (2015). Drop attacks, falls and atonic seizures in the video-eeg monitoring unit [Journal Article]. *Seizure*, *32*, 4-8. Retrieved from https://www.ncbi.nlm.nih.gov/pubmed/26552554 doi: 10.1016/j.seizure.2015.08.001

Bastany, Z. J. R., Askari, S., Dumont, G. A., Kellinghaus, C., Kazemi, A., & Gorji, A. (2020). Association of cortical spreading depression and seizures in patients with medically intractable epilepsy [Journal Article]. *Clin Neurophysiol*, *131*(12), 2861-2874. Retrieved from https://www.ncbi.nlm.nih.gov/pubmed/33152524 doi: 10.1016/j.clinph.2020.09.016

Beaulieu-Laroche, L., Toloza, E. H. S., van der Goes, M. S., Lafourcade, M., Barnagian, D., Williams, Z. M., ... Harnett, M. T.

(2018). Enhanced dendritic compartmentalization in human cortical neurons [Journal Article]. *Cell*, *175*(3), 643-651 e14. Retrieved from https://www.ncbi.nlm.nih.gov/pubmed/30340039 doi: 10.1016/j.cell.2018.08.045

Bellot-Saez, A., Kekesi, O., Morley, J. W., & Buskila, Y. (2017). Astrocytic modulation of neuronal excitability through k(+) spatial buffering [Journal Article]. *Neurosci Biobehav Rev*, *77*, 87-97. Retrieved from https://www.ncbi.nlm.nih.gov/pubmed/28279812 doi: 10.1016/j.neubiorev.2017.03.002

Beniczky, S., & Schomer, D. L. (2020). Electroencephalography: basic biophysical and technological aspects important for clinical applications [Journal Article]. *Epileptic Disord*, *22*(6), 697-715. Retrieved from https://www.ncbi.nlm.nih.gov/pubmed/33270023 doi: 10.1684/epd.2020.1217

Bere, Z., Obrenovitch, T. P., Kozak, G., Bari, F., & Farkas, E. (2014). Imaging reveals the focal area of spreading depolarizations and a variety of hemodynamic responses in a rat microembolic stroke model [Journal Article]. *J Cereb Blood Flow Metab*, *34*(10), 1695-705. Retrieved from https://www.ncbi.nlm.nih.gov/pubmed/25074743 doi: 10.1038/jcbfm.2014.136

Berger, M., Speckmann, E. J., Pape, H. C., & Gorji, A. (2008). Spreading depression enhances human neocortical excitability in vitro [Journal Article]. *Cephalalgia*, *28*(5), 558-62. Retrieved from https://www.ncbi.nlm.nih.gov/pubmed/18399818 doi: 10.1111/j.1468-2982.2008.01556.x

Berndt, A., Schoenenberger, P., Mattis, J., Tye, K. M., Deisseroth, K., Hegemann, P., & Oertner, T. G. (2011). High-efficiency channelrhodopsins for fast neuronal stimulation at low light levels [Journal Article]. *Proc Natl Acad Sci U S A*, *108*(18), 7595-600. Retrieved from https://www.ncbi.nlm.nih.gov/pubmed/21504945 doi: 10.1073/pnas.1017210108

Blumenfeld, H., Varghese, G. I., Purcaro, M. J., Motelow, J. E., Enev, M., McNally, K. A., ... Spencer, S. S. (2009). Cortical and subcortical networks in human secondarily generalized tonic-clonic seizures [Journal Article]. *Brain*, *132*(Pt 4), 999-1012. Retrieved from https://www.ncbi.nlm.nih.gov/pubmed/19339252 doi: 10.1093/brain/awp028

Bogdanov, V. B., Middleton, N. A., Theriot, J. J., Parker, P. D., Abdullah, O. M., Ju, Y. S., ... Brennan, K. C. (2016). Susceptibility of primary sensory cortex to spreading depolarizations [Journal Article]. *J Neurosci*, *36*(17), 4733-43. Retrieved from https://www.ncbi.nlm.nih.gov/pubmed/27122032 doi: 10.1523/JNEUROSCI.3694-15.2016

Boison, D. (2007). Adenosine as a modulator of brain activity [Journal Article]. *Drug News Perspect*, *20*(10), 607-11. Retrieved from https://www.ncbi.nlm.nih.gov/pubmed/18301794 doi: 10.1358/dnp.2007.20.10.1181353

Bolay, H., Reuter, U., Dunn, A. K., Huang, Z., Boas, D. A., & Moskowitz, M. A. (2002). Intrinsic brain activity triggers trigeminal meningeal afferents in a migraine model [Journal Article]. *Nat Med*, *8*(2), 136-42. Retrieved from https://www.ncbi.nlm.nih.gov/pubmed/11821897 doi: 10.1038/nm0202-136

Bonaccini Calia, A., Masvidal-Codina, E., Smith, T. M., Schafer, N., Rathore, D., Rodriguez-Lucas, E., ... Garrido, J. A. (2021). Full-bandwidth electrophysiology of seizures and epileptiform activity enabled by flexible graphene microtransistor depth neural probes [Journal Article]. *Nat Nanotechnol*. Retrieved from https://www.ncbi.nlm.nih.gov/pubmed/34937934 doi: 10.1038/s41565-021-01041-9

Boyden, E. S., Zhang, F., Bamberg, E., Nagel, G., & Deisseroth, K. (2005). Millisecond-timescale, genetically targeted optical control of neural activity [Journal Article]. *Nat Neurosci*, *8*(9), 1263-8. Retrieved from https://www.ncbi.nlm.nih.gov/pubmed/16116447 doi: 10.1038/nn1525

Brennan, E. K. W., Sudhakar, S. K., Jedrasiak-Cape, I., John, T. T., & Ahmed, O. J. (2020). Hyperexcitable neurons enable precise and persistent information encoding in the superficial retrosplenial cortex [Journal Article]. *Cell Rep*, *30*(5), 1598-1612 e8. Retrieved from https://www.ncbi.nlm.nih.gov/pubmed/32023472 doi: 10.1016/j.celrep.2019.12.093

Bretag, A. H. (2017). The glass micropipette electrode: A history of its inventors and users to 1950 [Journal Article]. *J Gen Physiol*, *149*(4), 417-430. Retrieved from https://www.ncbi.nlm.nih.gov/pubmed/28298356 doi: 10.1085/jgp.201611634

Bu, F., Du, R., Li, Y., Quinn, J. P., & Wang, M. (2016). Nr2a contributes to genesis and propagation of cortical spreading depression in rats [Journal Article]. *Sci Rep*, *6*, 23576. Re-

trieved from https://www.ncbi.nlm.nih.gov/pubmed/27001011 doi: 10.1038/srep23576

Bugay, V., Bozdemir, E., Vigil, F. A., Chun, S. H., Holstein, D. M., Elliott, W. R., ... Brenner, R. (2020). A mouse model of repetitive blast traumatic brain injury reveals post-trauma seizures and increased neuronal excitability [Journal Article]. *J Neurotrauma*, *37*(2), 248-261. Retrieved from https://www.ncbi.nlm.nih.gov/pubmed/31025597 doi: 10.1089/neu.2018.6333

Bumanglag, A. V., & Sloviter, R. S. (2008). Minimal latency to hippocampal epileptogenesis and clinical epilepsy after perforant pathway stimulation-induced status epilepticus in awake rats [Journal Article]. *J Comp Neurol*, *510*(6), 561-80. Retrieved from https://www.ncbi.nlm.nih.gov/pubmed/18697194 doi: 10.1002/cne.21801

Buzsaki, G., Anastassiou, C. A., & Koch, C. (2012a). The origin of extracellular fields and currents–eeg, ecog, lfp and spikes [Journal Article]. *Nat Rev Neurosci*, *13*(6), 407-20. Retrieved from https://www.ncbi.nlm.nih.gov/pubmed/22595786 doi: 10.1038/nrn3241

Buzsaki, G., Anastassiou, C. A., & Koch, C. (2012b). The origin of extracellular fields and currents–eeg, ecog, lfp and spikes [Journal Article]. *Nat Rev Neurosci*, *13*(6), 407-20. Retrieved from https://www.ncbi.nlm.nih.gov/pubmed/22595786 doi: 10.1038/nrn3241

Cammarota, M., Losi, G., Chiavegato, A., Zonta, M., & Carmignoto, G. (2013). Fast spiking interneuron control of seizure propagation in a cortical slice model of focal epilepsy [Journal Article]. *J Physiol*, *591*(4), 807-22. Retrieved from https://www.ncbi.nlm.nih.gov/pubmed/23207591 doi: 10.1113/jphysiol.2012.238154

Cela, E., & Sjostrom, P. J. (2020). A step-by-step protocol for optogenetic kindling [Journal Article]. *Front Neural Circuits*, *14*, 3. Retrieved from https://www.ncbi.nlm.nih.gov/pubmed/32116570 doi: 10.3389/fncir.2020.00003

Cha, S. S., Bucklin, M. E., & Han, X. (2020). Removable cranial window for sustained wide-field optical imaging in mouse neocortex. *bioRxiv*. Retrieved from https://www.biorxiv.org/content/early/2020/01/15/2020.01.14.905851 doi: 10.1101/2020.01.14.905851

Charles, A. C., & Baca, S. M. (2013). Cortical spreading depression and migraine [Journal Article]. *Nat Rev Neurol*, *9*(11), 637-44. Retrieved from https://www.ncbi.nlm.nih.gov/pubmed/24042483 doi: 10.1038/nrneu-

rol.2013.192

Chatzikonstantinou, A. (2014). Epilepsy and the hippocampus [Journal Article]. *Front Neurol Neurosci*, *34*, 121-42. Retrieved from https://www.ncbi.nlm.nih.gov/pubmed/24777136 doi: 10.1159/000356435

Chauveau, N., Franceries, X., Doyon, B., Rigaud, B., Morucci, J. P., & Celsis, P. (2004a). Effects of skull thickness, anisotropy, and inhomogeneity on forward eeg/erp computations using a spherical three-dimensional resistor mesh model [Journal Article]. *Hum Brain Mapp*, *21*(2), 86-97. Retrieved from https://www.ncbi.nlm.nih.gov/pubmed/14755596 doi: 10.1002/hbm.10152

Chauveau, N., Franceries, X., Doyon, B., Rigaud, B., Morucci, J. P., & Celsis, P. (2004b). Effects of skull thickness, anisotropy, and inhomogeneity on forward eeg/erp computations using a spherical three-dimensional resistor mesh model [Journal Article]. *Hum Brain Mapp*, *21*(2), 86-97. Retrieved from https://www.ncbi.nlm.nih.gov/pubmed/14755596 doi: 10.1002/hbm.10152

Choi, K. D., & Choi, J. H. (2016). Episodic ataxias: Clinical and genetic features [Journal Article]. *J Mov Disord*, *9*(3), 129-35. Retrieved from https://www.ncbi.nlm.nih.gov/pubmed/27667184 doi: 10.14802/jmd.16028

Choy, M., Dadgar-Kiani, E., Cron, G. O., Duffy, B. A., Schmid, F., Edelman, B. J., ... Lee, J. H. (2021). Repeated hippocampal seizures lead to brain-wide reorganization of circuits and seizure propagation pathways [Journal Article]. *Neuron*. Retrieved from https://www.ncbi.nlm.nih.gov/pubmed/34706219 doi: 10.1016/j.neuron.2021.10.010

Cianchetti, C., Avanzini, G., Dainese, F., & Guidetti, V. (2017). The complex interrelations between two paroxysmal disorders: headache and epilepsy [Journal Article]. *Neurol Sci*, *38*(6), 941-948. Retrieved from https://www.ncbi.nlm.nih.gov/pubmed/28341968 doi: 10.1007/s10072-017-2926-5

Coenen, A. M., & Van Luijtelaar, E. L. (1987). The wag/rij rat model for absence epilepsy: age and sex factors [Journal Article]. *Epilepsy Res*, *1*(5), 297-301. Retrieved from https://www.ncbi.nlm.nih.gov/pubmed/3143552 doi: 10.1016/0920-1211(87)90005-2

Collaborators, G. B. D. H. (2018). Global, regional, and national burden of migraine and tension-type headache, 1990-2016: a systematic analysis for the global

burden of disease study 2016 [Journal Article]. *Lancet Neurol*, *17*(11), 954-976. Retrieved from https://www.ncbi.nlm.nih.gov/pubmed/30353868 doi: 10.1016/S1474-4422(18)30322-3

Cozzolino, O., Marchese, M., Trovato, F., Pracucci, E., Ratto, G. M., Buzzi, M. G., ... Santorelli, F. M. (2018). Understanding spreading depression from headache to sudden unexpected death [Journal Article]. *Front Neurol*, *9*, 19. Retrieved from https://www.ncbi.nlm.nih.gov/pubmed/29449828 doi: 10.3389/fneur.2018.00019

Curatolo, J. M., Macdonell, R. A., Berkovic, S. F., & Fabinyi, G. C. (2000). Intraoperative monitoring to preserve central visual fields during occipital corticectomy for epilepsy [Journal Article]. *J Clin Neurosci*, *7*(3), 234-7. Retrieved from https://www.ncbi.nlm.nih.gov/pubmed/10833622 doi: 10.1054/jocn.1999.0208

Dana, H., Chen, T. W., Hu, A., Shields, B. C., Guo, C., Looger, L. L., ... Svoboda, K. (2014). Thy1-gcamp6 transgenic mice for neuronal population imaging in vivo [Journal Article]. *PLoS One*, *9*(9), e108697. Retrieved from https://www.ncbi.nlm.nih.gov/pubmed/25250714 doi: 10.1371/journal.pone.0108697

Dana, H., Sun, Y., Mohar, B., Hulse, B. K., Kerlin, A. M., Hasseman, J. P., ... Kim, D. S. (2019). High-performance calcium sensors for imaging activity in neuronal populations and microcompartments [Journal Article]. *Nat Methods*, *16*(7), 649-657. Retrieved from https://www.ncbi.nlm.nih.gov/pubmed/31209382 doi: 10.1038/s41592-019-0435-6

D'Antuono, M., Inaba, Y., Biagini, G., D'Arcangelo, G., Tancredi, V., & Avoli, M. (2006). Synaptic hyperexcitability of deep layer neocortical cells in a genetic model of absence seizures [Journal Article]. *Genes Brain Behav*, *5*(1), 73-84. Retrieved from https://www.ncbi.nlm.nih.gov/pubmed/16436191 doi: 10.1111/j.1601-183X.2005.00146.x

de Curtis, M., & Avoli, M. (2015). Initiation, propagation, and termination of partial (focal) seizures [Journal Article]. *Cold Spring Harb Perspect Med*, *5*(7), a022368. Retrieved from https://www.ncbi.nlm.nih.gov/pubmed/26134843 doi: 10.1101/cshperspect.a022368

Dehghani, A., & Karatas, H. (2019). Mouse models of familial hemiplegic migraine for studying migraine pathophysiology [Journal Article]. *Curr Neuropharmacol*, *17*(10), 961-973. Retrieved

from https://www.ncbi.nlm.nih.gov/pubmed/31092180 doi: 10.2174/1570159X17666190513085013

Delanty, N., Vaughan, C. J., & French, J. A. (1998). Medical causes of seizures [Journal Article]. *Lancet*, *352*(9125), 383-90. Retrieved from https://www.ncbi.nlm.nih.gov/pubmed/9717943 doi: 10.1016/S0140-6736(98)02158-8

Deng, X., Gu, L., Sui, N., Guo, J., & Liang, J. (2019). Parvalbumin interneuron in the ventral hippocampus functions as a discriminator in social memory [Journal Article]. *Proc Natl Acad Sci U S A*, *116*(33), 16583-16592. Retrieved from https://www.ncbi.nlm.nih.gov/pubmed/31358646 doi: 10.1073/pnas.1819133116

Desai, S. A., Rolston, J. D., Guo, L., & Potter, S. M. (2010). Improving impedance of implantable microwire multi-electrode arrays by ultrasonic electroplating of durable platinum black [Journal Article]. *Front Neuroeng*, *3*, 5. Retrieved from https://www.ncbi.nlm.nih.gov/pubmed/20485478 doi: 10.3389/fneng.2010.00005

Destexhe, A. (1998). Spike-and-wave oscillations based on the properties of gabab receptors [Journal Article]. *J Neurosci*, *18*(21), 9099-111. Retrieved from https://www.ncbi.nlm.nih.gov/pubmed/9787013

Di Guilmi, M. N., Wang, T., Inchauspe, C. G., Forsythe, I. D., Ferrari, M. D., van den Maagdenberg, A. M., ... Uchitel, O. D. (2014). Synaptic gain-of-function effects of mutant cav2.1 channels in a mouse model of familial hemiplegic migraine are due to increased basal [ca2+]i [Journal Article]. *J Neurosci*, *34*(21), 7047-58. Retrieved from https://www.ncbi.nlm.nih.gov/pubmed/24849341 doi: 10.1523/JNEUROSCI.2526-13.2014

Ding, K., Gupta, P. K., & Diaz-Arrastia, R. (2016). Epilepsy after traumatic brain injury [Book Section]. In D. Laskowitz & G. Grant (Eds.), *Translational research in traumatic brain injury.* Boca Raton (FL). Retrieved from https://www.ncbi.nlm.nih.gov/pubmed/26583175

Dodick, D. W. (2018). A phase-by-phase review of migraine pathophysiology [Journal Article]. *Headache*, *58 Suppl 1*, 4-16. Retrieved from https://www.ncbi.nlm.nih.gov/pubmed/29697154 doi: 10.1111/head.13300

Donmez-Demir, B., Erdener, S. E., Karatas, H., Kaya, Z., Ulusoy, I., & Dalkara, T. (2020). Kcl-induced cortical spreading depression waves more heterogeneously propagate than optogenetically-induced waves in lissencephalic brain:

an analysis with optical flow tools [Journal Article]. *Sci Rep*, *10*(1), 12793. Retrieved from https://www.ncbi.nlm.nih.gov/pubmed/32732932 doi: 10.1038/s41598-020-69669-6

Dreier, J. P. (2011). The role of spreading depression, spreading depolarization and spreading ischemia in neurological disease [Journal Article]. *Nat Med*, *17*(4), 439-47. Retrieved from https://www.ncbi.nlm.nih.gov/pubmed/21475241 doi: 10.1038/nm.2333

Dreier, J. P., & Reiffurth, C. (2015). The stroke-migraine depolarization continuum [Journal Article]. *Neuron*, *86*(4), 902-922. Retrieved from https://www.ncbi.nlm.nih.gov/pubmed/25996134 doi: 10.1016/j.neuron.2015.04.004

During, M. J., & Spencer, D. D. (1992). Adenosine: a potential mediator of seizure arrest and postictal refractoriness [Journal Article]. *Ann Neurol*, *32*(5), 618-24. Retrieved from https://www.ncbi.nlm.nih.gov/pubmed/1449242 doi: 10.1002/ana.410320504

Eickhoff, M., Kovac, S., Shahabi, P., Ghadiri, M. K., Dreier, J. P., Stummer, W., ... Gorji, A. (2014). Spreading depression triggers ictaform activity in partially disinhibited neuronal tissues [Journal Article]. *Exp Neurol*, *253*, 1-15. Retrieved from https://www.ncbi.nlm.nih.gov/pubmed/24368193 doi: 10.1016/j.expneurol.2013.12.008

Emmady, P. D., & Anilkumar, A. C. (2021). Eeg abnormal waveforms [Book Section]. In *Statpearls.* Treasure Island (FL). Retrieved from https://www.ncbi.nlm.nih.gov/pubmed/32491587

England, M. J., Liverman, C. T., Schultz, A. M., & Strawbridge, L. M. (2012). Epilepsy across the spectrum: promoting health and understanding. a summary of the institute of medicine report [Journal Article]. *Epilepsy Behav*, *25*(2), 266-76. Retrieved from https://www.ncbi.nlm.nih.gov/pubmed/23041175 doi: 10.1016/j.yebeh.2012.06.016

Erdener, S. E., & Dalkara, T. (2014). Modelling headache and migraine and its pharmacological manipulation [Journal Article]. *Br J Pharmacol*, *171*(20), 4575-94. Retrieved from https://www.ncbi.nlm.nih.gov/pubmed/24611635 doi: 10.1111/bph.12651

Evangelista, E., Benar, C., Bonini, F., Carron, R., Colombet, B., Regis, J., & Bartolomei, F. (2015). Does the thalamo-cortical synchrony play a role in seizure termination? [Journal Article]. *Front Neurol*, *6*, 192. Retrieved from https://www.ncbi.nlm.nih.gov/pubmed/26388834 doi:

10.3389/fneur.2015.00192

Falco-Walter, J. J., & Bleck, T. (2016). Treatment of established status epilepticus [Journal Article]. *J Clin Med*, *5*(5). Retrieved from https://www.ncbi.nlm.nih.gov/pubmed/27120626 doi: 10.3390/jcm5050049

Falco-Walter, J. J., Scheffer, I. E., & Fisher, R. S. (2018). The new definition and classification of seizures and epilepsy [Journal Article]. *Epilepsy Res*, *139*, 73-79. Retrieved from https://www.ncbi.nlm.nih.gov/pubmed/29197668 doi: 10.1016/j.eplepsyres.2017.11.015

Fioravanti, B., Kasasbeh, A., Edelmayer, R., Skinner, J., D. P., Hartings, J. A., Burklund, R. D., ... Vanderah, T. W. (2011). Evaluation of cutaneous allodynia following induction of cortical spreading depression in freely moving rats [Journal Article]. *Cephalalgia*, *31*(10), 1090-100. Retrieved from https://www.ncbi.nlm.nih.gov/pubmed/21700643 doi: 10.1177/0333102411410609

Fischer, L. F., Mojica Soto-Albors, R., Buck, F., & Harnett, M. T. (2020). Representation of visual landmarks in retrosplenial cortex [Journal Article]. *Elife*, *9*. Retrieved from https://www.ncbi.nlm.nih.gov/pubmed/32154781 doi: 10.7554/eLife.51458

Freilinger, T., Anttila, V., de Vries, B., Malik, R., Kallela, M., Terwindt, G. M., ... International Headache Genetics, C. (2012). Genome-wide association analysis identifies susceptibility loci for migraine without aura [Journal Article]. *Nat Genet*, *44*(7), 777-82. Retrieved from https://www.ncbi.nlm.nih.gov/pubmed/22683712 doi: 10.1038/ng.2307

Fujiwara-Tsukamoto, Y., Isomura, Y., Imanishi, M., Ninomiya, T., Tsukada, M., Yanagawa, Y., ... Takada, M. (2010). Prototypic seizure activity driven by mature hippocampal fast-spiking interneurons [Journal Article]. *J Neurosci*, *30*(41), 13679-89. Retrieved from https://www.ncbi.nlm.nih.gov/pubmed/20943908 doi: 10.1523/JNEUROSCI.1523-10.2010

Galvani, L. (1792). De viribus electricitatis in motu musculari commentarius, cum j. aldini dissertatione et notis. acc. epistolae ad animalis electricitatis theoriam pertinentes. [Journal Article]. *Mutinae : Soc. Typog., 1792. Tab. II EPB 23921/C*.

Garcia-Cortadella, R., Schwesig, G., Jeschke, C., Illa, X., Gray, A. L., Savage, S., ... Garrido, J. A. (2021). Graphene active sensor arrays for long-term and wireless mapping of wide frequency band epicortical brain

activity [Journal Article]. *Nat Commun*, *12*(1), 211. Retrieved from https://www.ncbi.nlm.nih.gov/pubmed/33431878 doi: 10.1038/s41467-020-20546-w

Genton, P., & Gelisse, P. (2013). The history of juvenile myoclonic epilepsy [Journal Article]. *Epilepsy Behav*, *28 Suppl 1*, S2-7. Retrieved from https://www.ncbi.nlm.nih.gov/pubmed/23756475 doi: 10.1016/j.yebeh.2013.01.002

Ghasemi, M., & Schachter, S. C. (2011). The nmda receptor complex as a therapeutic target in epilepsy: a review [Journal Article]. *Epilepsy Behav*, *22*(4), 617-40. Retrieved from https://www.ncbi.nlm.nih.gov/pubmed/22056342 doi: 10.1016/j.yebeh.2011.07.024

Gnatkovsky, V., Francione, S., Cardinale, F., Mai, R., Tassi, L., Lo Russo, G., & de Curtis, M. (2011). Identification of reproducible ictal patterns based on quantified frequency analysis of intracranial eeg signals [Journal Article]. *Epilepsia*, *52*(3), 477-88. Retrieved from https://www.ncbi.nlm.nih.gov/pubmed/21269289 doi: 10.1111/j.1528-1167.2010.02931.x

Goldenberg, M. M. (2010). Overview of drugs used for epilepsy and seizures: etiology, diagnosis, and treatment [Journal Article]. *P T*, *35*(7), 392-415. Retrieved from https://www.ncbi.nlm.nih.gov/pubmed/20689626

Golomb, D., Donner, K., Shacham, L., Shlosberg, D., Amitai, Y., & Hansel, D. (2007). Mechanisms of firing patterns in fast-spiking cortical interneurons [Journal Article]. *PLoS Comput Biol*, *3*(8), e156. Retrieved from https://www.ncbi.nlm.nih.gov/pubmed/17696606 doi: 10.1371/journal.pcbi.0030156

Gorji, A., & Speckmann, E. J. (2004). Spreading depression enhances the spontaneous epileptiform activity in human neocortical tissues [Journal Article]. *Eur J Neurosci*, *19*(12), 3371-4. Retrieved from https://www.ncbi.nlm.nih.gov/pubmed/15217393 doi: 10.1111/j.0953-816X.2004.03436.x

Gradinaru, V., Zhang, F., Ramakrishnan, C., Mattis, J., Prakash, R., Diester, I., ... Deisseroth, K. (2010). Molecular and cellular approaches for diversifying and extending optogenetics [Journal Article]. *Cell*, *141*(1), 154-165. Retrieved from https://www.ncbi.nlm.nih.gov/pubmed/20303157 doi: 10.1016/j.cell.2010.02.037

Gursoy-Ozdemir, Y., Qiu, J., Matsuoka, N., Bolay, H., Bermpohl, D., Jin, H., ... Moskowitz, M. A. (2004). Cortical spreading depression activates

and upregulates mmp-9 [Journal Article]. *J Clin Invest*, *113*(10), 1447-55. Retrieved from https://www.ncbi.nlm.nih.gov/pubmed/15146242 doi: 10.1172/JCI21227

Haan, J., Terwindt, G. M., van den Maagdenberg, A. M., Stam, A. H., & Ferrari, M. D. (2008). A review of the genetic relation between migraine and epilepsy [Journal Article]. *Cephalalgia*, *28*(2), 105-13. Retrieved from https://www.ncbi.nlm.nih.gov/pubmed/18197881 doi: 10.1111/j.1468-2982.2007.01460.x

Han, X., Chow, B. Y., Zhou, H., Klapoetke, N. C., Chuong, A., Rajimehr, R., ... Boyden, E. S. (2011). A high-light sensitivity optical neural silencer: development and application to optogenetic control of non-human primate cortex [Journal Article]. *Front Syst Neurosci*, *5*, 18. Retrieved from https://www.ncbi.nlm.nih.gov/pubmed/21811444 doi: 10.3389/fnsys.2011.00018

Harshe, D. G., Harshe, S. D., Harshe, G. R., & Harshe, G. G. (2016). Abdominal epilepsy in an adult: A diagnosis often missed [Journal Article]. *J Clin Diagn Res*, *10*(10), VD01-VD02. Retrieved from https://www.ncbi.nlm.nih.gov/pubmed/27891434 doi: 10.7860/JCDR/2016/19873.8600

Hartings, J. A., Li, C., Hinzman, J. M., Shuttleworth, C. W., Ernst, G. L., Dreier, J. P., ... Carlson, A. P. (2017). Direct current electrocorticography for clinical neuromonitoring of spreading depolarizations [Journal Article]. *J Cereb Blood Flow Metab*, *37*(5), 1857-1870. Retrieved from https://www.ncbi.nlm.nih.gov/pubmed/27286981 doi: 10.1177/0271678X16653135

Hatcher, A., Yu, K., Meyer, J., Aiba, I., Deneen, B., & Noebels, J. L. (2020). Pathogenesis of peritumoral hyperexcitability in an immunocompetent crispr-based glioblastoma model [Journal Article]. *J Clin Invest*, *130*(5), 2286-2300. Retrieved from https://www.ncbi.nlm.nih.gov/pubmed/32250339 doi: 10.1172/JCI133316

Hébert, C., Masvidal-Codina, E., Suarez-Perez, A., Calia, A. B., Piret, G., Garcia-Cortadella, R., ... Garrido, J. A. (2018). Flexible graphene solution-gated field-effect transistors: Efficient transducers for micro-electrocorticography [Journal Article]. *Advanced Functional Materials*, *28*(12), 1703976. Retrieved from https://onlinelibrary.wiley.com/doi/abs/10.1002/adfm.201703976 doi: https://doi.org/10.1002/adfm.201703976

Heinemann, U., Lux, H. D., & Gutnick, M. J. (1977). Extracellular free calcium and potassium during paroxsmal activity in the cerebral cortex of the cat [Journal Article]. *Exp Brain Res*, *27*(3-4), 237-43. Retrieved from https://www.ncbi.nlm.nih.gov/pubmed/880984 doi: 10.1007/BF00235500

Henneberger, C., & Rusakov, D. A. (2012). Monitoring local synaptic activity with astrocytic patch pipettes [Journal Article]. *Nat Protoc*, *7*(12), 2171-9. Retrieved from https://www.ncbi.nlm.nih.gov/pubmed/23196973 doi: 10.1038/nprot.2012.140

Hess, L. H., Seifert, M., & Garrido, J. A. (2013). Graphene transistors for bioelectronics [Journal Article]. *Proceedings of the IEEE, vol. 101, no. 7, pp. 1780-1792, July 2013*. doi: doi: 10.1109/JPROC.2013.2261031

Hochbaum, D. R., Zhao, Y., Farhi, S. L., Klapoetke, N., Werley, C. A., Kapoor, V., ... Cohen, A. E. (2014). All-optical electrophysiology in mammalian neurons using engineered microbial rhodopsins [Journal Article]. *Nat Methods*, *11*(8), 825-33. Retrieved from https://www.ncbi.nlm.nih.gov/pubmed/24952910 doi: 10.1038/nmeth.3000

Hodgkin, A. L., & Huxley, A. F. (1952). A quantitative description of membrane current and its application to conduction and excitation in nerve [Journal Article]. *J Physiol*, *117*(4), 500-44. Retrieved from https://www.ncbi.nlm.nih.gov/pubmed/12991237 doi: 10.1113/jphysiol.1952.sp004764

Houben, T., Loonen, I. C., Baca, S. M., Schenke, M., Meijer, J. H., Ferrari, M. D., ... Tolner, E. A. (2017). Optogenetic induction of cortical spreading depression in anesthetized and freely behaving mice [Journal Article]. *J Cereb Blood Flow Metab*, *37*(5), 1641-1655. Retrieved from https://www.ncbi.nlm.nih.gov/pubmed/27107026 doi: 10.1177/0271678X16645113

Huber, A., Padrun, V., Deglon, N., Aebischer, P., Mohler, H., & Boison, D. (2001). Grafts of adenosine-releasing cells suppress seizures in kindling epilepsy [Journal Article]. *Proc Natl Acad Sci U S A*, *98*(13), 7611-6. Retrieved from https://www.ncbi.nlm.nih.gov/pubmed/11404469 doi: 10.1073/pnas.131102898

Huberfeld, G., Wittner, L., Clemenceau, S., Baulac, M., Kaila, K., Miles, R., & Rivera, C. (2007). Perturbed chloride homeostasis and gabaergic signaling in human temporal lobe epilepsy [Journal Article]. *J Neurosci*, *27*(37), 9866-73. Retrieved from https://www.ncbi.nlm.nih.gov/pubmed/17855601 doi:

10.1523/JNEUROSCI.2761-07.2007

Imad, H., Zelano, J., & Kumlien, E. (2015). Hypoglycemia and risk of seizures: a retrospective cross-sectional study [Journal Article]. *Seizure*, *25*, 147-9. Retrieved from https://www.ncbi.nlm.nih.gov/pubmed/25455725 doi: 10.1016/j.seizure.2014.10.005

Jailani, M., Mubarak, M., Sarkhouh, M., Al Mahrezi, A., Abdulnabi, H., Naiser, M., ... Kamal, A. (2020). The effect of low-doses of caffeine and taurine on convulsive seizure parameters in rats [Journal Article]. *Behav Sci (Basel)*, *10*(2). Retrieved from https://www.ncbi.nlm.nih.gov/pubmed/32012788 doi: 10.3390/bs10020043

Jansen, N. A., Schenke, M., Voskuyl, R. A., Thijs, R. D., van den Maagdenberg, A., & Tolner, E. A. (2019). Apnea associated with brainstem seizures in cacna1a (s218l) mice is caused by medullary spreading depolarization [Journal Article]. *J Neurosci*, *39*(48), 9633-9644. Retrieved from https://www.ncbi.nlm.nih.gov/pubmed/31628185 doi: 10.1523/JNEUROSCI.1713-19.2019

Jaseja, H., & Jaseja, B. (2012). Eeg spike versus eeg sharp wave: differential clinical significance in epilepsy [Journal Article]. *Epilepsy Behav*, *25*(1), 137. Retrieved from https://www.ncbi.nlm.nih.gov/pubmed/22809496 doi: 10.1016/j.yebeh.2012.05.023

Jia, H., Rochefort, N. L., Chen, X., & Konnerth, A. (2011). In vivo two-photon imaging of sensory-evoked dendritic calcium signals in cortical neurons [Journal Article]. *Nat Protoc*, *6*(1), 28-35. Retrieved from https://www.ncbi.nlm.nih.gov/pubmed/21212780 doi: 10.1038/nprot.2010.169

Jobst, B. C., & Cascino, G. D. (2015). Resective epilepsy surgery for drug-resistant focal epilepsy: a review [Journal Article]. *JAMA*, *313*(3), 285-93. Retrieved from https://www.ncbi.nlm.nih.gov/pubmed/25602999 doi: 10.1001/jama.2014.17426

Jouhanneau, J. S., & Poulet, J. F. A. (2019). Multiple two-photon targeted whole-cell patch-clamp recordings from monosynaptically connected neurons in vivo [Journal Article]. *Front Synaptic Neurosci*, *11*, 15. Retrieved from https://www.ncbi.nlm.nih.gov/pubmed/31156420 doi: 10.3389/fnsyn.2019.00015

Juavinett, A. L., Bekheet, G., & Churchland, A. K. (2019). Chronically implanted neuropixels probes enable high-yield recordings in freely moving mice [Journal Article]. *Elife*, *8*. Retrieved

from https://www.ncbi.nlm.nih.gov/pubmed/31411559 doi: 10.7554/eLife.47188

Kang, J. Y., Rabiei, A. H., Myint, L., & Nei, M. (2017). Equivocal significance of post-ictal generalized eeg suppression as a marker of sudep risk [Journal Article]. *Seizure*, *48*, 28-32. Retrieved from https://www.ncbi.nlm.nih.gov/pubmed/28380395 doi: 10.1016/j.seizure.2017.03.017

Karoly, P. J., Freestone, D. R., Boston, R., Grayden, D. B., Himes, D., Leyde, K., ... Cook, M. J. (2016). Interictal spikes and epileptic seizures: their relationship and underlying rhythmicity [Journal Article]. *Brain*, *139*(Pt 4), 1066-78. Retrieved from https://www.ncbi.nlm.nih.gov/pubmed/26912639 doi: 10.1093/brain/aww019

Katzel, D., Zemelman, B. V., Buetfering, C., Wolfel, M., & Miesenbock, G. (2011). The columnar and laminar organization of inhibitory connections to neocortical excitatory cells [Journal Article]. *Nat Neurosci*, *14*(1), 100-7. Retrieved from https://www.ncbi.nlm.nih.gov/pubmed/21076426 doi: 10.1038/nn.2687

Keezer, M. R., Sisodiya, S. M., & Sander, J. W. (2016). Comorbidities of epilepsy: current concepts and future perspectives [Journal Article]. *Lancet Neurol*, *15*(1), 106-15. Retrieved from https://www.ncbi.nlm.nih.gov/pubmed/26549780 doi: 10.1016/S1474-4422(15)00225-2

Kendall, L. V., Hansen, R. J., Dorsey, K., Kang, S., Lunghofer, P. J., & Gustafson, D. L. (2014). Pharmacokinetics of sustained-release analgesics in mice [Journal Article]. *J Am Assoc Lab Anim Sci*, *53*(5), 478-84. Retrieved from https://www.ncbi.nlm.nih.gov/pubmed/25255070

Ketzef, M., & Gitler, D. (2014). Epileptic synapsin triple knockout mice exhibit progressive long-term aberrant plasticity in the entorhinal cortex [Journal Article]. *Cereb Cortex*, *24*(4), 996-1008. Retrieved from https://www.ncbi.nlm.nih.gov/pubmed/23236212 doi: 10.1093/cercor/bhs384

Khateb, M., Bosak, N., & Herskovitz, M. (2021). The effect of anti-seizure medications on the propagation of epileptic activity: A review [Journal Article]. *Front Neurol*, *12*, 674182. Retrieved from https://www.ncbi.nlm.nih.gov/pubmed/34122318 doi: 10.3389/fneur.2021.674182

Khodagholy, D., Doublet, T., Quilichini, P., Gurfinkel, M., Leleux, P., Gh-

estem, A., ... Malliaras, G. G. (2013). In vivo recordings of brain activity using organic transistors [Journal Article]. *Nat Commun*, *4*, 1575. Retrieved from https://www.ncbi.nlm.nih.gov/pubmed/23481383 https://www.ncbi.nlm.nih.gov/pmc/articles/PMC3615373/pdf/ncomms2573.pdf doi: 10.1038/ncomms2573

Kim, C. K., Adhikari, A., & Deisseroth, K. (2017). Integration of optogenetics with complementary methodologies in systems neuroscience [Journal Article]. *Nat Rev Neurosci*, *18*(4), 222-235. Retrieved from https://www.ncbi.nlm.nih.gov/pubmed/28303019 doi: 10.1038/nrn.2017.15

Kim, J. M., Hwa, J., Garriga, P., Reeves, P. J., RajBhandary, U. L., & Khorana, H. G. (2005). Light-driven activation of beta 2-adrenergic receptor signaling by a chimeric rhodopsin containing the beta 2-adrenergic receptor cytoplasmic loops [Journal Article]. *Biochemistry*, *44*(7), 2284-92. Retrieved from https://www.ncbi.nlm.nih.gov/pubmed/15709741 doi: 10.1021/bi048328i

Kirchner, A., Veliskova, J., & Velisek, L. (2006). Differential effects of low glucose concentrations on seizures and epileptiform activity in vivo and in vitro [Journal Article]. *Eur J Neurosci*, *23*(6), 1512-22. Retrieved from https://www.ncbi.nlm.nih.gov/pubmed/16553614 doi: 10.1111/j.1460-9568.2006.04665.x

Kirchner, T., Grohl, J., Herrera, M. A., Adler, T., Hernandez-Aguilera, A., Santos, E., & Maier-Hein, L. (2019). Photoacoustics can image spreading depolarization deep in gyrencephalic brain [Journal Article]. *Sci Rep*, *9*(1), 8661. Retrieved from https://www.ncbi.nlm.nih.gov/pubmed/31209253 doi: 10.1038/s41598-019-44935-4

Kiziltan, M., Gunduz, A., Ser Hazal, M., Yeni Naz, S., Ozkara, C., Demirbilek, V., ... Günes, K. (2020). The association between causes and electrophysiology in myoclonus: When and why electrophysiology? *Neurological Sciences and Neurophysiology*, *37*(4), 176-182. Retrieved from http://www.nsnjournal.org/article.asp?issn=2636-865X;year=2020;volume=37;issue doi: 10.4103/NSN.$NSN_8 2_2 0$

Klapoetke, N. C., Murata, Y., Kim, S. S., Pulver, S. R., Birdsey-Benson, A., Cho, Y. K., ... Boyden, E. S. (2014). Independent optical excitation of distinct neural populations [Journal Article]. *Nat Methods*, *11*(3), 338-46. Retrieved from https://www.ncbi.nlm.nih.gov/pubmed/24509633 doi: 10.1038/nmeth.2836

Kloiber, O., Bockhorst, K., Hoehn-Berlage, M., & Hossmann, K. A. (1993). Effect of hypoxia on bicuculline seizures of rat: Nmr spectroscopy and bioluminescence imaging [Journal Article]. *NMR Biomed*, *6*(5), 333-8. Retrieved from https://www.ncbi.nlm.nih.gov/pubmed/8268066 doi: 10.1002/nbm.1940060509

Kodankandath, T. V., Theodore, D., & Samanta, D. (2021). Generalized tonic-clonic seizure [Book Section]. In *Statpearls.* Treasure Island (FL). Retrieved from https://www.ncbi.nlm.nih.gov/pubmed/32119383

Kornreich, B. G. (2007). The patch clamp technique: principles and technical considerations [Journal Article]. *J Vet Cardiol*, *9*(1), 25-37. Retrieved from https://www.ncbi.nlm.nih.gov/pubmed/17689466 doi: 10.1016/j.jvc.2007.02.001

Kors, E. E., Terwindt, G. M., Vermeulen, F. L., Fitzsimons, R. B., Jardine, P. E., Heywood, P., ... Ferrari, M. D. (2001). Delayed cerebral edema and fatal coma after minor head trauma: role of the cacna1a calcium channel subunit gene and relationship with familial hemiplegic migraine [Journal Article]. *Ann Neurol*, *49*(6), 753-60. Retrieved from https://www.ncbi.nlm.nih.gov/pubmed/11409427 doi: 10.1002/ana.1031

Krendl, R., Lurger, S., & Baumgartner, C. (2008). Absolute spike frequency predicts surgical outcome in tle with unilateral hippocampal atrophy [Journal Article]. *Neurology*, *71*(6), 413-8. Retrieved from https://www.ncbi.nlm.nih.gov/pubmed/18614768 doi: 10.1212/01.wnl.0000310775.87331.90

Krimer, L. S., & Goldman-Rakic, P. S. (2001). Prefrontal microcircuits: membrane properties and excitatory input of local, medium, and wide arbor interneurons [Journal Article]. *J Neurosci*, *21*(11), 3788-96. Retrieved from https://www.ncbi.nlm.nih.gov/pubmed/11356867

Kwon, S. J., Han, T. H., Ko, T. Y., Li, N., Kim, Y., Kim, D. J., ... Lee, T. W. (2018). Extremely stable graphene electrodes doped with macromolecular acid [Journal Article]. *Nat Commun*, *9*(1), 2037. Retrieved from https://www.ncbi.nlm.nih.gov/pubmed/29795168 doi: 10.1038/s41467-018-04385-4

Lado, F. A., & Moshe, S. L. (2008). How do seizures stop? [Journal Article]. *Epilepsia*, *49*(10), 1651-64. Retrieved from https://www.ncbi.nlm.nih.gov/pubmed/18503563 doi: 10.1111/j.1528-1167.2008.01669.x

Larsen, R. S., & Waters, J. (2018). Neuromodulatory correlates of pupil dilation [Journal Article]. *Front Neural Circuits*, *12*, 21. Retrieved from https://www.ncbi.nlm.nih.gov/pubmed/29593504 doi: 10.3389/fncir.2018.00021

Lauritzen, M., Dreier, J. P., Fabricius, M., Hartings, J. A., Graf, R., & Strong, A. J. (2011). Clinical relevance of cortical spreading depression in neurological disorders: migraine, malignant stroke, subarachnoid and intracranial hemorrhage, and traumatic brain injury [Journal Article]. *J Cereb Blood Flow Metab*, *31*(1), 17-35. Retrieved from https://www.ncbi.nlm.nih.gov/pubmed/21045864 doi: 10.1038/jcbfm.2010.191

Laxpati, N. G., Mahmoudi, B., Gutekunst, C. A., Newman, J. P., Zeller-Townson, R., & Gross, R. E. (2014). Real-time in vivo optogenetic neuromodulation and multielectrode electrophysiologic recording with neurorighter [Journal Article]. *Front Neuroeng*, *7*, 40. Retrieved from https://www.ncbi.nlm.nih.gov/pubmed/25404915 doi: 10.3389/fneng.2014.00040

Leao, A. A. (1947). Further observations on the spreading depression of activity in the cerebral cortex [Journal Article]. *J Neurophysiol*, *10*(6), 409-14. Retrieved from https://www.ncbi.nlm.nih.gov/pubmed/20268874 doi: 10.1152/jn.1947.10.6.409

Leao, A. A. P., & Morison, R. S. (1945). Propagation of spreading cortical depression. *Journal of Neurophysiology*, *8*(1), 33-45. Retrieved from https://doi.org/10.1152/jn.1945.8.1.33 doi: 10.1152/jn.1945.8.1.33

Lee, M., Lee, S., Kim, J., Lim, J., Lee, J., Masri, S., ... Yang, S. (2021). Graphene-electrode array for brain map remodeling of the cortical surface [Journal Article]. *NPG Asia Materials*, *13*(1), 65. Retrieved from https://doi.org/10.1038/s41427-021-00334-8 doi: 10.1038/s41427-021-00334-8

Leech, C. A., & Holz, G. G. t. (1994). Application of patch clamp methods to the study of calcium currents and calcium channels [Journal Article]. *Methods Cell Biol*, *40*, 135-51. Retrieved from https://www.ncbi.nlm.nih.gov/pubmed/8201974 doi: 10.1016/s0091-679x(08)61113-9

Levesque, M., Salami, P., Gotman, J., & Avoli, M. (2012). Two seizure-onset types reveal specific patterns of high-frequency oscillations in a model of temporal lobe epilepsy [Journal Article]. *J Neurosci*, *32*(38), 13264-72.

Retrieved from https://www.ncbi.nlm.nih.gov/pubmed/22993442 doi: 10.1523/JNEUROSCI.5086-11.2012

Lhatoo, S. D., Faulkner, H. J., Dembny, K., Trippick, K., Johnson, C., & Bird, J. M. (2010). An electroclinical case-control study of sudden unexpected death in epilepsy [Journal Article]. *Ann Neurol*, *68*(6), 787-96. Retrieved from https://www.ncbi.nlm.nih.gov/pubmed/20882604 doi: 10.1002/ana.22101

Lin, J. Y., Knutsen, P. M., Muller, A., Kleinfeld, D., & Tsien, R. Y. (2013). Reachr: a red-shifted variant of channelrhodopsin enables deep transcranial optogenetic excitation [Journal Article]. *Nat Neurosci*, *16*(10), 1499-508. Retrieved from https://www.ncbi.nlm.nih.gov/pubmed/23995068 doi: 10.1038/nn.3502

Lin, M. Z., & Schnitzer, M. J. (2016). Genetically encoded indicators of neuronal activity [Journal Article]. *Nat Neurosci*, *19*(9), 1142-53. Retrieved from https://www.ncbi.nlm.nih.gov/pubmed/27571193 doi: 10.1038/nn.4359

Liou, J. Y., Ma, H., Wenzel, M., Zhao, M., Baird-Daniel, E., Smith, E. H., ... Schevon, C. A. (2018). Role of inhibitory control in modulating focal seizure spread [Journal Article]. *Brain*, *141*(7), 2083-2097. Retrieved from https://www.ncbi.nlm.nih.gov/pubmed/29757347 doi: 10.1093/brain/awy116

Liou, J. Y., Smith, E. H., Bateman, L. M., Bruce, S. L., McKhann, G. M., Goodman, R. R., ... Abbott, L. F. (2020). A model for focal seizure onset, propagation, evolution, and progression [Journal Article]. *Elife*, *9*. Retrieved from https://www.ncbi.nlm.nih.gov/pubmed/32202494 doi: 10.7554/eLife.50927

Lisgaras, C. P., & Scharfman, H. E. (2022). Robust chronic convulsive seizures, high frequency oscillations, and human seizure onset patterns in an intrahippocampal kainic acid model in mice [Journal Article]. *Neurobiol Dis*, *166*, 105637. Retrieved from https://www.ncbi.nlm.nih.gov/pubmed/35091040 doi: 10.1016/j.nbd.2022.105637

Liu, J., Li, F., Wang, Y., Pan, L., Lin, P., Zhang, B., ... Ling, D. (2020). A sensitive and specific nanosensor for monitoring extracellular potassium levels in the brain [Journal Article]. *Nat Nanotechnol*, *15*(4), 321-330. Retrieved from https://www.ncbi.nlm.nih.gov/pubmed/32042163 doi: 10.1038/s41565-020-0634-4

Liu, X., Ren, C., Lu, Y., Hattori, R., Shi, Y., Zhao, R., ... Kuzum, D. (2019). Decoding ecog high gamma power from cellular calcium response using transpar-

ent graphene microelectrodes. In *2019 9th international ieee/embs conference on neural engineering (ner)* (p. 710-713). doi: 10.1109/NER.2019.8717147

Loonen, I. C. M., Jansen, N. A., Cain, S. M., Schenke, M., Voskuyl, R. A., Yung, A. C., ... Tolner, E. A. (2019). Brainstem spreading depolarization and cortical dynamics during fatal seizures in cacna1a s218l mice [Journal Article]. *Brain*, *142*(2), 412-425. Retrieved from https://www.ncbi.nlm.nih.gov/pubmed/30649209 doi: 10.1093/brain/awy325

Lu, C. L., Chang, Y. H., Sun, Y., & Li, C. Y. (2018). A population-based study of epilepsy incidence in association with type 2 diabetes and severe hypoglycaemia [Journal Article]. *Diabetes Res Clin Pract*, *140*, 97-106. Retrieved from https://www.ncbi.nlm.nih.gov/pubmed/29608979 doi: 10.1016/j.diabres.2018.03.020

Mably, A. J., & Colgin, L. L. (2018). Gamma oscillations in cognitive disorders [Journal Article]. *Curr Opin Neurobiol*, *52*, 182-187. Retrieved from https://www.ncbi.nlm.nih.gov/pubmed/30121451 doi: 10.1016/j.conb.2018.07.009

Macfarlane, A., & Greenhalgh, T. (2018). Sodium valproate in pregnancy: what are the risks and should we use a shared decision-making approach? [Journal Article]. *BMC Pregnancy Childbirth*, *18*(1), 200. Retrieved from https://www.ncbi.nlm.nih.gov/pubmed/29859057 doi: 10.1186/s12884-018-1842-x

Magloire, V., Cornford, J., Lieb, A., Kullmann, D. M., & Pavlov, I. (2019a). Kcc2 overexpression prevents the paradoxical seizure-promoting action of somatic inhibition [Journal Article]. *Nat Commun*, *10*(1), 1225. Retrieved from https://www.ncbi.nlm.nih.gov/pubmed/30874549 doi: 10.1038/s41467-019-08933-4

Magloire, V., Cornford, J., Lieb, A., Kullmann, D. M., & Pavlov, I. (2019b). Kcc2 overexpression prevents the paradoxical seizure-promoting action of somatic inhibition [Journal Article]. *Nat Commun*, *10*(1), 1225. Retrieved from https://www.ncbi.nlm.nih.gov/pubmed/30874549 doi: 10.1038/s41467-019-08933-4

Magloire, V., Mercier, M. S., Kullmann, D. M., & Pavlov, I. (2019). Gabaergic interneurons in seizures: Investigating causality with optogenetics [Journal Article]. *Neuroscientist*, *25*(4), 344-358. Retrieved from https://www.ncbi.nlm.nih.gov/pubmed/30317911 doi: 10.1177/1073858418805002

Maki, B. A., Cummings, K. A., Paganelli, M. A., Murthy, S. E., & Popescu, G. K. (2014). One-channel cell-attached patch-clamp recording [Journal Article]. *J Vis Exp*(88). Retrieved from https://www.ncbi.nlm.nih.gov/pubmed/24961614 doi: 10.3791/51629

Marvin, J. S., Borghuis, B. G., Tian, L., Cichon, J., Harnett, M. T., Akerboom, J., ... Looger, L. L. (2013). An optimized fluorescent probe for visualizing glutamate neurotransmission [Journal Article]. *Nat Methods*, *10*(2), 162-70. Retrieved from https://www.ncbi.nlm.nih.gov/pubmed/23314171 doi: 10.1038/nmeth.2333

Masvidal-Codina, E., Illa, X., Dasilva, M., Calia, A. B., Dragojevic, T., Vidal-Rosas, E. E., ... Guimera-Brunet, A. (2019). High-resolution mapping of infraslow cortical brain activity enabled by graphene microtransistors [Journal Article]. *Nat Mater*, *18*(3), 280-288. Retrieved from https://www.ncbi.nlm.nih.gov/pubmed/30598536 doi: 10.1038/s41563-018-0249-4

Masvidal-Codina, E., Smith, T. M., Rathore, D., Gao, Y., Illa, X., Prats-Alfonso, E., ... Wykes, R. C. (2021). Characterization of optogenetically-induced cortical spreading depression in awake mice using graphene microtransistor arrays [Journal Article]. *J Neural Eng*, *18*(5). Retrieved from https://www.ncbi.nlm.nih.gov/pubmed/33690187 doi: 10.1088/1741-2552/abecf3

Mathern, G. W., Adelson, P. D., Cahan, L. D., & Leite, J. P. (2002). Hippocampal neuron damage in human epilepsy: Meyer's hypothesis revisited [Journal Article]. *Prog Brain Res*, *135*, 237-51. Retrieved from https://www.ncbi.nlm.nih.gov/pubmed/12143344 doi: 10.1016/s0079-6123(02)35023-4

Matsuura, T., & Bures, J. (1971a). The minimum volume of depolarized neural tissue required for triggering cortical spreading depression in rat [Journal Article]. *Exp Brain Res*, *12*(3), 238-49. Retrieved from https://www.ncbi.nlm.nih.gov/pubmed/5553371 doi: 10.1007/BF00237916

Matsuura, T., & Bures, J. (1971b). The minimum volume of depolarized neural tissue required for triggering cortical spreading depression in rat [Journal Article]. *Exp Brain Res*, *12*(3), 238-49. Retrieved from https://www.ncbi.nlm.nih.gov/pubmed/5553371 doi: 10.1007/BF00237916

Meneret, A., Gaudebout, C., Riant, F., Vidailhet, M., Depienne, C.,

& Roze, E. (2013). Prrt2 mutations and paroxysmal disorders [Journal Article]. *Eur J Neurol*, *20*(6), 872-8. Retrieved from https://www.ncbi.nlm.nih.gov/pubmed/23398397 doi: 10.1111/ene.12104

Messier, J. E., Chen, H., Cai, Z. L., & Xue, M. (2018). Targeting light-gated chloride channels to neuronal somatodendritic domain reduces their excitatory effect in the axon [Journal Article]. *Elife*, *7*. Retrieved from https://www.ncbi.nlm.nih.gov/pubmed/30091701 doi: 10.7554/eLife.38506

Mies, G., Iijima, T., & Hossmann, K. A. (1993). Correlation between peri-infarct dc shifts and ischaemic neuronal damage in rat [Journal Article]. *Neuroreport*, *4*(6), 709-11. Retrieved from https://www.ncbi.nlm.nih.gov/pubmed/8347812 doi: 10.1097/00001756-199306000-00027

Nagel, G., Szellas, T., Huhn, W., Kateriya, S., Adeishvili, N., Berthold, P., ... Bamberg, E. (2003). Channelrhodopsin-2, a directly light-gated cation-selective membrane channel [Journal Article]. *Proc Natl Acad Sci U S A*, *100*(24), 13940-5. Retrieved from https://www.ncbi.nlm.nih.gov/pubmed/14615590 doi: 10.1073/pnas.1936192100

Neher, E., & Sakmann, B. (1976). Single-channel currents recorded from membrane of denervated frog muscle fibres [Journal Article]. *Nature*, *260*(5554), 799-802. Retrieved from https://www.ncbi.nlm.nih.gov/pubmed/1083489 doi: 10.1038/260799a0

Nguyen, R., Venkatesan, S., Binko, M., Bang, J. Y., Cajanding, J. D., Briggs, C., ... Kim, J. C. (2020). Cholecystokinin-expressing interneurons of the medial prefrontal cortex mediate working memory retrieval [Journal Article]. *J Neurosci*, *40*(11), 2314-2331. Retrieved from https://www.ncbi.nlm.nih.gov/pubmed/32005764 doi: 10.1523/JNEUROSCI.1919-19.2020

Nissinen, J., Halonen, T., Koivisto, E., & Pitkanen, A. (2000). A new model of chronic temporal lobe epilepsy induced by electrical stimulation of the amygdala in rat [Journal Article]. *Epilepsy Res*, *38*(2-3), 177-205. Retrieved from https://www.ncbi.nlm.nih.gov/pubmed/10642046 doi: 10.1016/s0920-1211(99)00088-1

Novak, P., Gorelik, J., Vivekananda, U., Shevchuk, A. I., Ermolyuk, Y. S., Bailey, R. J., ... Korchev, Y. E. (2013). Nanoscale-targeted patch-clamp recordings

of functional presynaptic ion channels [Journal Article]. *Neuron*, *79*(6), 1067-77. Retrieved from https://www.ncbi.nlm.nih.gov/pubmed/24050398 doi: 10.1016/j.neuron.2013.07.012

Oakley, C. B., & Kossoff, E. H. (2014). Migraine and epilepsy in the pediatric population [Journal Article]. *Curr Pain Headache Rep*, *18*(3), 402. Retrieved from https://www.ncbi.nlm.nih.gov/pubmed/24500640 doi: 10.1007/s11916-013-0402-3

Ogren, J. A., Bragin, A., Wilson, C. L., Hoftman, G. D., Lin, J. J., Dutton, R. A., ... Staba, R. J. (2009). Three-dimensional hippocampal atrophy maps distinguish two common temporal lobe seizure-onset patterns [Journal Article]. *Epilepsia*, *50*(6), 1361-70. Retrieved from https://www.ncbi.nlm.nih.gov/pubmed/19054395 doi: 10.1111/j.1528-1167.2008.01881.x

Olesen, J., Burstein, R., Ashina, M., & Tfelt-Hansen, P. (2009). Origin of pain in migraine: evidence for peripheral sensitisation [Journal Article]. *Lancet Neurol*, *8*(7), 679-90. Retrieved from https://www.ncbi.nlm.nih.gov/pubmed/19539239 doi: 10.1016/S1474-4422(09)70090-0

Oliveira-Ferreira, A. I., Winkler, M. K., Reiffurth, C., Milakara, D., Woitzik, J., & Dreier, J. P. (2012). Spreading depolarization, a pathophysiological mechanism of stroke and migraine aura [Journal Article]. *Future Neurology*, *7*(1), 45-64. Retrieved from https://www.futuremedicine.com/doi/abs/10.2217/fnl.11.69 doi: 10.2217/fnl.11.69

Oron, D., Papagiakoumou, E., Anselmi, F., & Emiliani, V. (2012). Two-photon optogenetics [Journal Article]. *Prog Brain Res*, *196*, 119-43. Retrieved from https://www.ncbi.nlm.nih.gov/pubmed/22341324 doi: 10.1016/B978-0-444-59426-6.00007-0

Packer, A. M., Peterka, D. S., Hirtz, J. J., Prakash, R., Deisseroth, K., & Yuste, R. (2012). Two-photon optogenetics of dendritic spines and neural circuits [Journal Article]. *Nat Methods*, *9*(12), 1202-5. Retrieved from https://www.ncbi.nlm.nih.gov/pubmed/23142873 doi: 10.1038/nmeth.2249

Pakozdy, A., Halasz, P., & Klang, A. (2014). Epilepsy in cats: theory and practice [Journal Article]. *J Vet Intern Med*, *28*(2), 255-63. Retrieved from https://www.ncbi.nlm.nih.gov/pubmed/24438024 doi: 10.1111/jvim.12297

Papagiakoumou, E., Ronzitti, E., & Emiliani, V. (2020). Scanless two-photon excitation with temporal focusing [Journal Article]. *Nat Methods*, *17*(6), 571-581. Retrieved from https://www.ncbi.nlm.nih.gov/pubmed/32284609 doi: 10.1038/s41592-020-0795-y

Park, D. W., Ness, J. P., Brodnick, S. K., Esquibel, C., Novello, J., Atry, F., ... Ma, Z. (2018). Electrical neural stimulation and simultaneous in vivo monitoring with transparent graphene electrode arrays implanted in gcamp6f mice [Journal Article]. *ACS Nano*, *12*(1), 148-157. Retrieved from https://www.ncbi.nlm.nih.gov/pubmed/29253337 https://pubs.acs.org/doi/10.1021/acsnano.7b04321 doi: 10.1021/acsnano.7b04321

Park, S. J., Lee, Y., Oh, H. K., Lee, H. E., Lee, Y., Ko, S. Y., ... Ryu, J. H. (2014). Oleanolic acid attenuates mk-801-induced schizophrenia-like behaviors in mice [Journal Article]. *Neuropharmacology*, *86*, 49-56. Retrieved from https://www.ncbi.nlm.nih.gov/pubmed/24997455 doi: 10.1016/j.neuropharm.2014.06.025

Parker, E., Aboghazleh, R., Mumby, G., Veksler, R., Ofer, J., Newton, J., ... Friedman, A. (2021). Concussion susceptibility is mediated by spreading depolarization-induced neurovascular dysfunction [Journal Article]. *Brain*. Retrieved from https://www.ncbi.nlm.nih.gov/pubmed/34927674 doi: 10.1093/brain/awab450

Parker, P. D., Suryavanshi, P., Melone, M., Sawant-Pokam, P. A., Reinhart, K. M., Kaufmann, D., ... Brennan, K. C. (2021). Non-canonical glutamate signaling in a genetic model of migraine with aura [Journal Article]. *Neuron*, *109*(4), 611-628 e8. Retrieved from https://www.ncbi.nlm.nih.gov/pubmed/33321071 doi: 10.1016/j.neuron.2020.11.018

Pelluru, D., Konadhode, R. R., Bhat, N. R., & Shiromani, P. J. (2016). Optogenetic stimulation of astrocytes in the posterior hypothalamus increases sleep at night in c57bl/6j mice [Journal Article]. *Eur J Neurosci*, *43*(10), 1298-306. Retrieved from https://www.ncbi.nlm.nih.gov/pubmed/26369866 doi: 10.1111/ejn.13074

Percie du Sert, N., & Rice, A. S. (2014). Improving the translation of analgesic drugs to the clinic: animal models of neuropathic pain [Journal Article]. *Br J Pharmacol*, *171*(12), 2951-63. Retrieved from https://www.ncbi.nlm.nih.gov/pubmed/24527763 doi: 10.1111/bph.12645

Picot, A., Dominguez, S., Liu, C., Chen, I. W., Tanese, D., Ronzitti, E., ... Emiliani, V. (2018). Temperature rise under two-photon optogenetic brain stimulation [Journal Article]. *Cell Rep*, *24*(5), 1243-1253 e5. Retrieved from https://www.ncbi.nlm.nih.gov/pubmed/30067979 doi: 10.1016/j.celrep.2018.06.119

Pietrobon, D. (2010a). Cav2.1 channelopathies [Journal Article]. *Pflugers Arch*, *460*(2), 375-93. Retrieved from https://www.ncbi.nlm.nih.gov/pubmed/20204399 doi: 10.1007/s00424-010-0802-8

Pietrobon, D. (2010b). Insights into migraine mechanisms and cav2.1 calcium channel function from mouse models of familial hemiplegic migraine [Journal Article]. *J Physiol*, *588*(Pt 11), 1871-8. Retrieved from https://www.ncbi.nlm.nih.gov/pubmed/20194127 doi: 10.1113/jphysiol.2010.188003

Pietrobon, D., & Moskowitz, M. A. (2014). Chaos and commotion in the wake of cortical spreading depression and spreading depolarizations [Journal Article]. *Nat Rev Neurosci*, *15*(6), 379-93. Retrieved from https://www.ncbi.nlm.nih.gov/pubmed/24857965 doi: 10.1038/nrn3770

Poh, M. Z., Loddenkemper, T., Reinsberger, C., Swenson, N. C., Goyal, S., Madsen, J. R., & Picard, R. W. (2012). Autonomic changes with seizures correlate with postictal eeg suppression [Journal Article]. *Neurology*, *78*(23), 1868-76. Retrieved from https://www.ncbi.nlm.nih.gov/pubmed/22539579 doi: 10.1212/WNL.0b013e318258f7f1

Postnikova, T. Y., Zubareva, O. E., Kovalenko, A. A., Kim, K. K., Magazanik, L. G., & Zaitsev, A. V. (2017). Status epilepticus impairs synaptic plasticity in rat hippocampus and is followed by changes in expression of nmda receptors [Journal Article]. *Biochemistry (Mosc)*, *82*(3), 282-290. Retrieved from https://www.ncbi.nlm.nih.gov/pubmed/28320269 doi: 10.1134/S0006297917030063

Pottkamper, J. C. M., Hofmeijer, J., van Waarde, J. A., & van Putten, M. (2020). The postictal state - what do we know? [Journal Article]. *Epilepsia*, *61*(6), 1045-1061. Retrieved from https://www.ncbi.nlm.nih.gov/pubmed/32396219 doi: 10.1111/epi.16519

Proix, T., Jirsa, V. K., Bartolomei, F., Guye, M., & Truccolo, W. (2018). Predicting the spatiotemporal diversity of seizure propagation and termination in human focal epilepsy [Journal Article]. *Nat Commun*, *9*(1), 1088. Retrieved from

https://www.ncbi.nlm.nih.gov/pubmed/29540685 doi: 10.1038/s41467-018-02973-y

Rathmann, T., Khaleghi Ghadiri, M., Stummer, W., & Gorji, A. (2020). Spreading depolarization facilitates the transition of neuronal burst firing from interictal to ictal state [Journal Article]. *Neuroscience*, *441*, 176-183. Retrieved from https://www.ncbi.nlm.nih.gov/pubmed/32450296 doi: 10.1016/j.neuroscience.2020.05.029

Reif, P. S., Strzelczyk, A., & Rosenow, F. (2016a). The history of invasive eeg evaluation in epilepsy patients [Journal Article]. *Seizure*, *41*, 191-5. Retrieved from https://www.ncbi.nlm.nih.gov/pubmed/27131772 doi: 10.1016/j.seizure.2016.04.006

Reif, P. S., Strzelczyk, A., & Rosenow, F. (2016b). The history of invasive eeg evaluation in epilepsy patients [Journal Article]. *Seizure*, *41*, 191-5. Retrieved from https://www.ncbi.nlm.nih.gov/pubmed/27131772 doi: 10.1016/j.seizure.2016.04.006

Reyes-Garcia, S. Z., Scorza, C. A., Araujo, N. S., Ortiz-Villatoro, N. N., Jardim, A. P., Centeno, R., ... Cavalheiro, E. A. (2018). Different patterns of epileptiform-like activity are generated in the sclerotic hippocampus from patients with drug-resistant temporal lobe epilepsy [Journal Article]. *Sci Rep*, *8*(1), 7116. Retrieved from https://www.ncbi.nlm.nih.gov/pubmed/29740014 doi: 10.1038/s41598-018-25378-9

Rich, S., Chameh, H. M., Rafiee, M., Ferguson, K., Skinner, F. K., & Valiante, T. A. (2019). Inhibitory network bistability explains increased interneuronal activity prior to seizure onset [Journal Article]. *Front Neural Circuits*, *13*, 81. Retrieved from https://www.ncbi.nlm.nih.gov/pubmed/32009908 doi: 10.3389/fncir.2019.00081

Rogawski, M. A., & Loscher, W. (2004). The neurobiology of antiepileptic drugs [Journal Article]. *Nat Rev Neurosci*, *5*(7), 553-64. Retrieved from https://www.ncbi.nlm.nih.gov/pubmed/15208697 doi: 10.1038/nrn1430

Ronzitti, E., Ventalon, C., Canepari, M., Forget, B. C., Papagiakoumou, E., & Emiliani, V. (2017, oct). Recent advances in patterned photostimulation for optogenetics. *Journal of Optics*, *19*(11), 113001. Retrieved from https://doi.org/10.1088/2040-8986/aa8299 doi: 10.1088/2040-8986/aa8299

Rossi, L. F., Kullmann, D. M., & Wykes, R. C. (2018). The enlightened brain: Novel imaging methods focus on epileptic networks at mul-

tiple scales [Journal Article]. *Front Cell Neurosci*, *12*, 82. Retrieved from https://www.ncbi.nlm.nih.gov/pubmed/29632475 doi: 10.3389/fncel.2018.00082

Rossi, L. F., Wykes, R. C., Kullmann, D. M., & Carandini, M. (2017). Focal cortical seizures start as standing waves and propagate respecting homotopic connectivity [Journal Article]. *Nat Commun*, *8*(1), 217. Retrieved from https://www.ncbi.nlm.nih.gov/pubmed/28794407 doi: 10.1038/s41467-017-00159-6

Royo, N. C., Vandenberghe, L. H., Ma, J. Y., Hauspurg, A., Yu, L., Maronski, M., ... Watson, D. J. (2008). Specific aav serotypes stably transduce primary hippocampal and cortical cultures with high efficiency and low toxicity [Journal Article]. *Brain Res*, *1190*, 15-22. Retrieved from https://www.ncbi.nlm.nih.gov/pubmed/18054899 doi: 10.1016/j.brainres.2007.11.015

Rubaiy, H. N. (2017). A short guide to electrophysiology and ion channels [Journal Article]. *J Pharm Pharm Sci*, *20*, 48-67. Retrieved from https://www.ncbi.nlm.nih.gov/pubmed/28459656 doi: 10.18433/J32P6R

Russell, M. B., & Ducros, A. (2011). Sporadic and familial hemiplegic migraine: pathophysiological mechanisms, clinical characteristics, diagnosis, and management [Journal Article]. *Lancet Neurol*, *10*(5), 457-70. Retrieved from https://www.ncbi.nlm.nih.gov/pubmed/21458376 doi: 10.1016/S1474-4422(11)70048-5

Santos, E., Scholl, M., Sanchez-Porras, R., Dahlem, M. A., Silos, H., Unterberg, A., ... Sakowitz, O. W. (2014). Radial, spiral and reverberating waves of spreading depolarization occur in the gyrencephalic brain [Journal Article]. *Neuroimage*, *99*, 244-55. Retrieved from https://www.ncbi.nlm.nih.gov/pubmed/24852458 doi: 10.1016/j.neuroimage.2014.05.021

Schachter, S. C. (2009). Seizure disorders [Journal Article]. *Med Clin North Am*, *93*(2), 343-51, viii. Retrieved from https://www.ncbi.nlm.nih.gov/pubmed/19272512 doi: 10.1016/j.mcna.2008.10.001

Scheffer, I. E., Berkovic, S., Capovilla, G., Connolly, M. B., French, J., Guilhoto, L., ... Zuberi, S. M. (2017). Ilae classification of the epilepsies: Position paper of the ilae commission for classification and terminology [Journal Article]. *Epilepsia*, *58*(4), 512-521. Re-

trieved from https://www.ncbi.nlm.nih.gov/pubmed/28276062 doi: 10.1111/epi.13709

Schindler, K., Elger, C. E., & Lehnertz, K. (2007). Increasing synchronization may promote seizure termination: evidence from status epilepticus [Journal Article]. *Clin Neurophysiol*, *118*(9), 1955-68. Retrieved from https://www.ncbi.nlm.nih.gov/pubmed/17644031 doi: 10.1016/j.clinph.2007.06.006

Sharma, S., Puttachary, S., Thippeswamy, A., Kanthasamy, A. G., & Thippeswamy, T. (2018). Status epilepticus: Behavioral and electroencephalography seizure correlates in kainate experimental models [Journal Article]. *Front Neurol*, *9*, 7. Retrieved from https://www.ncbi.nlm.nih.gov/pubmed/29410648 doi: 10.3389/fneur.2018.00007

Shemesh, O. A., Tanese, D., Zampini, V., Linghu, C., Piatkevich, K., Ronzitti, E., ... Emiliani, V. (2017). Temporally precise single-cell-resolution optogenetics [Journal Article]. *Nat Neurosci*, *20*(12), 1796-1806. Retrieved from https://www.ncbi.nlm.nih.gov/pubmed/29184208 https://www.nature.com/articles/s41593-017-0018-8.pdf doi: 10.1038/s41593-017-0018-8

Shen, Y., Gong, Y., Ruan, Y., Chen, Z., & Xu, C. (2021). Secondary epileptogenesis: Common to see, but possible to treat? [Journal Article]. *Front Neurol*, *12*, 747372. Retrieved from https://www.ncbi.nlm.nih.gov/pubmed/34938259 doi: 10.3389/fneur.2021.747372

Shibata, M., & Bures, J. (1972). Reverberation of cortical spreading depression along closed-loop pathways in rat cerebral cortex [Journal Article]. *J Neurophysiol*, *35*(3), 381-8. Retrieved from https://www.ncbi.nlm.nih.gov/pubmed/5029956 doi: 10.1152/jn.1972.35.3.381

Shibata, M., & Suzuki, N. (2017). Exploring the role of microglia in cortical spreading depression in neurological disease [Journal Article]. *J Cereb Blood Flow Metab*, *37*(4), 1182-1191. Retrieved from https://www.ncbi.nlm.nih.gov/pubmed/28155572 doi: 10.1177/0271678X17690537

Silfverhuth, M. J., Kortelainen, J., Ruohonen, J., Suominen, K., Niinimaki, J., Sonkajarvi, E., ... Seppanen, T. (2011). A characteristic time sequence of epileptic activity in eeg during dynamic penicillin-induced focal epilepsy–a preliminary study [Journal Article]. *Seizure*, *20*(7), 513-9. Retrieved from https://www.ncbi.nlm.nih.gov/pubmed/21511498 doi:

10.1016/j.seizure.2011.03.006

Smart, S. L., Lopantsev, V., Zhang, C. L., Robbins, C. A., Wang, H., Chiu, S. Y., ... Tempel, B. L. (1998). Deletion of the k(v)1.1 potassium channel causes epilepsy in mice [Journal Article]. *Neuron*, *20*(4), 809-19. Retrieved from https://www.ncbi.nlm.nih.gov/pubmed/9581771 doi: 10.1016/s0896-6273(00)81018-1

Smith, P. D., McLean, K. J., Murphy, M. A., Turnley, A. M., & Cook, M. J. (2005). Seizures, not hippocampal neuronal death, provoke neurogenesis in a mouse rapid electrical amygdala kindling model of seizures [Journal Article]. *Neuroscience*, *136*(2), 405-15. Retrieved from https://www.ncbi.nlm.nih.gov/pubmed/16226389 doi: 10.1016/j.neuroscience.2005.07.055

Smith, S. J. (2005). Eeg in the diagnosis, classification, and management of patients with epilepsy [Journal Article]. *J Neurol Neurosurg Psychiatry*, *76 Suppl 2*, ii2-7. Retrieved from https://www.ncbi.nlm.nih.gov/pubmed/15961864 doi: 10.1136/jnnp.2005.069245

Soares-Silva, B., Beserra-Filho, J. I. A., Morera, P. M. A., Custodio-Silva, A. C., Maria-Macedo, A., Silva-Martins, S., ... Ribeiro, A. M. (2021). The bee venom active compound melittin protects against bicuculline-induced seizures and hippocampal astrocyte activation in rats [Journal Article]. *Neuropeptides*, *91*, 102209. Retrieved from https://www.ncbi.nlm.nih.gov/pubmed/34808488 doi: 10.1016/j.npep.2021.102209

Srienc, A. I., Chiang, P. P., Schmitt, A. J., & Newman, E. A. (2019). Cortical spreading depolarizations induced by surgical field blood in a mouse model of neurosurgery [Journal Article]. *J Neurosurg*, *132*(6), 1820-1828. Retrieved from https://www.ncbi.nlm.nih.gov/pubmed/30952117 doi: 10.3171/2018.12.JNS181130

Sripanidkulchai, K., & Wyss, J. M. (1986). Thalamic projections to retrosplenial cortex in the rat [Journal Article]. *J Comp Neurol*, *254*(2), 143-65. Retrieved from https://www.ncbi.nlm.nih.gov/pubmed/3794004 doi: 10.1002/cne.902540202

Stafstrom, C. E., & Carmant, L. (2015). Seizures and epilepsy: an overview for neuroscientists [Journal Article]. *Cold Spring Harb Perspect Med*, *5*(6). Retrieved from https://www.ncbi.nlm.nih.gov/pubmed/26033084 doi: 10.1101/cshperspect.a022426

Staley, K. J., White, A., & Dudek, F. E. (2011). Interictal spikes: harbingers

or causes of epilepsy? [Journal Article]. *Neurosci Lett*, *497*(3), 247-50. Retrieved from https://www.ncbi.nlm.nih.gov/pubmed/21458535 doi: 10.1016/j.neulet.2011.03.070

Stam, A. H., Luijckx, G. J., Poll-The, B. T., Ginjaar, I. B., Frants, R. R., Haan, J., ... van den Maagdenberg, A. M. (2009). Early seizures and cerebral oedema after trivial head trauma associated with the cacna1a s218l mutation [Journal Article]. *J Neurol Neurosurg Psychiatry*, *80*(10), 1125-9. Retrieved from https://www.ncbi.nlm.nih.gov/pubmed/19520699 https://core.ac.uk/download/189729280.pdf doi: 10.1136/jnnp.2009.177279

Strzelczyk, A., Griebel, C., Lux, W., Rosenow, F., & Reese, J. P. (2017). The burden of severely drug-refractory epilepsy: A comparative longitudinal evaluation of mortality, morbidity, resource use, and cost using german health insurance data [Journal Article]. *Front Neurol*, *8*, 712. Retrieved from https://www.ncbi.nlm.nih.gov/pubmed/29312132 doi: 10.3389/fneur.2017.00712

Sztriha, L., Joo, F., & Szerdahelyi, P. (1985). Accumulation of calcium in the rat hippocampus during kainic acid seizures [Journal Article]. *Brain Res*, *360*(1-2), 51-7. Retrieved from https://www.ncbi.nlm.nih.gov/pubmed/4075183 doi: 10.1016/0006-8993(85)91219-3

Tada, M., Takeuchi, A., Hashizume, M., Kitamura, K., & Kano, M. (2014). A highly sensitive fluorescent indicator dye for calcium imaging of neural activity in vitro and in vivo [Journal Article]. *Eur J Neurosci*, *39*(11), 1720-8. Retrieved from https://www.ncbi.nlm.nih.gov/pubmed/24405482 doi: 10.1111/ejn.12476

Takagaki, M., Feuerstein, D., Kumagai, T., Gramer, M., Yoshimine, T., & Graf, R. (2014). Isoflurane suppresses cortical spreading depolarizations compared to propofol–implications for sedation of neurocritical care patients [Journal Article]. *Exp Neurol*, *252*, 12-7. Retrieved from https://www.ncbi.nlm.nih.gov/pubmed/24246282 doi: 10.1016/j.expneurol.2013.11.003

Takahashi, T., Yoshihara, K., Watanabe, M., Kubota, M., Johnson, R., Derguini, F., & Nakanishi, K. (1991). Photoisomerization of retinal at 13-ene is important for phototaxis of chlamydomonas reinhardtii: simultaneous measurements of phototactic and photophobic responses [Journal Article]. *Biochem Biophys Res Commun*, *178*(3), 1273-9. Retrieved from https://www.ncbi.nlm.nih.gov/pubmed/1872847 doi: 10.1016/0006-

291x(91)91031-7

Tamim, I., Chung, D. Y., de Morais, A. L., Loonen, I. C. M., Qin, T., Misra, A., ... Ayata, C. (2021). Spreading depression as an innate antiseizure mechanism [Journal Article]. *Nat Commun*, *12*(1), 2206. Retrieved from https://www.ncbi.nlm.nih.gov/pubmed/33850125 doi: 10.1038/s41467-021-22464-x

Tas, Y. C., Solaroglu, I., & Gursoy-Ozdemir, Y. (2019). Spreading depolarization waves in neurological diseases: A short review about its pathophysiology and clinical relevance [Journal Article]. *Curr Neuropharmacol*, *17*(2), 151-164. Retrieved from https://www.ncbi.nlm.nih.gov/pubmed/28925885 doi: 10.2174/1570159X15666170915160707

Tfelt-Hansen, P. C. (2010). History of migraine with aura and cortical spreading depression from 1941 and onwards [Journal Article]. *Cephalalgia*, *30*(7), 780-92. Retrieved from https://www.ncbi.nlm.nih.gov/pubmed/19740119 doi: 10.1111/j.1468-2982.2009.02015.x

Thijs, R. D., Surges, R., O'Brien, T. J., & Sander, J. W. (2019). Epilepsy in adults [Journal Article]. *Lancet*, *393*(10172), 689-701. Retrieved from https://www.ncbi.nlm.nih.gov/pubmed/30686584 doi: 10.1016/S0140-6736(18)32596-0

Torres-Martinez, N., Cretallaz, C., Ratel, D., Mailley, P., Gaude, C., Costecalde, T., ... Sauter-Starace, F. (2019). Evaluation of chronically implanted subdural boron doped diamond/cnt recording electrodes in miniature swine brain [Journal Article]. *Bioelectrochemistry*, *129*, 79-89. Retrieved from https://www.ncbi.nlm.nih.gov/pubmed/31125924 doi: 10.1016/j.bioelechem.2019.05.007

Tottene, A., Pivotto, F., Fellin, T., Cesetti, T., van den Maagdenberg, A. M., & Pietrobon, D. (2005). Specific kinetic alterations of human cav2.1 calcium channels produced by mutation s218l causing familial hemiplegic migraine and delayed cerebral edema and coma after minor head trauma [Journal Article]. *J Biol Chem*, *280*(18), 17678-86. Retrieved from https://www.ncbi.nlm.nih.gov/pubmed/15743764 doi: 10.1074/jbc.M501110200

Tozzi, A., de Iure, A., Di Filippo, M., Costa, C., Caproni, S., Pisani, A., ... Calabresi, P. (2012). Critical role of calcitonin gene-related peptide receptors in cortical spreading depression [Journal Article]. *Proc Natl Acad Sci U S A*, *109*(46), 18985-90. Retrieved from https://www.ncbi.nlm.nih.gov/pubmed/23112192 doi:

10.1073/pnas.1215435109

Trevelyan, A. J., Sussillo, D., Watson, B. O., & Yuste, R. (2006). Modular propagation of epileptiform activity: evidence for an inhibitory veto in neocortex [Journal Article]. *J Neurosci*, *26*(48), 12447-55. Retrieved from https://www.ncbi.nlm.nih.gov/pubmed/17135406 doi: 10.1523/JNEUROSCI.2787-06.2006

Turley, J. A., Zalewska, K., Nilsson, M., Walker, F. R., & Johnson, S. J. (2017). An analysis of signal processing algorithm performance for cortical intrinsic optical signal imaging and strategies for algorithm selection [Journal Article]. *Sci Rep*, *7*(1), 7198. Retrieved from https://www.ncbi.nlm.nih.gov/pubmed/28775255 doi: 10.1038/s41598-017-06864-y

Turski, L., Ikonomidou, C., Turski, W. A., Bortolotto, Z. A., & Cavalheiro, E. A. (1989). Review: cholinergic mechanisms and epileptogenesis. the seizures induced by pilocarpine: a novel experimental model of intractable epilepsy [Journal Article]. *Synapse*, *3*(2), 154-71. Retrieved from https://www.ncbi.nlm.nih.gov/pubmed/2648633 doi: 10.1002/syn.890030207

Umpierre, A. D., Bystrom, L. L., Ying, Y., Liu, Y. U., Worrell, G., & Wu, L. J. (2020). Microglial calcium signaling is attuned to neuronal activity in awake mice [Journal Article]. *Elife*, *9*. Retrieved from https://www.ncbi.nlm.nih.gov/pubmed/32716294 doi: 10.7554/eLife.56502

Vafaiee, M., Vossoughi, M., Mohammadpour, R., & Sasanpour, P. (2019). Gold-plated electrode with high scratch strength for electrophysiological recordings [Journal Article]. *Sci Rep*, *9*(1), 2985. Retrieved from https://www.ncbi.nlm.nih.gov/pubmed/30814648 doi: 10.1038/s41598-019-39138-w

van den Maagdenberg, A. M., Pizzorusso, T., Kaja, S., Terpolilli, N., Shapovalova, M., Hoebeek, F. E., ... Ferrari, M. D. (2010). High cortical spreading depression susceptibility and migraine-associated symptoms in ca(v)2.1 s218l mice [Journal Article]. *Ann Neurol*, *67*(1), 85-98. Retrieved from https://www.ncbi.nlm.nih.gov/pubmed/20186955 doi: 10.1002/ana.21815

Van Dycke, A., Raedt, R., Dauwe, I., Sante, T., Wyckhuys, T., Meurs, A., ... Boon, P. (2010). Continuous local intrahippocampal delivery of adenosine reduces seizure frequency in rats with spontaneous

seizures [Journal Article]. *Epilepsia*, *51*(9), 1721-8. Retrieved from https://www.ncbi.nlm.nih.gov/pubmed/20726873 doi: 10.1111/j.1528-1167.2010.02700.x

Van Gompel, J. J., Bower, M. R., Worrell, G. A., Stead, M., Chang, S. Y., Goerss, S. J., ... Lee, K. H. (2014). Increased cortical extracellular adenosine correlates with seizure termination [Journal Article]. *Epilepsia*, *55*(2), 233-44. Retrieved from https://www.ncbi.nlm.nih.gov/pubmed/24483230 doi: 10.1111/epi.12511

Vanni, M. P., Chan, A. W., Balbi, M., Silasi, G., & Murphy, T. H. (2017). Mesoscale mapping of mouse cortex reveals frequency-dependent cycling between distinct macroscale functional modules [Journal Article]. *J Neurosci*, *37*(31), 7513-7533. Retrieved from https://www.ncbi.nlm.nih.gov/pubmed/28674167 doi: 10.1523/JNEUROSCI.3560-16.2017

Vecchia, D., Tottene, A., van den Maagdenberg, A. M., & Pietrobon, D. (2015). Abnormal cortical synaptic transmission in cav2.1 knockin mice with the s218l missense mutation which causes a severe familial hemiplegic migraine syndrome in humans [Journal Article]. *Front Cell Neurosci*, *9*, 8. Retrieved from https://www.ncbi.nlm.nih.gov/pubmed/25741235 doi: 10.3389/fncel.2015.00008

Verkhratsky, A., & Parpura, V. (2014). History of electrophysiology and the patch clamp [Journal Article]. *Methods Mol Biol*, *1183*, 1-19. Retrieved from https://www.ncbi.nlm.nih.gov/pubmed/25023299 doi: 10.1007/978-1-4939-1096-0_1

Veronesi, M. C., Kubek, D. J., & Kubek, M. J. (2008). Isoflurane exacerbates electrically evoked seizures in amygdala-kindled rats during recovery [Journal Article]. *Epilepsy Res*, *82*(1), 15-20. Retrieved from https://www.ncbi.nlm.nih.gov/pubmed/18674885 doi: 10.1016/j.eplepsyres.2008.06.007

Victor, T. W., Hu, X., Campbell, J. C., Buse, D. C., & Lipton, R. B. (2010). Migraine prevalence by age and sex in the united states: a life-span study [Journal Article]. *Cephalalgia*, *30*(9), 1065-72. Retrieved from https://www.ncbi.nlm.nih.gov/pubmed/20713557 doi: 10.1177/0333102409355601

Viitanen, T., Ruusuvuori, E., Kaila, K., & Voipio, J. (2010). The k+-cl cotransporter kcc2 promotes gabaergic excitation in the mature rat hippocampus [Journal Article]. *J Physiol*, *588*(Pt 9), 1527-40. Retrieved from

https://www.ncbi.nlm.nih.gov/pubmed/20211979 doi: 10.1113/jphysiol.2009.181826

Vinck, M., Oostenveld, R., van Wingerden, M., Battaglia, F., & Pennartz, C. M. (2011). An improved index of phase-synchronization for electrophysiological data in the presence of volume-conduction, noise and sample-size bias [Journal Article]. *Neuroimage*, *55*(4), 1548-65. Retrieved from https://www.ncbi.nlm.nih.gov/pubmed/21276857 doi: 10.1016/j.neuroimage.2011.01.055

Vinogradova, L. V., Rysakova, M. P., & Pavlova, I. V. (2020). Small damage of brain parenchyma reliably triggers spreading depolarization [Journal Article]. *Neurol Res*, *42*(1), 76-82. Retrieved from https://www.ncbi.nlm.nih.gov/pubmed/31900075 doi: 10.1080/01616412.2019.1709745

Vinogradova, L. V., Suleymanova, E. M., & Medvedeva, T. M. (2021). Transient loss of interhemispheric functional connectivity following unilateral cortical spreading depression in awake rats [Journal Article]. *Cephalalgia*, *41*(3), 353-365. Retrieved from https://www.ncbi.nlm.nih.gov/pubmed/33164563 doi: 10.1177/0333102420970172

Vinogradova, L. V., Vinogradov, V. Y., & Kuznetsova, G. D. (2006). Unilateral cortical spreading depression is an early marker of audiogenic kindling in awake rats [Journal Article]. *Epilepsy Res*, *71*(1), 64-75. Retrieved from https://www.ncbi.nlm.nih.gov/pubmed/16806830 doi: 10.1016/j.eplepsyres.2006.05.014

Viventi, J., Kim, D. H., Vigeland, L., Frechette, E. S., Blanco, J. A., Kim, Y. S., ... Litt, B. (2011). Flexible, foldable, actively multiplexed, high-density electrode array for mapping brain activity in vivo [Journal Article]. *Nat Neurosci*, *14*(12), 1599-605. Retrieved from https://www.ncbi.nlm.nih.gov/pubmed/22081157 doi: 10.1038/nn.2973

Voge, C. M., & Stegemann, J. P. (2011). Carbon nanotubes in neural interfacing applications [Journal Article]. *J Neural Eng*, *8*(1), 011001. Retrieved from https://www.ncbi.nlm.nih.gov/pubmed/21245526 doi: 10.1088/1741-2560/8/1/011001

Walker, M. C. (2018). Pathophysiology of status epilepticus [Journal Article]. *Neurosci Lett*, *667*, 84-91. Retrieved from https://www.ncbi.nlm.nih.gov/pubmed/28011391 doi: 10.1016/j.neulet.2016.12.044

Wang, C., Zhang, J., & Schroeder, J. I. (2017). Two-electrode voltage-clamp

recordings in xenopus laevis oocytes: Reconstitution of abscisic acid activation of slac1 anion channel via pyl9 aba receptor [Journal Article]. *Bio Protoc*, *7*(2). Retrieved from https://www.ncbi.nlm.nih.gov/pubmed/28516122 doi: 10.21769/BioProtoc.2114

Weiss, S. A., Alvarado-Rojas, C., Bragin, A., Behnke, E., Fields, T., Fried, I., ... Staba, R. (2016). Ictal onset patterns of local field potentials, high frequency oscillations, and unit activity in human mesial temporal lobe epilepsy [Journal Article]. *Epilepsia*, *57*(1), 111-21. Retrieved from https://www.ncbi.nlm.nih.gov/pubmed/26611159 doi: 10.1111/epi.13251

Weiss, S. A., Lemesiou, A., Connors, R., Banks, G. P., McKhann, G. M., Goodman, R. R., ... Schevon, C. A. (2015). Seizure localization using ictal phase-locked high gamma: A retrospective surgical outcome study [Journal Article]. *Neurology*, *84*(23), 2320-8. Retrieved from https://www.ncbi.nlm.nih.gov/pubmed/25972493 doi: 10.1212/WNL.0000000000001656

Wenzel, M., Hamm, J. P., Peterka, D. S., & Yuste, R. (2019). Acute focal seizures start as local synchronizations of neuronal ensembles [Journal Article]. *J Neurosci*, *39*(43), 8562-8575. Retrieved from https://www.ncbi.nlm.nih.gov/pubmed/31427393 doi: 10.1523/JNEUROSCI.3176-18.2019

Wyrwicz, A. M., Conboy, C. B., Ryback, K. R., Nichols, B. G., & Eisele, P. (1987). In vivo 19f-nmr study of isoflurane elimination from brain [Journal Article]. *Biochim Biophys Acta*, *927*(1), 86-91. Retrieved from https://www.ncbi.nlm.nih.gov/pubmed/3790622 doi: 10.1016/0167-4889(87)90069-3

Wyss, J. M., & Van Groen, T. (1992). Connections between the retrosplenial cortex and the hippocampal formation in the rat: a review [Journal Article]. *Hippocampus*, *2*(1), 1-11. Retrieved from https://www.ncbi.nlm.nih.gov/pubmed/1308170 doi: 10.1002/hipo.450020102

Xiao, D., Vanni, M. P., Mitelut, C. C., Chan, A. W., LeDue, J. M., Xie, Y., ... Murphy, T. H. (2017). Mapping cortical mesoscopic networks of single spiking cortical or sub-cortical neurons [Journal Article]. *Elife*, *6*. Retrieved from https://www.ncbi.nlm.nih.gov/pubmed/28160463 doi: 10.7554/eLife.19976

Xu, H., Zhu, H., Luo, L., & Zhang, R. (2021). Altered gray mat-

ter volume in mri-negative focal to bilateral tonic-clonic seizures [Journal Article]. *Acta Neurol Belg*, *121*(6), 1525-1533. Retrieved from https://www.ncbi.nlm.nih.gov/pubmed/32449136 doi: 10.1007/s13760-020-01383-6

Yang, C., Liu, Z., Wang, Q., Luan, G., & Zhai, F. (2020). Epileptic seizures in a heterogeneous excitatory network with short-term plasticity [Journal Article]. *Cognitive Neurodynamics*. doi: 10.1007/s11571-020-09582-w

Yang, G., Li, L., Lee, W. B., & Ng, M. C. (2018). Structure of graphene and its disorders: a review [Journal Article]. *Sci Technol Adv Mater*, *19*(1), 613-648. Retrieved from https://www.ncbi.nlm.nih.gov/pubmed/30181789 doi: 10.1080/14686996.2018.1494493

Yao, X., Smith, A. J., Jin, B. J., Zador, Z., Manley, G. T., & Verkman, A. S. (2015). Aquaporin-4 regulates the velocity and frequency of cortical spreading depression in mice [Journal Article]. *Glia*, *63*(10), 1860-9. Retrieved from https://www.ncbi.nlm.nih.gov/pubmed/25944186 doi: 10.1002/glia.22853

Yi, M. H., Liu, Y. U., Umpierre, A. D., Chen, T., Ying, Y., Zheng, J., ... Wu, L. J. (2021). Optogenetic activation of spinal microglia triggers chronic pain in mice [Journal Article]. *PLoS Biol*, *19*(3), e3001154. Retrieved from https://www.ncbi.nlm.nih.gov/pubmed/33739978 doi: 10.1371/journal.pbio.3001154

Yizhar, O., Fenno, L. E., Davidson, T. J., Mogri, M., & Deisseroth, K. (2011). Optogenetics in neural systems [Journal Article]. *Neuron*, *71*(1), 9-34. Retrieved from https://www.ncbi.nlm.nih.gov/pubmed/21745635 doi: 10.1016/j.neuron.2011.06.004

Zakharov, A., Chernova, K., Burkhanova, G., Holmes, G. L., & Khazipov, R. (2019). Segregation of seizures and spreading depolarization across cortical layers [Journal Article]. *Epilepsia*, *60*(12), 2386-2397. Retrieved from https://www.ncbi.nlm.nih.gov/pubmed/31755112 https://www.ncbi.nlm.nih.gov/pmc/articles/PMC7164417/pdf/nihms-1056638.pdf doi: 10.1111/epi.16390

Zariwala, H. A., Borghuis, B. G., Hoogland, T. M., Madisen, L., Tian, L., De Zeeuw, C. I., ... Chen, T. W. (2012). A cre-dependent gcamp3 reporter mouse for neuronal imaging in vivo [Journal Article]. *J Neurosci*, *32*(9), 3131-41. Retrieved from https://www.ncbi.nlm.nih.gov/pubmed/22378886 doi: 10.1523/JNEUROSCI.4469-11.2012

Zemelman, B. V., Lee, G. A., Ng, M., & Miesenbock, G. (2002). Selective photo-

stimulation of genetically charged neurons [Journal Article]. *Neuron*, *33*(1), 15-22. Retrieved from https://www.ncbi.nlm.nih.gov/pubmed/11779476 doi: 10.1016/s0896-6273(01)00574-8

Zhang, X., Levy, D., Kainz, V., Noseda, R., Jakubowski, M., & Burstein, R. (2011). Activation of central trigeminovascular neurons by cortical spreading depression [Journal Article]. *Ann Neurol*, *69*(5), 855-65. Retrieved from https://www.ncbi.nlm.nih.gov/pubmed/21416489 doi: 10.1002/ana.22329

Zhang, X., Levy, D., Noseda, R., Kainz, V., Jakubowski, M., & Burstein, R. (2010). Activation of meningeal nociceptors by cortical spreading depression: implications for migraine with aura [Journal Article]. *J Neurosci*, *30*(26), 8807-14. Retrieved from https://www.ncbi.nlm.nih.gov/pubmed/20592202 doi: 10.1523/JNEUROSCI.0511-10.2010

Zhao, H. T., Tuohy, M. C., Chow, D., Kozberg, M. G., Kim, S. H., Shaik, M. A., & Hillman, E. M. C. (2021a). Neurovascular dynamics of repeated cortical spreading depolarizations after acute brain injury [Journal Article]. *Cell Rep*, *37*(1), 109794. Retrieved from https://www.ncbi.nlm.nih.gov/pubmed/34610299 doi: 10.1016/j.celrep.2021.109794

Zhao, H. T., Tuohy, M. C., Chow, D., Kozberg, M. G., Kim, S. H., Shaik, M. A., & Hillman, E. M. C. (2021b). Neurovascular dynamics of repeated cortical spreading depolarizations after acute brain injury [Journal Article]. *Cell Rep*, *37*(1), 109794. Retrieved from https://www.ncbi.nlm.nih.gov/pubmed/34610299 doi: 10.1016/j.celrep.2021.109794

Zhao, J., & Levy, D. (2018). Dissociation between csd-evoked metabolic perturbations and meningeal afferent activation and sensitization: Implications for mechanisms of migraine headache onset [Journal Article]. *J Neurosci*, *38*(22), 5053-5066. Retrieved from https://www.ncbi.nlm.nih.gov/pubmed/29703787 doi: 10.1523/JNEUROSCI.0115-18.2018

Ziemann, A. E., Schnizler, M. K., Albert, G. W., Severson, M. A., Howard, r., M. A., Welsh, M. J., & Wemmie, J. A. (2008). Seizure termination by acidosis depends on asic1a [Journal Article]. *Nat Neurosci*, *11*(7), 816-22. Retrieved from https://www.ncbi.nlm.nih.gov/pubmed/18536711 doi: 10.1038/nn.2132

Zipfel, W. R., Williams, R. M., & Webb, W. W. (2003). Nonlinear magic: multiphoton microscopy in the biosciences [Jour-

nal Article]. *Nat Biotechnol*, *21*(11), 1369-77. Retrieved from https://www.ncbi.nlm.nih.gov/pubmed/14595365 doi: 10.1038/nbt899

Zubler, F., Steimer, A., Gast, H., & Schindler, K. A. (2014). Seizure termination [Journal Article]. *Int Rev Neurobiol*, *114*, 187-207. Retrieved from https://www.ncbi.nlm.nih.gov/pubmed/25078503 doi: 10.1016/B978-0-12-418693-4.00008-X